Side chain functional poly(2-oxazoline)s for biomedical applications

Dissertation zur Erlangung des naturwissenschaftlichen Doktorgrades
der Julius-Maximilians-Universität Würzburg

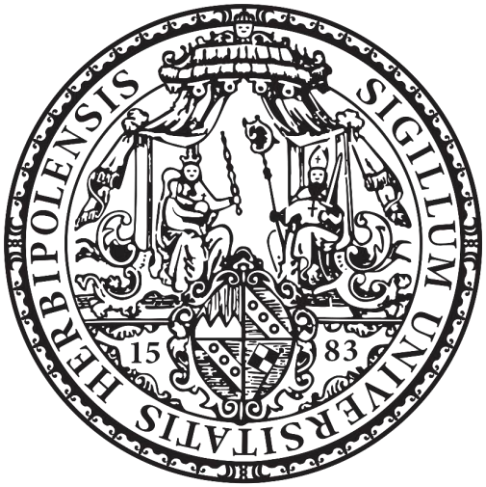

vorgelegt von

Julia Liebscher, geb. Blöhbaum
(M. Sc. Chemie)

aus Leipzig

Würzburg 2019

Eingereicht bei der Fakultät für Chemie und Pharmazie am

_____

Gutachter der schriftlichen Arbeit

1. Gutachter: _____
2. Gutachter: _____

Prüfer des öffentlichen Promotionskolloquiums

1. Prüfer: _____
2. Prüfer: _____
3. Prüfer: _____

Datum des öffentlichen Promotionskolloquiums

_____

Doktorurkunde ausgehändigt am

_____

Die vorliegende Arbeit wurde in der Abteilung für Funktionswerkstoffe der Medizin und Zahnheilkunde, Universität Würzburg, Würzburg, Deutschland in der Zeit von Juli 2014 bis Dezember 2018 unter der Leitung von Herrn Prof. Dr. Jürgen Groll angefertigt.

COPYRIGHT REMARKS

Parts of this thesis have been previously published and are adapted with permission from:

Julia Blöhbaum, Ilona Paulus, Ann-Christin Pöppler, Jörg Tessmar and Jürgen Groll, Influence of charged groups on the cross-linking efficiency and release of guest molecules from thiol-ene cross-linked poly(2-oxazoline) hydrogels, *Journal of Materials Chemistry B* **2019**, *7*, 1782-1794.

Julia Blöhbaum, Oliver Berberich, Stefanie Hölscher-Doht, Rainer Meffert, Jörg Teßmar, Torsten Blunk, Jürgen Groll; Catechol-modified Poly(oxazoline)s with Tunable Degradability Facilitate Cell Invasion and Lateral Cartilage Integration, *Journal of Industrial and Engineering Chemistry* **2019**, *80*, 757-769.

Julia Liebscher, Jörg Tessmar, Jürgen Groll; In situ polymer analogue generation of azlactone functions at poly(oxazoline)s for peptide conjugation, *Macromolecular Chemistry and Physics*, November 2019, accepted.

Table of contents

Abbreviations

ACN	acetonitrile
a. u.	arbitrary units
BDAA	2-oxo-1,3-benzo-dioxole-5-acetic acid
Boc	*tert*-butyloxycarbonyl
BP	boiling point
BSA	bovine serum albumin
ButEnOx	2-(3-butenyl)-2-oxazoline
CG3F	peptide with amino sequence CGGGF
CKF	peptide with amino sequence CKFKFQF
CP	cross-polarization
CROP	cationic ring opening polymerization
Đ	dispersity
d	day
Da	Dalton
DBU	1,8-diazabicyclo[5.4.0]undec-7-ene
DCC	*N,N*-dicyclohexylcarbodiimide
DecEnOx	2-decenyl-2-oxazoline
DMAP	4-(dimethylamino)pyridine
DMF	dimethylformamide
DMPP	dimethylphenylphosphine
DMSO	dimethylsulfoxide
DOPA	3,4-dihydroxyphenylalanine
DSC	*N,N*-disuccinimidyl carbonate
ECM	extracellular membrane
EDC	1-ethyl-3-(3-dimethylaminopropyl)carbodiimide
EI-MS	electron ionization - mass spectrometry
eq.	equivalent
et al.	et alii / et aliae (and others)
EtOx	2-ethyl-2-oxazoline
EWG	electron withdrawing group
FITC	fluorescein isothiocyanate
FSN	fluorescein sodium salt
GAG	glycosaminoglycan
h	hour
HA	hyaluronic acid
HPLC	high performance liquid chromatography
I2959	Irgacure 2959: 2-hydroxy-1-[4-(hydroxyethoxy)-phenyl]-2-methyl-1-propanone
iPrOx	2-isopropyl-2-oxazoline

IR	infrared
LCST	lower critical solution temperature
LDA	lithium diisopropylamide
M_n	number-average molar mass
M_w	mass-average molar mass
MAS	Magic Angle Spinning
MB	methylene blue
MeOH	methanol
MeOx	2-methyl-2-oxazoline
MeOTf	methyl triflate
MeTos	methyl tosylate
M	molarity (mol/L)
min	minute
Mol%	molar percentage
MOMA	*N*-(3-mercapto-1-oxopropyl)-2-methyl-alanine
MPAA	4-mercaptophenylacetic acid
MWCO	molecular weight cut-off
NCL	native chemical ligation
NHS	N-hydroxysuccinimide
NMR	nuclear magnetic resonance
Pip	piperidine
n-PropOx	2-*n*-propyl-2-oxazoline
PBS	phosphate buffered saline
PCL	polycaprolactone
PDMS	poly(dimethyl siloxane)
PE	polyethylene
PhOx	2-phenyl-2-oxazoline
Pip	piperidine
PDLA	poly(D-lactic acid)
PEG	poly(ethylene glycol)
PEtOx	poly(2-ethyl-2-oxazoline)
PGA	poly(glycolic acid)
PLGA	poly(lactic-*co*-glycolic acid)
PLLA	poly(L-lactic acid)
PMeOx	poly(2-methyl-2-oxazoline)
PMMA	poly(methyl methacrylate)
PNIPAAm	poly(N-isopropylacrylamide)
PP	polypropylene
PPG	poly(propylene glycol)
ppm	parts per million
PPrOx	poly(*n*-propyl-2-oxazoline)

POx	poly(2-alkyl-2-oxazoline)
PTFE	poly(tetrafluoroethylene)
PVC	poly(vinyl chloride)
rt	room temperature
SD	swelling degree
SEC	size exclusion chromatography
SEM	scanning electron microscopy
T_{CP}	cloud point temperature
TCEP	tris(2-carboxyethyl)phosphine
THF	tetrahydrofuran
UV	ultraviolet
V	volume
VDM	2-vinyl-4,4-dimethylazlactone
Vis	visible
Wt%	weight percent
YM	Young’s modulus

1 Objective of the thesis

Macromolecules or polymers, which are molecules of high molar mass consisting of repetitive units of molecules with low molecular mass, i.e. monomers, have found application in the biomedical field soon after their discovery about a hundred years ago. Since then, a wide range of natural and synthetic polymers have been explored for biomedical applications.

Natural polymers, such as polysaccharides and proteins, are often used in the field of tissue engineering due to their similarity to the extracellular matrix [1-3]. In addition, they offer a certain biodegradability which many synthetic polymers do not possess to an extent relevant for temporary clinical applications in patients.

However, many synthetic polymers offer chemical versatility of their backbone and functional groups together with a tuneability of molar mass, which allows to adjust chemical as well as physical properties. These can ultimately be influenced by external stimuli after application in the patient [4].

Network structured, cross-linked materials which can hold up large quantities of water, so called hydrogels, have been the basis for many biomaterials. Hydrogels are usually synthesized from biocompatible polymers with multiple, orthogonal functional groups. The variety of these functional groups is huge allowing physical and chemical, covalent cross-linking strategies [5-7].

One prominent hydrophilic synthetic polymer that has been widely used for different biomedical applications is poly(ethylene glycol) (PEG). Cross-linked PEG has been used for drug releasing hydrogel formulations, while polymer-conjugated PEG has been applied for use in antifouling coatings of implants. Moreover, drug or protein conjugates with PEG are used to prolong circulation time, as well as drug half-lives for the parenteral delivery of highly potent but sensitive drug substances [4]. PEG exhibits a unique feature, the so called “stealth” effect. PEG-functionalized products show reduced unspecific protein adsorption and hence a longer blood circulation is ensured [8]. However, concerns have been raised due to the first findings of PEG-antibodies and hypersensitivity reactions in patients [8-10].

A promising alternative to PEG, which has recently captured the interest of many researchers, are poly(2-alkyl-2-oxazoline)s (POx). POx derivatives, as acyl substituted poly(ethyleneimine)s, belong to the so-called class of pseudo-peptides [11]. They are not new polymers, as their polymerization was already reported in the sixties by several research groups [12-15]. However, the relatively long synthesis times discouraged further extensive research until reaction times were sped up by

the use of commercial microwave reactors in the early 2000s [16-18]. In contrast to bifunctional PEG, POx polymers are highly versatile as they do not only allow functionalization at the α- and ω-terminus, but also at the side chain of the polymer through functional monomers [19-24], which even allows the introduction of thermo-responsive behavior [11]. The desirable stealth effect seen in PEG, is also observed for POx polymers [9, 25] and many comparable applications of POx based biomaterials have been reported in current literature [26-29].

In the last decade, hydrogels based on a variety of cross-linked POx have appeared as well, with applications in drug delivery and regenerative medicine [30-35]. POx based block-copolymers have also shown great promises as polymeric micelles in delivering hydrophobic drugs [36, 37] and accordingly activated POx has been conjugated to proteins and antibodies for therapeutic applications [28, 38]. The chemistry behind these biomedical applications is manifold and needs to be specifically tailored to the desired application in the human body.

Hence, it was the **aim of this thesis** to synthesize different poly(2-alkyl-*co*-alkenyl-2-oxazoline) copolymers and equip these with new functional groups via a subsequent post-polymerization functionalization. The approach should be efficient and straight-forward for which thiol-ene chemistry proved to be well suited. Different new functional groups were studied for applications in the biomedical field, one focus was their use for the preparation of hydrogels suited for the delivery of small and large molecules or as degradable adhesives for cartilage regeneration. The second focus was on new chemo-selective functional groups in order to bind thiol-bearing peptides to the side chains of polymers towards the generation of multiple peptide conjugates.

Chapter 2 gives an overview of the relevant literature starting with the variety of polymers available for biomedical applications in *Section 2.1* followed by a more detailed insight into poly(2-oxazolines) and their synthesis in *Section 2.2*. An insight into the basic concepts of thiol-ene chemistry is given in *Section 2.3*. Furthermore, in *Section 2.4* and *2.5*, an introduction into hydrogels, their synthesis and characterization, especially into hydrogels based on poly(2-oxazoline)s in *Section 2.6*, and their application is presented. *Section 2.7* elucidates the chemistry behind the catechol group and its application in context with macromolecules. The final section this chapter, *Section 2.8*, deals with the variety of polymer conjugates, their synthesis and application.

Chapter 3 is divided into three sections. The first section covers the synthesis and characterization of poly(2-oxazoline) homopolymers, see *Section 3.1.1*, and of randomly copolymerized poly(2-oxazoline) copolymers, see *Section 3.1.2* and *3.1.3*. Their functionalization with different functional groups is presented in the second section, showing the functionalization at the side chain with thiols, *Section 3.2.1*, with catechols, *Section 3.2.2*, with thiolactones, *Section 3.2.3* and with azlactones, *Section 3.2.4*. The last section presents the different applications of the functionalized poly(2-oxazoline) copolymers. The preparation and characterization of thiol-ene cross-linked hydrogels based on the afore mentioned thiol functionalized copolymers is shown in *Section 3.3.1*. In addition to the swelling behavior and mechanical properties, these hydrogels were characterized by solid-state NMR, *Section 3.3.1.2.3*, by cryo-scanning electron microscopy, *Section 3.3.1.2.4*, and on their cytotoxicity, *Section 3.3.1.2.5*. The hydrogels were further loaded with fluorescently-labeled dextran molecules or dyes and the diffusion out of the hydrogel network was analyzed, see *Sections 3.3.1.3* and *3.3.1.4*.
Hydrogels were also synthesized through the oxidation of catechol-functionalized copolymers for the application in cartilage regeneration. Their synthesis and characterization are presented in *Section 3.3.2*.
The last part of the final section, *Section 3.3.3*, shows the attachment of a model peptide through thiol-ene chemistry, *Section 3.3.3.1*, through the cyclic thioester, a thiolactone, *Section 3.3.3.2* and through the azlactone group, see *Section 3.3.3.3*.

Chapter 4 comprises a conclusion of the thesis in English and German.

Chapter 5 includes all materials and methods used and a detailed description of all experiments performed. A full characterization of all polymers, hydrogels and polymer conjugates is presented.

2 Theoretical Background

Parts of this chapter have already been published in

Julia Blöhbaum, Ilona Paulus, Ann-Christin Pöppler, Jörg Tessmar and Jürgen Groll; Influence of charged groups on the cross-linking efficiency and release of guest molecules from thiol-ene cross-linked poly(2-oxazoline) hydrogels, *Journal of Materials Chemistry B* **2019**, *7*, p. 1782-1794.

Julia Blöhbaum, Oliver Berberich, Stefanie Hölscher-Doht, Rainer Meffert, Jörg Teßmar, Torsten Blunk, Jürgen Groll; Catechol-modified Poly(oxazoline)s with Tunable Degradability Facilitate Cell Invasion and Lateral Cartilage Integration, *Journal of Industrial and Engineering Chemistry* **2019**, *80*, p. 757-769.

Julia Liebscher, Jörg Tessmar, Jürgen Groll; In situ polymer analogue generation of azlactone functions at poly(oxazoline)s for peptide conjugation, *Macromolecular Chemistry and Physics*, November 2019, accepted.

2.1 Polymers for Biomedical Applications

Polymers have been omnipresent in our everyday life since their discovery in the early twentieth century by Leo Hendrik Baekeland (Bakelite), John Wesley Hyatt (Celluloid) and Fritz Klatte (poly(vinyl chloride)). In 1922, Hermann Staudinger developed the first theories on macromolecules for which he later won the Nobel prize in Chemistry [39]. These newly invented polymers were applied for products of everyday life like spectacle frames and buttons but were also used as first "biomaterials" in denture fabrication [40].

Since then, a wide range of natural and synthetic polymers that can be used for biomedical applications were discovered and developed, as polymers are closer to biological tissue than inorganic materials due to their carbon-based chemistry [4]. An overview of several polymers in use is given in Table 1. Natural polymers have been used for a long time in human medicine, but synthetic polymers caught up after the Second World War in relation to their variety and application possibilities. Their huge advantage is the tunability in respect to their chemical and physical properties which can be controlled by the choice of monomer and polymerization reaction. In addition, there exists the possibility of synthesizing copolymers, whose composition can be tuned accordingly, or the option for post-polymerization functionalization [4].

Table 1: Overview of natural and synthetic polymers used for biomedical applications [1, 4, 41].

Natural polymers	Synthetic polymers
Polysaccharides • Starch • Cellulose • Dextran • Pectin • Chitosan • Alginate • Hyaluronic acid *Proteins* • Collagen • Silk • Fibrin • Elastin	*Non-degradable* • Polyurethanes • Polyamides • Polyethers • Polyacrylates *Degradable* • Polylactides • Polyesters • Polyanhydrides • Polyacetals

Synthetic polymers can also offer unique mechanical properties that can sometimes be influenced by external stimuli like pH, temperature, light or magnetic field. One of the main disadvantages of synthetic polymers however is that they are often not biodegradable, or their degradation products are toxic, if non-natural monomers are used.

Figure 1 shows the chemical structure of two natural polymers, alginate and hyaluronic acid, which are often used for wound dressings, drug delivery or tissue engineering applications [2, 3], and two synthetic polymers, poly(ethylene glycol) (PEG) and poly(methyl methacrylate) (PMMA). PEG is often used for drug conjugates, hydrogel formulations or antifouling coatings and PMMA can be used for bone cement formulations, contact lenses and intraocular lenses or as dialysis membranes [4].

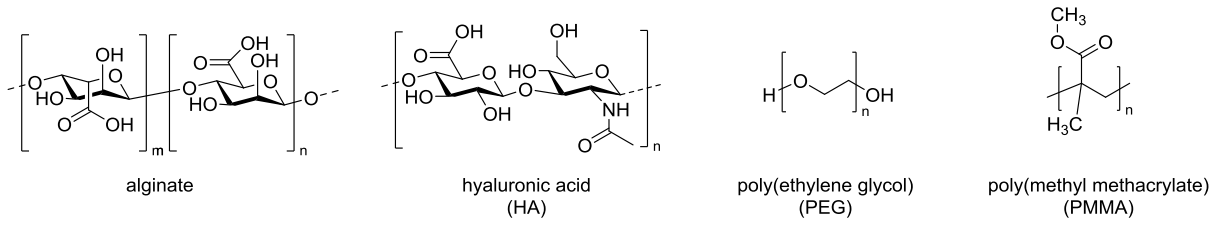

Figure 1: Chemical structure of natural polymers: alginate and hyaluronic acid, and synthetic polymers: PEG and PMMA.

Natural polymers are often preferred in biomedical applications due to their similarity to native extracellular matrix (ECM) and other macromolecules occurring in the body. In many cases, they can also be modified chemically making them more versatile for specific applications.

One major class of natural polymers that are used in biomedicine are polysaccharides, like starch, cellulose, dextran, hyaluronic acid and alginate. One can differentiate between homopolysaccharides consisting of only one monomer unit and heteropolysaccharides made from two or more monomer units [1].

Starch and cellulose are obtained from plants. Starch has so far been combined with other synthetic polymers for the manufacturing of porous scaffolds [1, 42]. Cellulose derivatives are most commonly applied in membranes for dialysis or for biosensors but scaffolds made from cellulose acetate have also shown potential for growing cardiac cell constructs [43].

Dextran, which is synthesized by bacteria, has shown great physio-chemical properties and is well tolerated in the human body. For these reasons, it has been

used for drug targeting, stabilization and solubilization reducing side effects and prolonging the release [1].

Another frequently used polysaccharide in biomedicine, which is also classified as glycosaminoglycan (GAG), is hyaluronic acid (also hyaluronan or sodium hyaluronate) (HA). It is composed of alternating D-glucuronic and *N*-acetyl-D-glucosamine residues and can be found in the ECM of soft connective tissue in vertebrates. Biological sources for HA in laboratory use are bacteria and animal tissues, like rooster combs, shark skin or bovine eyeballs, and the molar mass ranges between several hundred thousands of Da up to 2.5 MDa [3]. HA is clinically applied in ophthalmologic, orthopedic and plastic surgery, but has also shown great potential for the formation of hydrogels for DNA and drug delivery [3].

Another naturally occurring anionic polysaccharide is alginate, which can be extracted from brown algae at low cost. It is composed of β-D-mannuronate and α-L-guluronate residues that alternate in blocks or individually along the chain. The molecular weight of commercially available alginate ranges between several ten to hundred thousand Da.

Alginate has shown great biocompatibility, low toxicity and structural similarity to the ECM. The gelation can be induced ionically by addition of bivalent cations, e.g. Ca^{2+} or through covalent cross-linking using diamines and simple NHS/EDC chemistry [44]. The viscosity of the alginate solution can be influenced by the pH as a protonation of the carboxylate groups at low pH leads to an increase in hydrogen bonds. Alginate hydrogels have been used as wound dressings, for the release of small drugs or large macromolecules like proteins, in cell culture and for tissue regeneration [2].

Another large class of natural polymers that are used for biomedical applications are proteins and poly(amino acids) like fibrin, elastin, silk and collagen. Fibrin, that consists of the two proteins, fibrinogen and thrombin both involved in blood clotting, is probably the most prominent example having been used for a long time as a biomaterial to prevent bleeding and ameliorate wound healing [45]. Fibrinogen is made up of three pairs of polypeptide chains connected by disulfide bonds. The six polypeptide chains are joined by their amino termini in the central region, which are cleaved by the proteolytic enzyme thrombin. This enzymatic cleavage produces a fibrin monomer which is “polymerized” into protofibrils by specific protein–protein interaction. The addition of more monomers leads to two-stranded protofibrils that

aggregate to fibers forming a three-dimensional mesh [45]. The commercial sources of fibrin are human or bovine plasma, which increases the risk of disease or prion transmission. In clinical application, there is the possibility to concentrate autologous fibrin, however this can take several hours, and the patient must be free of any clotting disorders. So far, fibrin has been used as a hemostatic glue, for wound repair, in drug and cell delivery and tissue engineering [45, 46].

Collagen is the most extensively studied natural polymer as it is the major component in all human connective tissue, like skin and bone. There exist 29 different types, of which five are known to form fibrils. Type I collagen, which represents 90 % of the total collagen in the human body, is so far, the most widely used to produce biomaterials. Collagen can be extracted from nearly any animal, but common sources are bovine and porcine skin, and rat tails [47].

The cross-linking of collagen can occur via physical, chemical or enzymatic pathways. Collagen hydrogels have been used for modulation of cardiovascular and musculoskeletal tissues or as microparticles for the delivery of cells [46, 48].

The last natural polymer that is described in this chapter is silk. Silk consists of fibrous proteins with repetitive sequences predominantly made of the amino acids alanine, glycine and serine [49]. Silk is produced by mulberry silkworms with the commercially available silk produced solely by the species *Bombyx mori* [50]. Its biocompatibility, low immunogenicity, non-toxicity and mechanical strength renders it the ideal candidate as a biomaterial and has already been used for wound healing, tissue engineering (cartilage, bone and tendon) and drug delivery [49, 50].

All of these natural biopolymers discussed have the advantage of being degradable, which is essential in tissue engineering as the engineered scaffold should be integrated into host tissue over time. Their biodegradability however strongly depends on the environmental conditions and is extremely variable. Most natural polymers are degraded via hydrolysis followed by oxidation under physiological conditions [1]. One can differ between enzymatically degradable polymers and non-enzymatically degradable polymers that decompose when in contact with water or serum. For example, hyaluronic acid can be degraded by reactive oxygen species at inflammatory sites or enzymatically by several hyaluronidases [3].

After this short overview of the most relevant natural polymers, the focus will further lie on the development of synthetic polymers for biomedical use.

Polyolefins like polyethylene (PE), polypropylene (PP), poly(tetrafluoroethylene) (PTFE) and poly(vinyl chloride) (PVC) were among the first industrial polymers that were manufactured at large scale and used in biomedical applications. PE can be synthesized with different percentages of crystallinity and molecular weights. Low density PE is used for packaging due to is low elastic modulus, but ultrahigh molecular weight PE can be employed as sliding surfaces of artificial joints with an elastic modulus of 1000 MPa – 2000 MPa. PP is similarly hydrophobic and biologically inert, and utilized for non-resorbable suture materials and hernia meshes [4]. PTFE is another hydrophobic and non-degradable polymer that has been used for vascular grafts, e.g. in mitral valve repair, surgical meshes, ligament and tendon repair [51]. PVC, which most people probably know from its use as flooring, is used mainly outside of the body, for example for blood storage bags, as its synthesis requires the use of stabilizers and plasticizers which would be toxic upon long term implantation in the body.

The non-carbon-based polymer silicone with a -Si-O- backbone can be manufactured with different chain lengths and cross-link degrees leading to materials with different physical properties, i.e., oils, gels or even rubbers. The advantage is that silicones do not need any plasticizers, but the biological compatibility ranges from well tolerated (in ophthalmologic application) to the occurrence of hematologic cancers [4]. Poly(dimethyl siloxane) (PDMS) is used for catheters, plastic surgery, intraocular lenses and dialysis membranes.

Polyacrylates are easiest obtained by radical polymerization which is also possible *in situ*, which has led to its wide application in dentistry, e.g. as dental fillings, and in orthopedics [51]. The polymerization of methyl methacrylate leads to tough PMMA, which is used as bone cement or as hard intraocular lenses [46]. Hydrogels can be prepared through the polymerization of the more hydrophilic monomer hydroxyethyl methacrylate which have been applied for soft contact lenses, hemocompatible coatings and lubricants due to its good anti-fouling properties. The polyacrylates are generally considered to be biologically inert, but there might be toxic effects due to remaining unpolymerized monomer, especially for *in situ* polymerized materials [4].

A popular group of polymers that are degradable by simple means of hydrolysis in the body are polyesters like poly(glycolic acid) (PGA), one of the first degradable polymers in biomedical use, and include poly(L-lactic acid) (PLLA) and poly(D-lactic acid) (PDLA). There are also several random copolymers of both with varying

compositions, namely poly(lactic-*co*-glycolic acid)s (PLGA). In general, poly(lactide)s are more hydrophobic and hence degrade more slowly than PGA. The degradation rate of these polymers principally depends on the molecular weight, crystallinity and also on the terminal ester or acid group. They degrade into their monomers glycolic acid or lactic acid, which are physiological metabolites and accordingly can be metabolized by the patient. However, based on the speed of degradation or the application site, there are concerns regarding a local decrease in pH being possibly harmful to neighboring cells and tissues. PGA has been used for a long time as a suture material and most recently also as short-term tissue engineering scaffolds. Highly crystalline PLLA on the other hand degrades rather slowly which can be improved by chemical modification or the copolymerization with other degradable polymers. It has been extensively used for tissue engineering applications such as bone, cartilage, tendon and vascular regeneration. The copolymer PLGA can be tailored to the specific application need through the composition and monomer sequence. A rapid degradation rate makes it the ideal candidate for drug delivery, and it has already been used to deliver chemotherapeutics, proteins, vaccines and antibiotics. In addition, PLGA scaffolds have demonstrated great cell adhesion and proliferation properties [4, 41].

The last class of synthetic polymers which will be presented in this short summary are polyethers. Research has mostly focused on poly(ethylene glycol) (PEG), also named poly(ethylene oxide) (PEO) if the molecular weight is above 20 kDa, and poly(propylene oxide) (PPO), as well as triblock copolymers of PEO and PPO, so called poloxamers or pluronics. Polyethers are in general not susceptible to hydrolytic degradation and enzymatic degradation in the human body has so far not been demonstrated. For this reason, it is recommended to use rather low molecular weight polyethers, so that they can still be excreted renally. Nevertheless, PEG with a molecular weight of 200 $gmol^{-1}$ has already demonstrated clastogenic effects in Chinese Hamster epithelial liver cells and should be employed with caution [4].

PEG is mostly used for protein and drug delivery systems as it prolongs the blood circulation time and ameliorates the pharmacokinetics. In these applications, PEG-functionalized (PEGylated) products are not recognized as foreign and so are not prematurely cleared from the body, previously described as the “stealth” effect. This characteristic still renders PEG the most widely used synthetic polymer for drug delivery applications [52]. In addition, PEG has been used to improve the delivery

properties of other polymers like PLA, PLGA and PCL, and can be used as hydrogel forming polymer upon cross-linking for tissue engineering applications, e.g., for ligament, cartilage or bone regeneration [41].

The pluronic polymer PF127, consisting of 30 % of a hydrophobic middle segment of PPO and two hydrophilic segments of PEO, has also been used for a wide range of biomedical applications. The hydrophobic core helps to encapsulate lipophilic drugs whereas the hydrophilic PEO segments prevent unspecific protein binding [53]. This feature can also be used for *in situ* gel systems. These can easily be prepared and do not require any organic solvent facilitating site-specific delivery and patient compliance [54, 55]. Disadvantages of PF127 are the rapid dissolution in physiological fluids, rapid clearance and weak mechanical strength which however can be overcome by changing the structure into polymeric micelles or hydrophobically modified thermogels [56].

A close multifunctional analogue to PEG, which can only have two reactive end-groups, is poly(glycidol) (PG). PG offers a hydroxyl -CH_2OH side chains per monomer unit incorporated. These can further be modified into carboxyl, amine or vinyl groups and increase the hydrophilicity of the polymer. The multifunctionality allows covalent immobilization of drugs [57], attachment of fluorescent labels [58], nanoparticle coatings [59] and the preparation of densely cross-linked hydrogels [60]. In addition, the coating of different surfaces like glass or gold with PG has shown that protein adsorption is reduced immensely [61]. It was also reported for hyperbranched PG that it is hemocompatible and well tolerated by mice when injected in high doses [62].

2.2 Poly(oxazoline)s

Another multifunctional alternative to PEG are poly(2-alkyl/aryl-2-oxazoline)s, in short poly(oxazoline)s (POx), which have shown great potential for biomedical applications in the last two decades. The general chemical structure of the monomer and the polymer are shown in Figure 2. Due to the living polymerization, POx offers the possibility to functionalize at the α- and ω-terminus of the polymer chain independently. Furthermore, possible modifications at the side chain, using functional monomers, make it very versatile concerning the tuning of chemical and physical properties. In addition, researchers have shown its great potential for biomedical applications in the last two decades.

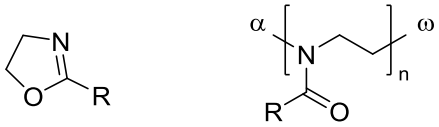

Figure 2: Chemical structure of the 2-oxazoline monomer (left) and the corresponding polymer POx (right) with R = alkyl or aryl.

2.2.1 "Living" Cationic Ring Opening Polymerization of 2-Oxazolines

The term "living" was first introduced by M. Szwarc in 1956 for the anionic polymerization of poly(styrene). In general, a polymerization starts with the initiation step, followed by the propagation and growth of the polymer is finally stopped by the termination step. However, "an interesting situation arises when a polymerization process does not involve a termination step. The polymeric molecules then 'live' for an indefinite period amount of time…" [63]. The polymeric chain can of course only grow if new monomer is available. The time of termination can be chosen by adding a terminating agent at a specific time point, until then, the living end in the reaction will be able to grow as long as new monomer is available [63]. This process is however somewhat limited to the viscosity of the reaction solution which will increase with increasing molecular weight of the polymer. A 'living' polymerization will yield narrow dispersities (Đ) if the reaction constant of the initiation is much greater than the reaction constant of the chain growth ($k_{ini} > k_{growth}$). Here, the limit is set at Đ < 1.2 for 'living' polymerizations. The 'living'/controlled nature of a polymerization can be carried out in radical, anionic and in cationic polymerizations.

The polymerization rate of a living polymerization is accordingly determined by the propagation rate and follows first-order kinetics as follows:

$$-\frac{d[M]}{dt} = k_p[P^*][M] \qquad \textbf{Eq. 1}$$

with [M] being the monomer concentration, [P*] the concentration of the living chains and k_p being the polymerization constant of the respective monomer. The concentration of living chain ends can be assumed to be equal to the initial initiator concentration $[I]_0$ under ideal living conditions, where immediate and complete initiation and no termination occurs. Eq. 1 can then be reformulated and integrated into:

$$ln\left(\frac{[M]_0}{[M]_t}\right) = k_p[I]_0 t \qquad \textbf{Eq. 2}$$

with $[M]_0$ being the initial monomer concentration and $[M]_t$ being the monomer concentration at any possible time point during the polymerization. In an ideal living polymerization, the slope from this first order kinetic plot, from which k_p can be deducted, should be linear.

In 1966 and 1967, several research groups reported the cationic ring opening polymerization of 2-oxazolines belonging to the group of poly(amide)s [12-15]. POx are generally considered as pseudo-peptides as they cannot form secondary structures like peptides due to the lack of chiral centers in the main chain [11].

The cationic ring opening polymerization of 2-oxazolines is schematically shown in Figure 3. The polymerization starts with the nucleophilic attack of the nitrogen atom of the cyclic imino ether to the electrophilic initiator and is governed by the initiation rate constant k_i. Initiation already occurs at room temperature, but very slowly, except when extremely reactive electrophiles like triflates are used.

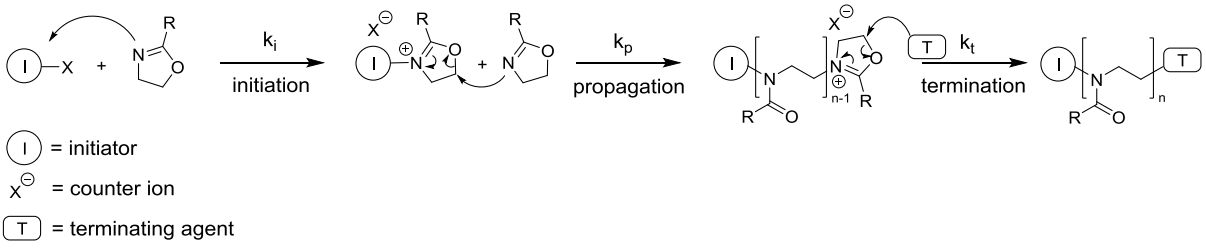

Figure 3: Synthesis scheme of the CROP of 2-oxazolines, adapted from [64] - © 2016 Elsevier Ltd.

There exists a range of different initiators like organic and inorganic (Lewis) acids, silyl and acid halides, chloroformates and alkyl halides, tosylates and triflates. Among which methyl triflate, methyl iodide, benzyl bromide and methyl tosylate are the most commonly used. The latter is preferred by many researchers due to its higher

stability [64]. The counter ion plays an important role for the equilibrium between the active cationic species and the covalent species (Figure 4), which also depends on the monomer and solvent chosen [65].

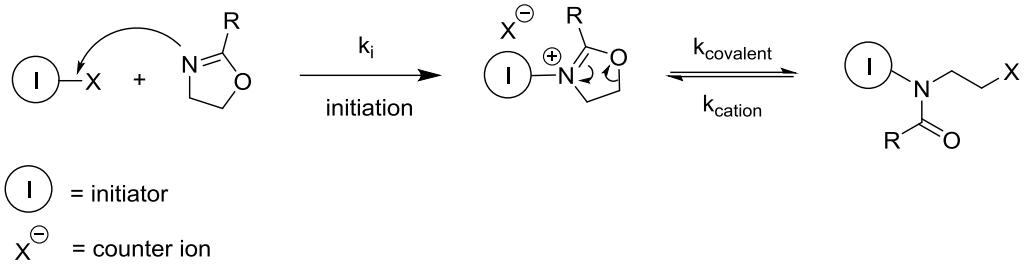

Figure 4: Initiation step of the CROP of 2-oxazolines showing the equilibrium that exists between the cationic and covalent species, adapted from [64] - © 2016 Elsevier Ltd.

The α-terminus of the polymer can be functionalized by choosing an appropriate functional initiator. Here, one should be careful that the functional group of the initiator is compatible with the requirements of the CROP. Functional initiators that have been used in the past comprise allyl, vinyl, styrene, anthracene and alkyne functional groups [64]. If the functional group is not compatible with the CROP, suitable protecting groups can be employed such as a *tert*-butyloxycarbonyl (Boc) group for protection of amines or thioesters for the protection of thiols. By choosing the appropriate initiator, it is also possible to synthesize complex architectures, for example star-shaped polymers, and graft or comb copolymers.

The first step of the propagation is the addition of the first monomer to the initiator salt with the rate constant $k_{p,1}$ which is also the rate determining step as this process is rather slow (Figure 5). The equilibrium between the cationic and covalent species prevails during propagation, however, it was found that the second pathway, the covalent propagation (i.e. bimolecular ionization, denotated with II) in Figure 5), is of minor importance and that the cationic active centers exclusively contribute to the chain growth [65].

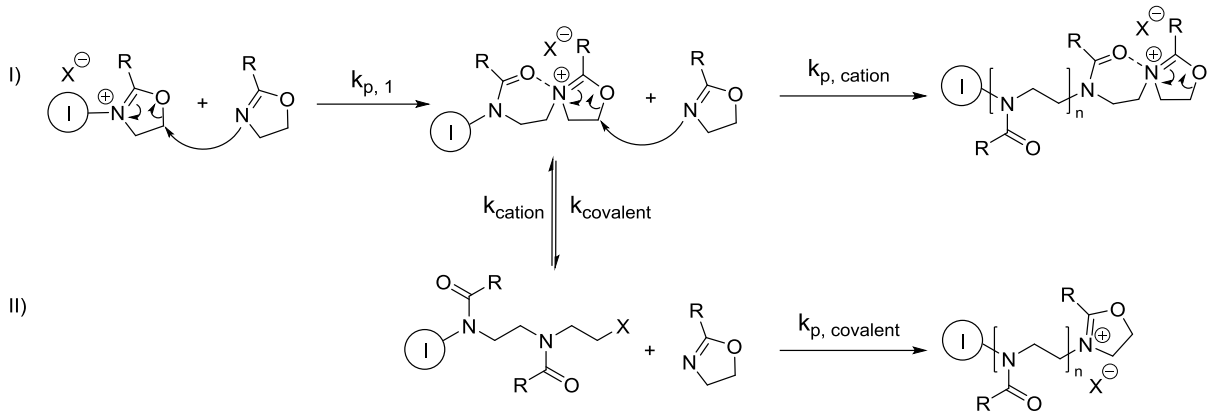

Figure 5: Propagation mechanism of the CROP of 2-oxazolines with I) via the cationic and II) the covalent propagation route, adapted from [64] - © 2016 Elsevier Ltd.

The neighboring oxygen of the amide induces an intra-molecular dipole-ion polarization effect which leads to a drastic increase of the propagation rate constant $k_{p,\ cation}$ and stabilizes the transition state. The stability of this transition state depends of course also on the ability of the counter ion to form a stable anionic species and on the nucleophilicity of the monomer itself. Besides these factors, the temperature and solvent have a strong influence [64].

Even though, CROP of 2-oxazolines has so far been described as living, it is nearly impossible to carry out the polymerization under truly living conditions in the laboratory. This fact becomes especially apparent if higher molecular weights are targeted (> 10 kDa). The polymerization is highly sensitive to nucleophilic impurities, for example water and ammonia (possible contaminant in the monomer) [66]. Litt *et al*. were the first to discuss a possible side reaction where the monomer does not act as a nucleophile but as a base and an E2 β-elimination reaction competes with the propagation reaction [67], see Figure 6 reaction scheme I). This enamine terminated polymer can subsequently react with a living polymer end leading to chain coupling/termination, see reaction scheme II) in Figure 6.

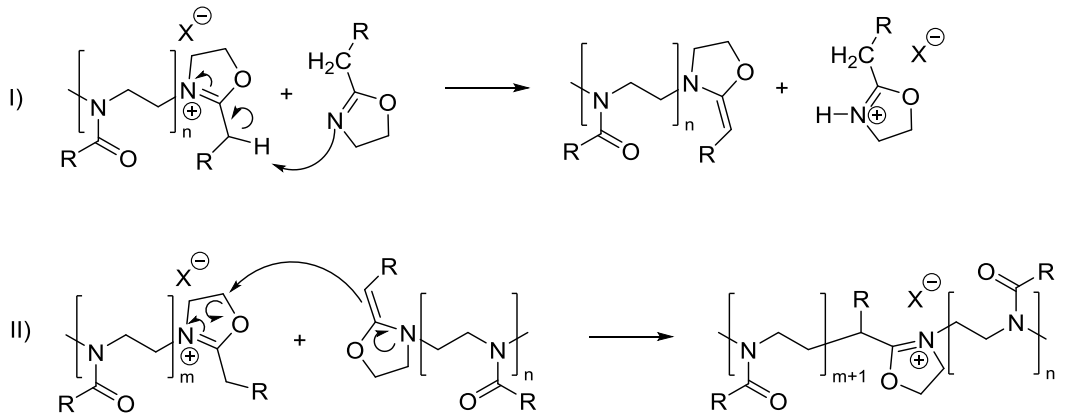

Figure 6: Side reaction mechanism as proposed by Litt *et al*. through I) chain transfer to the monomer via β-elimination and II) chain coupling of the enamine terminated polymer to a living polymer end [67].

Monnery *et al*. proposed another possible chain-transfer reaction based on their findings of polymerizing the monomer 2-ethyl-2-oxazoline (EtOx) whilst attempting a molecular weight of 300 kDa with a dispersity below 1.2 [66] (Figure 7). They questioned the acidity of the abstracted hydrogen atom in the β-elimination proposed by Litt *et al*. Instead, they hypothesized a tautomerization of the monomer and cationic oxazolinium species. The tautomerization of the cationic oxazolinium species leads to a proton transfer to the monomer resulting in the same chain-transfer product as described by Litt *et al*. The second mechanism that is proposed is that the monomer will undergo tautomerization to its enamine form and will react with the living chain end by nucleophilic attack resulting in a protonated oxazolinium end group. Monnery *et al*. suggested that either further monomer is added to this chain end or it will transfer the proton to another monomer initiating a new chain whilst being deactivated [66].

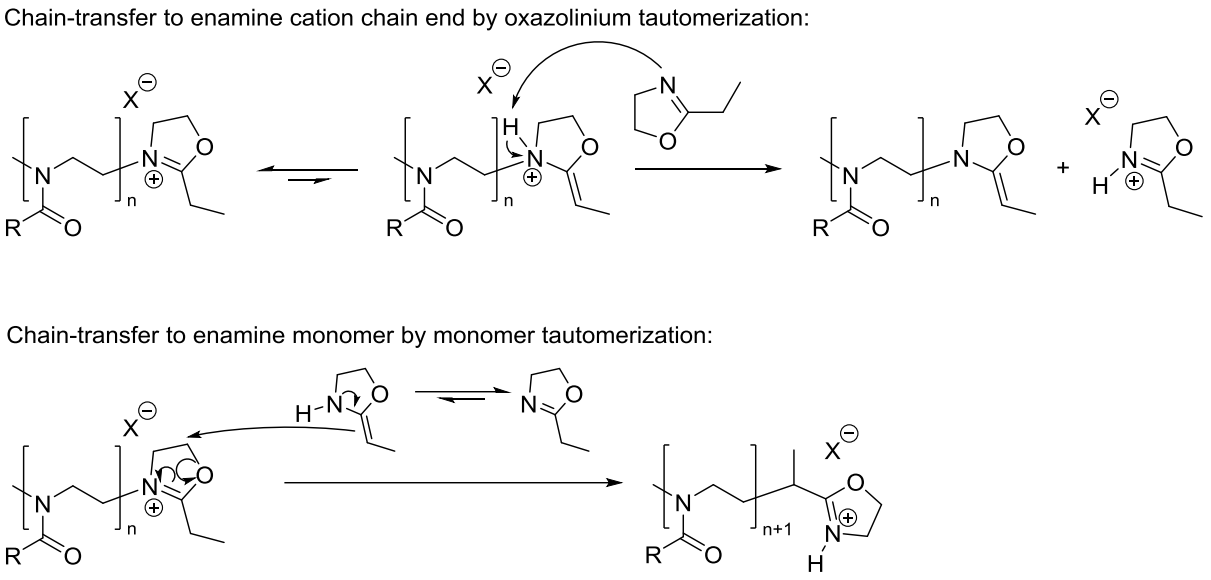

Figure 7: Proposed mechanisms of chain-transfer during the propagation of EtOx through oxazolinium tautomerization or monomer tautomerization, adapted from Monnery *et al*. [66].

The Monnery group confirmed the newly proposed tautomerization of the monomer by deuterating the side chain of EtOx at 140 °C in deuterated acetonitrile. A deuterium exchange could not be observed at 40 °C. Whilst the monomer concentration is the rate-limiting step for the side reactions involving monomer tautomerization or the β-elimination mechanism described by Litt, the concentration of living cationic chain ends is the key factor for the chain-transfer reaction by oxazolinium tautomerization.

Monnery *et al*. applied an extensive purification protocol but could not obtain P(EtOx) without low molecular mass tailing and higher molar mass peaks when polymerizing at 140 °C in acetonitrile. They switched to a different solvent, chlorobenzene, lower temperatures (40 °C), an oxazolinium salt as initiator and performed the polymerization by static distillation under high vacuum. By these means, they were able to synthesize P(EtOx) with a molecular weight up to 58 kDa with dispersities below 1.06. Polymers with a mass of 60 kDa to 300 kDa had dispersity values between 1.1 – 1.2. A major drawback of this synthesis approach are the long reaction times (20 to 28 days) and the fact that a slight increase of the reaction temperature to 60 °C already yielded in higher dispersities. By determining the chain transfer coefficients via the chain length distribution, Monnery *et al*. found that the probability of chain-transfer reactions is mostly dependent of the concentration of oxazolinium chain ends so that their suggested mechanism of oxazolinium tautomerization is predominantly responsible for higher dispersities.

Sedlacek *et al*. recently tried to apply the synthesis protocol of Monnery *et al*. to the monomer 2-methyl-2-oxazoline (MeOx) to receive polymers with a molar mass higher than 20 kDa. However, they found that dispersities broadened as soon as repeating units with higher numbers (> 100) were targeted and dispersities could only be kept < 1.3 for molar masses below 15 kDa. Sedlacek *et al*. explain the higher chain-transfer rate of MeOx by the lower steric hindrance of the α-proton of MeOx [68] being in line with the β-elimination theory of Litt *et al*. In summary, the chain-transfer reaction mechanism that does occur is not yet fully understood and is difficult to verify. Depending on the monomer, different mechanisms could be applicable.

The mechanistic theories on the termination rely on a study performed by Nuyken *et al*. in 1996 [69]. They found that there exists a kinetically driven termination at the 2-position of the oxazoline ring and a thermodynamically driven termination at the 5-position of the oxazoline ring. In general, the latter is the favored mechanism.

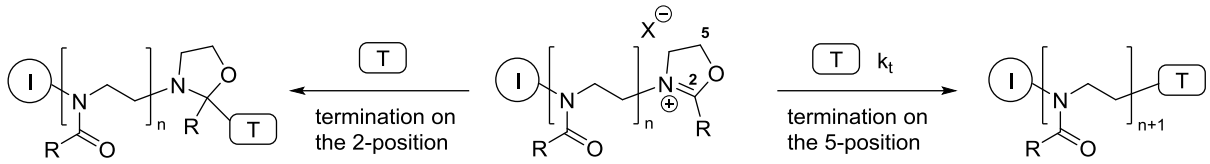

Figure 8: Termination mechanisms with left arrow showing the kinetically driven termination and right arrow showing the thermodynamically driven termination [69].

A typical terminating agent for the kinetically controlled pathway is water resulting in a secondary amine and ester end group. Typical terminating agents for the thermodynamically driven pathway are amines and amides, carboxylates, methanolic potassium hydroxide and thiolates [64]. The most commonly used terminating agents are piperidine, boc-piperazine, or methanolic solutions of potassium or sodium hydroxide which are usually added in excess. The terminating reaction can be carried out at room temperature but is often performed at temperatures of 40 – 45 °C to speed up the terminating process or in the case of allylamine elevated temperatures are a must as primary amines are rather weak terminating agents [70].

2.2.2 Oxazolines

2-oxazolines, or more correctly 2-substituted 4,5-dihydrooxazoles, belong to the group of cyclic imino ethers. Cyclic imino ethers all bear the same –N=C–O– motif in their ring structure. The ring size ranges from five to seven atoms following the nomenclature oxazoline, oxazine and oxazepine respectively, see Figure 9A. When

the double bond is located in the 2-position the molecule is called a 2-oxazoline but the double bond can also be located at the 3- or 4-position, see Figure 9B. The heterocyclic ring can also be substituted at the position 2, 4, 5 or at 2 and 4, see Figure 9C.

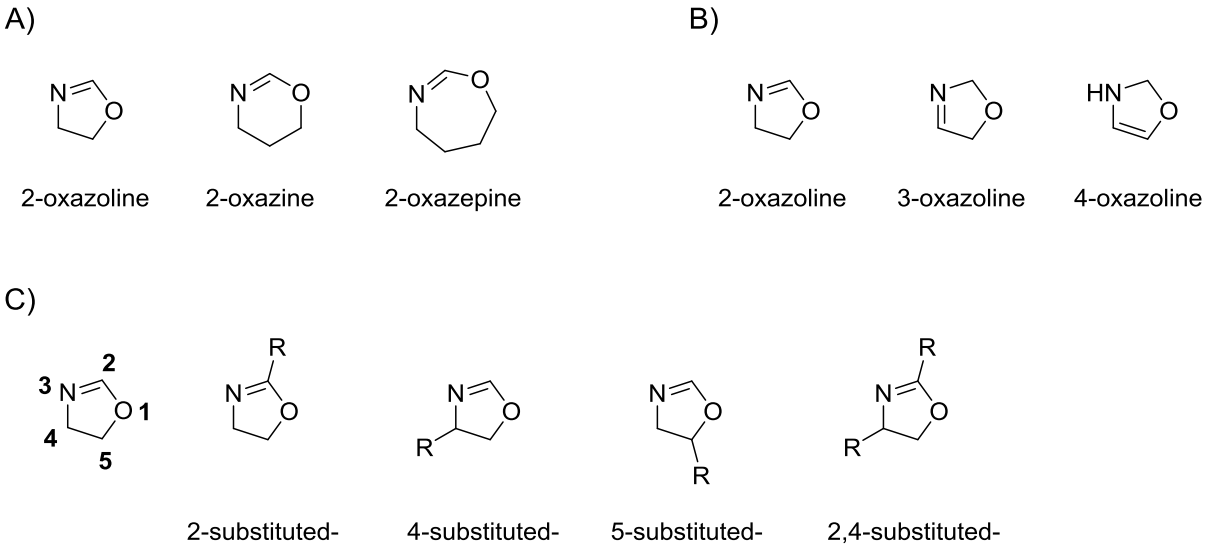

Figure 9: Nomenclature of cyclic imino ethers, depending on A) ring size, B) location of double bond within ring structure and C) position of substituents, adapted from [71] - © WILEY-VCH Verlag GmbH & Co. KGaA.

The most common and commercially available 2-oxazolines are 2-methyl-2-oxazoline (MeOx), 2-ethyl-2-oxazoline (EtOx), 2-isopropyl-2-oxazoline (iPrOx), 2-*n*-propyl-2-oxazoline (nPrOx) and 2-phenyl-2-oxazoline (PhOx), see Figure 10.

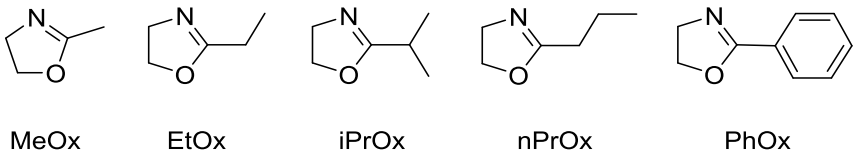

Figure 10: Chemical structure of commercially available 2-oxazolines.

The most popular synthesis strategy for 2-oxazoline is the procedure developed by Witte and Seeliger. In this single-stage synthesis, an accordingly substituted nitrile is heated with α, β-amino alcohols (e.g. ethanolamine) with catalytic amounts of zinc or cadmium salts [72] under the development of ammonia. In case that the substituent is not compatible with the nitrile approach the (modified) Wenker synthesis [73] is an option.

Synthesis by Witte and Seeliger:

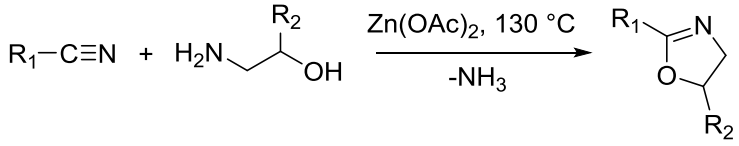

Synthesis by Wenker:

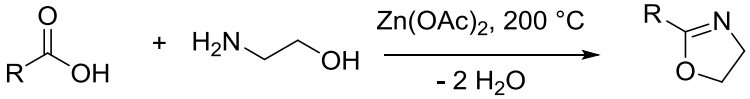

Modified Wenker synthesis:

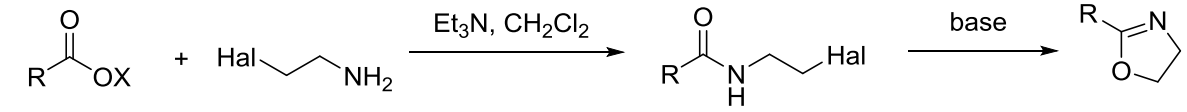

X = OEt, Hal

Synthesis by Persigehl *et al*.:

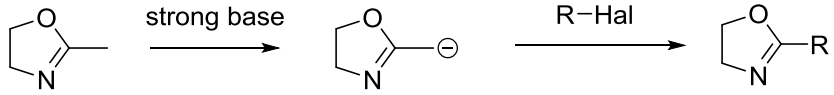

Figure 11: Possible strategies for the synthesis of 2-oxazolines.

In the original Wenker synthesis, a carboxylic acid is reacted with ethanolamine at very high temperatures. The modified version comprises a two-step synthesis were the activated acid is reacted with an halogenethylene amine chloride, e.g. 2-chloroethylamine hydrochloride, forming 2-halogenethylamide. The ring closure follows through the addition of a base [74, 75]. This synthesis strategy has often been used for the preparation of 2-substituted oxazoline monomers with functionalities that allow post-polymerization functionalization such as 2-(3-butenyl)-2-oxazoline (ButEnOx) or 2-decenyl-2-oxazoline (DecEnOx). The forth option is to deprotonate the methyl group of MeOx with a strong base such as *n*-butyllithium or lithium diisopropylamide (LDA) introduced by Persigehl *et al*. [76]. The substituted alkyl halide will then react by nucleophilic substitution at the 2-position of the oxazoline ring. This approach was for example used by Dargaville *et al*. to synthesize ButEnOx starting from MeOx using LDA and allyl bromide [77].

The side chain of the 2-oxazoline monomer determines the solubility of the later obtained polymer in organic solvents as well as in water. Polymers made of MeOx are water soluble without any limitations, but POx with two to three carbons in the

side chain exhibit a lower critical solution temperature (LCST) or cloud point temperature (T_{CP}), see Figure 13. Polymers with a LCST become insoluble upon heating as the intra- and intermolecular hydrogen bonding between polymer chains is in favor of the solubilization with water molecules at a certain temperature. This process is entropically driven as the water molecules are released from the polymer chain. In addition, the polymer undergoes a coil-to-globule transition due to the dehydration [78]. POx with a side chain of four or more carbons are not water soluble at all. However, in case of PEtOx, this LCST behavior only starts when the polymer is at least 100 repeating units long [79] and ranges from 66 °C – 94 °C depending on the degree of polymerization (DP) [80]. In line with this observation, Christova *et al*. found that PEtOx follows a classical Type I Flory-Huggins behavior, meaning that the cloud point (T_{CP}) decreases with increasing molecular weight, which was used for the formation of temperature-responsive hydrogels [79]. The LCST is defined as the lowest T_{CP} which was determined to be around 60 °C to 63 °C by Lin *et al*. for PEtOx with a molecular weight of 50 kDa – 500 kDa at a concentration of 3 wt% [81].

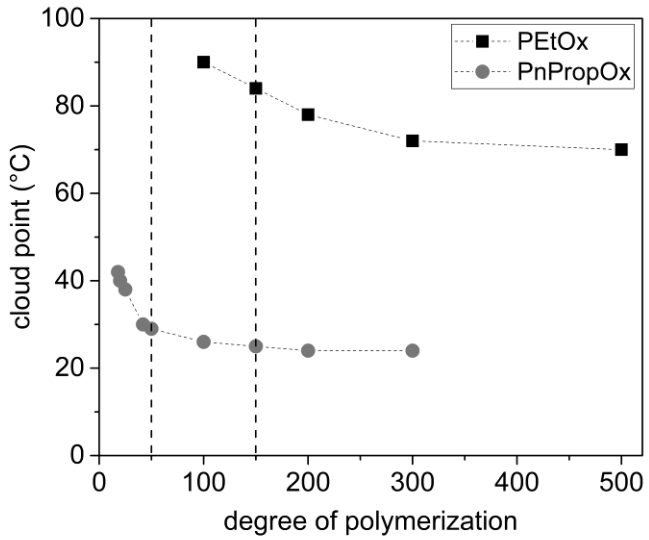

Figure 12: Dependence of the cloud point depending on the degree of polymerization of PEtOx and P*n*PrOx, reproduced and adapted from [80] with permission from The Royal Society of Chemistry.

Besides the molecular weight, the presence and concentration of ions can have a strong influence on T_{CP} as demonstrated by Demirel *et al*. where the addition of just 0.2 M Na_2CO_3 to a 1 wt% solution of PEtOx induced a decrease of the T_{CP} to 27 °C [82]. Other salts, such as NaSCN, can also induce a slight increase of T_{CP}. The concentration of the polymer solution itself also influences the cloud point for which

reason, the concentration should always be stated with T_{CP}. Another factor is the topology of the backbone. It was shown that a star-shaped PEtOx has a lower T_{CP} than its linear analogue by Kowalczuk *et al*. [83].

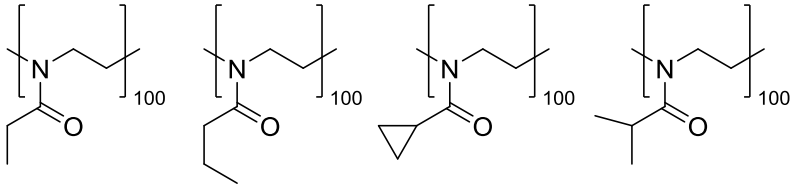

	PEtOx	PnPrOx	PcPrOx	PiPrOx
T_{CP} (°C)	94	27	30	44

Figure 13: Cloud point temperature of water soluble POx with DP = 100 [80, 84].

The polymers of the isomers of 2-propyl-2-oxazoline (*n*-, cyclo- and iso-propyl-2-oxazoline) also exhibit a LCST behavior with poly(2-isopropy-2-oxazoline) (PiPOx) being the most popular as its T_{CP} is close to the body temperature and also follows type I Flory-Huggins behavior. In case of PiPrOx, Obeid *et al*. also demonstrated that the cloud point temperature strongly depends on the hydrophilicity of end-group (hydroxyl/methyl vs. *n*-octadecyl) of the polymer, especially for shorter chains [85]. The most hydrophobic polymer among the propyl-isomers, namely poly(2-*n*-propyl-2-oxazoline (P*n*PrOx) also exhibits the lowest LCST. The dependence of the molar mass and the concentration plays a less significant role due to the more hydrophobic character of the linear propyl side chain [86].

To fine tune the thermo-responsive behavior for specific applications, it is possible to blend/mix different homopolymers, for example PiPrOx with poly(*N*-vinylcaprolactam) to obtain a cooperative behavior. Another possibility is to copolymerize different monomers into statistical or block copolymers. For example, EtOx was statistically copolymerized with *n*PrOx which resulting in copolymers with cloud points ranging from 24 °C to 97 °C where a higher content on *n*PrOx and a higher DP led to a lower T_{CP} [80]. Diehl *et al*. synthesized statistical copolymers of iPrOx and ButEnOx which were afterwards modified with long alkyl chains, alcohols, carboxylic acids or glycopyranose by post-polymerization functionalization using thiol-ene chemistry leading to a variety of cloud points [87].

2.2.3 “Defined” Copolymers

A copolymer, consisting of usually two monomers, but also more are possible, can be polymerized in a way so that there is a statistical distribution of the monomers along the polymer chain. For this kind of copolymer, the monomers are added to the reaction mixture at the same time. A fully statistical copolymer is however only achieved if the reaction constants of both monomers are the same. If one monomer reacts faster than the other, a gradient copolymer is typically received, unless the monomer concentrations in the feedstock are constantly adjusted to account for the different reactivity, e.g. by using syringe pumps. It is also possible to first polymerize only one monomer until complete consumption of the first monomer (first block) and then add the second monomer (second block). Accordingly synthesized polymers are called block copolymers. The last option are graft polymers, here it is possible to graft the second monomer to, from or through the linear polymer chain of the first monomer (Figure 14).

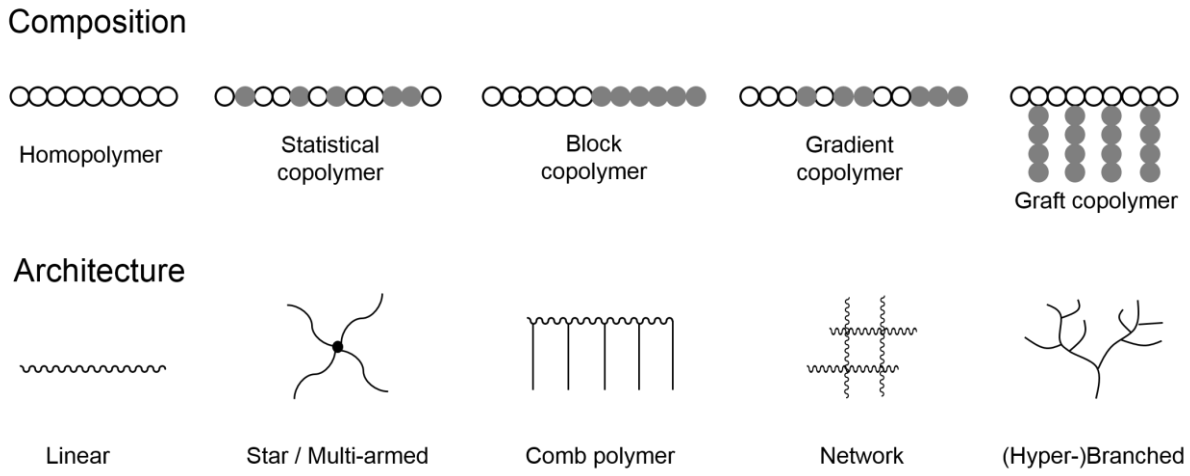

Figure 14: Composition and architecture possibilities of copolymers – adapted from [88], © Elsevier.

Due to the living character of the polymerization of POx, many groups have polymerized block copolymers of an AB-type diblock or ABA-type triblock structure. For example, Luxenhofer *et al*. polymerized a diblock and a triblock copolymer from EtOx and *n*PrOx with the *n*PrOx block in the middle of the triblock and characterized their efficacy in the solubilization of the hydrophobic drug Paclitaxel [36]. In general, the hydrophilic block of POx copolymers consists of the hydrophilic monomers MeOx, EtOx or iPrOx while the hydrophobic block often consists of monomers with long aliphatic chains such as 2-nony-2-oxazoline or 2-phenyl-2-oxazoline. These

copolymers, with a hydrophilic and a hydrophobic part, form micelles and the specific monomer combination determines the morphology of the resulting micelles, e.g. rod-like or spherical [89, 90].

In addition to linear architectures (Figure 14), also star shaped POx [83], comb copolymers with POx at the side chain in combination with a methacrylate backbone [91, 92], or hyperbranched structures have been synthesized. The latter were generated using propargyl tosylate as initiator and potassium ethylxanthate as terminating agent allowing for thiol-yne chemistry to receive a highly branched structure [93]. In addition, networks of POx have been formed to receive hydrogels, which can be used for biomedical applications, with a large toolbox of cross-linking chemistries [94].

One of the most often used cross-linking chemistries is the thiol-ene reaction because of its straight-forward nature and minimal amounts of cross-linking initiator that need to be employed. As an “ene” functionality is needed for this reaction, the hydrophobic monomers ButEnOx or DecEnOx were randomly copolymerized with hydrophilic monomers MeOx or EtOx to maintain the overall water solubility of the copolymer [21, 22, 77]. It was observed by Dargaville *et al*. that the monomer MeOx polymerized slightly faster than ButEnOx or DecEnOx leading rather to a gradient than a truly statistical distribution of the vinyl moieties along the polymer chain [77]. Interestingly, the monomer EtOx polymerizes slower than DecEnOx [22] but faster than ButEnOx [21]. In line with the observation by Dargaville *et al*. that DecEnOx polymerizes faster than ButEnOx [77], for yet unknown reasons, the following order of the reaction speed, starting with the fastest, can be assumed as MeOx > DecEnOx > EtOx > ButEnOx.

2.3 Thiol-ene “Click” Chemistry

Sharpless *et al.* defined the term “click chemistry” in 2001 with the following words: “The reaction must be *modular*, *wide in scope*, give *very high yields*, generate only *inoffensive byproducts* that can be removed by nonchromatographic methods, and be *stereospecific* […] The required process characteristics include *simple reaction conditions*, *readily available starting materials and reagents*, the use of *no solvent or a solvent that is benign or easily removed* and *simple production isolation*” [95].

The concept of “click” chemistry has since then had a major impact on polymer chemistry as highly efficient reactions without side products and major purification

protocols are of great importance for the design and synthesis of functionalized macromolecular architectures (Figure 15) [96].

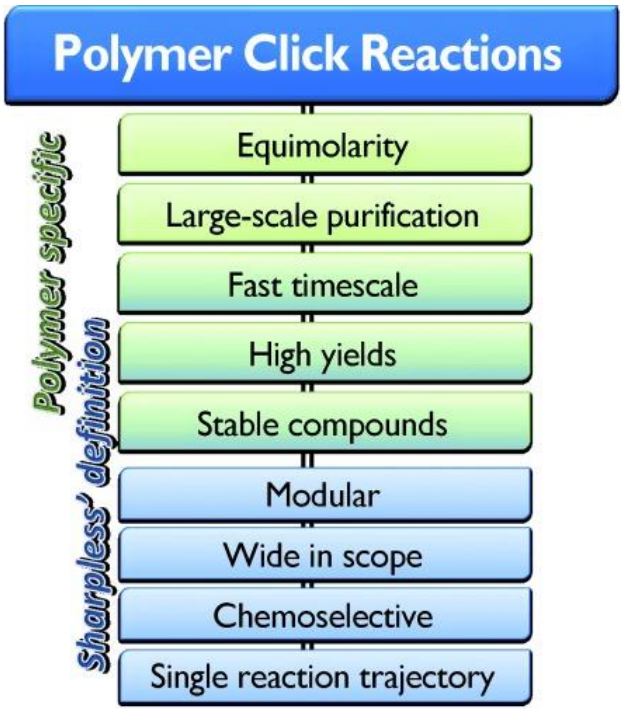

Figure 15: Requirements for click reactions involving one or more polymeric reagents (blue: originally defined by Sharpless; green and blue-green: adapted requirement related to synthetic polymer chemistry) – from [96], Copyright © 2011 WILEY-VCH Verlag GmbH & Co. KGaA, Weinheim.

The reaction of a thiol to a C=C bond, also known as the thiol-ene reaction, has been known for over 100 years [97]. The hydrothiolation can proceed through the radical pathway, catalytic processes mediated by nucleophiles, acids and bases and even in the absence of a catalyst in highly polar solvents [98]. In addition, a variety of thiols and enes can be used. In case of the thiols, nearly any thiol can be used however the reactivity strongly depends on the S–H bond strength. In case of the ene, activated as well as non-activated species and multiple-substituted olefinic bonds can be employed with the reactivity depending on the reaction mechanism and the substitution pattern [98]. In general, the radical or base/nucleophile-mediated addition of the thiol to the C=C double bond are the most widely used approaches. In the following, it will be distinguished between radical thiol-ene and thiol-Michael reaction. The radical thiol-ene reaction starts with the formation of a thiyl radical through addition of a radical initiator, typically a photoinitiator which is activated by irradiation at the appropriate wavelength (Figure 16, left).

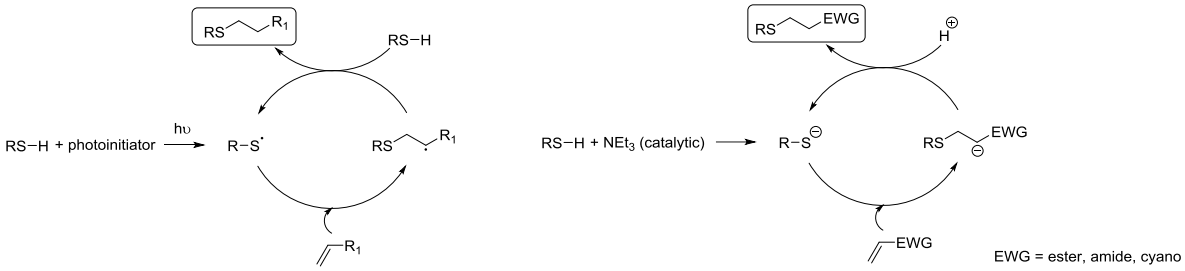

Figure 16: Mechanism of hydrothiolation in the presence of a photoinitiator (radical thiol-ene) (left) and a base (thiol-Michael) (right) – adapted from [98].

The initiation step is followed by a propagation step, where the thiyl radical directly adds to the C=C bond forming an intermediate carbon centered radical which is followed by a chain transfer to another thiol molecule with the simultaneous formation of new thiyl radical. The thiol-ene addition product is received with anti-Markovnikov orientation. In general, it can be stated that the ene reactivity for radical thiol-ene reaction decreases with decreasing electron density at the double bond and that terminal enes are more reactive than enes within longer alkenyl chains.

If the ene is activated by the presence of an electron withdrawing group (EWG), the thiol addition can also proceed through mild basic catalysis (thiol-Michael addition). Usually, a mild base like triethylamine (Net_3) is sufficient to deprotonate the thiol and form a thiolate (Figure 16, right). The thiolate adds to the electrophilic β-carbon forming an intermediate carbon-centered anion. The enolate abstracts a proton from another present thiol or the earlier formed base cation and the thiol-ene product is received, again by regioselective formation of the anti-Markovnikov product [98]. Besides triethylamine, primary or secondary amines like hexylamine or di-*n*-propylamine and phosphines like dimethylphenylphosphine (DMPP) can be used as a catalyst. However, the activation mechanism for primary/secondary amines and phosphines is assumed to be different as those catalysts rather act as a nucleophile than a base. They attack the activated ene generating an intermediate, strong (zwitterionic) enolate base which will further deprotonate the thiol. After this step, the thiol-ene product is formed in the same manner as it is the case for the base catalyzed system.

The radical thiol-ene reaction has become popular in recent years for post-polymerization functionalization of (co)polymers, for example by Gress *et al*. who added methyl-3-mercaptopropionate, thioacetic acid or 2,3,4,6-tetra-*O*-acetyl-1-thio-*β*-D-glucopyranose to PbutEnOx in THF under UV irradiation without addition of an

initiator [21]. The radical thiol-ene reaction is also a popular tool to synthesize hydrogels bringing along several advantages. For example, the radical thiol-ene reaction is rather oxygen insensitive (especially favorable if cells are present), can be performed in many (organic) solvents as well as in water and the initiator can be applied at very low concentrations which are non-toxic to cells [99].

2.4 Hydrogels

Wichterle *et al*. were the first to state that solid plastics are not very suitable for most medical applications and that they should possess: "(1) a structure permitting the desired water content, (2) inertness to normal biological processes (including resistance to the degradation of the polymer and to reactions unfavorable to the organism), (3) permeability for metabolites" [100]. They presented the first hydrogel based on glycolmonomethacrylate and glycoldimethacrylate which was also tested *in vivo*.

The conception of the properties, that a hydrogel should bring along for biomedical application, has since then somewhat changed concerning the inertness to biological processes and degradability. In the last decade, researchers have designed hydrogels in a fashion that cells can interact with the material, for example through the incorporation cell adhesion motives, signaling molecules and growth factors to induce cell proliferation. In addition, depending on the application, degradability can be desirable which can be achieved by degradable polymers or degradable cross-linking points.

In general, hydrogels can be formed via chemical and physical cross-linking. The advantage of a covalently cross-linked hydrogel is their higher mechanical strength, but they usually degrade much slower than physically cross-linked hydrogels as chemical bonds have to be cleaved to yield individual soluble polymer chains. Physical hydrogels are formed by noncovalent interactions such as hydrophobic or ionic interaction, and hydrogen bonding. Hydrogels have been prepared from natural polymers or synthetic polymers, and combinations of both, then often called biohybrid hydrogels. An enumeration of popular hydrophilic polymers that have been used for hydrogel matrices is shown in Table 2. Alginate has often been used as a very prominent polymer for hydrogel applications, as already described in Section 2.1. By addition of a bivalent cation, such as Ca^{2+}, an ionotropic hydrogel is formed. If a

polymeric cation, such as polylysine, is added, a polyion complex hydrogel is formed, (Figure 17A).

Table 2: List of hydrophilic polymers used for hydrogel formation – adapted from [5] – Copyright © 2002 Elsevier Science B.V.

Polymer type	Examples
Natural polymers and their derivatives	
Anionic	Hyaluronic acid, alginic acid, pectin, carrageenan, chondroitin sulfate, dextran sulfate
Cationic	Chitosan, polylysine
Amphipathic	Collagen, gelatin, carboxymethyl chitin, fibrin
Neutral	Dextran, agarose, pullulan
Synthetic polymers	
Polyesters	PEG-PLA-PEG, PEG-PLGA-PEG, PEG-PCL-PEG, PLA-PEG-PLA, PHB, P(PF-co-EG)±acrylate end groups, P(PEG/PBO terephthalate)
Other	PEG-bis-(PLA-acrylate), PEG±CDs, PEG-g-P(Aam-co-Vamine), PAAm, P(NIPAAm-co-Aac)
Combinations of natural and synthetic polymers	P(PEG-co-peptides), alginate-g-(PEO-PPO-PEO), P(PLGA-serine), collagen-acrylate, alginate-acrylate, P(HEMA/Matrigel®), HA-g-NIPAAm

Hydrogels based on synthetic polymers are often formed by free radical polymerization using unsaturated monomers with a cross-linker, or macromers with unsaturated monomers or cross-linkers which are then copolymerized into a hydrogel network. Inside the hydrogel, it is also possible to polymerize a second monomer leading to an interpenetrating network which usually possesses a higher mechanical strength (Figure 17B).

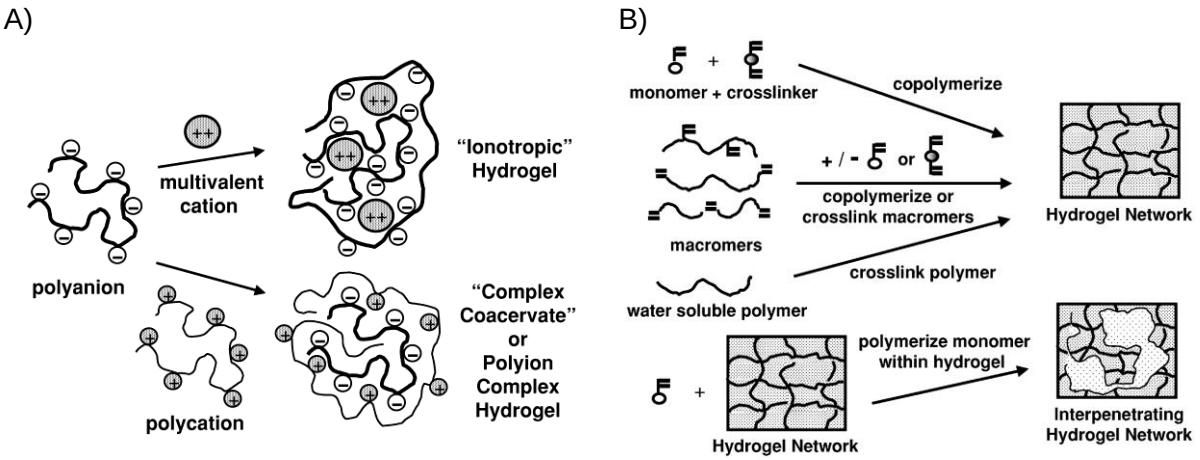

Figure 17: A) Schematic of the possibilities to form ionic hydrogels and B) schematic of the formation of cross-linked hydrogels by free radical polymerization – adapted from [5] - Copyright © 2002 Elsevier Science B.V.

The physical characteristics of a swollen hydrogel are influenced by the molecular weight of the polymer chain between the cross-links of the hydrogel ($\bar{M}_c$, Figure 18), the possible existing charges, the cross-linking density and physical interactions. A hydrogel network which is made of a large polymer offering multiple cross-linking sites is usually more robust than a network made of small polymer chains. Here, higher concentrations are needed to create hydrogels with sufficient rigidity. The cross-linking density determines the elastic modulus and stiffness of the network which logically increases with increasing cross-linking density [101]. It also determines how well molecules like drugs and peptides can diffuse through the network. The average distance between the consecutive cross-links is described by the mesh size (**ξ**, Figure 18) which correlates to the maximum size of a solute that can pass through the network [102].

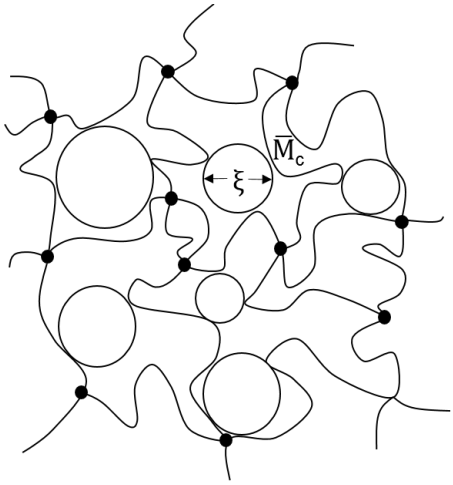

Figure 18: Schematic of the cross-linked structure of a hydrogel with cross-links (black dots), molecular weight of the polymer chains between cross-links ($\bar{M}_c$) and the average mesh size (ξ) – reproduced from [102].

The exact mesh size is difficult to directly determine experimentally, but it is generally possible using scattering techniques [103, 104]. Hence, it is usually calculated. Here, the presumption that the equilibrium polymer volume fraction ($\nu_{2,s}$), which is the ratio of the volume of the polymer to the volume of the swollen gel, is inversely proportional to the equilibrium swelling degree (SD) has often been applied. For example, the SD can be determined gravimetrically by equilibrium swelling experiments. In addition, the number-average molecular weight between cross-links, $\bar{M}_c$, can be related to the degree of cross-linking, *X*, as follows [105]:

$$\bar{M}_c = M_0/2X \qquad \textbf{Eq. 3}$$

with M_0 being the molecular weight of the repeating unit of the polymer.

Peppas *et al*. stated in 1989 that the mesh size relates to the equilibrium polymer volume fraction in a swollen gel at high polymer concentrations as follows [102]:

$$\xi \sim \nu_{2,s}^{-1/2} \qquad \textbf{Eq. 4}$$

There exists a variety of scaling laws and equations to determine the number average weight between cross-links from the polymer volume fraction but the most popular, especially for biomedical hydrogels, is probably the one developed by Flory and Rehner [105-107]:

$$\frac{1}{\bar{M}_c} = \frac{2}{\bar{M}_n} - \frac{(\bar{v}/V_1)\left[\ln\left(1 - v_{2,s}\right) + v_{2,s} + \chi_{12} {v_{2,s}}^2\right]}{\left({v_{2,s}}^{1/3} - v_{2,s}/2\right)} \qquad \textbf{Eq. 5}$$

2.5 Application of Hydrogels

Hydrogels have been used for a variety of biomedical applications, including tissue culture and engineering, wound healing and surgery and for drug delivery purposes. In tissue culture, it is essential that the hydrogel can mimic the biological environment of the cells and that the transport of nutrients and waste products is taken care of. However, there are sometimes issues with the diffusion of larger molecules, like proteins, which can be limited by the mesh size of the hydrogel. This problem can be circumvented by the incorporation of peptide or protein segments in the polymer that can be degraded by exoproteases released by the cultured cells. Another property that is advantageous for cell culture is their low mechanical modulus, which is more similar to their natural surrounding than the solid cell culture plastics. Accordingly, it was demonstrated that the mere elastic modulus of a material can affect the differentiation of stem cells [108].

Hydrogels have also been applied in clinics to support wound healing for a long time. In this application, hydrogels keep a moist environment and thereby provide a good healing environment by allowing oxygen diffusion and oftentimes being antibacterial.

Concerning drug delivery, hydrogels offer a fast and controllable diffusion rate of small molecular weight substances and can be applied in the form of films for surface delivery, as depots for implantation or as small nanoparticles for long term blood circulation [108]. Injectable *in situ* forming gel systems are also favored which can be easily achieved through thermo-reversible hydrogels that are liquid at room temperature but solidify at body temperature. An example for this is a polylactide-

PEG block copolymer (industrial name Regel®) which has been clinically tested for the release of the anti-tumor drug paclitaxel or insulin [108].

2.6 Hydrogels Based on Poly(2-oxazoline)s

A variety of chemically cross-linked POx hydrogels, based on multivalent monomers, macro-crosslinkers or side chain functionalized polymer precursors [94] has already been presented in the literature. The drawback of using multivalent monomers, such as bis(2-oxazoline), or macro-crosslinkers, (meth)acrylic α- and ω-end functionalized POx, for hydrogel preparation is that they cannot be synthesized *in situ* as those hydrogels are usually formed in organic solvents such as methanol [79], ethanol [109], and dichloromethane [33], which must be later evaporated to ensure sufficient biocompatibility. Using side chain functionalized polymers in combination with a chemoselective reaction, like the UV initiated thiol–ene reaction, can therefore be advantageous for several reasons. It has been shown that the photoinitiator used for radical formation can be added at such low concentrations that no cytotoxic effects occur [99]. Additionally, thiol-ene reactions mediated by radical formation are rather oxygen insensitive, which is favorable for present cells [110]. In combination with a cytocompatible hydrophilic polymer and an appropriate light source, this route for hydrogel formation can be highly advantageous for in vivo applications allowing the preparation of complex shaped hydrogels under minimally invasive conditions even inside the patient's body [111]. POx copolymers of MeOx or EtOx in combination with unsaturated monomers DecEnOx or ButEnOx have been synthesized and cross-linked with a variety of small molecular weight dithiols like dithiothreitol [77], 2,2'-(ethylenedioxy)-diethanol, glycol dimercaptoacetate [22, 112] and 1,3-propanethiol to 1,9-nonanedithiol [113], which always bear the risk of cellular toxicity and moreover have to be accurately weighed in order to minimize dangling crosslinking points due to small excess of thiol groups. Hydrogels fabricated by the small molecule crosslinker route are usually pre-fabricated and then rehydrated before their intended biomedical application [114] because of the poor solubility of the dithiol in water or because of the high amounts of dithiol needed, which usually exceeds the LC_{50} of most of the compounds [113]. One alternative to this approach is the replacement of the small dithiol molecule with a thiol side chain functionalized polymer which has been demonstrated by Stichler *et al*. [60], who were able to 3D print cytocompatible, mechanically strong and complex hydrogel structures via a rapid UV mediated thiol-

ene reaction. The presented approach could also be a strategy for the synthesis of POx hydrogels. The first POx with thiol side chain functionality was reported by Cesana *et al*. [20], who introduced thiols via a monomer with protected thiol side chains, but no further study or application was reported for this specific polymer.

2.7 Catechol-functional Polymers

For the use as a tissue adhesive, hydrogels are usually equipped with chemical functionalities that allow for a covalent binding of tissue surfaces, which are exposed in the defect sites. In this regard, an emerging functionality is the catechol group, which naturally occurs in the amino acid 3,4-dihydroxyphenylalanine (DOPA). This amino acid plays a key role in the mussel foot protein, which allows mussels to attach to many different types of surfaces with fast curing kinetics even in wet environments. Under oxidizing conditions the catechol group becomes highly reactive and forms a *o*-quinone which can self-polymerize or react with a variety of nucleophiles, like amino or thiol groups, undergoing Michael addition or Schiff base formation [115] (Figure 19).

Therefore, it is a perfect candidate for reactions with nucleophiles like cysteinyl, histidyl or lysyl groups that are present on many natural tissue surfaces [116]. The catechol group can also form metal complexes in the presence of metal ions like Fe^{3+} or bind to inorganic surfaces via hydrogen bonding.

The most common method is to polymerize dopamine with other monomers, for example, Mehdizadeh *et al*. polymerized citric acid with PEG and dopamine in a condensation reaction resulting in a biodegradable polymer which could be used as a tissue adhesive for wound closure [117]. In addition, the catechol functionality has already been attached to amino- or NHS-functionalized PEG using 3,4-dihydroxyhydrocinnamic acid or dopamine HCl [118, 119]. It was also attached to biomacromolecules, for example to carboxylated silk fibroin [120] or to gelatin by simple EDC/NHS chemistry [121]. Further, it has been already polymerized as dopamine acrylamide or dopamine hydrochloride to form three-dimensional networks [122, 123].

During the synthesis and modification, it can be quite helpful to protect the catechol group to prevent unwanted oxidation or chemical side reactions. The protecting group needs to remain intact during the synthetic chemical reaction/linkage to e.g.

the polymer side chain and its deprotection should not compromise the final polymer [124].

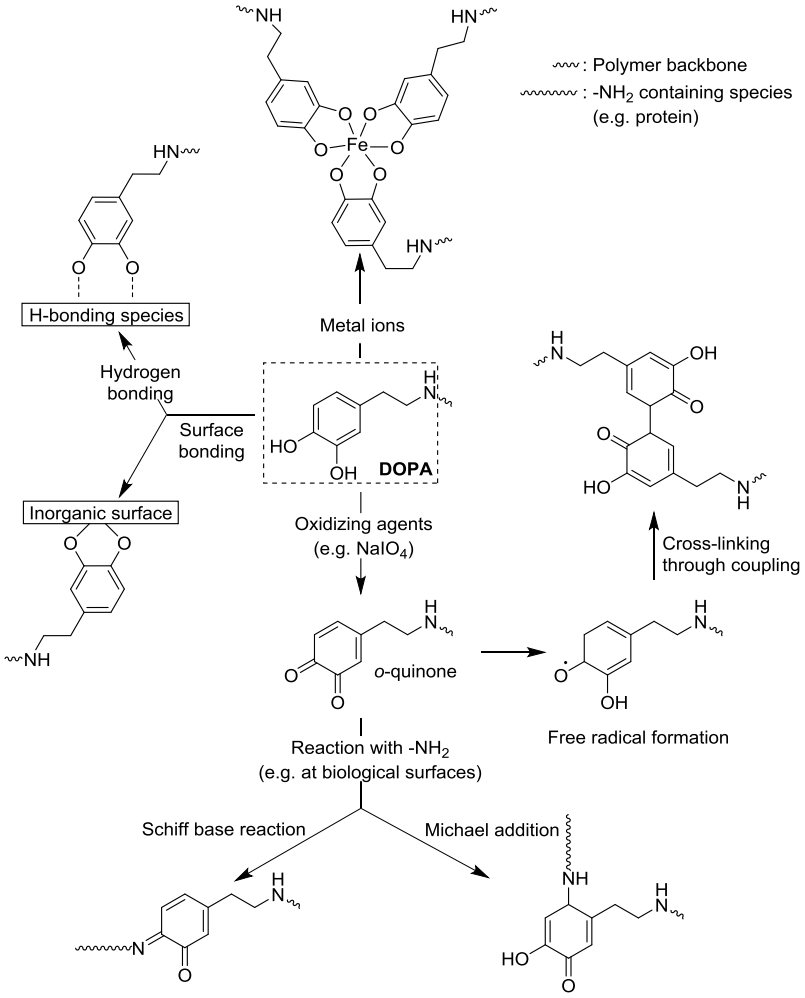

Figure 19: Schematic of the possible pathways of cross-linking and surface binding of the catechol group bound to a polymer – adapted from [117].

Protecting groups for the two catechol hydroxyl groups have been cyclic ethyl orthoformate (which can be cleaved in 1 M trifluoroacetic acid) [125], acetonide using 2,2-dimethoxypropane (cleavage under acidic conditions) [126], bis(*t*-butyldimethylsiloxy) using *t*-butyldimethylsilyl chloride (TBDMS-Cl) (removal with tetrabutylammonium fluoride) [127] and cyclic carbonate using diphenylcarbonate or *N,N*-disuccinimidyl carbonate (which is already cleaved in water by hydrolysis) [128, 129].

A variety of catechol containing hydrogel systems, degradable and non-degradable, have been synthesized. These systems can also be self-healing when metal-catechol coordination is used as the cross-linking mechanism. The intended applications have

been biomedical sealants and adhesives, anti-fouling and cell-resistant coatings and coatings for gold and silver nanoparticles in anti-tumor therapy [124].

2.8 Polymer Conjugates

Polymer conjugates is a term comprising polymer-drug, polymer-peptide and polymer-protein conjugates which emerged in the 1960s. The most widely used polymer for these conjugates is the hydrophilic PEG which brings along a very important property, the “stealth”-effect which was already described in section 2.1.
When binding a peptide or protein to a macromolecule, it is usually essential to keep their structure and by this, their function, intact. For this reason, chemoselective reactions are preferred. One ligation reaction, which was originally used solely in peptide chemistry, but has found its way into polymer-peptide conjugation, is the native chemical ligation (NCL). NCL has become increasingly popular since Kent *et al*. demonstrated in 1994 that the reaction is chemoselective and can even be applied to unprotected peptides [130]. The NCL is based on a capture/rearrangement concept. The first step, the capture, is based on a reversible thiol-thioester exchange between an electrophilic (aryl) ester and a nucleophilic thiol of a cysteine residue. In peptide chemistry, the thioester is located at the C terminus of a peptide and the thiol/cysteine at the N terminus of the other peptide. In the rearrangement step, the cysteine-thioester undergoes an intramolecular S→N transfer, via a 5-membered ring intermediate, to form a stable amide bond. The rearrangement is unique to the terminal cysteine as any internal cysteine residues, which only participate in the capture step, rapidly exchange backwards because the S→N shift is not possible [131].

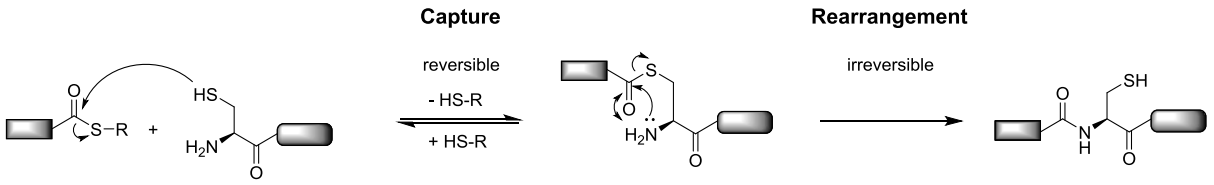

Figure 20: Schematic of native chemical ligation mechanism between a thioester and a cysteine terminal molecule.

In peptide chemistry, NCL is usually performed in an aqueous buffer system containing guanidine HCl salt (to unfold the peptide), sodium dihydrogen phosphate and tris(2-carboxyethyl)phosphine (TCEP) (reducing agent for formed disulfides).

Usually, an additional thiol catalyst must be added as the alkyl thioesters, which are employed due to easy preparation and long-term storage capability, are relatively unreactive. A popular thiol catalyst is 4-mercaptophenylacetic acid (MPAA) which converts the alkyl thioester in a reactive aryl thioester so that the transthioesterification can proceed much faster and efficiently.

The NCL cannot only be performed with linear thioesters but also with cyclic thiolactones. The advantage of a cyclic thioester is that no byproduct (R-SH) is formed which can potentially be toxic. For example, Chen *et al*. coupled sterically demanding peptides with a β-thiolactone terminal peptide [132] and Fan *et al*. synthesized polypeptide hydrogels with γ-thiolactone (Figure 21, left) functionalized poly(γ-glutamic acid) and cysteine functionalized ε-poly(lysine) in aqueous buffer solutions [133].

Another interesting functionality to attach peptides to polymers, which has attracted researchers' interest in the last decade, is it the azlactone functionality (Figure 21, right). The electrophilic azlactone, which is basically a "masked" amino acid [134], can react with amines, hydroxyls and thiols [135] without the formation of a by-product. It could therefore be an interesting alternative to the N-hydroxysuccinimide active esters used in many conjugation reactions [136-138]. Schmitt *et al*. demonstrated that the azlactone functionality also reacts with cysteine terminal peptides through a capture/rearrangement process similar to NCL [139].

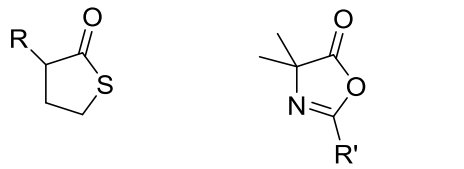

γ–Thiolactone 4,4-Dimethyl azlactone

Figure 21: Chemical structure of γ-thiolactone and 4,4'-dimethyl azlactone.

Thiol-ene coupling has also been employed to attach peptides to polymers and Geng *et al*. found that thiol-ene coupling is comparable to copper mediated coupling [140]. Heise and co-workers synthesized poly(γ-benzyl-L-glutamate-*co*-cysteine and attached poly(ethylene glycol) methyl ether acrylate to the thiol group using AIBN as initiator [141]. Anseth and co-workers were able to selectively photo-pattern hydrogels with cysteine terminal peptides using UV mediated thiol-ene chemistry with the radical initiators I2959 or lithium phenyl-2,4,6-trimethylbenzoyl-phosphinate [142].

However, it was also found that the efficiency of the thiol-ene reaction strongly depends on the molecular environment. Not all buffers, such as HEPES, are compatible and some amino acids decrease coupling efficiency. In addition, it was observed by Colak *et al*. that the position of the cysteine in the peptide chain plays an important role and peptides with non-terminal cysteines should be preferred [143].

It is also possible to use the pendant amino group of the amino acid lysine, which is a common acid on the surface of proteins [144], to attach polymers via a variety of functions which are displayed in Figure 22.

Regarding POx peptide-polymer conjugates, Luxenhofer *et al*. attached a cyclic azide modified RGD peptide using copper mediated click chemistry [145, 146]. Schmitz *et al*. attached thioester functional peptides to a multifunctional cysteine POx copolymer using NCL chemistry [147]. Nawroth *et al*. synthesized maleimide terminal POx to which glutathione and an elastin-like polypeptide bearing cysteine groups was attached by Michael-thiol addition [148].

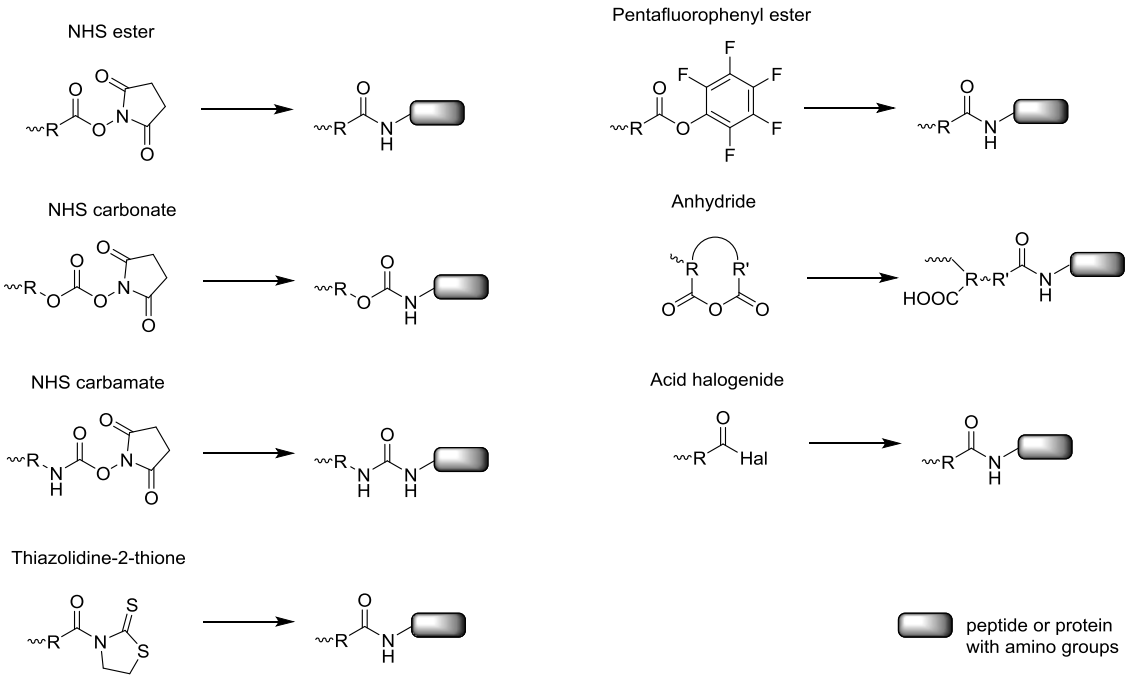

Figure 22: Coupling methods for the amino group of peptides or proteins to functional polymers [144].

The strategies described so far are also known as the ‘grafting to’ approach. It is also possible to attach peptides by the ‘grafting from’ approach using specific peptide macroinitiators from which the synthetic polymer can be polymerized through nitroxide-mediated, atom transfer radical or reversible addition-fragmentation chain transfer polymerization [149].

2.9 Applications of Polymer Conjugates

There exists a variety of medical applications for polymer conjugates, for example, in drug delivery as anticancer nanomedicines, in tissue regeneration and repair, in chronic wound healing and promotion of bone regeneration [150].
Peptide/protein-polymer conjugates are especially interesting due to their hierarchical structure, biocompatibility and stimuli responsiveness. The different classes of polymer-drug conjugates are displayed in Figure 23 and examples of such are listed in Table 3. The standard polymer, which is applied for the synthesis of polymer-protein conjugates, is PEG. The sterical repulsion of PEG has several advantages. It reduces the immunogenicity, prevents premature degradation by proteolytic enzymes and opsonization followed by clearance by the mononuclear phagocyte system. In addition, a longer circulation time in the blood stream is achieved through the increase in molar mass and hydrodynamic radius of the drug. The first PEG-protein conjugate that received clinical approval in 1990 was Adagen® [151].

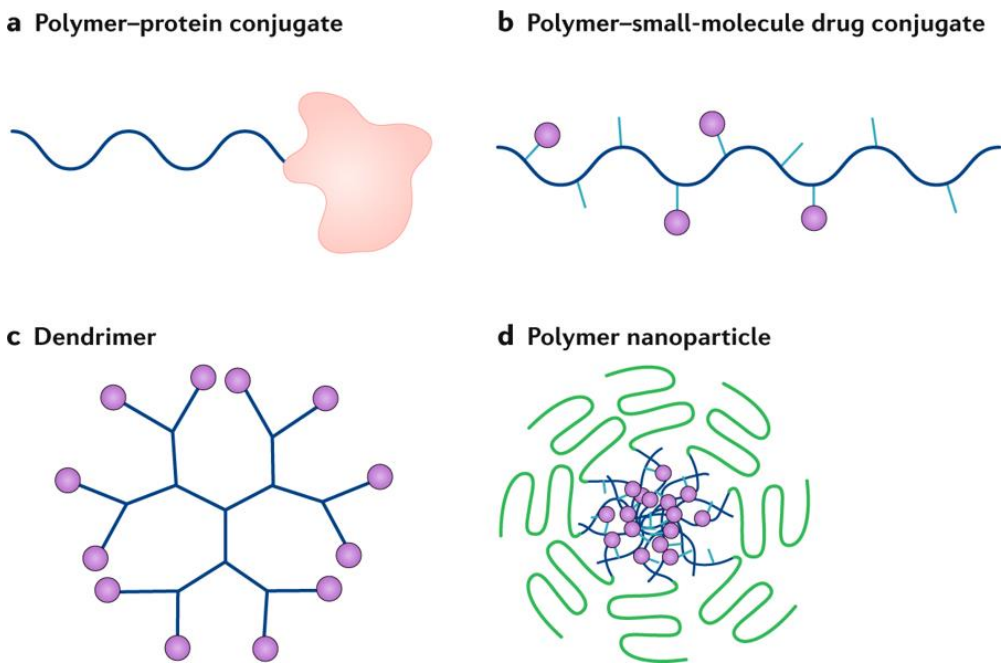

Figure 23: Classes of polymer-drug conjugates on the market or in clinical development – from [151], copyright 2019 by Springer Nature.

A major drawback of the polymer PEG is its non-degradability. For this reason, only molecular masses below 40 kDa are applied for polymer-drug conjugates which is

close to the glomerular filtration threshold of PEG. In addition, PEGylation does not improve the delivery of proteins through biological barriers like the cellular membrane [28]. Alternatively, biopolymers such as dextran, polysialic acid, hyaluronic acid and polypeptides have been used.

Synthetic polymers that are similar to PEG and have become the focus of interest since the first reports on the immunogenicity and antigenicity of PEG conjugate proteins are POx [28] and polypeptoids [152]. Proteins like catalase, trypsin, BSA, ribonuclease, uricase and insulin have been linked to PMeOx or PEtOx by simple NHS ester chemistry [28]. Hu *et al*. demonstrated that conjugation of the polypeptoid polysarcosine to human interferon-α2b (IFN) led to an increased potency against tumor growth and a decrease in antibody formation compared to PEG-IFN conjugates [152].

Table 3: Examples of polymer conjugates used in therapeutics and clinical development from [150].

Sub class	Examples	Composition	Status
Polymer-drug conjugate	CT-2103; Xyotax;	Poly-glutamic acid (PGA)-paclitaxel	Phase II/III
	Opaxio	HPMA-copolymer-DACH platinate	Phase II
	Prolindac	Multiarm PEG-camptothecin derivative	Phase II
	PEG-SN38	Polyacetal-camptothecin conjugate	Phase I
	XMT-1001	PEG-naloxone	Phase III
	NKTR-118	Styrene maleic anhydride-neocarzino-statin	Market (Japan) Phase I/II
Polymer-protein conjugates	Zinostatin Stimaler	Polysialylated insulin	
	SuliXen	PEG-anti-TNF Fab	Market
PEGylated proteins	Cimzia	PEG-EPO	Market
	Mircera	PEG-Interferon alpha 2b	Market
	Peg-intron	PEG-Interferon alpha 2a	Market
	Pegasys	PEG-hrGCSF	Market
	Neulasta	PEG-uricase	Market
	Uricase-PEG 20	PEG-aptamer (apatanib)	Market
PEGylated-aptamer	Macugen	PEG-anti-PDGF aptamer	Phase II
	E10030	PEG-anti-platelet-binding function of von Willebrand Factor	Phase II
	ARC1779		

Serina Therapeutics, Inc. developed an antibody drug conjugate SER-214 which is a copolymer of EtOx with 10 % 2-pentynyl-2-oxazoline with a molecular weight of 20 kDa. Rotigotine, which is a potent dopamine antagonist, is bound to the pendant alkine side chains by copper “click chemistry” [38]. It is currently in Phase II clinical trials to treat Parkinson’s disease and restless legs syndrome.

In addition to direct linkage of the drug to the polymer, another common method to solubilize drugs are amphiphilic micelles. Polymeric micelles are advantageous due

to their high thermodynamic stability, their low critical micelle concentration, which increases their stability upon dilution in the blood stream, and their inherent stealth effect caused by the hydrophilic polymer shell. Triblock copolymers of POx, for example, PMeOx-PBuOx-PMeOx, have been used to solubilize poorly water soluble anti-cancer drugs like paclitaxel and docetaxel with great success and have already been tested in *in vivo* mouse models [37, 153]. PMeOx has also been used to shield proteinaceous nanoparticles, such as the tobacco mosaic virus, with higher efficiency than PEG [25].

Peptide-polymer conjugates can also be used in tissue engineering. The most popular example is probably the modification of polymers with the RGD (R: arginine; G: glycine; D: aspartic acid) peptide sequence since it has been found to promote cell adhesion [154]. RGD is not the only cell recognition motif, however, it is unique concerning its effectiveness and broad distribution among many ECM proteins [155]. For example, Farrugia *et al*. synthesized P(MeOx-*co*-DecEnOx) copolymers and coupled CRGDSG peptides to the polymer by photoinitiated radical thiol-ene chemistry to 5 %, 10 % and 25 % of the present alkene groups of the polymer. The residual alkene groups could then be used to induce cross-linking with the dithiol DTT to form hydrogels. There was a significant increase in fibroblast cells that attached to the hydrogels loaded with the RGD peptide. The RGD content also influenced the cell morphology [34].

It was also shown by Hammer *et al*. that proteins can be incorporated into hydrogels. They developed a system where they first PEGylated lysozyme, a model protein, and afterwards synthesized a hydrogel network using copper mediated click chemistry. Through degradable carbamate links, the protein was gradually released over a time frame of four weeks [156].

3 Results and Discussion

Parts of this chapter have already been published in

Julia Blöhbaum, Ilona Paulus, Ann-Christin Pöppler, Jörg Tessmar and Jürgen Groll; Influence of charged groups on the cross-linking efficiency and release of guest molecules from thiol-ene cross-linked poly(2-oxazoline) hydrogels, *Journal of Materials Chemistry B* **2019**, *7*, p. 1782-1794.

Julia Blöhbaum, Oliver Berberich, Stefanie Hölscher-Doht, Rainer Meffert, Jörg Teßmar, Torsten Blunk, Jürgen Groll; Catechol-modified Poly(oxazoline)s with Tunable Degradability Facilitate Cell Invasion and Lateral Cartilage Integration, *Journal of Industrial and Engineering Chemistry* **2019**, *80*, p. 757-769.

Julia Liebscher, Jörg Tessmar, Jürgen Groll; In situ polymer analogue generation of azlactone functions at poly(oxazoline)s for peptide conjugation, *Macromolecular Chemistry and Physics*, November 2019, accepted.

3.1 Synthesis and Characterization of Poly(oxazoline)s

In this chapter, the synthesis of poly(oxazoline) (POx) homo- as well as copolymers will be presented. The presentation of the synthesis and analysis of the POx homopolymers will be the basis for the subsequent copolymer synthesis. The synthesis and analysis (^{1}H NMR, SEC, T_{CP}) of the copolymers will be shown in the second part of the chapter.

3.1.1 Homopolymer Synthesis

Homopolymers based on the commercially available monomers 2-methyl-2-oxazoline (MeOx) and 2-ethyl-2-oxazoline (EtOx) as well as self-synthesized 2-*n*-propyl-2-oxazoline (*n*PropOx) (Figure 24) were prepared according to literature [16] using methyl tosylate as initiator and acetonitrile as solvent for the cationic ring opening polymerization under water-free and inert conditions.

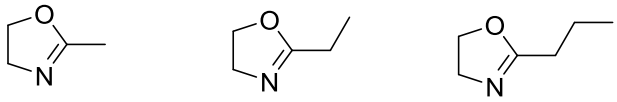

Figure 24: Commercially available monomers 2-methyl-2-oxazoline (MeOx) and 2-ethyl-2-oxazoline (EtOx) as well as synthesized 2-*n*-propyl-2-oxazoline (*n*PropOx).

An overview of the different synthesis parameters (solvent, temperature, theoretical repeating units and heating device) of the prepared homopolymers are given in Table 4.

Table 4: Overview of the synthesis parameters used for the preparation of homopolymers.

Monomer	Solvent	Repeating units$_{theo}$	Temperature (°C)	Heating device
MeOx	Acetonitrile	30 50	100 140	Microwave
EtOx	Acetonitrile	20 25 30 50 60	70 100 140	Oil bath Microwave
*n*PropOx	Benzonitrile Acetonitrile	100 200 300 400	100 120	Oil bath Microwave

The microwave vial only allows reaction volumes up to 25 mL. This is the reason why large-scale polymerizations were usually carried out in a round-bottom flask. For the polymerization of poly(*n*-propyl-2-oxazoline) (PPrOx), where a large amount of polymer was needed for a collaboration partner, benzonitrile was used as solvent as it allows to polymerize at higher temperatures than acetonitrile (bp = 81 °C compared to 191 °C for benzonitrile). To study the influence of the temperature on the polymerization, syntheses were carried out at 100 °C and 140 °C for PEtOx and PMeOx in the microwave reactor. PPrOx was also synthesized at 120 °C in the microwave reactor to keep reaction times short whilst aiming for a higher number of repeating units (> 100).

The initiator to monomer ratio determines the repeating units of the polymer chain. Homopolymers based on EtOx were synthesized in varying chain length from 20 to 60 repeating units, whereas polymers based on PMeOx were synthesized with a constant chain length of 50 repeating units. PPrOx was synthesized with a higher number of repeating units, namely from 100 to 400 repeating units as it was intended to be used for melt electro writing.

As terminating agents, nucleophiles like piperidine, creating an inert terminus, methanolic KOH, creating a hydroxyl functional chain end or allyl amine, equipping the terminus with an allyl functionality, were used in excess. The termination with piperidine or KOH can be carried out at room temperature but can also be sped up by using elevated temperatures (~45 °C). The termination with allyl amine needs to be performed at elevated temperatures (45 °C) for 48 h because primary amines are weaker nucleophiles. The termination with piperidine, however, can be carried out at room temperature for 12 hours.

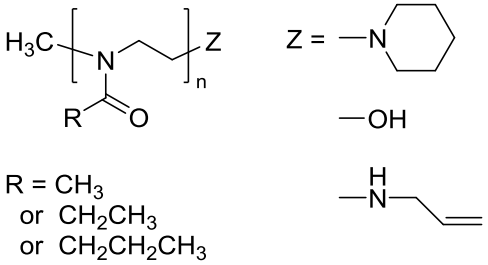

Figure 25: Chemical structure of synthesized POx homopolymers.

The theoretical chain length that had been set by the initiator to monomer ratio was usually achieved within 5 – 10 % deviation as determined by ^{1}H NMR spectroscopy (Table 5 and section 5.3.2). The signal of the methyl group (**a**) of the initiator at

2.96 ppm (doublet, 2 protons) and at 2.86 ppm (singlet, 1 proton) can be used as internal reference to determine the number of repeating units and thereby the number average molar mass (Figure 26). The doublet structure of the methyl group was already examined by Nuyken *et al*. in 1996, who found that the methyl group can rotate around the amide function leading to a *syn*- and *anti*-conformer [69].

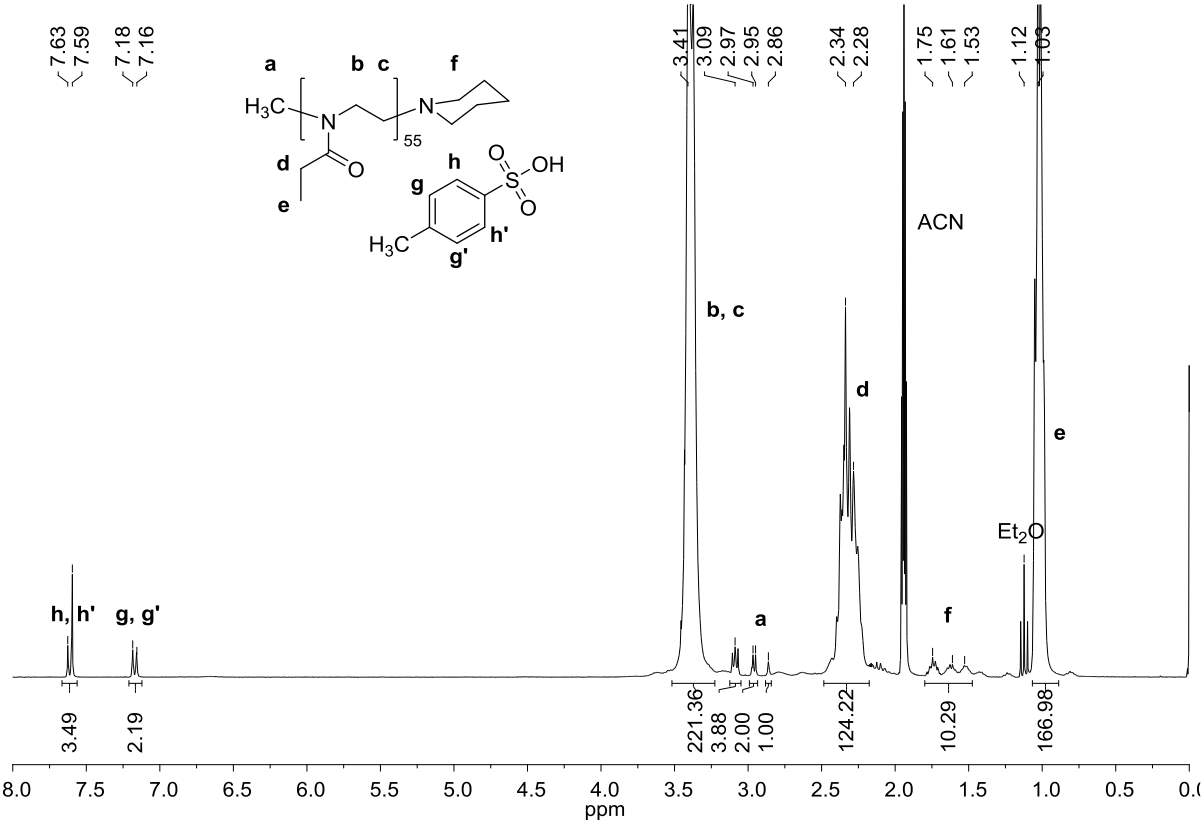

Figure 26: ^{1}H NMR of PEtOx with 55 repeating units in CD_3CN.

The broad multiplet signal at 3.41 ppm belongs to the backbone of the polymer and the signals at 2.30 and 1.03 ppm belong to the side chain. Below the signal for the CH_2 group of the side chain also lies the signal of the methyl group of the initiator counter ion toluene sulfonate. The aromatic signals of toluene sulfonate are visible at 7.62 and 7.17 ppm (two doublets). There is another prominent signal at 3.09 ppm that was only observed when the polymerization was terminated with piperidine, never with KOH or allylamine. A possible hypothesis (there exists no literature on this observation so far) could be that piperidine reacts with the toluene sulfonate salt. This would result in the appearance of a triplet at higher ppm than for piperidine alone (2.69 ppm) for the protons adjacent to the nitrogen atom (indicated with **i** in Figure 27), in accordance for the ^{1}H NMR signals of 1-tosylpiperidine found in literature

[157]. Especially as the integral value in all measured NMR spectra of this signal is ~4 protons in relation to the aromatic protons.

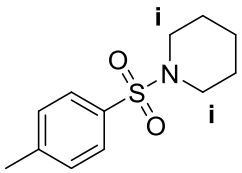

Figure 27: Possible side product of p-toluene sulfonate with piperidine.

The triplet always disappeared after dialysis of the polymer against water, which confirms the assumption that the signal is not related to the polymer but that it originates from a small molecular weight compound.

The number average molecular weight (M_n) determined by size exclusion chromatography (SEC) was in general 1.05 to 1.15 times higher than the one determined by ^{1}H NMR end-group analysis (Table 5). Considering that SEC is only a relative method, the obtained values for the molecular weight are within a satisfying range. The dispersity of all PEtOx polymers was below 1.15 when the polymerization was carried out at 100 °C. To accelerate the polymerization, the reaction was also performed at 140 °C in the microwave reactor but the dispersity increased to 1.32 when the initiator MeTos was used and to even 1.49 when the initiator methyl triflate (MeOTf) was used. An increase for the probability of side reactions at an increased reaction temperature has already been described in literature and could also explain the higher dispersity values [66]. The distribution of the synthesized PEtOx polymers can be described as monomodal even though some elugrams showed a very small shoulder at smaller retention volume (higher molecular weight), which can be explained by the possible side reaction described in section 2.2.1. The dispersity for PMeOx was also below 1.20 but the SEC elugrams showed a bimodal distribution with a shoulder at smaller retention volume (high molecular weight), which was very prominent when the polymerization had been performed at 140 °C. The bimodal distribution did not occur when the polymerization was terminated with allylamine instead of piperidine. Based on the experiments performed during the master thesis of Ilona Paulus [158], the reason for this phenomena could not be clarified. Different initiators (MeTos and MeOTf), solvents (acetonitrile and benzonitrile), temperatures (70 °C, 100 °C and 110 °C) and heating options (microwave reactor and oil bath) had been applied but the shoulder was always visible when using piperidine as the terminating agent. There were only slight improvements when the synthesis was

carried out at 70 °C or when benzonitrile was used as solvent. The prominent shoulder was always reduced through dialysis against water. The dialysis membrane used had a molecular weight cut-off of 1 kDa, which should remove only small polymer chains. Therefore, the shrinking of the fraction of polymer chains with high molecular weight is difficult to explain. Hence, it was speculated that agglomerates form which can be dispersed through dialysis and removal of impurities. In addition, a recent publication by Sedláček *et al*. also showed that the chain transfer coefficient, which is the ratio of chain transfer events to propagation steps, is much higher for MeOx than for EtOx. This observation was explained by the lower steric hindrance of the MeOx proton at the α-position leading to chain transfer [68].

Table 5: Characterization of synthesized homopolymers by ^{1}H NMR spectroscopy and size exclusion chromatography.

Sample name	Repeating units$_{theo}$	Repeating units$_{exp}$*	M_n (g/mol)*	M_n (g/mol)	Đ#	Temperature (°C)	Terminating agent
			PEtOx				
P1§	50	n. d.	n.d.	3617	1.32	140	piperidine
P2§	50	55	5445	3765	1.08	100	piperidine
P4#	50	58	5782	6549	1.11	100	KOH
P8#	50	46.5	4681	5041	1.12	100	allylamine
			PMeOx				
P11§	50	46	4014	4481	1.18$	140	piperidine
P12#	50	42	3683	7254	1.12$	100	piperidine
P13#	30	26	2282	3904	1.02	100	allylamine
			PPrOx				
P14	100	102	11559	13090	1.10$	140	piperidine
P15	200	207	23558	26170	1.11$	120	piperidine
P16	300	343	38886	37710	1.19$	120	piperidine
P17	400	391	44314	41600	1.27	120	piperidine
P18	400	397	44993	41720	1.30	100	piperidine

*determined by 1H NMR spectroscopy #measured on Malvern SEC system (triple detection) §measured on PSS SEC system (conventional calibration) $bimodal distribution

Homopolymers based on *n*PropOx also showed a bimodal distribution with dispersities below 1.20 for polymers with 100 to 350 repeating units. The dispersity increased to ~1.30 for 400 repeating units, however, the shoulder at smaller retention volume was less prominent for these polymers which might also be caused by the upper exclusion limit of the columns (100,000 g/mol for pullulan). Figure 28 shows an exemplary SEC elugram of P(PrOx)$_{100}$ from a self-synthesized polymer and a purchased polymer from Ultroxa® with the same molecular weight. The shoulder at smaller retention volume is also visible for the commercial product even though the group of company of R. Hoogenboom polymerizes with very pure reagents and with black vacuum (< 10^{-5} torr) [66]. As it is known from literature, the polymerization of

POx is in general considered as a “living” polymerization. However, depending on the monomer and with increasing chain length and polymerization temperature, the risk of chain coupling and the formation of branching points increases [64, 66] (section 2.2.1), which can explain that there also exist species with a higher molecular weight (earlier retention time).

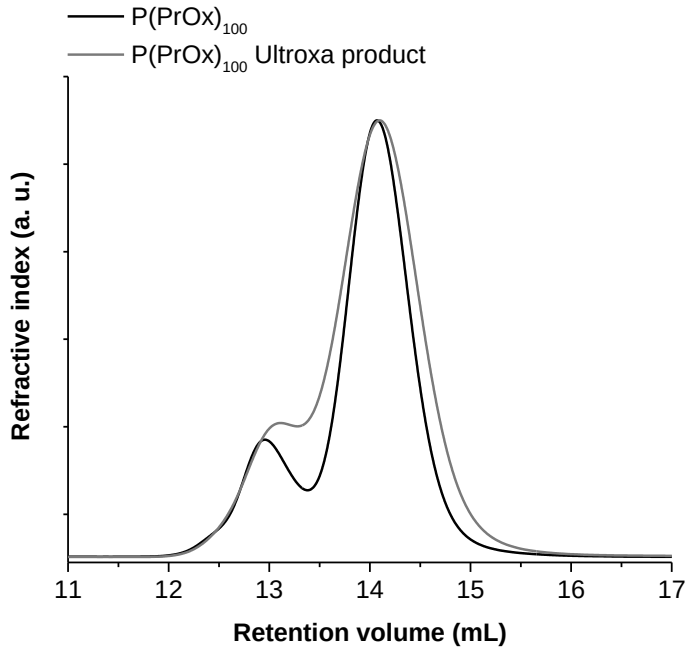

Figure 28: SEC elugram of synthesized and purchased $P(PrOx)_{100}$ from Ultroxa measured in DMF.

3.1.2 Copolymer Synthesis

To synthesize copolymers with vinyl side functionalities, two oxazoline monomers, namely 2-(3-butenyl)-2-oxazoline (ButEnOx) [21] and 2-decenyl-2-oxazoline (DecEnOx) [159], with varying side chain length were synthesized (analysis see 5.3.1.1 and 5.3.1.2). The monomer ButEnOx was received with 54 % yield, which is in accordance to literature (53 % by Gress *et al*.) [21] and the ^{1}H NMR spectrum did not show any impurities. The monomer DecEnOx was received in a good yield of 69 % (78 % by Kempe *et al.* [159]) and the ^{1}H NMR showed a clean product.

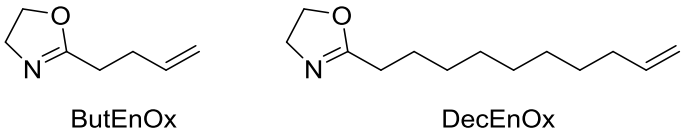

ButEnOx DecEnOx

Figure 29: Chemical structure of self-synthesized 2-(3-butenyl)-2-oxazoline (ButEnOx) and 2-decenyl-2-oxazoline (DecEnOx).

The percentage of vinyl functionalities in the copolymer is tunable by the amount of monomer that is added to the polymerization reaction. The self-synthesized monomers were randomly copolymerized with MeOx or EtOx. The longer alkyl side chain increases the overall hydrophobicity of the copolymer. In consequence, the amount of ButEnOx or DecEnOx that can be incorporated into the copolymer whilst maintaining sufficient water solubility will be lower for copolymers consisting of EtOx instead of MeOx as co-monomer. The vinyl functionality at the side chain will serve for further functionalization. For example, thiol-ene click chemistry can be used opening the route for various functional groups, for example, amino, hydroxyl, carboxylic acid and thiol groups, which cannot be brought into the copolymer by functional monomers as these groups would interfere with the CROP.

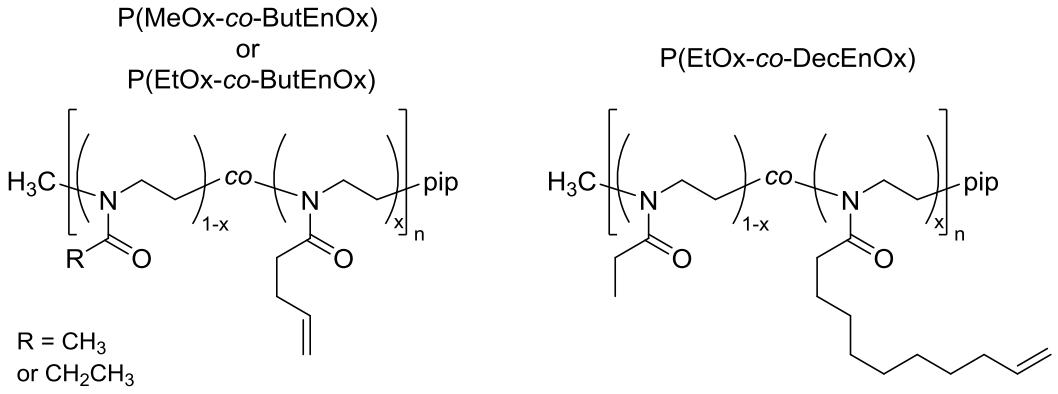

Figure 30: Chemical structure of copolymers P(MeOx-*co*-ButEnOx), R = CH_3, P(EtOx-*co*-ButEnOx) and P(EtOx-*co*-DecEnOx), R = CH_2CH_3.

Copolymers consisting of EtOx and ButEnOx or DecEnOx as well as of MeOx and ButEnOx were polymerized in the microwave reactor using methyl tosylate (MeTos) as initiator, acetonitrile as solvent and piperidine as terminating agent. The total number of repeating units was kept constant at 50 and the amount of ButEnOx in P(EtOx-*co*-ButEnOx) copolymers was gradually increased by 5 repeating units ranging from 10 mol% to 40 mol% ButEnOx (for PEtOx-*co*-ButEnOx) and 10 mol% to 20 mol% (for PMeOx-*co*-ButEnOx) in the monomer feed. In case of PEtOx-*co*-DecEnOx, three different copolymers with theoretically 9 mol%, 13 mol% and 20 mol% DecEnOx were synthesized. It was also tried to synthesize copolymers of EtOx or MeOx with ButEnOx with a higher number of repeating units of 80. For P(EtOx-*co*-ButEnOx) copolymers, the experimental amount of ButEnOx, found by ^{1}H NMR end-group analysis, was very close to the intended theoretical amount (Table 6)

and for P(MeOx-*co*-ButEnOx), the mol% incorporated into the copolymer was 8.9 mol% and 18.4 mol% for a total of 50 repeating units. For P(EtOx-*co*-DecEnOx) copolymers, the experimental amount of DecEnOx, found by ^{1}H NMR end-group analysis, was 7.3 mol%, 11.3 mol% and 17.2 mol%. The chain length and composition of the copolymer was determined with ^{1}H NMR end-group analysis by using the methyl initiator signal as an internal reference (Figure 31, Figure 32 and Figure 33). The theoretical value (set by the monomer feed) was usually met with a deviation of 5 – 10 % (Table 6). The molecular weight obtained from SEC analysis was approximately 20 % higher than the value obtained from ^{1}H NMR analysis for copolymers consisting of EtOx. The deviation was much higher for copolymers consisting of MeOx, which can be explained by the prominent shoulder at shorter retention times (higher molecular weight) as already observed in section 3.1.1 for PMeOx homopolymers. Here, the dispersity was also ~1.30 in contrast to ~1.10 for P(EtOx-*co*-ButEnOx) copolymers, where only a small shoulder at lower retention volumes could be observed. The prominent shoulder for P(MeOx-*co*-ButEnOx) could however be reduced by purification via dialysis against water (Figure 34). Here the same assumption as for PMeOx homopolymers must be made and it is expected that temporary adducts might form, too. A logic explanation how the terminating agent piperidine is involved in this cannot be given.

Table 6: Characterization of synthesized copolymers by ^{1}H NMR spectroscopy and by size exclusion chromatography.

Sample name	**Repeating units$_{theo}$**		**Repeating units$_{exp}$***		**mol% "ene"**	**M_n (g/mol)***	**M_n (g/mol)$^{\#}$**	**Đ$^{\#}$**
	EtOx	**ButEnOx**	**EtOx**	**ButEnOx**				
P19	50	5	51	5	8.9	5782	6907	1.09
P20	45	5	50	6	10.7	5801	6799	1.09
P21	40	10	42	11	20.8	5633	7557	1.11
P22	35	15	43	19	30.6	6732	6746	1.08
P23	30	20	34	23	40.4	6341	7243	1.10
P24	77	5	85	6	6.6	9277	12700	1.18
	EtOx	**DecEnOx**	**EtOx**	**DecEnOx**				
P25	50	5	51	4	7.3	5986	6974	1.13
P26	50	7.5	63	8	11.3	8012	8101	1.14
P27	40	10	48	10	17.2	7335	8362	1.14
	MeOx	**ButEnOx**	**MeOx**	**ButEnOx**				
P28	50	5	51	5	8.9	5986	8264	1.23$^{\$}$
P29	40	10	40	9	18.4	4631	6821	1.29$^{\$}$
P30	72	8	71	8	10.3	7143	14930	1.27$^{\$}$

*determined by 1H NMR spectroscopy $^{\#}$measured on Malvern SEC system (triple detection) $^{\$}$bimodal distribution

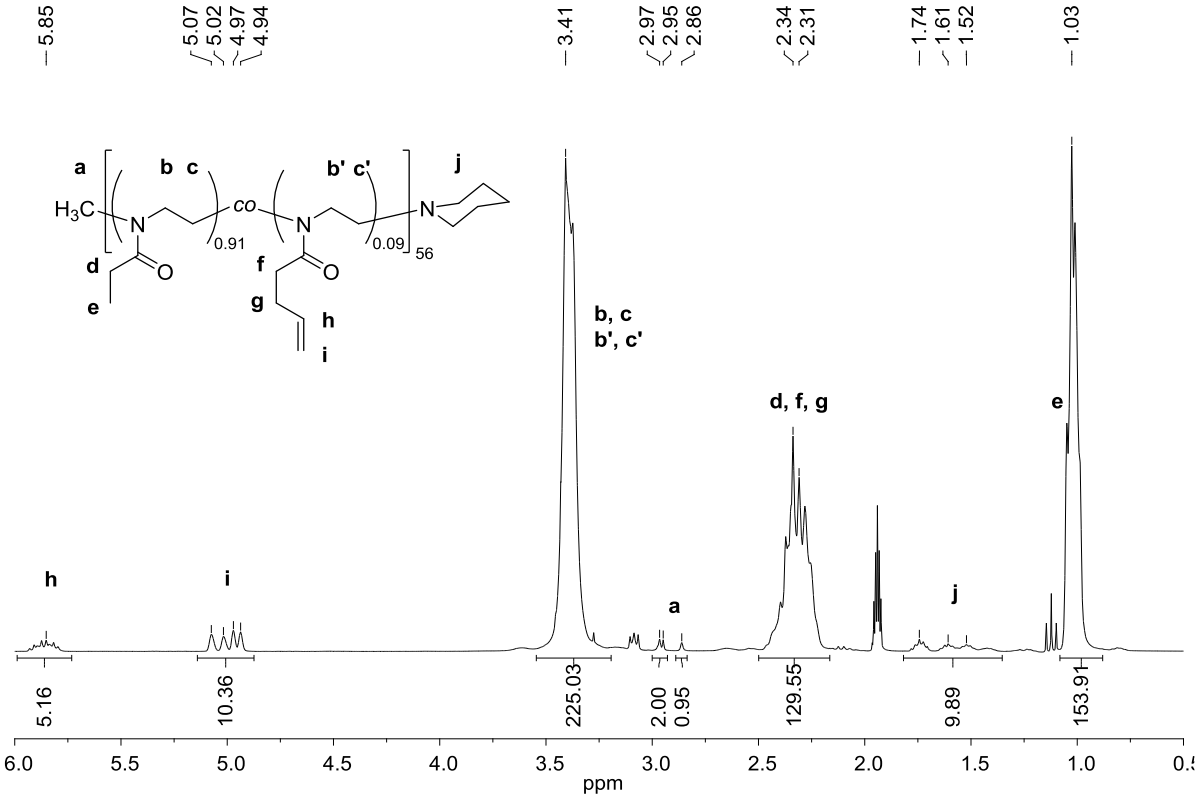

Figure 31: ^{1}H NMR of P(EtOx$_{0.91}$-*co*-ButEnOx$_{0.09}$)$_{56}$ (P19) measured in CD_3CN.

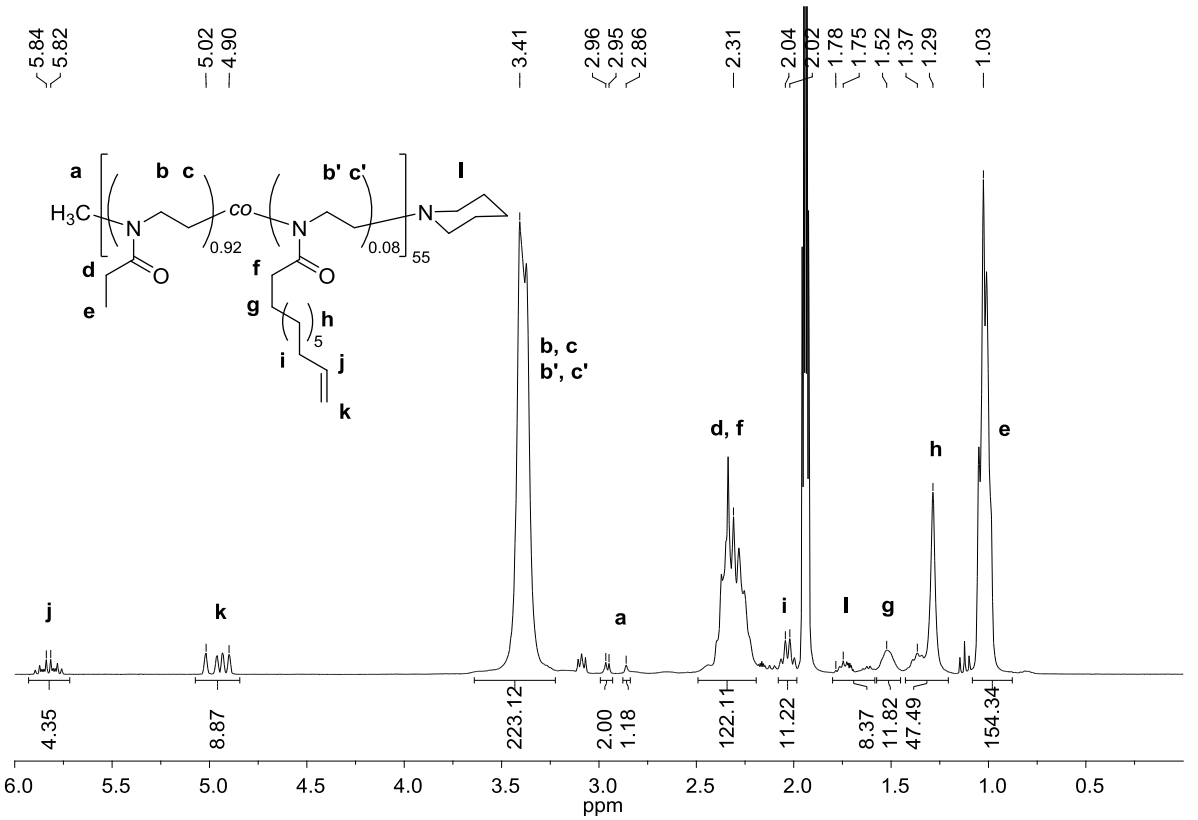

Figure 32: ^{1}H NMR of P(EtOx$_{0.92}$-*co*-DecEnOx$_{0.08}$)$_{55}$ (P25) measured in CD_3CN.

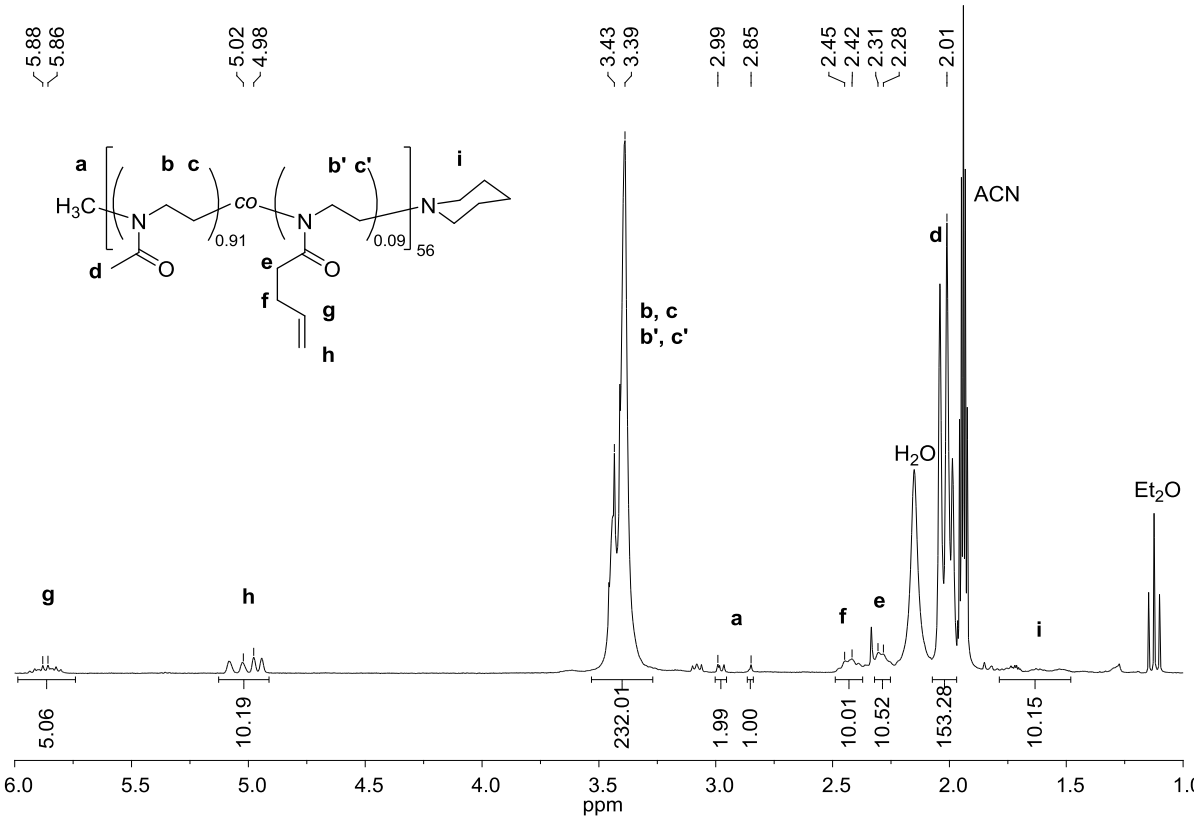

Figure 33: ^{1}H NMR of P(MeOx$_{0.91}$-*co*-ButEnOx$_{0.09}$)$_{56}$ (P28) measured in CD_3CN.

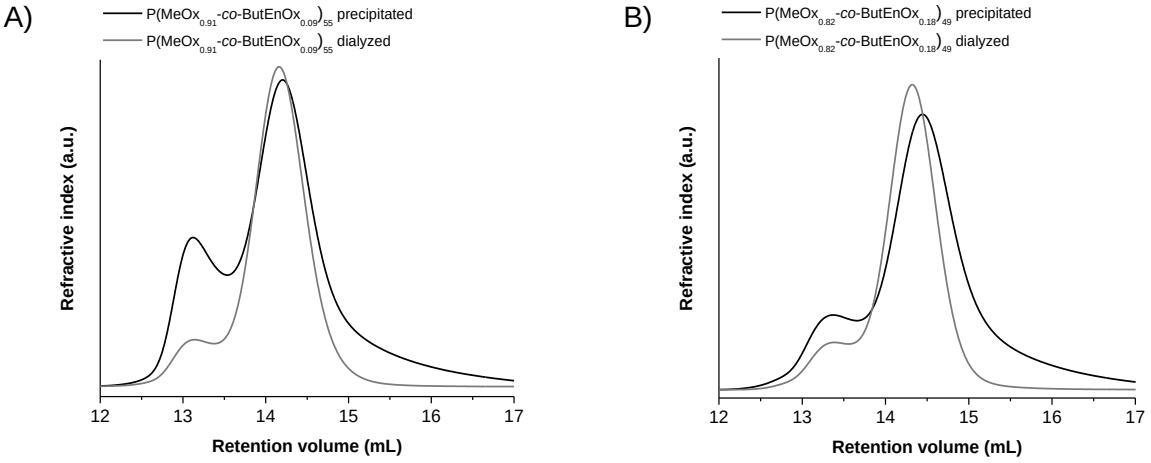

Figure 34: SEC elugram of polymers A) P28 and B) P29 which were only precipitated in comparison to dialyzed polymer.

As the incorporation of monomers with a longer alkyl chain reduced the water solubility of the whole polymer, the cloud point temperature (T_{CP}), i.e. the temperature above which the polymer is no longer soluble in water and the solution becomes

turbid, was determined. 1 wt% aqueous solutions of copolymers with varying vinyl content were prepared and measured by dynamic light scattering, increasing the temperature in 0.5 °C steps. The cloud point temperature was reached when the count rate of the measurement increased drastically. The results for the differently substituted polymers are shown in Figure 35. It becomes clear that the water solubility is compromised by incorporating monomers with longer alkyl side chains. The effect is more drastic for copolymer combinations with EtOx than with MeOx which can compensate with its hydrophilicity for the hydrophobicity of ButEnOx. P(EtOx-*co*-ButEnOx) with ~10 mol% ButEnOx does not exhibit a cloud point temperature, but the T_{CP} gradually decreases to 25 °C when the ButEnOx content is increased up to 40 mol%. The cloud point temperature for P(EtOx-*co*-DecEnOx) with 7.3 mol% DecEnOx is already at 25 °C and decreases to 12 °C for 11.3 mol% DecEnOx and the copolymer is no longer water soluble for a DecEnOx content of 17.2 mol%.

The increased hydrophobicity of ButEnOx containing copolymers was also observed when measuring HPLC (Figure 36). A reverse phase C18 column was used with a gradient flow starting with 10 % acetonitrile/ 90 % water to 90 % acetonitrile/ 10 % water. HPLC is an interaction-based method and a hydrophobic compound will remain longer on the column as they will interact with the hydrophobic column material. The HPLC elugrams show that the higher the content of ButEnOx in the polymer, the longer the polymer remains on the column. The elugram of P($EtOx_{0.89}$-*co*-$ButEnOx_{0.11}$)$_{56}$ is not a smooth curve as one is used to from SEC. In contrast, there are several spikes visible. Each spike could represent a fraction with a similar ButEnOx content and the polymer chains with the smallest amount of ButEnOx will elute the earliest. The elugrams of the copolymers with higher ButEnOx content become smoother as there exists a larger variety of possibilities of how many ButEnOx monomers were incorporated into the polymer chain.

In summary, copolymers based on MeOx and EtOx in combination with ButEnOx or DecEnOx were successfully synthesized. The theoretical number of repeating units was met with a deviation of 5 – 10 %. The dispersity of the copolymers was usually below 1.2, indicating a “living” type polymerization except for copolymers based on MeOx, where a bimodal distribution was observed in the SEC elugrams. This seems to be related to the less sterically hindered α-proton of the MeOx monomer resulting in more side reactions, like chain coupling [68].

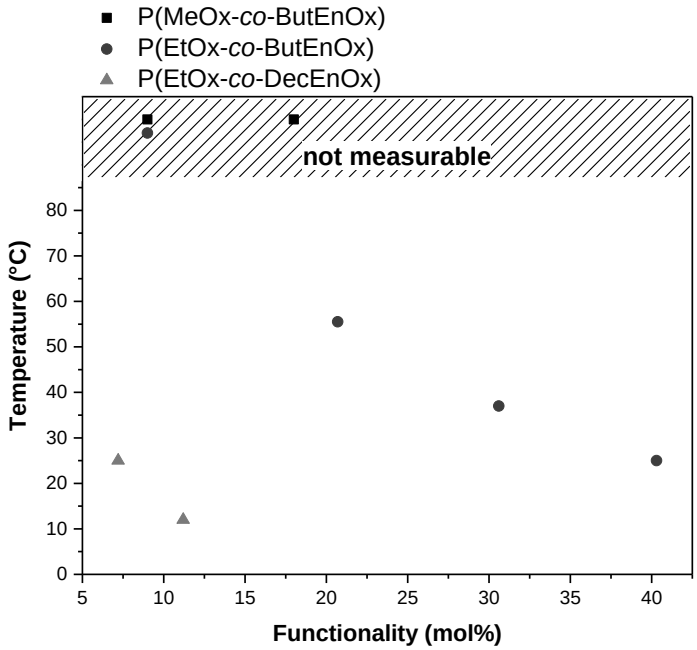

Figure 35: Cloud point temperature of aqueous solution of POx copolymers with varying vinyl functionality degree.

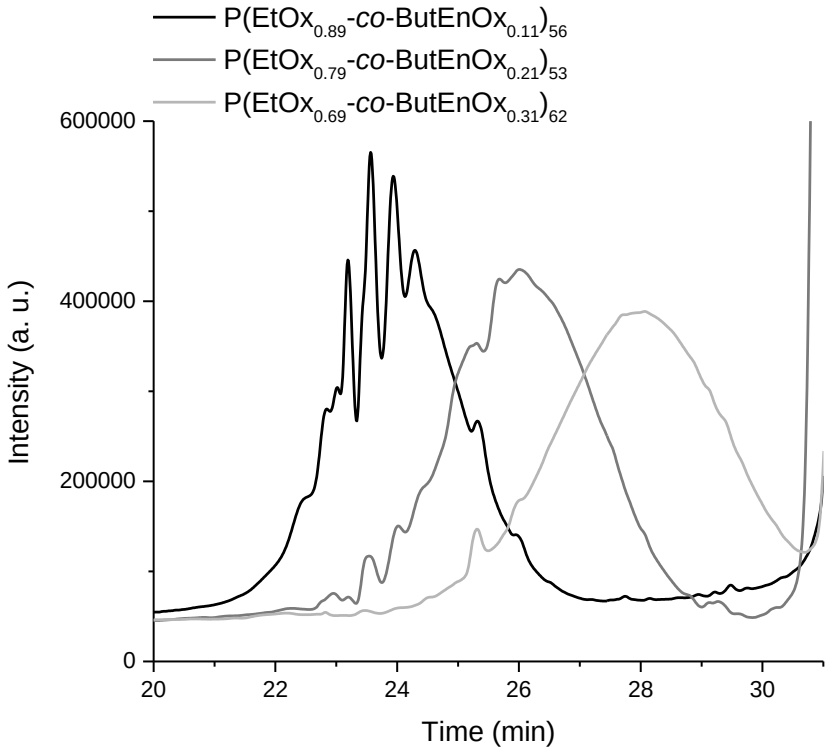

Figure 36: HPLC measurement of P(EtOx-*co*-ButEnOx) with increasing amount of ButEnOx at 210 nm.

3.1.3 Cytocompatibility of Copolymers

The cell toxicity of copolymers with ~10 and ~20 mol% vinyl content for different concentrations, namely 15, 5, 1 and 0.1 mg/mL, were tested with the CellTiter-Glo® luminescent cell viability assay using mouse fibroblasts (L 929 CC1). The luminescent signal depends on the luciferase reaction that takes place between the assay reagent Luciferin and adenosine triphosphate (ATP), which is produced from viable cells. Hence, the intensity of the luminescent signal is proportional to the number of viable cells. As negative control, poly(styrene) was used, which is known to not affect cell growth. As positive control, the eluate of poly(vinylchloride) (PVC) plates, of which it is known to be very cell toxic, was used. Figure 37 and Figure 38 show the results of the cell viability test. The results are evaluated according to the generally applied limits of cell toxicity as follows: 100 % – 80 % viable cells means no cell toxicity, 79 % – 60 % viable cells means weak cytotoxicity, 59 % – 30 % viable cells means moderate cytotoxicity and below 30 % viable cells means strong cytotoxicity. At the highest concentration, 15 mg/mL, all copolymers demonstrate a weak cytotoxicity except for P(EtOx-*co*-ButEnOx) with 20 mol%, which is non-toxic. The copolymer P(MeOx-*co*-ButEnOx) with the higher amount of ButEnOx is also less toxic than the one with less ButEnOx at 15 mg/mL. It seems that the increased hydrophobicity of the copolymer favors a decrease in cell toxicity. At concentrations of 5 mg/mL and lower, none of the copolymers showed any cytotoxic effects. Overall, the copolymers based on EtOx seem to be less cytotoxic in direct comparison to the copolymers based on MeOx.

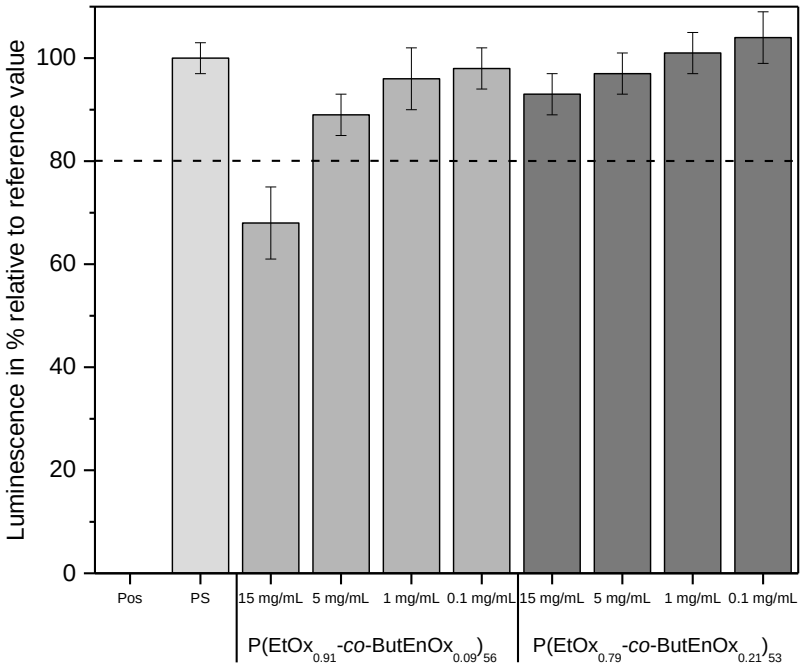

Figure 37: Results of the CellTiter-Glo® luminescent cell viability assay for different concentrations of P(EtOx-*co*-ButEnOx) copolymers.

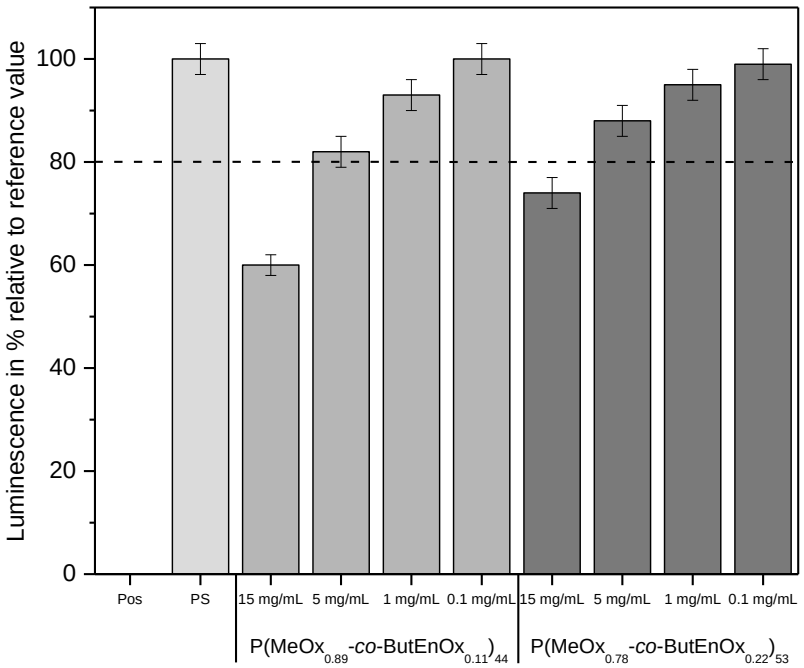

Figure 38: Results of the CellTiter-Glo® luminescent cell viability assay for different concentrations of P(MeOx-*co*-ButEnOx) copolymers.

3.2 Functionalization of Copolymers

The vinyl functionality at the side chain of the polymer allows for subsequent thiol-ene functionalization, which is a reliable reaction with conversions up to 100 % [98]. Monothiols like cysteamine, 2-mercaptoethanol or thioglycolic acid can be easily attached to the side chain of the POx copolymers to yield amino, hydroxyl or carboxylic acid side functional polymers. These can, for example, further be used for esterification or amidation reactions.

3.2.1 Polymer-analogue Thiol Functionalization

The polymer-analogue thiol functionalization of side functional POx copolymers is a two-step synthesis starting by attaching a protected thiol, a thiocarboxylic acid, to the polymer side chain forming a thioester which is, in the second step, deprotected. It was first tried to follow the protocol of Stichler *et al*. [60] and cleave the thioester under basic conditions with sodium hydroxide at 100 °C. However, as also already observed by Lambermont-Thijs *et al.* [90], these conditions lead to a degradation of the polymer, i.e. the cleavage of the side chains, which can be observed in the GPC elugram (Figure 39), where the molecular weight distribution is shifted to lower molecular weights/longer retention time (grey line).

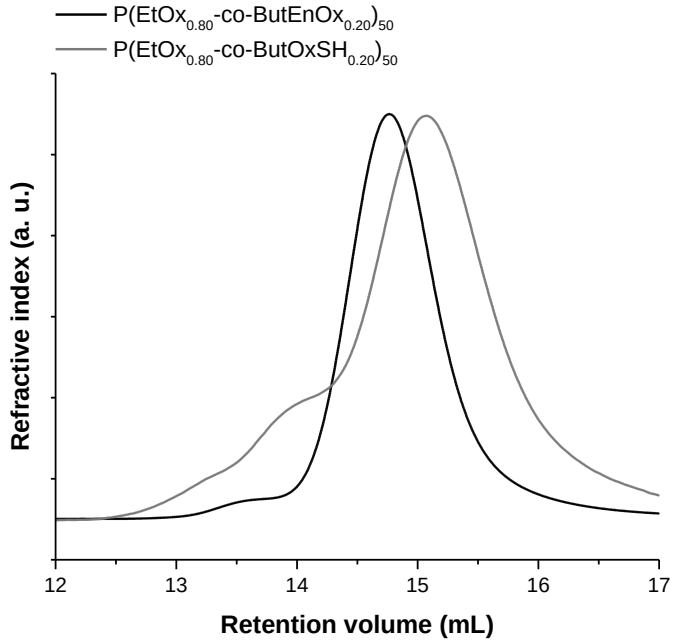

Figure 39: SEC elugram of POx copolymer before and after functionalization with thiols via basic deprotection.

In order to prevent the cleavage of the side chains, a new synthetic route was developed, which will be explained in the following.

Copolymers based on P(EtOx-*co*-ButEnOx) and P(MeOx-*co*-ButEnOx) with ~10 mol% and ~20 mol% vinyl content were functionalized with thioacetic acid via thiol-ene chemistry in methanol under UV irradiation, as depicted in Figure 40. The success of the thiol-ene reaction could be observed by the disappearance of the double bond signal in the ^{1}H NMR spectrum. The conversion of the vinyl group to the thioester was always 100 %. After removal of the excess thioacetic acid by precipitation of the modified polymer, the obtained thioester was cleaved using cysteine, which would react with the thioester in a “native chemical ligation” manner under reductive conditions, using sodium borohydride ($NaBH_4$). By “native chemical ligation manner” is meant that the deprotonated thiol of the cysteine attacks the carbonyl of the thioester. The close proximity of the amino group then leads to a rearrangement leading to a stable amide bond and the release of the deprotected thiol at the side chain (Figure 41).

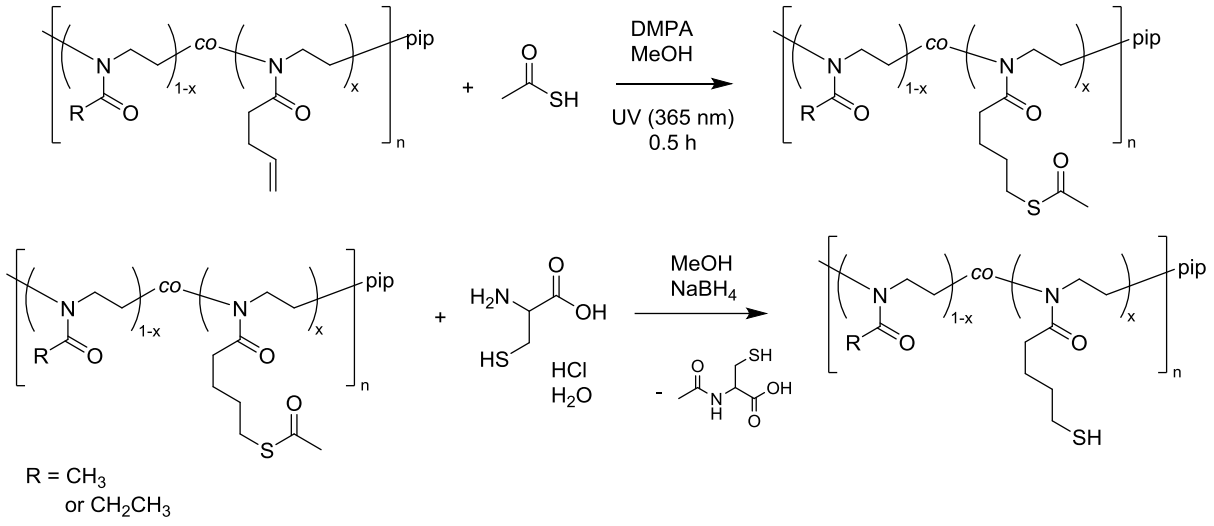

Figure 40: Synthesis scheme of the thiol side functionalization of POx copolymers.

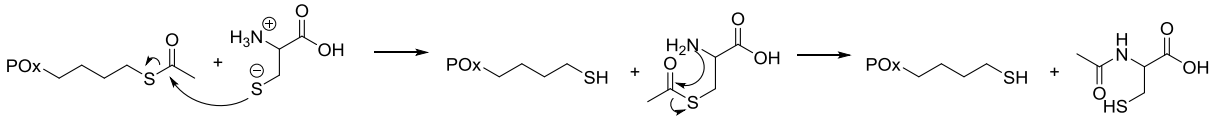

Figure 41: Deprotection mechanism of cysteine attacking the thioester at the side chain of POx.

The side product acetylcysteine was visible in the NMR spectrum of the precipitated polymer (Figure 42) and could be removed through dialysis (Figure 43). The chemical shift of the methyl group to 4.41 ppm leads to the conclusion that indeed acetylcysteine and not the intermediate product was formed.

In the final spectrum, there are no signals of the original double bond visible but there is a new set of signals at 2.57 ppm – 2.59 ppm, which belongs to the -CH_2 adjacent to the introduced thiol group.

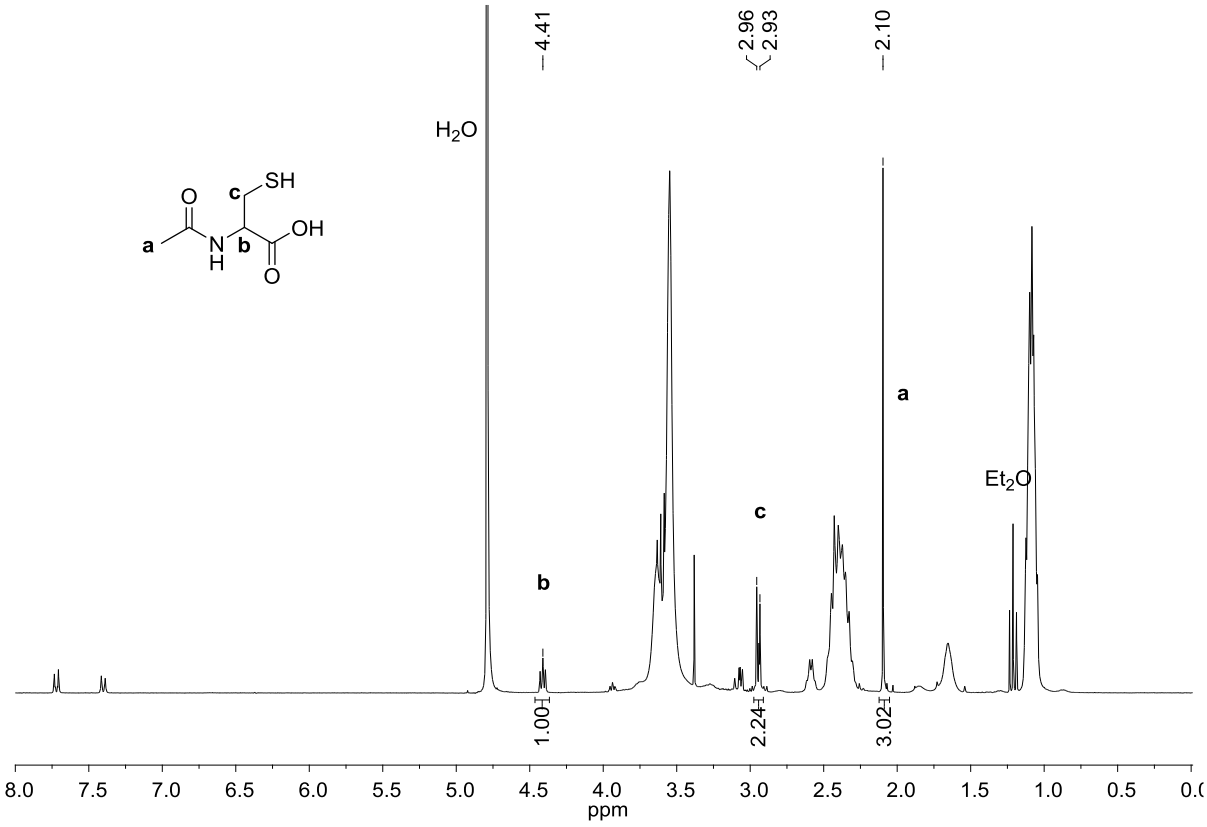

Figure 42: ^1H NMR in D_2O of precipitated polymer after deprotection showing side product acetylcysteine.

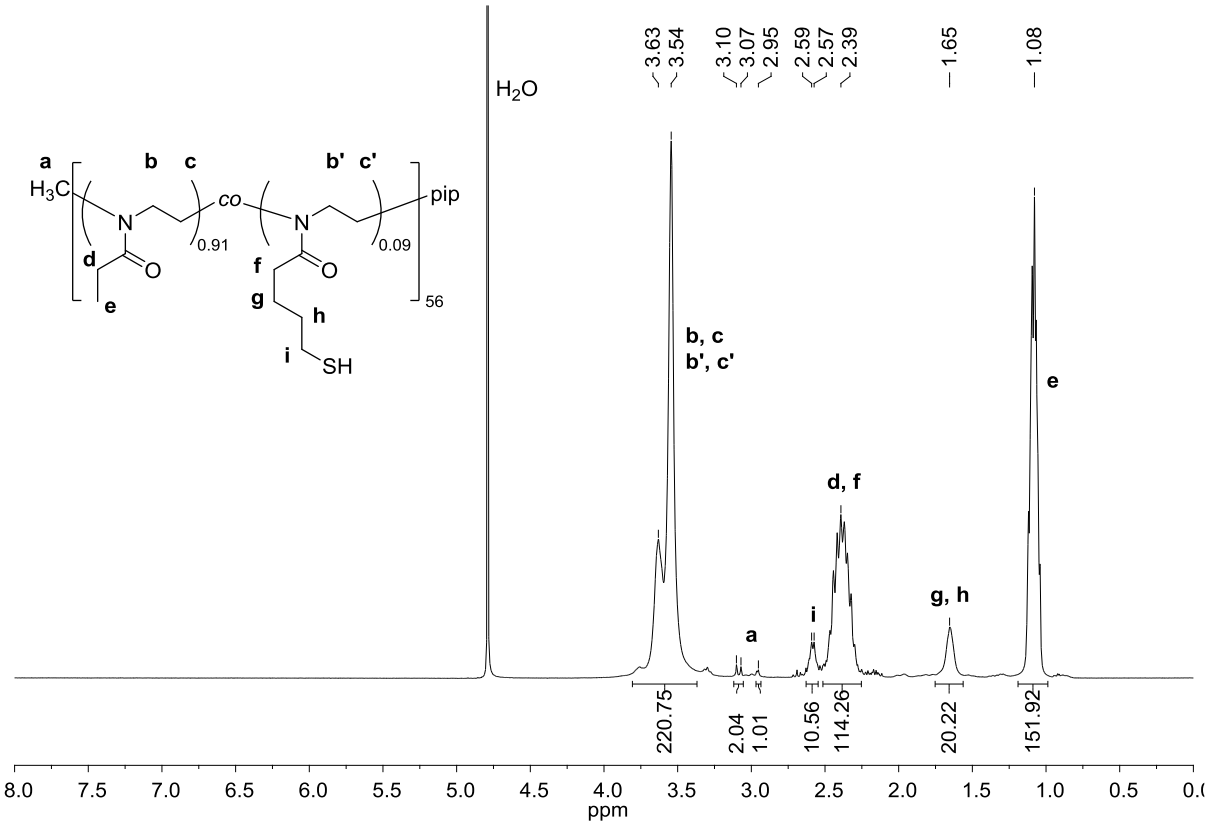

Figure 43: ^{1}H NMR of thiol functionalized POx after dialysis, measured in D_2O.

Figure 44A shows the SEC elugrams of one of the original parent copolymers, which was further functionalized with thioacetic acid resulting in an apparent increase in molecular weight as the peak maximum is shifted to a smaller retention volume. This shift can also be caused by a different chemical environment causing the polymer to coil and interact with the column material differently. After deprotection, the peak maximum is again shifted to its original retention volume, but the peak has widened with a shoulder at smaller retention volume. This might be caused by aggregation of the polymer chains or by a different interaction with the column material due to the thiol groups. In contrast to the deprotection method with NaOH, the SEC elugram does not display any degradation of the polymer at higher retention volume. Figure 44B shows the Raman spectra of two exemplary thiol functionalized copolymers. No disulfide signals are visible in the area of 430 cm^{-1} – 550 cm^{-1} [160] but there is a strong signal at 2570 cm^{-1}, which belongs to the vibration of the thiol groups. The signal increases in intensity with increasing amount of thiol attached to the polymer.

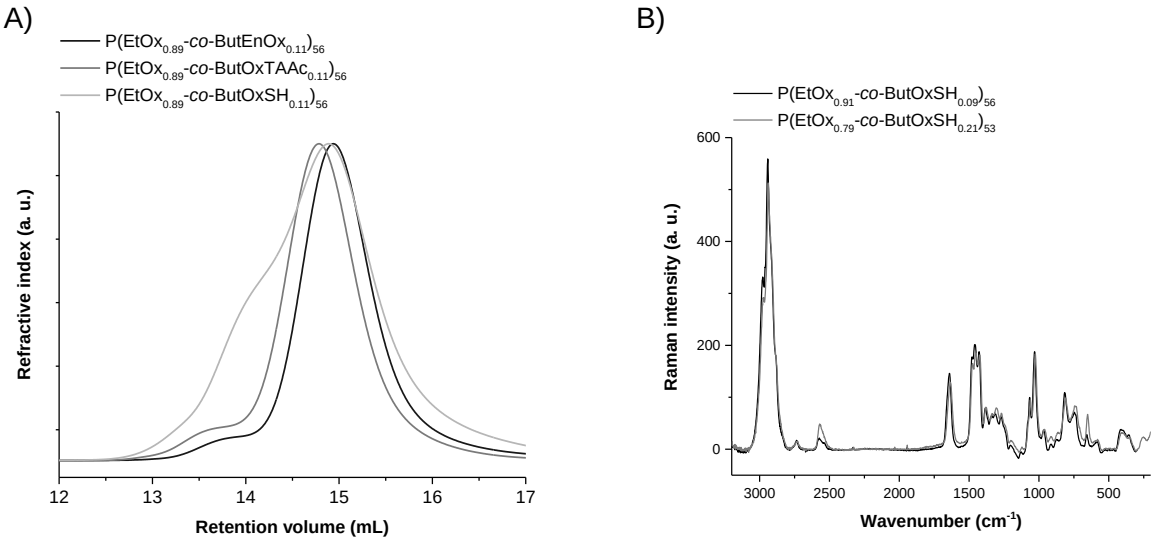

Figure 44: A) SEC elugram of parent polymer P(EtOx$_{0.89}$-*co*-ButEnOx$_{0.11}$)$_{56}$, after functionalization with thioacetic acid and after deprotection, B) exemplary Raman spectra of P(EtOx-*co*-ButOxSH) with increasing amount of thiol.

The copolymers were further analyzed with an Ellman's assay to quantitively determine the number of thiols per polymer chain. The mol% of thiols that was identified by the assay matched well with the number that had been found by ^{1}H NMR end group analysis.

In addition, a cloud point temperature was observed for P(EtOx-*co*-ButOxSH) copolymers, which ranged from 53 °C for polymers with 10 mol% functionality to 23.5 °C for polymers with 20 mol% functionality. Copolymers based on MeOx did not display any T_{CP}, which can be explained by the higher hydrophilicity of the monomer MeOx.

The thiol functional copolymers with ~10 mol% and ~20 mol%, except for P(EtOx-*co*-ButOxSH) with 20 mol% functionality as its T_{CP} was below 37 °C, were also tested on their cytotoxicity in the same fashion as the vinyl functional copolymers described earlier. The results of the cell viability assay are shown in Figure 45. At the highest concentration, thiol functionalized copolymers demonstrated a moderate cytotoxicity, which decreased with decreasing concentration. At 1 mg/mL, none of the copolymers showed any cytotoxicity. These results indicate that the functionalization with the reactive thiols increases the cytotoxicity. As already observed for the vinyl functional polymers, the cytotoxicity of copolymers based on EtOx is lower than for copolymers based on MeOx.

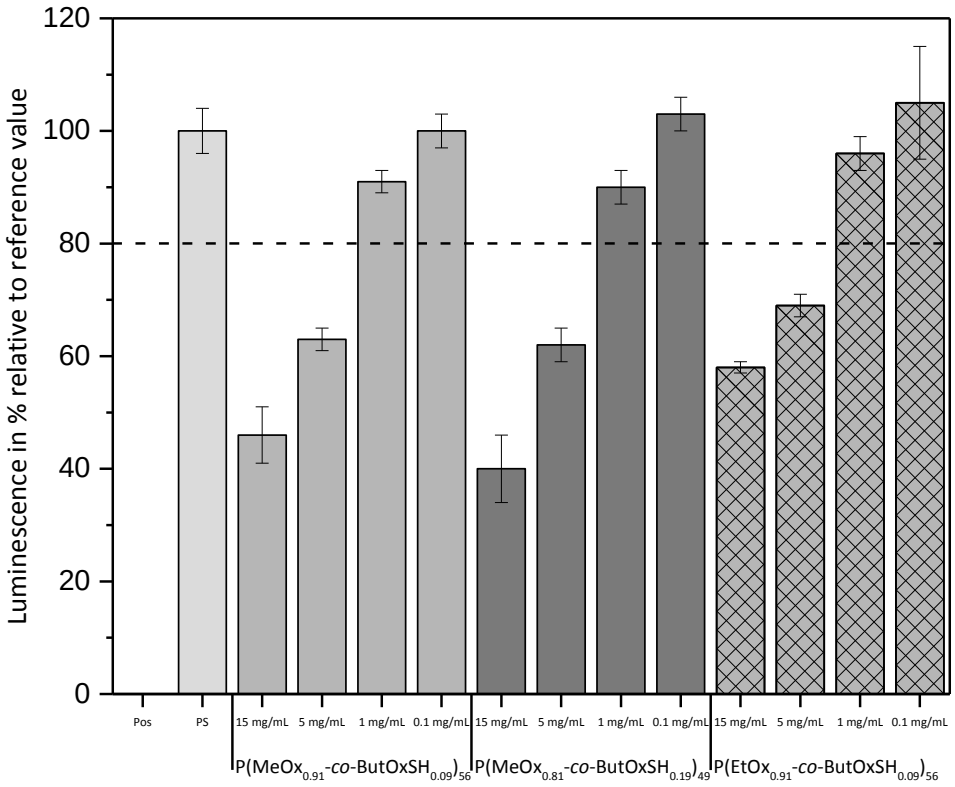

Figure 45: Results of the CellTiter-Glo® luminescent cell viability assay for different concentrations of thiol-functionalized copolymers.

3.2.2 Catechol Functionalization

The polymer side chains of POx copolymers were equipped with a degradable and a non-degradable bond to be able to tune the degradation rate. An ester bond was chosen for the degradable bond as it can be degraded enzymatically and by hydrolysis. The non-degradable bond was an amide bond. The synthesis scheme of the side functionalization using a protected catechol molecule is shown in Figure 46.

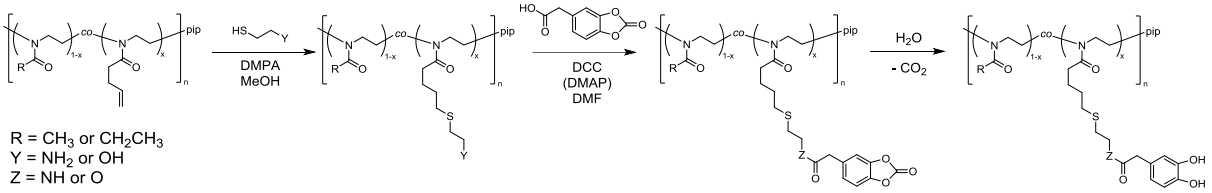

Figure 46: Synthesis scheme of the catechol functionalization at the side chain of POx copolymers.

The catechol building block, which was synthesized according to Li Shao and Xiaohu Zhang [129], was 2-oxo-1,3-benzo-dioxole-5-acetic acid (BDAA) starting from 3,4-dihydroxyphenylacetic acid. To attach the acid functionality of the catechol molecule to the polymer without side reactions between the phenolic hydroxyls and the hydroxyl or amine function at the polymer side chain, the two phenolic hydroxyls had to be protected using *N,N*-disuccinimidyl carbonate (DSC) catalyzed by triethylamine (Figure 47). The product BDAA was received as a white powder in good yield (~59 %) and was analyzed via NMR and EI-MS, see Figure 48 and section 5.3.3.4 for more details.

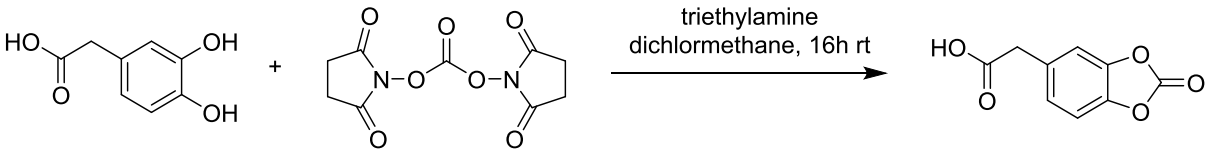

Figure 47: Synthesis scheme of 2-oxo-1,3-benzo-dioxole-5-acetic acid (BDAA) using DSC.

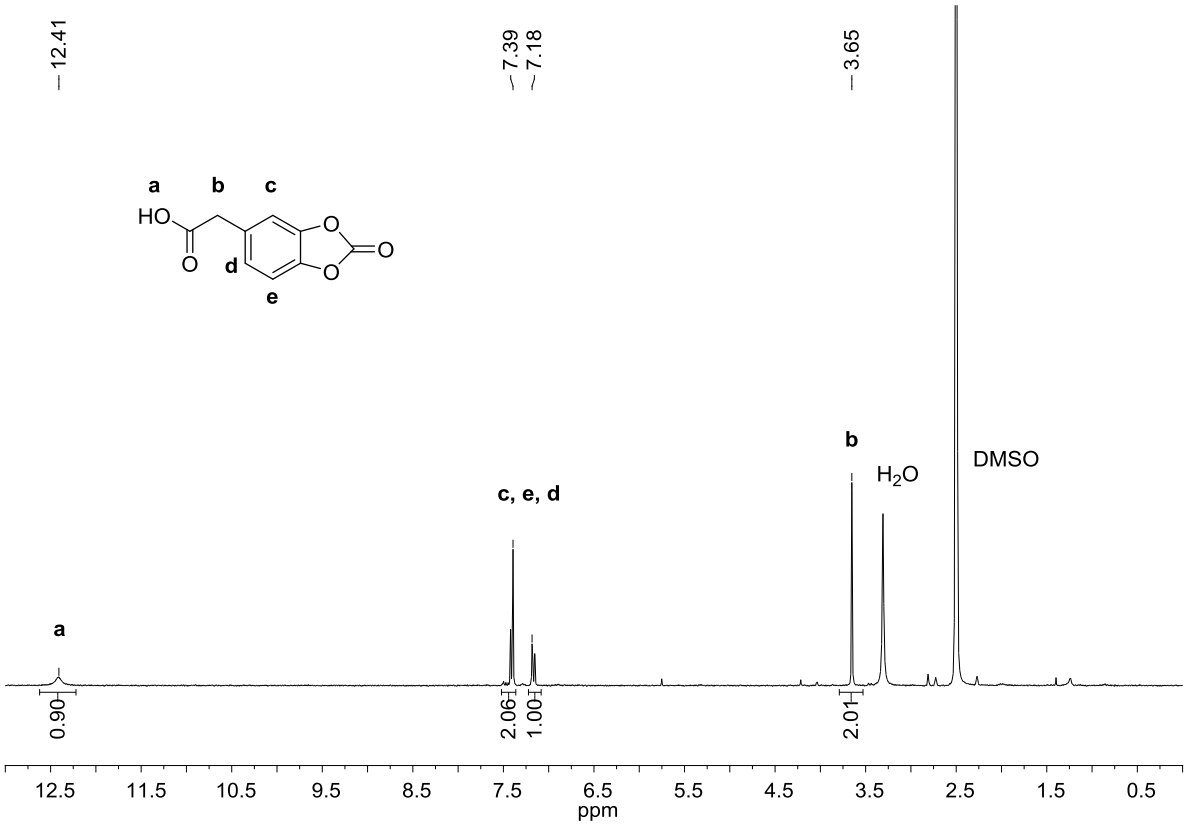

Figure 48: ^{1}H NMR of 2-oxo-1,3-benzo-dioxole-5-acetic acid measured in DMSO-d_6.

Two different copolymers, namely P(EtOx$_{0.93}$-*co*-ButEnOx$_{0.07}$)$_{91}$ and P(MeOx$_{0.90}$-*co*-ButEnOx$_{0.10}$)$_{79}$, were functionalized at the side chain. From earlier experiments, it was known that there was a limit on the percentage of catechol that could be incorporated when using P(EtOx-*co*-ButEnOx), as the longer side chain would render the polymer hydrophobic. This limit was higher for P(MeOx-*co*-ButEnOx) so that a copolymer with 10 mol% ButEnOx instead of 7 mol% could be used due to the more hydrophilic co-monomer MeOx.

3.2.2.1 Synthesis of P(EtOx-*co*-ButOxDOPAm)

The copolymer P(EtOx$_{0.93}$-*co*-ButEnOx$_{0.07}$)$_{91}$-pip was functionalized with an amine group at the side chain via thiol-ene reaction with cysteamine in methanol. After dialysis removing excess cysteamine and lyophilization, the polymer P[(EtOx)$_{0.93}$-*co*-(ButOxNH$_2$)$_{0.07}$]$_{91}$-pip was received. The catechol molecule BDAA (3 eq. per amine group) was added to the amine functionality using *N,N*-dicyclohexylcarbodiimide (DCC) in dry DMF. After dialysis in acidified water, the polymer was received as a white powder after freeze-drying. ^{1}H NMR spectroscopy showed that not all side chains were functionalized with the catechol group, which could be quantified by the

integral of the amide proton (H-**l**) and the integrals of the catechol protons (H-**n**, **p**, **q**, **o**, **o'**), showing that ~4 of the possible ~6 side chains had been functionalized (Figure 49).

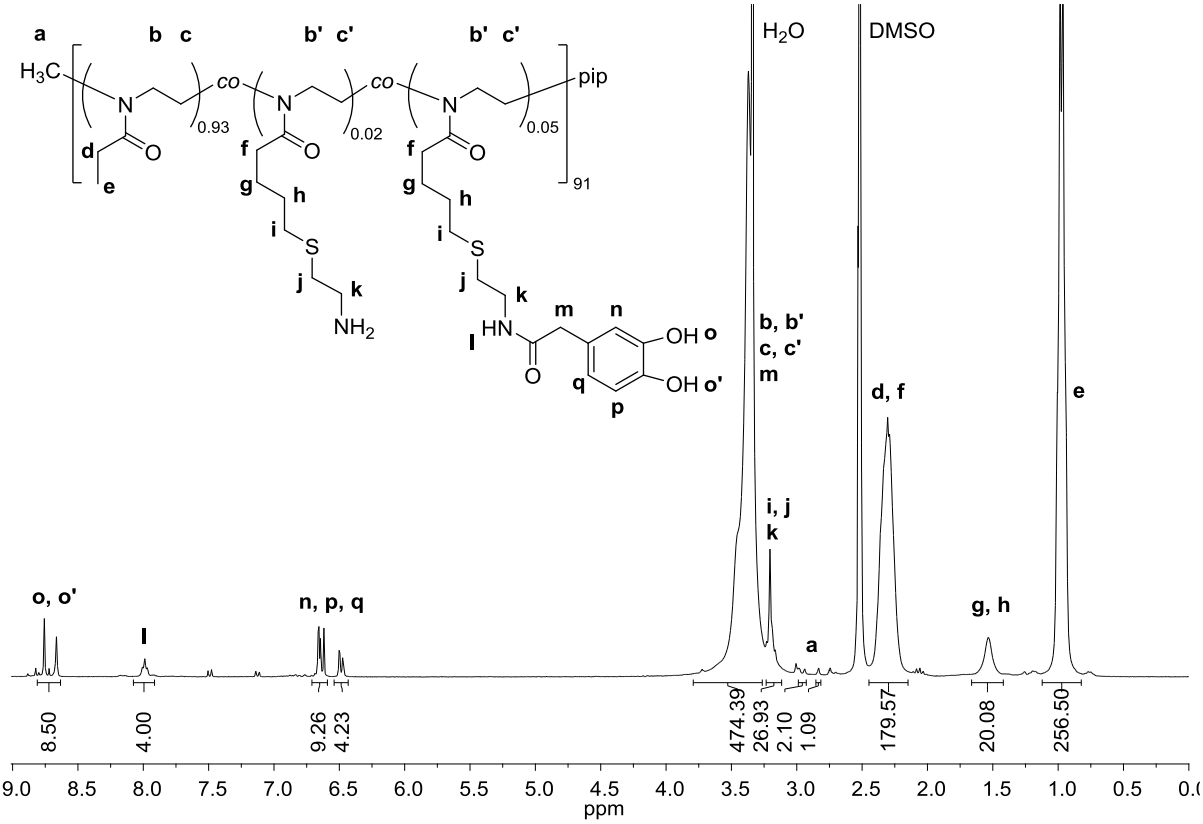

Figure 49: ^{1}H NMR of P[(EtOx)$_{0.93}$-*co*-(ButOxNH$_2$)$_{0.02}$-*co*-(ButOxDOPAm)$_{0.05}$]$_{91}$-pip in DMSO-d$_6$.

3.2.2.2 Synthesis of P(EtOx-*co*-ButOxDOPAc)

The copolymer P(EtOx$_{0.93}$-*co*-ButEnOx$_{0.07}$)$_{91}$-pip was functionalized at the side chain with a hydroxyl group via thiol-ene chemistry with 2-mercaptoethanol in methanol. After purification via precipitation in ice-cold diethyl ether, the polymer was dissolved in dry DMF and the catechol molecule BDAA (3 eq.) and as catalysts, 10 mol% of 4-(dimethylamino)pyridine (DMAP) and DCC (3 eq. per hydroxyl), were added. After the reaction, the polymer was purified by dialysis against DMF and afterwards precipitated in diethyl ether. The ^{1}H NMR end group analysis showed the protons that are distinct for the catechol molecule (H-**l** – **o**) and their integral value indicated that ~4 of the 6 side chains had been functionalized with the catechol functionality (Figure 50). It was not possible to measure an ^{1}H NMR spectrum of the functionalized copolymer without protecting groups as the water molecules, which are needed for the hydrolysis, would have also partially cleaved the ester bond at the side chain.

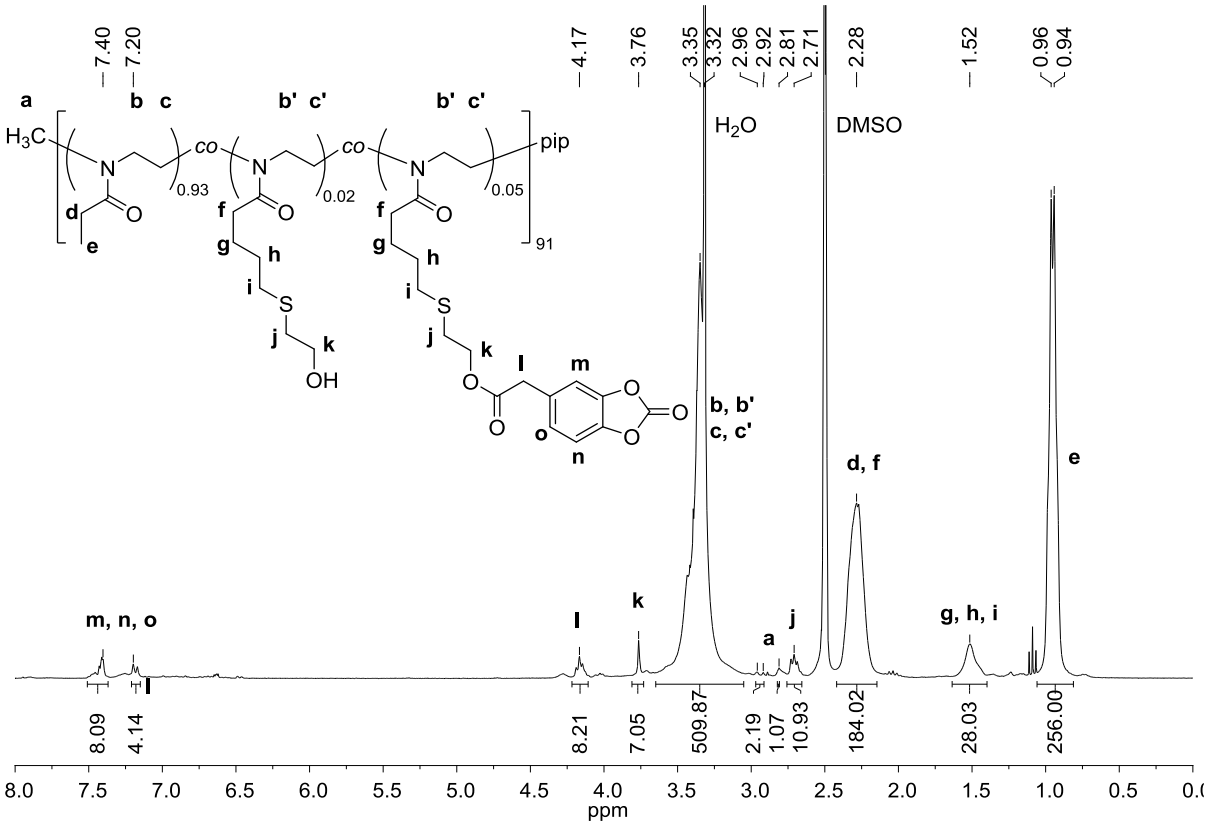

Figure 50: ^{1}H NMR of P(EtOx$_{0.93}$-*co*-ButOxOH$_{0.02}$-*co*-ButOxDOPAc$_{0.05}$)$_{91}$-pip in DMSO-d$_6$.

3.2.2.3 Synthesis of P(MeOx-*co*-ButOxDOPAm)

The polymer P(MeOx$_{0.90}$-*co*-ButEnOx$_{0.10}$)$_{79}$-pip was functionalized with thioglycolic acid by thiol-ene reaction in methanol. An earlier experiment had shown that the copolymer functionalized with amine side chains was not soluble in DMF. Hence, a different synthesis route was chosen to functionalize the MeOx containing copolymer with catechol by an amide bond. After purification through precipitation, the polymer was dissolved in DMF and N-hydroxysuccinimide (NHS), 1-ethyl-3-(3-dimethylaminopropyl)carbodiimide hydrochloride (EDC) and dopamine hydrochloride were added. After reaction overnight, the polymer was purified by dialysis against acidified water. The ^{1}H NMR end group analysis showed that ~6.7 of ~8 side chains had been functionalized with dopamine, which could be determined by the integral value of the catechol protons (H-**j**, **m** – **p**) (Figure 51).

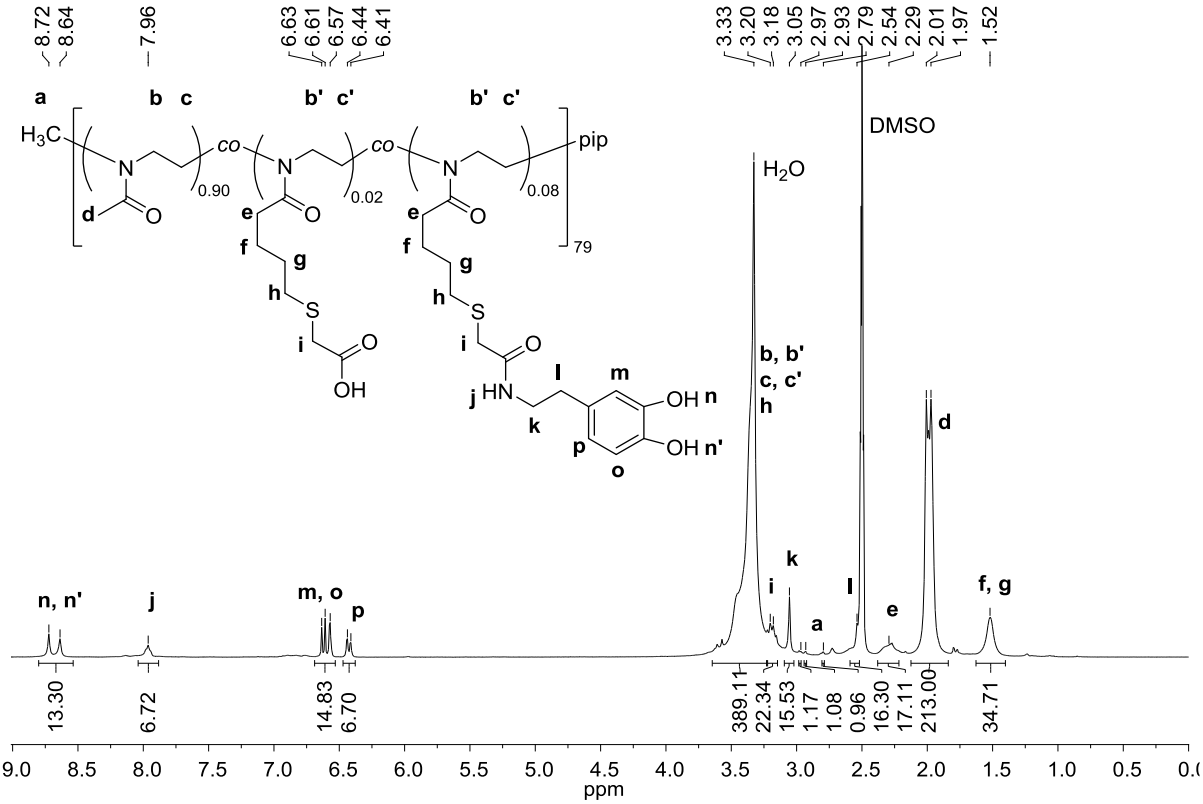

Figure 51: ^{1}H NMR of P(MeOx$_{0.90}$-*co*-ButOxCOOH$_{0.02}$-*co*-ButOxDOPAm$_{0.08}$)$_{79}$-pip in DMSO-d$_6$.

3.2.2.4 Synthesis of P(MeOx-*co*-DOPAc)

The polymer P(MeOx$_{0.90}$-*co*-ButEnOx$_{0.10}$)$_{79}$-pip was functionalized with 2-mercaptoethanol through thiol-ene chemistry at the side chain in methanol. After multiple precipitation in cold diethyl ether, the hydroxyl functional copolymer was dissolved in dry DMF and BDAA and the catalysts DMAP and DCC were added. The polymer was purified by dialysis against DMF and afterwards precipitated from chloroform/methanol (1:1 v/v) in cold diethyl ether. The ^{1}H NMR end group analysis showed that ~4.6 of possible 8 side chains had been functionalized with the catechol group (Figure 52).

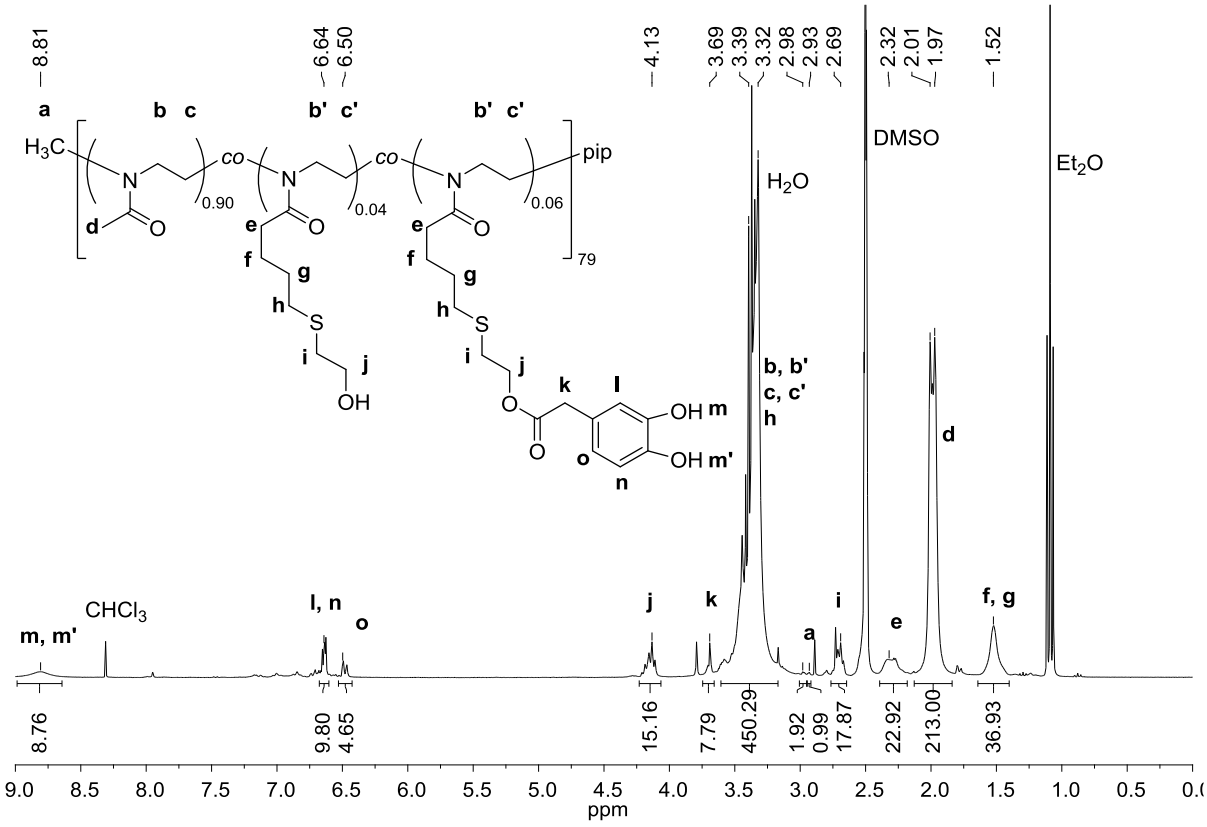

Figure 52: ^{1}H NMR of P(MeOx$_{0.90}$-*co*-ButOxOH$_{0.04}$- *co*-ButOxDOPAc$_{0.06}$)$_{79}$-pip in DMSO-d$_6$.

It was tried to analyze the catechol-functionalized polymers by SEC but the elugram showed that the polymer interacted strongly with the column resulting in a very broad signal. Hence, SEC was not considered as an appropriate tool to analyze these polymers.

However, the aromatic ring of dopamine is UV/Vis active (Figure 53) and absorbs at 280 nm. The functionalized copolymers were dissolved at 0.1 mg/mL in water and measured by UV/Vis spectroscopy. All spectra show the characteristic peak for

dopamine at 280 nm (Figure 54). The intensity of the peak increases in accordance to the results obtained by NMR analysis (Table 7) with P(MeOx-*co*-ButOxDOPAm) having the highest content of catechol functionality. The peak intensity of P(EtOx-*co*-ButOxDOPAm) and P(EtOx-*co*-ButOxDOPAc) is nearly similar, which corroborates with the NMR analysis.

Table 7: Overview of overall percentage of catechol functionality.

Copolymer	Percentage of catechol functionality (%)
P(EtOx-*co*-ButOxDOPAm)	5
P(EtOx-*co*-ButOxDOPAc)	5
P(MeOx-*co*-ButOxDOPAm)	8
P(MeOx-*co*-ButOxDOPAc)	6

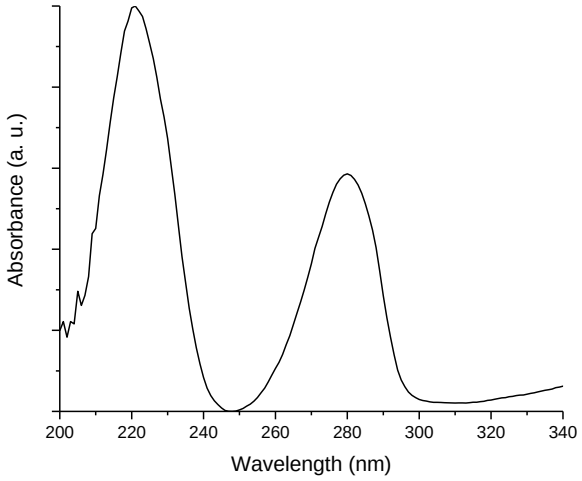

Figure 53: UV/Vis spectrum of dopamine in water.

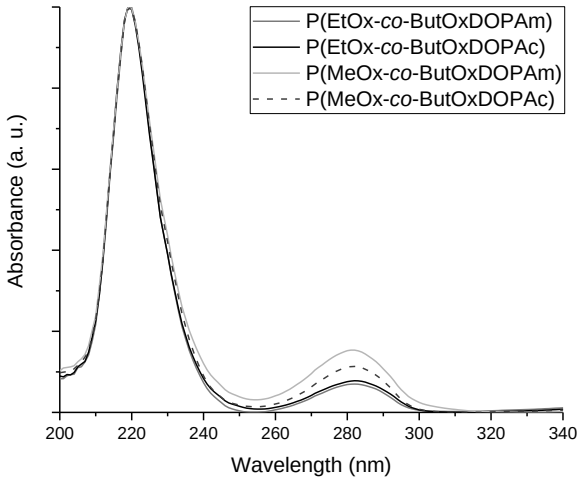

Figure 54: Stacked UV/Vis spectra of the catechol-functionalized copolymers.

3.2.3 Thiolactone Functionalization

A self-synthesized thiolactone compound with vinyl functionality was attached to thiol functionalized copolymers via thiol-Michael addition. Thiolactone acrylamide was synthesized according to Reinicke *et al*. [161] starting from homocysteine thiolactone hydrochloride and acryloyl chloride (Figure 55 and Figure 56).

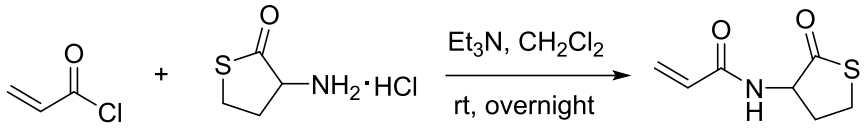

Figure 55: Synthesis scheme of thiolactone acrylamide.

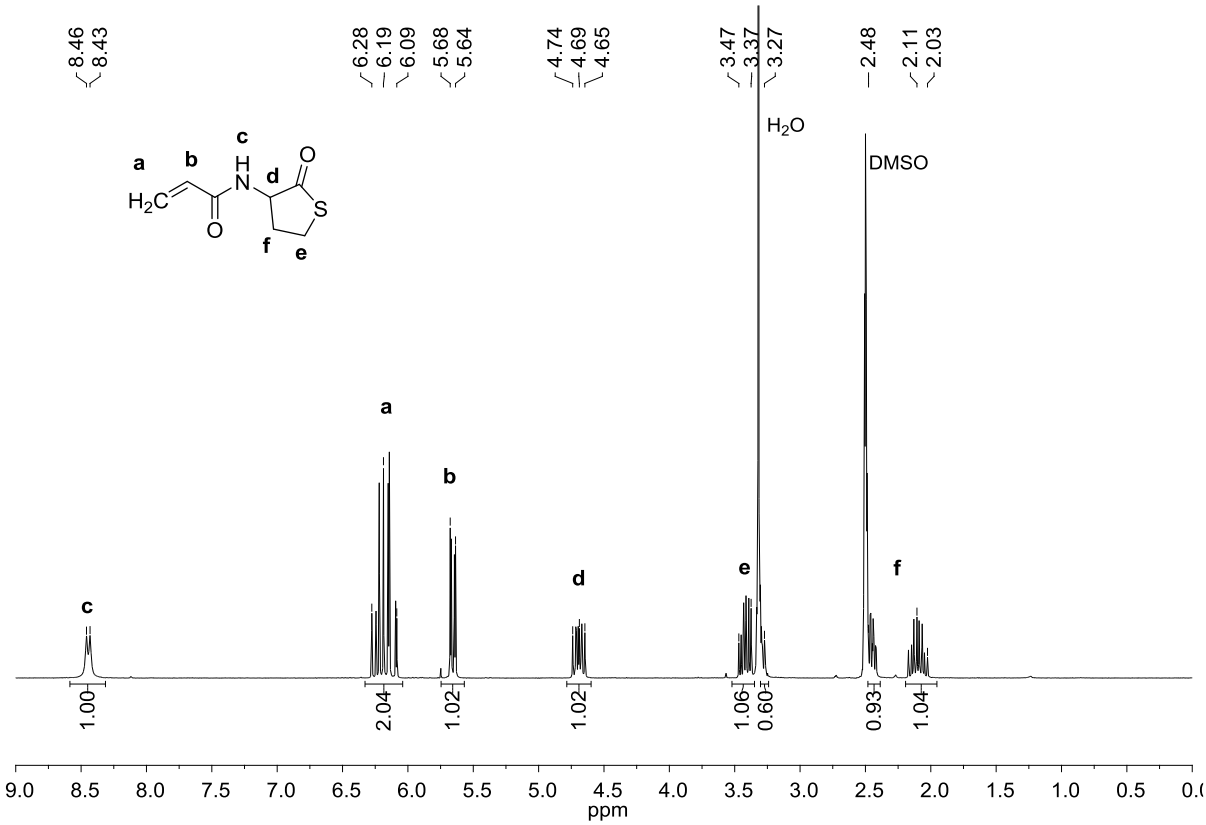

Figure 56: ^{1}H NMR of thiolactone acrylamide in DMSO-d_6

The acryl group could then be used to add the compound to P(EtOx$_{0.89}$-*co*-ButOxSH$_{0.11}$)$_{56}$ and P(EtOx$_{0.79}$-*co*-ButOxSH$_{0.21}$)$_{53}$ via thiol-Michael addition using dimethylphenylphosphine (DMPP) as co-reagent to activate the double bond. DMPP could not be completely removed by precipitation of the polymer and was still visible in the NMR spectrum. A successful addition of the thiolactone molecule could be observed by a change of the signal of the CH_2 group, which was formerly adjacent to the thiol group and additional signals of the thiolactone molecule, see exemplary

^{1}H NMR of P(EtOx$_{0.89}$-*co*-ButOxLac$_{0.11}$)$_{56}$ (Figure 57). For example, the signal of the CH group is visible at 4.57 ppm as well as the signal of the CH_2 group of the thiolactone ring at 2.76 ppm. In addition, the signals for the vinyl group have disappeared. This could also be caused by an effective activation by the co-reagent DMPP [98], but as the thiolactone molecule was used in excess to DMPP, the absence of the signal is probably due to a successful addition to the polymer side chain. The SEC elugram of the functionalized copolymers (Figure 133) in the experimental section, showed a slight widening of the peak with a minimal increase in dispersity, the calculated molecular weight however did not increase. The peak widening might be caused through an interaction of the thiolactone groups with the column material or through incomplete saturation of the thiol groups with the thiolactone molecule, which could have led to chain coupling via the formation of thioesters. The specific thiolactone vibrations at 3274 cm^{-1} (amide, NH valency) and 1702 cm^{-1} (C=O valency, amide band I) are also visible in the IR spectrum of the functionalized polymer (Figure 58).

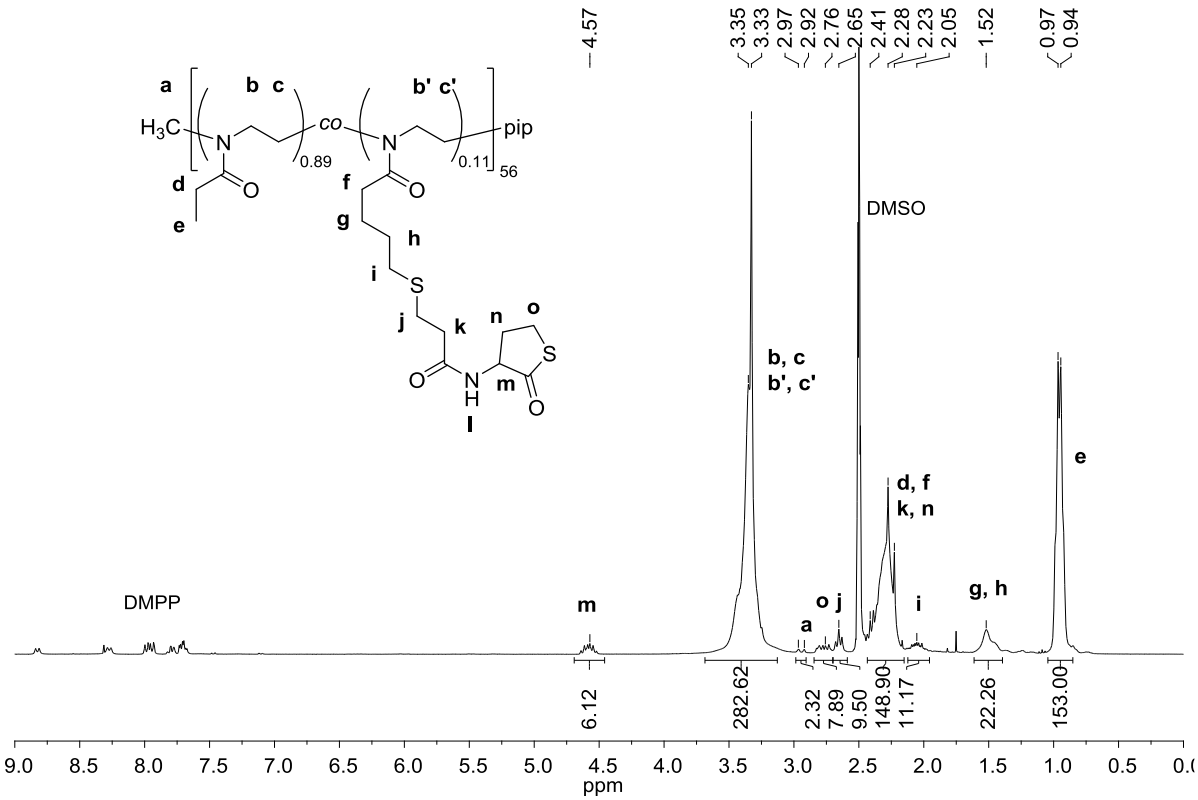

Figure 57: ^{1}H NMR of P(EtOx$_{0.89}$-*co*-ButOxLac$_{0.11}$)$_{56}$ in DMSO-d$_6$.

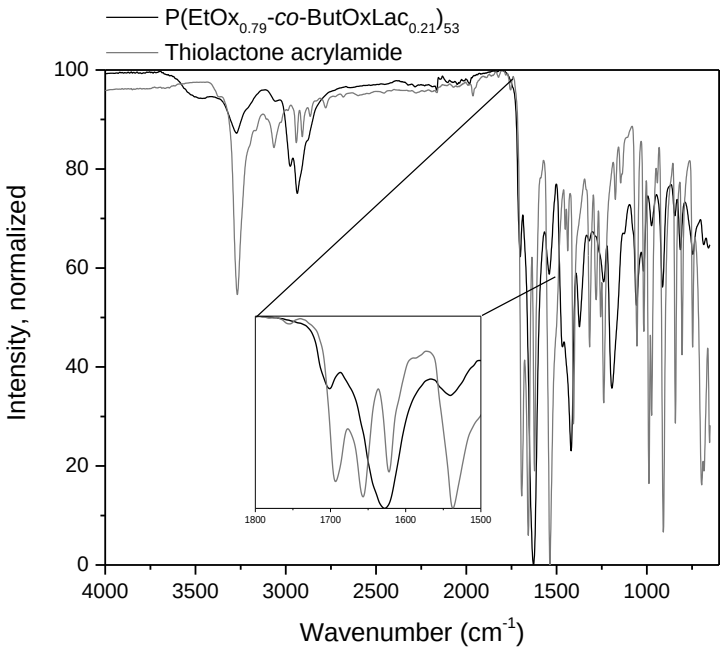

Figure 58: IR spectrum of $P(EtOx_{0.79}\text{-}co\text{-}ButOxLac_{0.21})_{53}$ (black line) and thiolactone acrylamide (grey line).

3.2.4 Azlactone Functionalization

Similar to the thiolactone side chain functionalization, it was tried to bind 2-vinyl-4,4-dimethylazlactone (VDM), which was synthesized according to Levere *et al*. [136] (Figure 59), to thiol-functionalized POx.

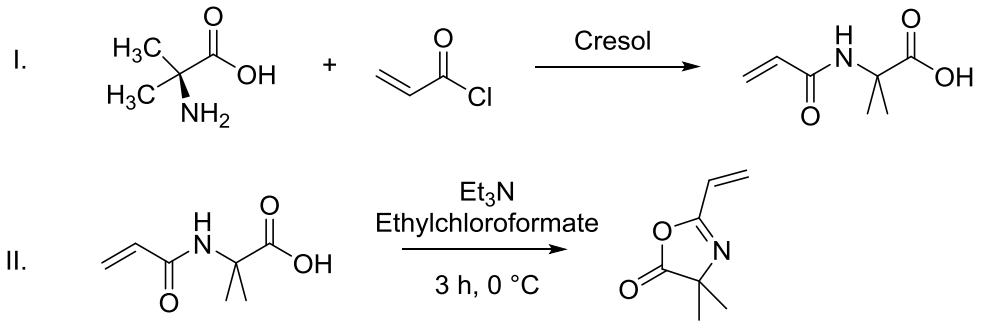

Figure 59: Synthesis scheme of 2-vinyl-4,4-dimethylazlactone (VDM).

It was first tried to attach VDM via radical mediated thiol-ene reaction using the photo-initiator 2,2-dimethoxy-2-phenylacetophenone (DMPA) (Figure 60). Two different solvents, methanol and chloroform, were used. After the reaction, the IR spectra showed the distinct peak of the carbonyl vibration of the azlactone ring at 1816 cm^{-1} (Figure 61A). However, the SEC elugrams showed a large shoulder at smaller retention volumes, especially for the product that had been formed in methanol (Figure 61B). Therefore, it was suspected, that especially in more polar

solvents, the possibility was high that thiols, which had not yet reacted with the vinyl group of VDM, could open the azlactone ring meaning that VDM unintentionally acts as a cross-linker.

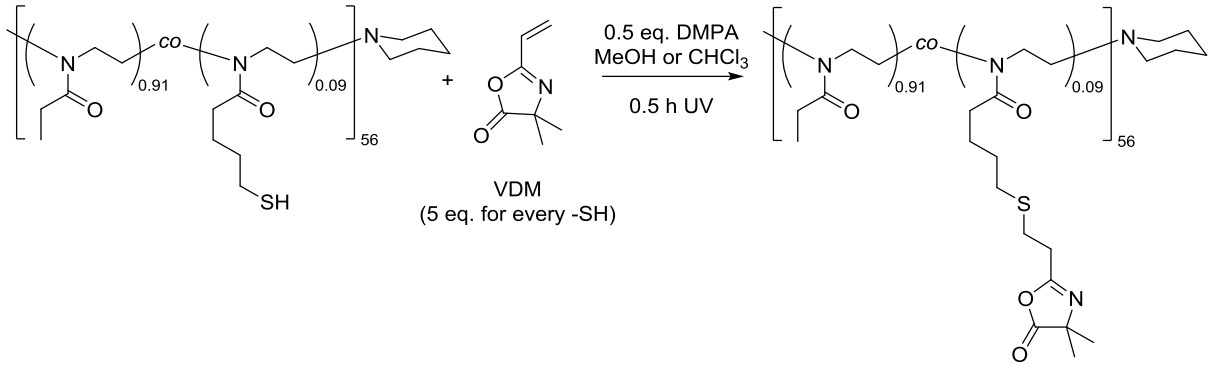

Figure 60: Synthesis scheme of radical mediated thiol-ene reaction between thiol functionalized POx and VDM.

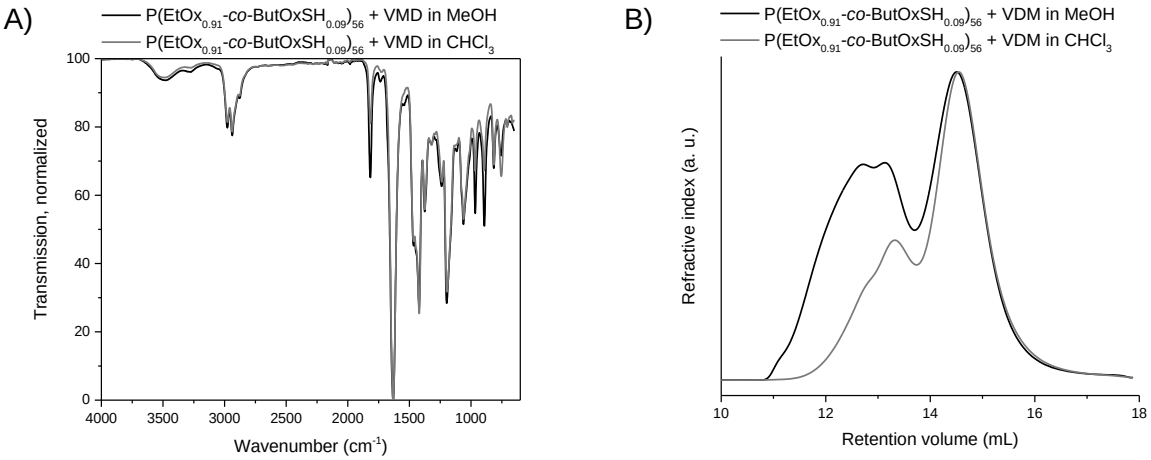

Figure 61: A) IR spectra and B) SEC elugrams (measured in DMF) of azlactone functionalized POx by radical mediated thiol-ene reaction.

It was also tested if the cross-linking side reaction occurred less when VDM was attached to the POx side chain via thiol-Michael addition. DMPP or 1,8-diazabicyclo[5.4.0]undec-7-ene (DBU) were used as catalyst in chloroform or in a more polar solvent, acetonitrile (Figure 62), according to Ho *et al*. [162], where VDM was attached to a polymer with a thiol end group using DMPP in tetrahydrofuran.

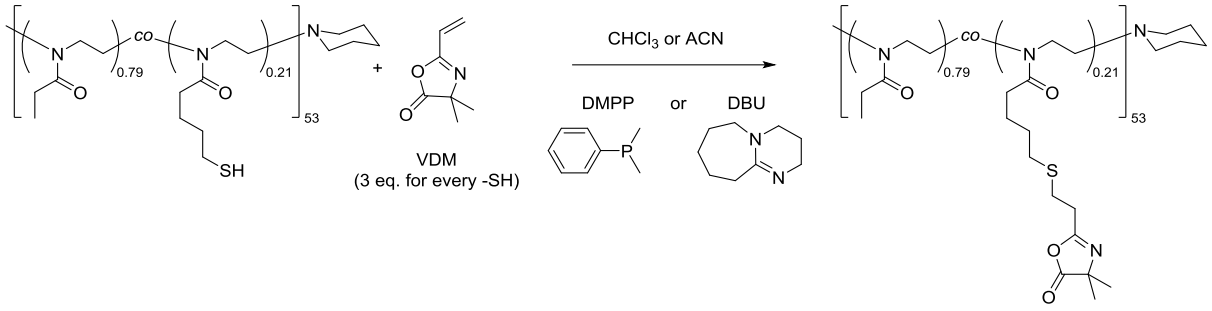

Figure 62: Synthesis scheme of thiol-Michael addition between thiol functionalized POx and VDM.

DMPP was tested solely in chloroform, whereas DBU was also tested in acetonitrile. For all three experiments, there were still signals of the vinyl group of VDM visible in the ^{1}H NMR spectrum, which had not been the case for the radical mediated conjugation. The IR spectra show the vibration of the azlactone ring carbonyl group. However, when these spectra are compared to the polymer, where VDM was attached via radical thiol-ene (Figure 63A, dashed line), the signal of the carbonyl is rather small. The polymer, which was used for the thiol-Michael addition, has twice the amount of thiol functionality available so one would expect the signal to be much greater in intensity. The SEC elugrams (Figure 63B) show no signs of cross-linking side products for the reaction with DMPP and DBU in acetonitrile, but a strong tailing to smaller molecular weights. The product of the reaction with DBU in chloroform shows not tailing to smaller molecular weights, but again a bimodal distribution with a shoulder at higher molecular weights. These findings lead to the conclusion that the radical mediated thiol-ene reaction seems to lead to complete conversion but also to side reactions and the Michael thiol-ene reaction leads to incomplete conversion of the functional groups but to less side reactions. It also seems to make a difference if only a terminal thiol is available for reaction, as in the work of Ho *et al*., or if the polymer contains thiols at the side chain, which might aggregate or lead to a different coiling behavior depending on the solvent used, which could explain the different results in polar and less polar solvents.

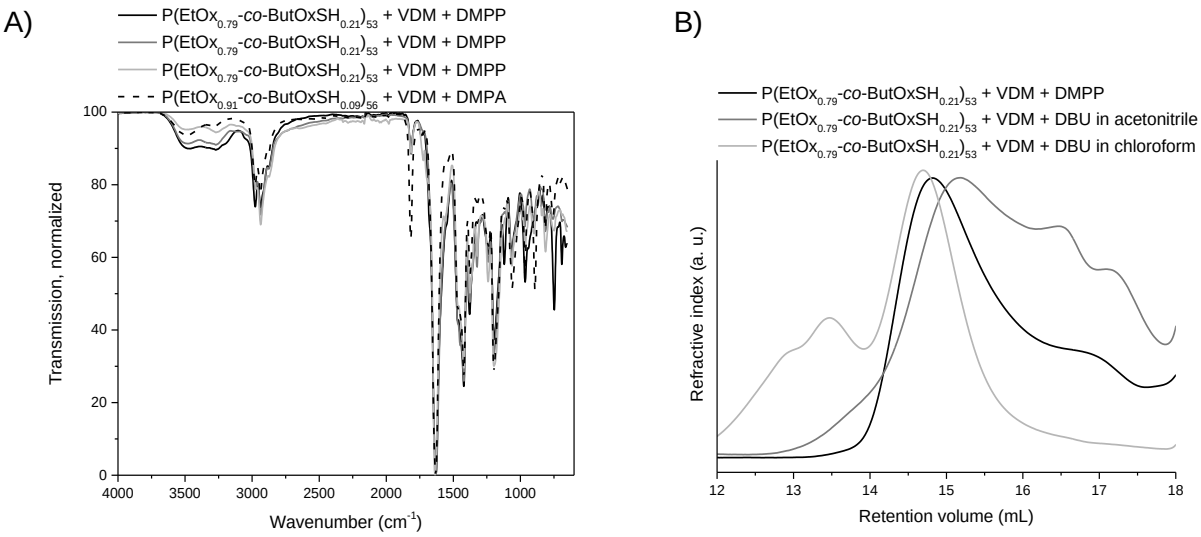

Figure 63: A) IR spectra and B) SEC elugrams (measured in DMF) of azlactone functionalized POx by thiol-Michael addition.

In accordance with these findings, it was tried to functionalize POx copolymers with azlactone in a way so that no available nucleophile could disturb the post-polymerization functionalization. One option would be to attach an azlactone precursor molecule to the side chain and close the azlactone ring *in situ* at the polymer chain.

Hence, a mercaptoacyl amino acid, namely *N*-(3-mercapto-1-oxopropyl)-2-methyl-alanine (MOMA), was synthesized with modifications according to Condon *et al*. [163]. The starting amino acid was aminoisobutyric acid providing two geminal methyl groups next to the amine group, which would later on facilitate the ring closure [164]. The amine group was transformed into an amide using 3-bromopropionyl chloride and subsequently decorated with a thioester, which could easily be deprotected in aqueous ammonia (Figure 64). The intermediate product *N*-[3-(benzoylthio)-1-oxopropyl]-2-methylalanine was obtained in 24 % yield, which is lower than the yield achieved for the functionalized amino acids in the work of Condon *et al*. (56 %). It is possible that the yield could be increased by fine-tuning the reaction conditions, nevertheless, as the educts that are needed for this reaction are rather inexpensive, the yield is acceptable. The intermediate product was deprotected with aqueous ammonia within two hours with a yield of 44 % leading to a thiol group, which could be used for thiol-ene reaction with the vinyl side chain of the synthesized POx

copolymers. The successful synthesis was shown by ^{1}H NMR (Figure 65) and ^{13}C NMR, EI-MS, IR and Raman spectroscopy (section 5.3.3.3).

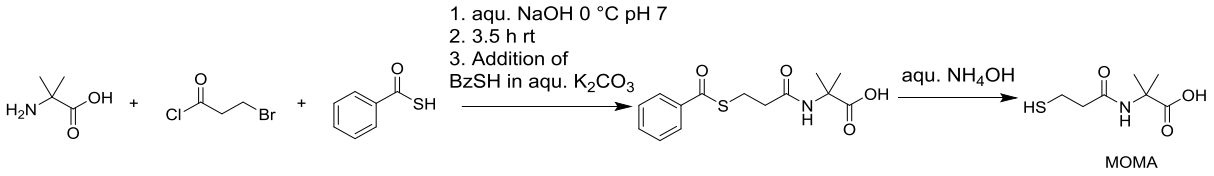

Figure 64: Synthesis scheme of *N*-(3-mercapto-1-oxopropyl)-2-methyl-alanine (MOMA).

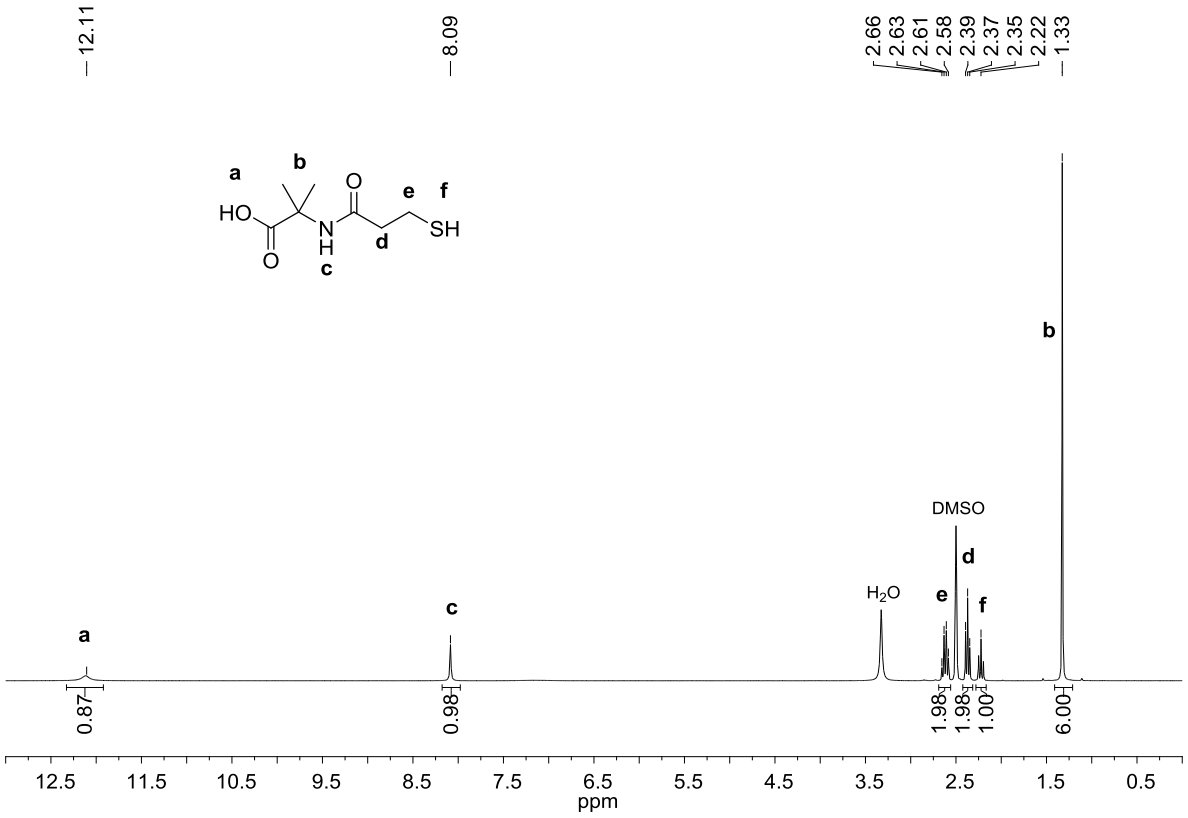

Figure 65: ^{1}H NMR of *N*-(3-mercapto-1-oxopropyl)-2-methyl-alanine (MOMA) in DMSO-d_6.

It was first tried to attach MOMA via radical mediated thiol-ene reaction with the photo-initiator Irgacure to the vinyl side chain of P(EtOx-*co*-ButEnOx) copolymers in water. The idea was to make the reaction more efficient through the addition of the reducing agent TCEP, which would suppress any disulfide formation of MOMA. First experiments were carried out with an excess of MOMA (1.5 eq. for every double bond available) and the ^{1}H NMR spectrum showed the disappearance of all signals belonging to the double bond. It was then tried to attach 0.5 and 0.75 eq. of MOMA for every double bond available to evaluate the possibility of keeping part of the vinyl functionality free for other reactions. Here, it was observed in the ^{1}H NMR spectrum,

that the integral of the signal of the double bond had diminished more than expected, which led to the conclusion that some of the double bonds might homopolymerize if there was not an excess of thiols available. This assumption was proven with two experiments, where the copolymer P(EtOx-*co*-ButEnOx) was dissolved either in water or in methanol and irradiated at 365 nm with the photo-initiator Irgacure (for water as solvent) or DMPA (for methanol as solvent). The ^{1}H NMR spectrum showed that the integral for the double bond had decreased when water was used as a solvent, in contrast to the experiment where methanol had been used. That indeed homo-polymerization had taken place could also be observed in the SEC elugrams of the two experiments (Figure 66). The peak of the water experiment shows a bimodal distribution with a large second peak at higher molecular weight whereas the distribution of the polymer in the methanol experiment is still monomodal. This leads to the conclusion that the aggregation of the hydrophobic vinyl side chains is much greater in water than in the less polar solvent methanol, which increases the likelihood for homo-polymerization.

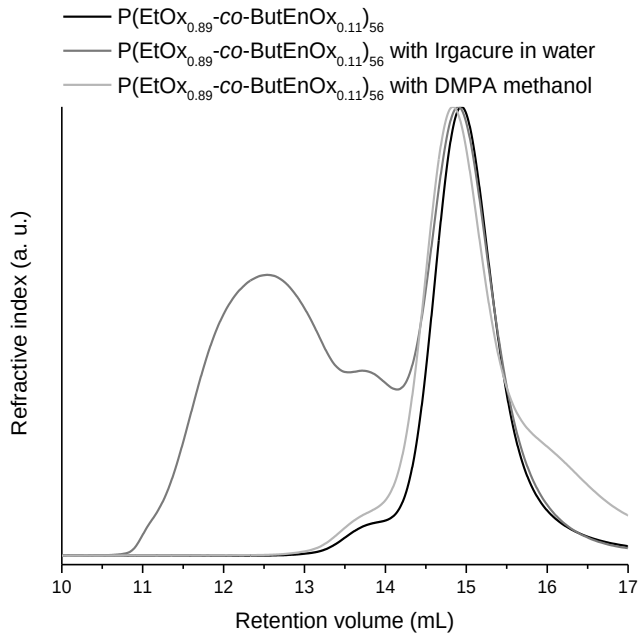

Figure 66: SEC elugram of parent polymer (black line), after reaction in water with photo-initiator (grey line) and after reaction with photo-initiator in methanol (light grey line).

After these findings, the thiol-ene reaction between the copolymer and MOMA was always carried out in methanol, which was degassed before the addition of MOMA to reduce the risk of disulfide formation due to dissolved oxygen. ^{1}H NMR spectroscopy confirmed the successful addition and complete conversion of all side chains after

dialysis of the polymer leading to P(EtOx-*co*-ButOxMOMA) (Figure 67). The SEC elugram also showed a monomodal distribution (Figure 136) and the IR spectrum showed the characteristic vibration of the carboxylic acid (C=O) at 1730 cm^{-1} and the bending vibration of the secondary amide (N-H) at 1540 cm^{-1} of the attached MOMA.

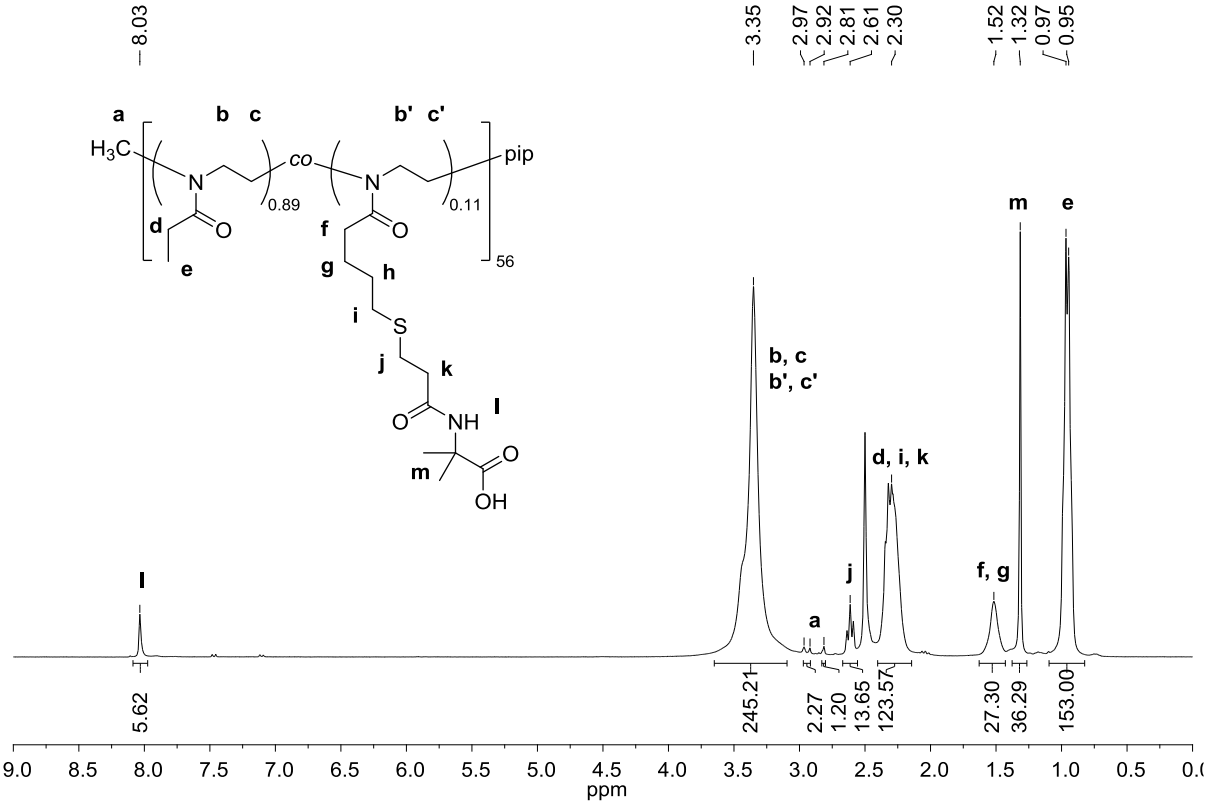

Figure 67: ^{1}H NMR of $P(EtOx_{0.89}\text{-}co\text{-}ButOxMOMA_{0.11})_{56}$ measured in DMSO-d_6.

The ring closure of MOMA to the azlactone ring was then performed under dry conditions using triethylamine and ethyl chloroformate in DMF following the protocol for the synthesis of VDM [136] (Figure 68). The base triethylamine catalyzes the reaction of ethyl chloroformate to the carboxylic acid of MOMA. Subsequently, the azlactone ring is closed through the attack of the carbonyl group at the carboxylic anhydride releasing ethyl hydrogen carbonate (Figure 69). The successful conversion could be detected by ^{1}H NMR spectroscopy, where the signal of the proton of the amide was no longer visible at 8.03 ppm (Figure 70), and by IR spectroscopy, where the vibrations for the carboxylic acid as well as for the secondary amide were also no longer present but the characteristic peak for the carbonyl group of the azlactone ring was visible at 1816 cm^{-1} [136]. The distribution of the functionalized polymer was still

monomodal and no peak widening was observed, showing that the experimental conditions had not led to any side reactions (Figure 72).

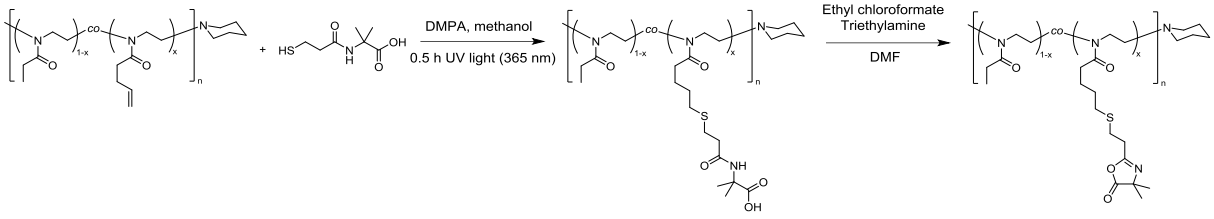

Figure 68: Synthesis scheme of azlactone functionalized P(EtOx-*co*-ButOxAL) starting from P(EtOx-*co*-ButEnOx).

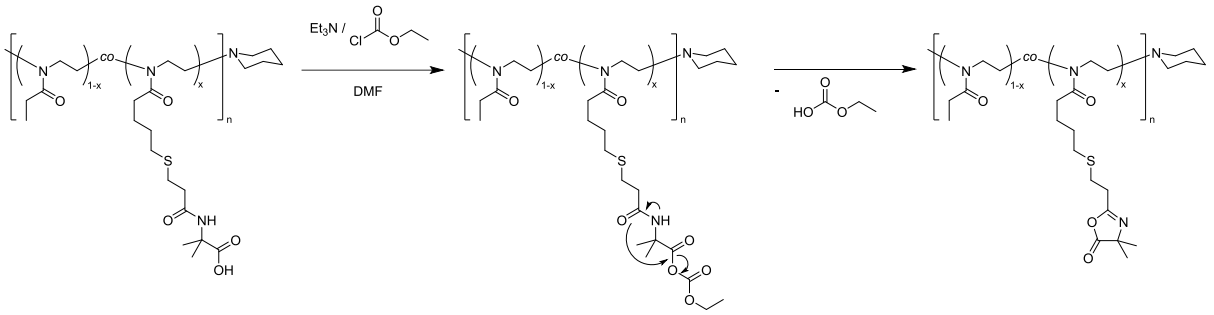

Figure 69: Reaction scheme of the *in-situ* azlactone ring closure at the polymer side chain.

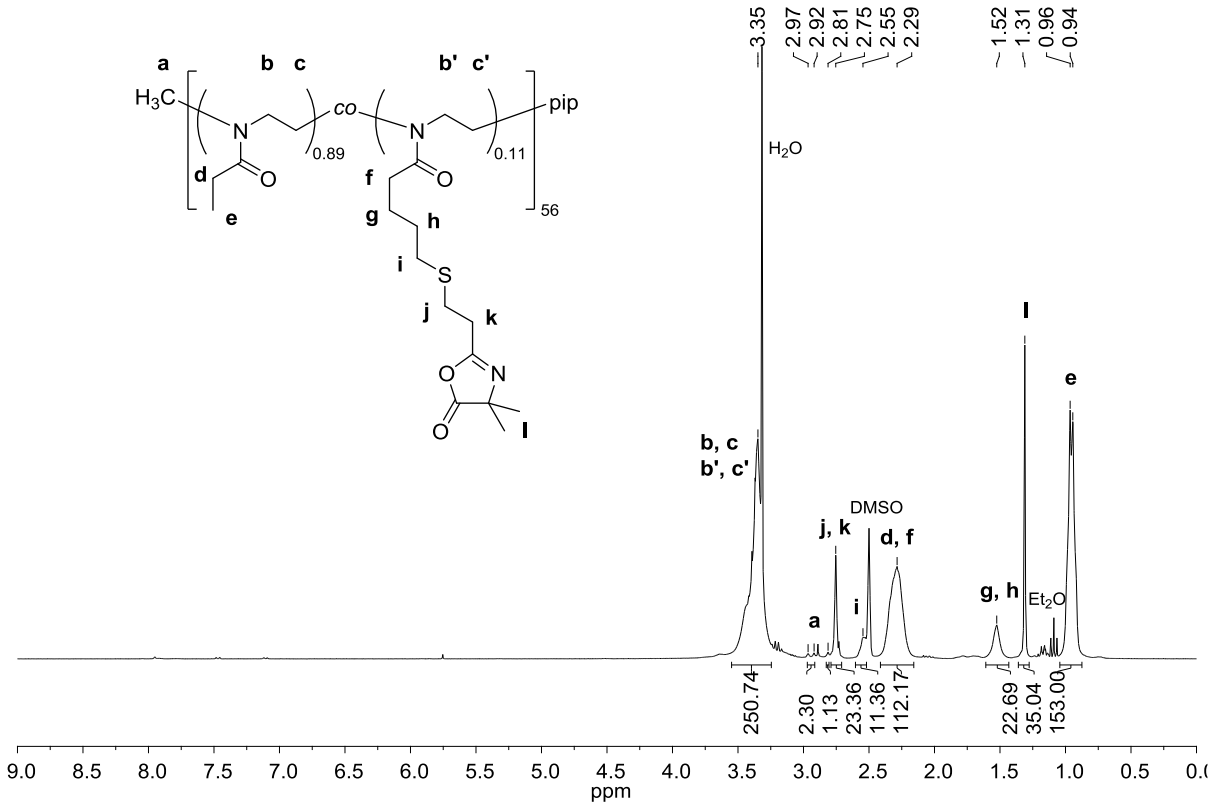

Figure 70: ^{1}H NMR of P(EtOx$_{0.89}$-*co*-ButOxAL$_{0.11}$)$_{56}$ measured in DMSO-d$_6$.

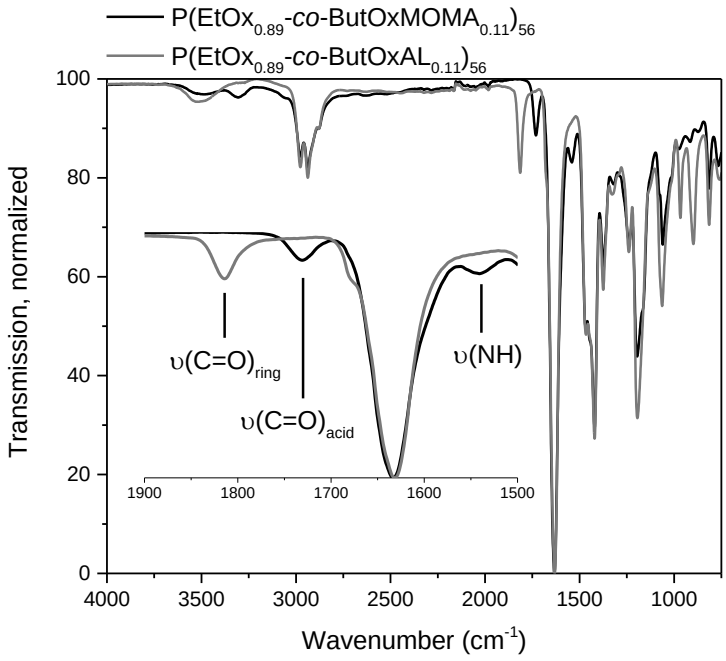

Figure 71: Stacked IR spectra of P(EtOx$_{0.89}$-*co*-ButOxMOMA$_{0.11}$)$_{56}$ and P(EtOx$_{0.89}$-*co*-ButOxAL$_{0.11}$)$_{56}$ showing the distinct vibrations for each functionality.

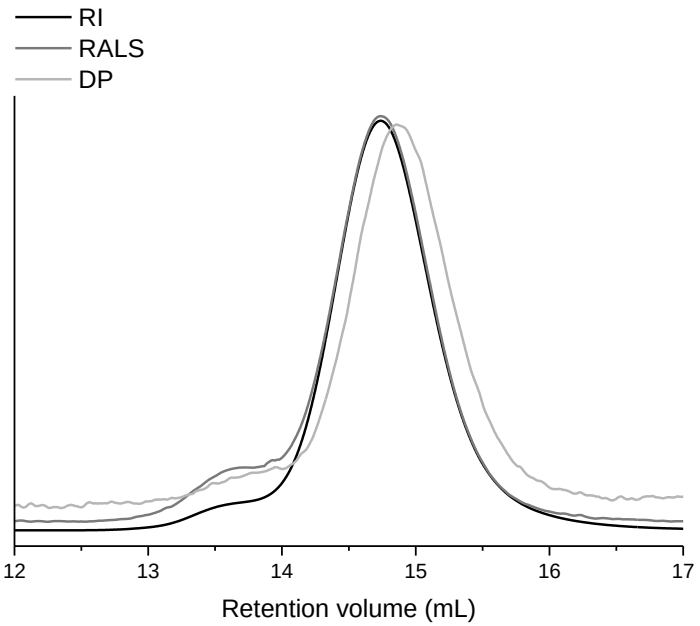

Figure 72: SEC elugram of P(EtOx$_{0.89}$-*co*-ButOxMOMA$_{0.11}$)$_{56}$ measured in DMF.

3.3 Application of Functionalized Poly(oxazoline)s

The functionalized copolymers described in chapter 3.2 were used to prepare hydrogels based on radical mediated thiol-ene chemistry or on catechol cross-linking through oxidation. Furthermore, the attachment of peptides to the side chain functional copolymers was performed using thiol-ene chemistry for vinyl functional copolymers or native chemical ligation for thiolactone and azlactone moieties under different reaction conditions. The results of the mentioned applications are shown in this chapter.

3.3.1 Thiol-ene Cross-linked Hydrogels

The vinyl and thiol side functional copolymers were used to fabricate hydrogels cross-linked via thiol-ene chemistry using the photo-initiator Irgacure 2959 in aqueous solution. The following polymer combinations were used to produce hydrogels:
P(EtOx$_{0.91}$-*co*-ButEnOx$_{0.09}$)$_{56}$ with P(EtOx$_{0.91}$-*co*-ButOxSH$_{0.09}$)$_{56}$;
P(EtOx$_{0.79}$-*co*-ButEnOx$_{0.21}$)$_{53}$ with P(EtOx$_{0.79}$-*co*-ButOxSH$_{0.21}$)$_{53}$;
P(MeOx$_{0.91}$-*co*-ButEnOx$_{0.09}$)$_{56}$ with P(MeOx$_{0.91}$-*co*-ButOxSH$_{0.09}$)$_{56}$ and
P(MeOx$_{0.81}$-*co*-ButEnOx$_{0.19}$)$_{49}$ with P(EtOx$_{0.81}$-*co*-ButOxSH$_{0.19}$)$_{49}$,
abbreviated **HGEt10**, **HGEt20**, **HGMe10** and **HGMe20** respectively.

3.3.1.1 Hydrogel Preparation

The functional copolymers were dissolved in water or 1xPBS buffer so that the ratio of vinyl functionality to thiol functionality was 1:1 and copolymers with the same percentage of functionality were combined. After complete dissolution, the photo-initiator Irgacure (concentration of the stock solution was 2.5 mg/mL) was added so that the overall concentration of the polymer was 15 wt% and the concentration of the photo-initiator was 0.05 wt%. The concentration of Irgacure was chosen to be 0.05 wt% as it had been shown that this amount is not cell toxic for various cell lines for irradiation times up to 10 min at 4 or 8 mW/cm^{-2} [99, 165]. The handlamp that was used for the fabrication of the hydrogels had a power of 1 mWcm^{-2} and the irradiation time was 15 min.

The synthesis scheme for the fabrication of the hydrogels is shown in Figure 73.

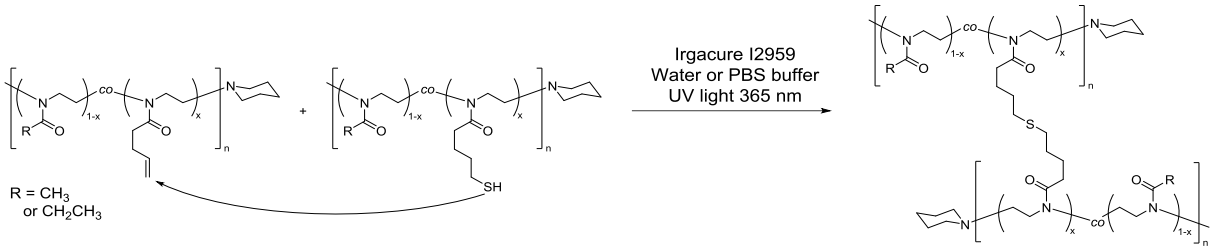

Figure 73: Synthesis scheme for the fabrication of thiol-ene cross-linked hydrogels.

The hydrogel precursor solution was pipetted into clear cylindrical silicon molds with a diameter of 4 mm and a height of 4 mm. The fabrication could be performed at room temperature except for the hydrogel precursor solution containing P(EtOx$_{0.79}$-*co*-ButOxSH$_{0.21}$)$_{53}$ (P21-thiol), which had to be cooled with ice due to its low cloud point.

As a control experiment, only vinyl functional polymer was dissolved to a concentration of 15 wt% with Irgacure as initiator and irradiated for 15 min. The solution stayed liquid, which indicates that homo-polymerization between the vinyl functionalities is not the main mechanism for the network formation as it had been observed for the preparation of hydrogels based on P(MeOx-*co*-DecEnOx) by Dargaville *et al.* [77] caused by hydrophobic interactions of the long alkyl chain. However, it cannot be excluded that homo-polymerization does not happen at all.

3.3.1.2 Hydrogel Characterization

3.3.1.2.1 Swelling Behavior

The polymer content was kept constant at 15 wt% to be able to compare how the cross-linking degree and the different hydrophilicity of the hydrogel network influences the hydrogel properties. The mass change over time (four weeks) was measured gravimetrically in 1xPBS at 37 °C (to mimic the human body environment) and at 4 °C, for the hydrogel specimens which had been fabricated from polymers with a T_{CP} (Figure 75 and Figure 76). The mass change that could be observed was not caused by a degradation of the network, but by the ability of the hydrogel network to bind water as the volume change was consistent with the mass change (Figure 77). In addition, the value for the gel fraction did not indicate any major loss of polymer except for HGMe10, where an incomplete cross-linking could be the reason

for a mass loss of ~23 % (Table 8). Hydrogels based on EtOx (HGEt10 and HGEt20) reached their equilibrium state after one week of incubation. Afterwards, no further significant change could be observed. Hydrogels based on MeOx (HGMe10 and HGMe20) reached their equilibrium state after two weeks of incubation and no further significant change until week four could be observed.

Hydrogel specimens with MeOx as main monomer and the lowest degree of functionalization (HGMe10) showed the highest mass increase (130 %) and the highest swelling degree (SD) of 8.1 at 37 °C after 24 h (Table 8). When the functionality was increased to 20 mol%, and hence the cross-linking degree increased, the hydrogel was less able to swell with a mass decrease to ~95 % and a SD of 4.9 at 37 °C. The gel fraction was only ~77 % for HGMe10 and it increased to ~85 % for HGMe20. The hydrophilicity of the polymer chains might on the hand lead to better dissolution in water and less entanglement resulting in a lower probability of the functional groups to bind to each other. On the other hand, the widened network can lead to a better diffusion of unbound polymer chains out of the network.

Hydrogels based on the more hydrophobic monomer EtOx with 10 mol% functionality showed a mass decrease to ~85 % after 24 h of incubation at 37 °C and a SD of 4.8, which is about two thirds of the SD of HGMe10, showing the extreme significance of the shorter alkyl chain of MeOx on the ability of the network to bind water, which had already been observed by Dargaville *et al.* [22] and Šrámková *et al*. [113]. When the degree of functionalization is increased to 20 mol%, the mass of the hydrogel specimens decreases to ~50 % after 24 h at 37 °C and the SD is lowered to 2.6. The gel fraction was ~83 % for HGEt10 and ~89 % for HGEt20. The high gel fraction, especially for HGEt20, might be caused by the collapsed network, which allows less unbound polymer chains to diffuse out of the gel. The collapse of the hydrogel network at temperatures above room temperature is not surprising as the T_{CP} of P(EtOx$_{0.79}$-*co*-ButOxSH$_{0.21}$)$_{53}$ was already at 23.5 °C and it was published that the formation of cross-links will lead to further decrease of the cloud point [79].

The highest swelling was, however, recorded for HGEt10 when it was incubated at 4 °C with a mass increase of ~150 % after 24 h, which is nearly twice the mass as at 37 °C. The same was observed for HGEt20, where the mass change was ~90 % at 4 °C instead of 50 % at 37 °C. The swelling degree increased accordingly to 9.4 for HGEt10 and 5.8 for HGEt20. This change could also be seen visually (Figure 74).

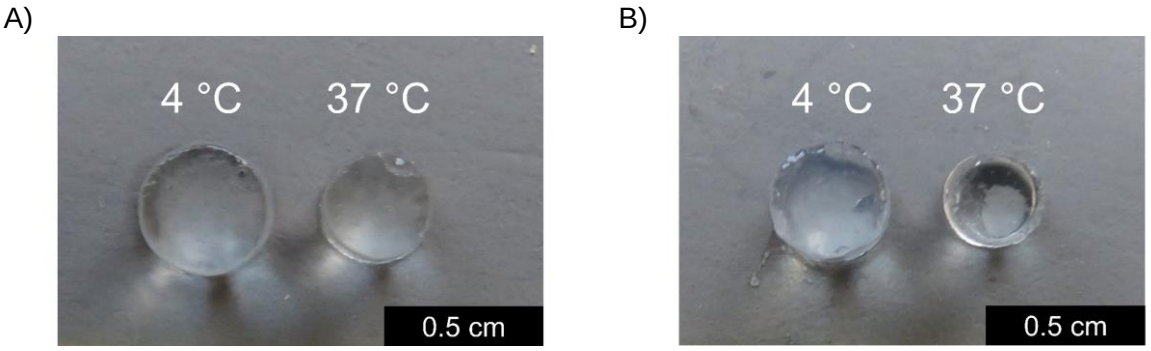

Figure 74: Photographs of exemplary hydrogels of A) HGEt10 and B) HGEt20 at 4 °C and 37 °C in PBS after 24 h.

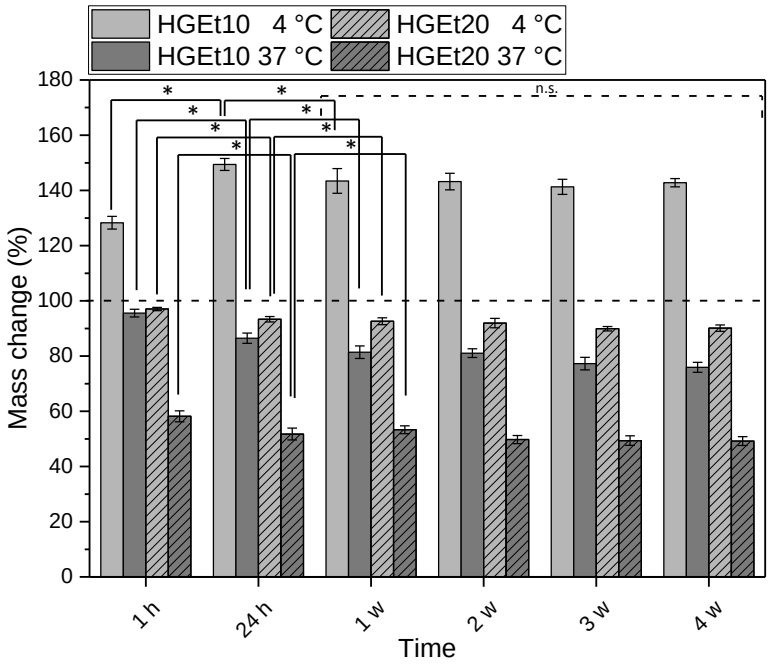

Figure 75: Swelling behavior of thiol-ene cross-linked hydrogels based on the co-monomer EtOx in 1xPBS at 4 °C and at 37 °C, over a time course of 4 weeks. Mean and standard deviation shown (n = 4). Statistical significance shown with * ($p < 0.050$) and n.s. (no significant difference between the same type of hydrogel on consecutive time points).

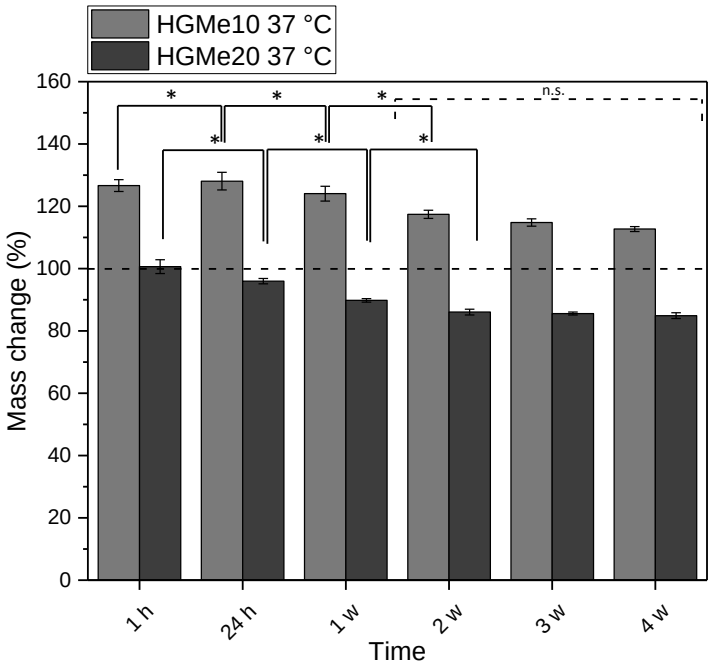

Figure 76: Swelling behavior of thiol-ene cross-linked hydrogels based on the co-monomer MeOx in 1xPBS at 37 °C, over a time course of 4 weeks. Mean and standard deviation shown (n = 4). Statistical significance shown with * ($p < 0.050$) and n.s. (no significant difference between the same type of hydrogel on consecutive time points).

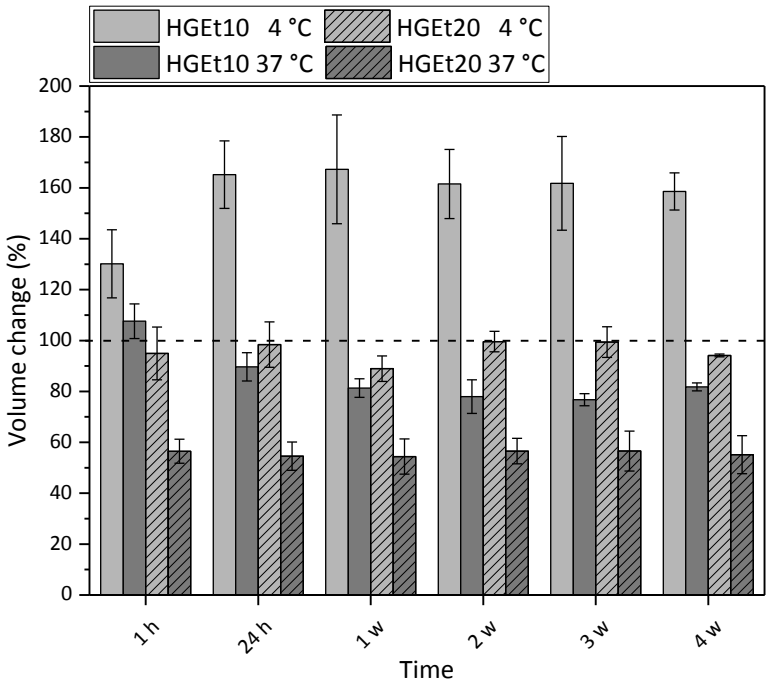

Figure 77: Volume change of thiol-ene cross-linked hydrogels based on the co-monomer EtOx in PBS at 4 °C and 37 °C, over the time course of 4 weeks. Mean and standard deviation shown (n = 4).

Table 8: Swelling degree and gel fraction of thiol-ene cross-linked hydrogels in PBS after 24 h at 37 °C or at 4 °C for thermo-responsive hydrogels. Mean and standard deviation shown (n = 3).

Hydrogel sample	Temperature (°C)	SD*	Gel fraction (%)[#]
HGEt10	37	4.8 ± 0.1	83.1 ± 0.3
HGEt10_4	4	9.4 ± 0.3	n.d.
HGEt20	37	2.6 ± 0.2	88.7 ± 2.3
HGEt20_4	4	5.8 ± 0.2	n.d.
HGMe10	37	8.1 ± 0.1	77.5 ± 1.9
HGMe20	37	4.9 ± 0.1	85.5 ± 0.5

*swelling degree (SD) = $(w_s-w_d)/w_d$, [#]Gel fraction = $w_g/w_i \cdot 100$

Christova *et al.* [79] had observed a Type I LCST behavior for PEtOx hydrogels synthesized by radical network formation. To determine whether the thiol-ene cross-linked hydrogels also showed the same behavior, HGEt20 was incubated first at 5 °C and the weight recorded and referenced as m_0. The hydrogel specimens were then incubated in continuous steps up to 60 °C with an incubation time of 24 h at each point (Figure 78). The slope shows a continuous deswelling of the hydrogel with increasing temperature, comparable to the finding of Christova *et al*., which indicates that these hydrogels also underly a Type I LCST behavior.

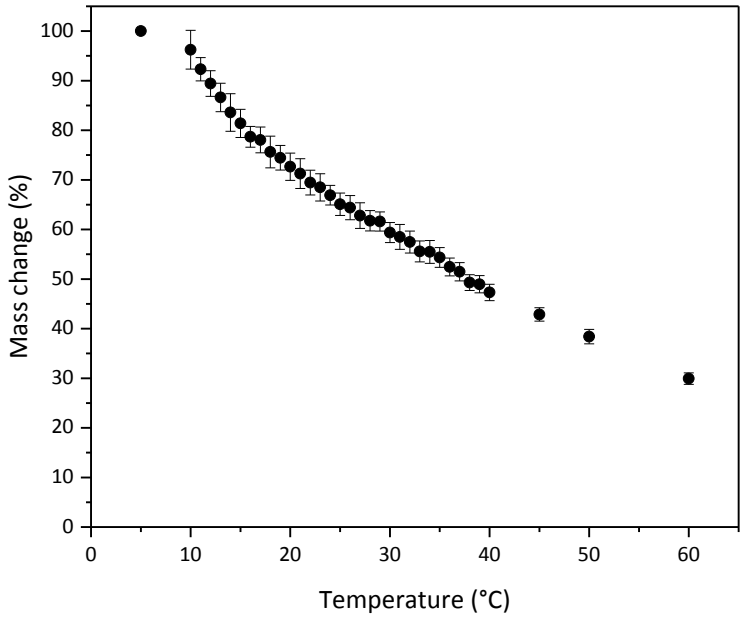

Figure 78: Mass change of HGEt20 in PBS starting from 5 °C to 60 °C. Mean and standard deviation shown (n = 3). Mean and standard deviation shown (n = 3). Figure was adapted from [166] – copyright by The Royal Society of Chemistry.

Besides the effect of temperature on the hydrogels, it was also observed that salts influenced the ability to swell of the hydrogels. When HGEt10 was incubated in ultrapure water, the mass increased to 120 % in contrast to 85 % in 1xPBS. This significant difference was maintained over a time course of four weeks (Figure 79). The influence of salts on the water binding capacity of poly(2-alkyl-2-oxazoline)s has already been examined by Bloksma *et al*. who observed that the LCST is lowered by various types of salts with an increasing influence with increasing salt concentration [167]. This effect can also be observed for cross-linked hydrogels which can hold up significantly less water molecules in buffered medium than in pure water.

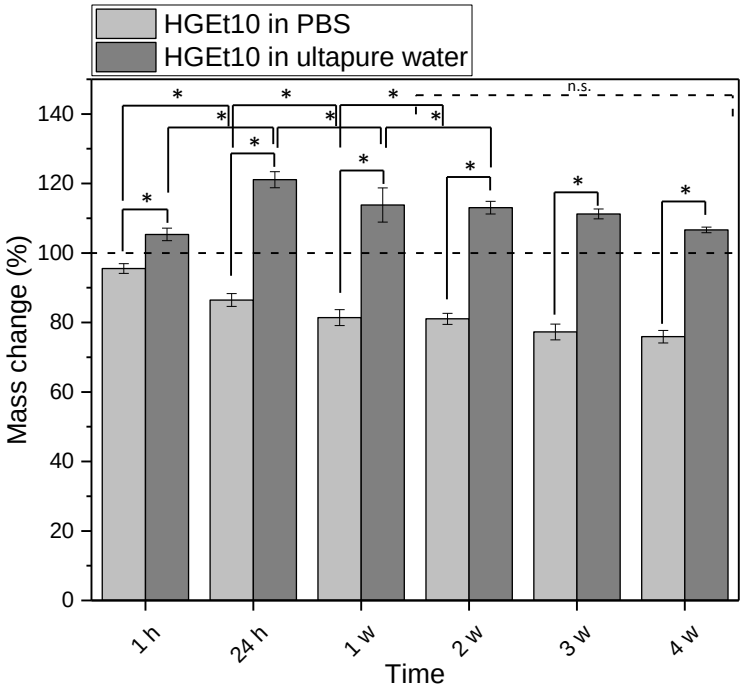

Figure 79: Swelling behavior of HGEt10 in PBS vs. ultrapure water over the time course of 4 weeks at 37 °C. Mean and standard deviation shown (n = 3).

3.3.1.2.2 Mechanical Properties

The Young's modulus (or compressive modulus) was measured at the same time points as the mass change, but it was found that the modulus did not change significantly after 24 h over the course of two weeks. The Young's modulus (YM) in relation to the swelling degree of each hydrogel type at 37 °C in PBS, and at 4 °C for hydrogels displaying a temperature dependent behavior is shown in Figure 80. The YM ranged from ~120 kPa (HGEt10) to ~375 kPa (HGEt20) for hydrogels at 37 °C.

Whereas the YM was comparable for hydrogels with only 10 % functionality but different polymer backbone, HGMe10 and HGEt10, the YM of hydrogels with 20 % functionality increased by 100 kPa from HGMe20 to HGEt20. As discussed before, the SD decreased for hydrogels with the same percentage of functionality but a greater hydrophobicity due to the longer alkyl chain of EtOx. Even though the SD of HGMe20 and HGEt10 is similar, the reduced cross-linking density leads to a weaker YM. The hydrogel with the lowest SD also exhibits the highest YM, i.e. HGEt20, which can be explained by the denser network in combination with the less hydrophilic polymer backbone. Hydrogels which were incubated at 4 °C showed a decrease in the YM compared to the same type incubated at 37 °C, but only of about ~35 kPa. The impact on the SD was much greater where values roughly doubled. Comparing HGMe10 with HGEt10 at 4 °C, it is interesting to note that the YM decreased with an increased SD, which makes sense as the network can bind more water molecules and is as a result softer. Comparing HGMe20 with HGEt20 at 4 °C, the YM is still far higher for HGEt20 even though the SD is slightly higher which again corroborates with the observation made earlier that the cross-linking degree influences the YM the most.

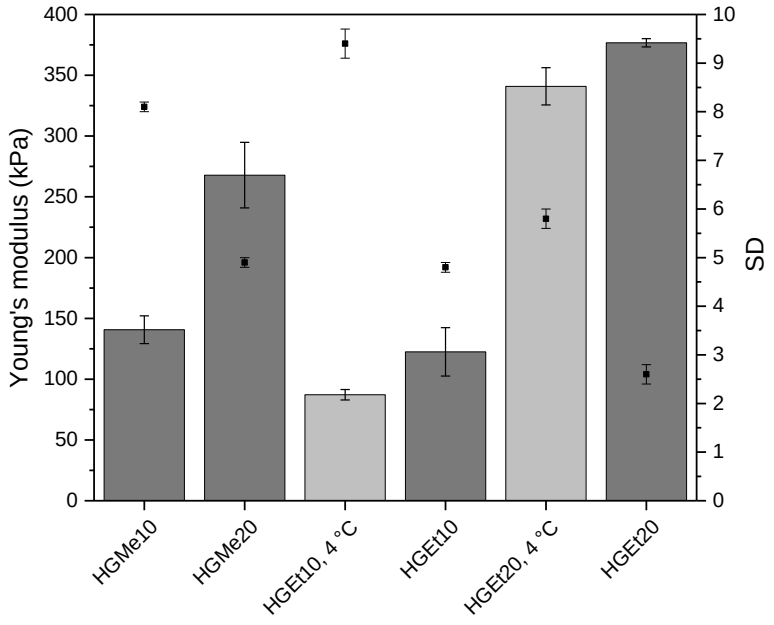

Figure 80: Young's modulus (columns) and swelling degree (squares) of thiol-ene cross-linked hydrogels after 24 h incubation in PBS at 37 °C (dark grey) and at 4 °C (light grey). Mean and standard deviation shown (n = 3).

3.3.1.2.3 Solid-state NMR of Hydrogels

^{1}H-^{13}C cross-polarization (CP) and Magic Angle Spinning (MAS) NMR spectra were recorded of the vinyl and thiol functional polymeric precursors as well as of the cross-linked hydrogel (Figure 81). The spectra of the functional polymers are very similar. The signals for the backbone, amide unity and ethyl moiety are visible in both spectra. There are also signals belonging to impurities which are comparable (grey boxes). The CH_2 groups of the vinyl side chain which are adjacent to the double bond are visible at 32.3 and 29.8 ppm. The signals of the vinyl unit can be found between 100 and 150 ppm. Two of the four CH_2 groups of the side chain of P(EtOx-*co*-ButOxSH) show signals at 32.9 ppm whereas the remaining CH_2 groups are overlaid by the main CH_2 resonance. There are no signals visible between 100 and 150 ppm for the thiol functionalized polymer. The same applies for the cross-linked hydrogel which indicates that all vinyl groups have reacted. Unfortunately, it was not possible to examine with this method if the vinyl groups mainly reacted with thiols or if also homo-polymerization between vinyl chains had taken place.

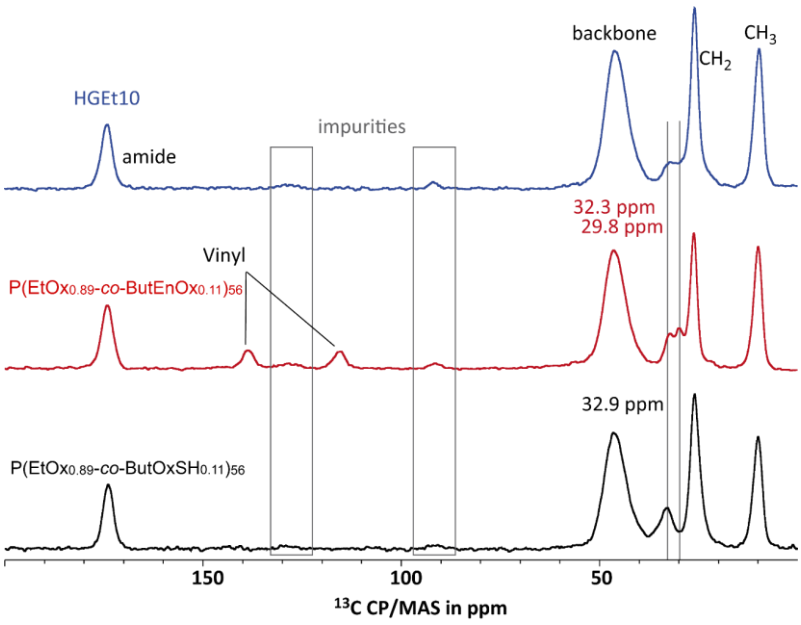

Figure 81: ^{1}H-^{13}C CP / MAS solid-state NMR spectra of the cross-linked hydrogel (blue) and the precursor polymers with vinyl (red) and thiol (black) side functionality.

3.3.1.2.4 Cryo SEM

Cryo scanning electron microscopy (SEM) was performed on freshly prepared samples of HGEt10 and HGEt20 in Milli-Q water. However, the hydrogels were only cross-linked for 5 min as the volume of each hydrogel was only a 2 µL – 3 µL. The 3D network structure is clearly visible for all samples (Figure 82). Nevertheless, the network seems wider for samples with a lower cross-linking degree (HGEt10) due to a lower functionalization of the precursor polymers. At higher magnification, finer structures with small pores are visible. These might be caused by an insufficient fast freezing of the hydrogels. Even though the samples were frozen as fast as possible in a self-made sample holder using slushed nitrogen, such structures could not be suppressed.

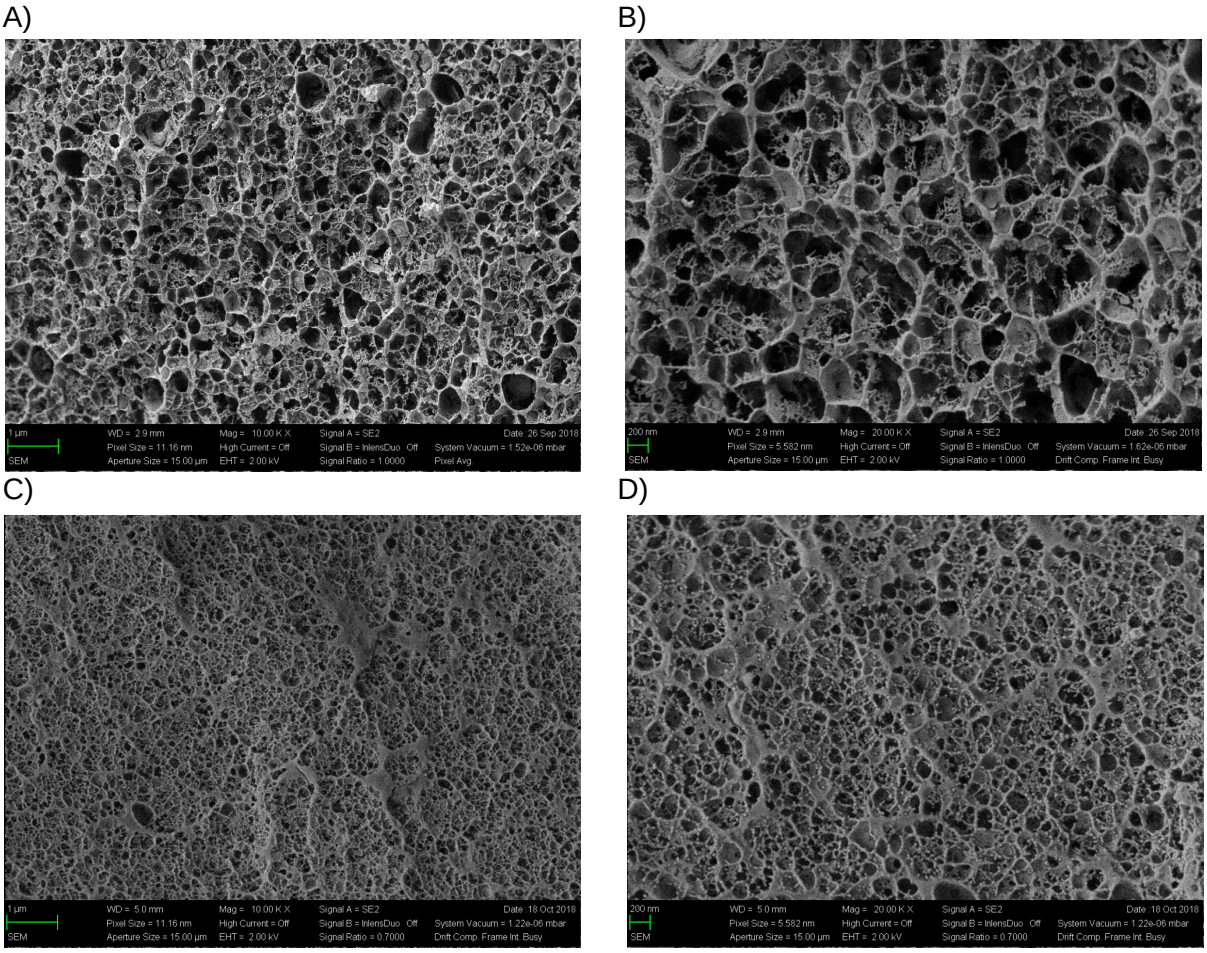

Figure 82: Cryo SEM images of A) HGEt10 at 10k magnification, B) HGEt10 at 20k magnification, C) HGEt20 at 10k magnification and D) HGEt20 at 20k magnification.

3.3.1.2.5 Cytotoxicity of Hydrogels

Hydrogels were synthesized in sterile PBS buffer and placed on top of a cell layer (mouse fibroblasts, L 929) in a 48-well plate. As a negative control, 2 wt% agarose hydrogels were used to eliminate any mechanical influence that the hydrogel specimen might have when placed on top of the cell layer and as positive control, the eluate of PVC plates was used. The hydrogels were incubated for 7 days. Afterwards, the cell proliferation reagent WST-1 solution was added, and the absorbance was measured. The cell viability was very good for all hydrogels (Figure 83) implying that the released amount of initiator and polymer chains, that were not incorporated into the network during incubation, are not cell toxic. These findings confirm the good cell compatibility, which had already been demonstrated in literature, for the same initiator system [34, 113].

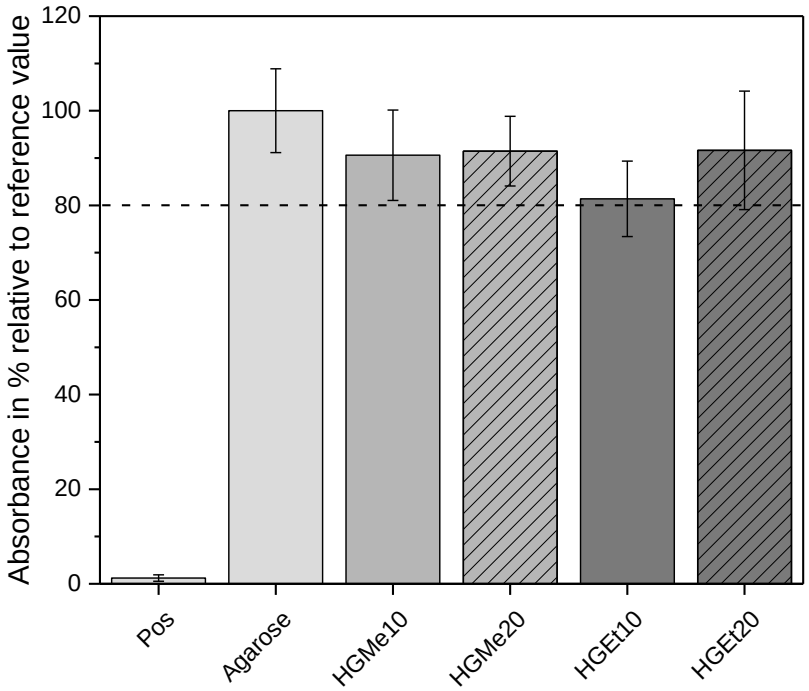

Figure 83: WST cell viability assay of thiol-ene cross-linked hydrogels after 7 d in direct cell contact.

3.3.1.3 Release of FITC-Dextran

The polymeric hydrogel precursor solutions of HGEt10 and HGEt20 were mixed with defined amounts of fluorescein isothiocyanate-labeled dextran (FITC-dextran) with a molecular weight of 4 kDa, 40 kDa and 500 kDa prior to cross-linking. The loaded hydrogels were incubated at 37 °C in PBS for 15 d, except for HGEt20 which was additionally incubated at 4 °C to observe the effect of a more swollen network on the release. In general, the FITC-dextran molecule with 4 kDa was released to the largest extent (22 % – 25 % of the total amount incorporated) compared to FITC-dextran with higher molecular weight (Figure 84). An exception to this is FITC-dextran with a molecular weight of 40 kDa, which was released from HGEt10 to 40 % of the total amount. One explanation for this could be that these samples were loaded with twice the amount of dextran per hydrogel specimen, as the FITC labeling was lower (0.001 mol – 0.008 mol FITC/mol glucose compared to 0.002 mol – 0.020 mol FITC/mol glucose for dextran with 4 and 500 kDa). Hence, it can be assumed that the network of HGEt10 is wide enough to be able to release macromolecules with a molecular weight of 40 kDa to the same extent as smaller macromolecules, whereas molecules with a molecular weight of 500 kDa are no longer able to diffuse so easily. FITC-dextran with 40 kDa and 500 kDa is released up to ~10 % for HGEt20 at 4 °C and up to ~19 % for HGEt20 at 37 °C. One would assume that the dextran molecules would be able to diffuse more easily from the hydrogel at 4 °C as it is more swollen at this temperature. However, the hydrogels had to be prepared in the cold to prevent precipitation. This means that the hydrogels shrunk when they were put from the cold silicon mold into the warm PBS solution. This could have led to the increased release at 37 °C as the dissolved macromolecules were pushed out of the network due to the collapse of the network structure. The release profile in the first 24 h (Figure 85) shows a burst release with a steady but rather small increase in released dextran over time. The system could however be improved by the incorporation of degradable bonds which would ensure complete release of the dextran molecules.

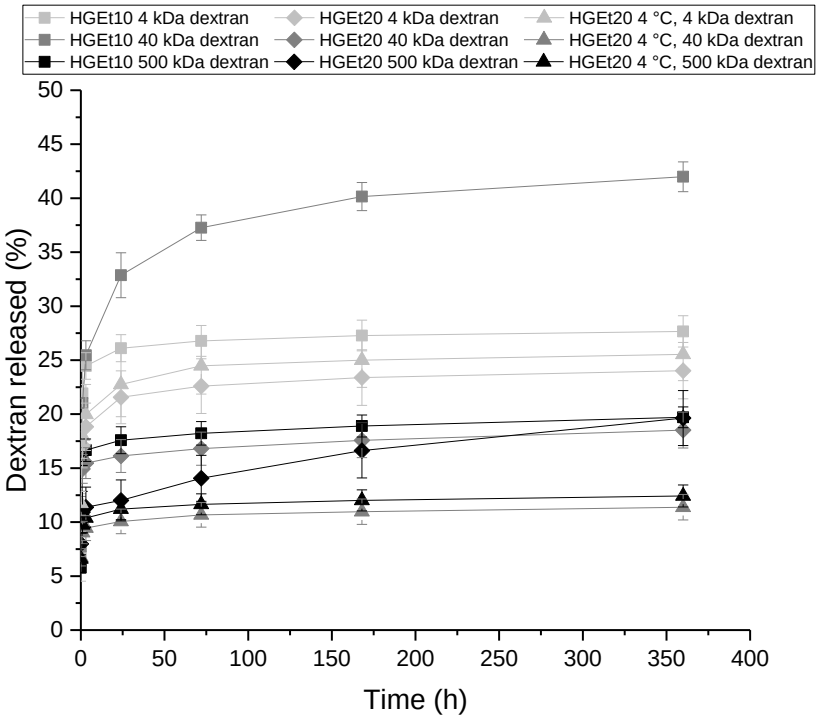

Figure 84: Release of FITC-dextran with 4 kDa, 40 kDa and 500 kDa molecular weight from HGEt10 at 37 °C and HGEt20 at 4 °C and 37 °C in PBS. Mean and standard deviation shown (n = 3).

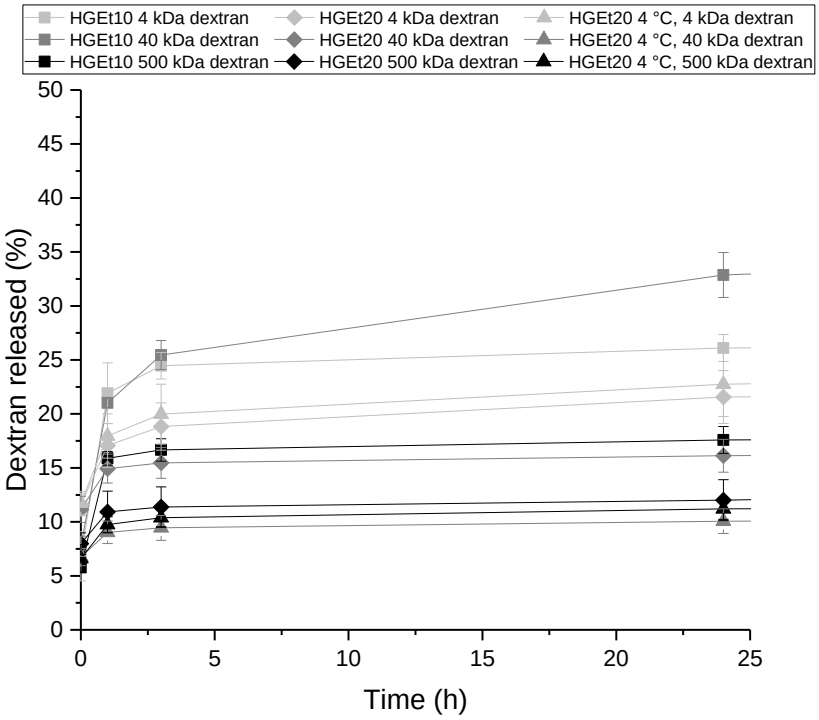

Figure 85: Zoom in on the first 24 h of the release of FITC-dextran with 4 kDa, 40 kDa and 500 kDa molecular weight from HGEt10 at 37 °C and HGEt20 at 4 °C and 37 °C in PBS. Mean and standard deviation shown (n = 3).

3.3.1.4 Interaction with Dyes

To test the influence of the hydrophilicity of the hydrogel network, two well detectable dyes, fluorescein sodium salt (FSN) and methylene blue (MB) (chemical structure Figure 86) were chosen. FSN is well soluble in water with 500 g/L and MB is less water soluble with only 43.6 g/L at room temperature. It was observed that MB was even less water soluble when stored in the cold, which could be confirmed by UV/Vis measurements showing a decrease in absorption. The maximum solubility at 4 °C was calculated to be 11.8 g/L from these measurements. All hydrogels were prepared as described and afterwards incubated in the dye solution at room temperature or additionally at 4 °C for the thermo-responsive HGEt10 and HGEt20 hydrogels. This approach was chosen since the dyes would interfere with the thiol-ene photo reaction and hence comparability of cross-linking was ensured.

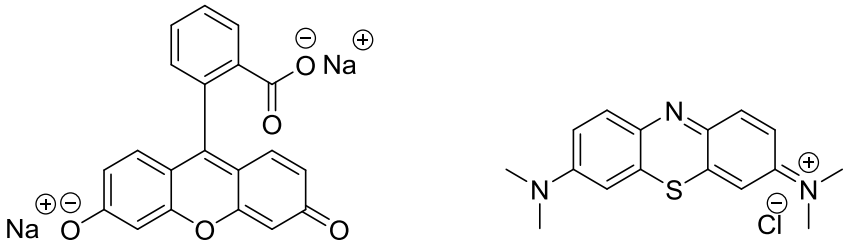

fluorescein sodium salt methylene blue

Figure 86: Chemical structure of dyes fluorescein sodium salt and methylene blue.

Under the assumption that the dye solution would equally diffuse into the hydrogel specimen, it was presumed from the concentration of the dye solution that every hydrogel would contain approximately 2 mg of MB or 3 mg of FSN based on the volume of the loaded hydrogel.

Figure 87 shows the amount of MB that had been released after 48 h incubation and Figure 88 displays the release profile. No further MB was released after 48 h, even though the hydrogels were still colored (Figure 91A). The hydrogel HGMe10, which was the most swollen and hydrophilic due to the polymer backbone mainly made of MeOx, was able to release the highest amount of MB (1.7 mg) in contrast to HGMe20 (0.3 mg) followed by hydrogels HGEt10 and HGEt20 (~0.2 mg). Hydrogels stored at 4 °C released even less dye, which might be caused by the inferior water solubility of MB at colder temperatures. Looking at the photographs, HGMe10 and HGMe20 are of a dark blue color indicating that more dye was able to diffuse into the network and

could also be retained by it. Hydrogels HGEt10 and HGEt20 were of a much lighter blue color, from which it can be concluded that MB was less able to diffuse into the network resulting in smaller quantities released. The release profile shows a burst release during the first 10 h, after which only small quantities in the nanogram scale were released.

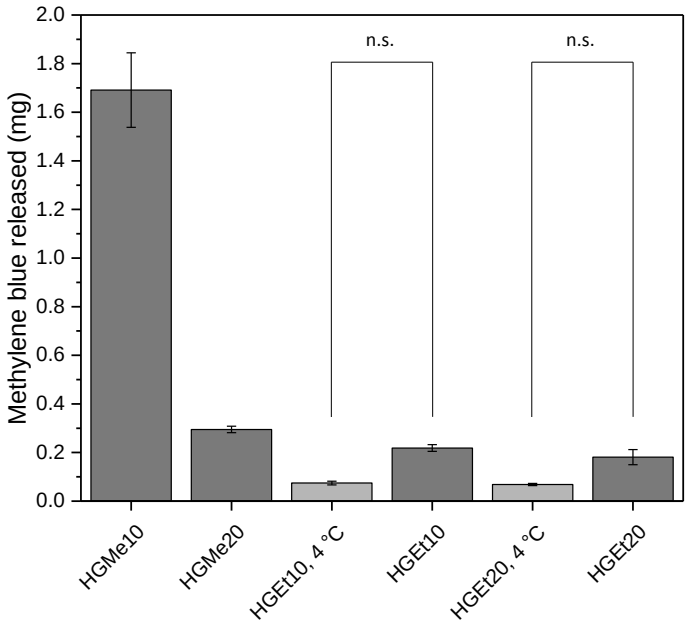

Figure 87: Amount of methylene blue released after 48 hours. There is a significant difference between the hydrogel types ($p < 0.05$) unless otherwise stated by n.s. (not significant). Mean and standard deviation shown ($n = 3$).

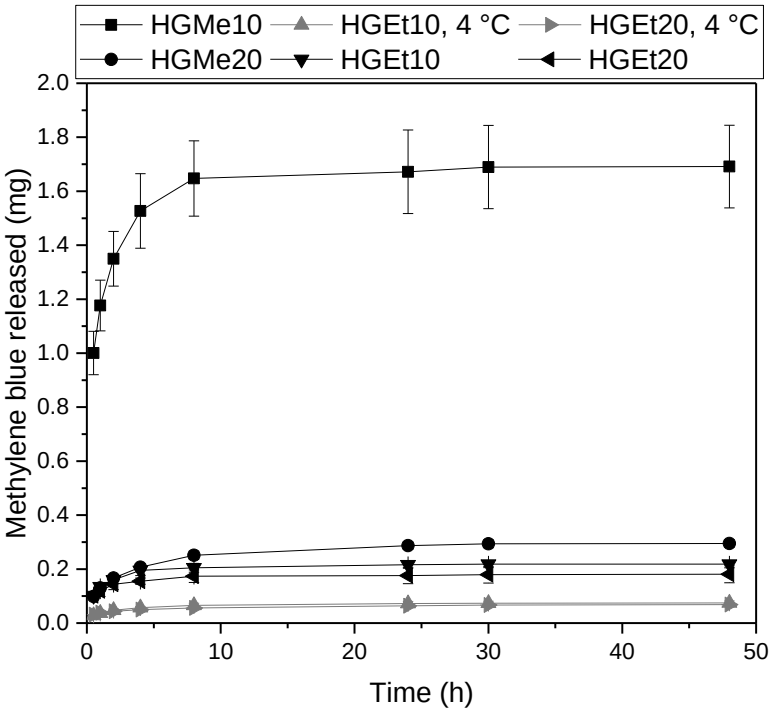

Figure 88: Release profile of methylene blue during the first 48 h. Mean and standard deviation shown (n = 3).

The hydrogels were also incubated in the more hydrophilic dye fluorescein sodium salt (FSN) for 24 h at 37 °C and at 4 °C for hydrogels HGEt10 and HGEt20. The amount released after 48 h was more equally distributed among the different hydrogel types (Figure 89). The cross-linking density played a less important role for the more hydrophilic network of HGMe10 and HGMe20 in contrast to the more hydrophobic network of HGEt10 and HGEt20, where HGEt20 released only two thirds of HGEt10. The most FSN was released from HGEt10 at 4 °C (~4 mg) which also displayed the highest swelling degree. The least FSN (2 mg) was released from HGEt20 at 37 °C, which had the lowest swelling degree. The release profile showed a similar burst release during the first 10 hours as it had been observed for MB (Figure 90). However, in contrast to MB, a release in the nanogram scale could still be observed up to 14 d, the end of the study. The coloring of the hydrogel specimens was rather uniform (Figure 91B) which fits the data of the mass that had been released. If one considers that there is still a lot of FSN retained in the hydrogel, which can be assumed from the strong coloring after 72 h, plus the amount that is already released, it becomes clear that FSN diffused into the hydrogel to a greater degree than it would have been possible by pure equilibrium during incubation. For an equal distribution, it had been assumed that 3 mg would diffuse into the hydrogel

volume. This amount is already exceeded by the amount that was released for all hydrogels except for HGEt20 at 37 °C. The high uptake and release behavior is in accordance with experiments performed by Luef *et al*. [112], where POx hydrogels were loaded with Eosin B, a dye very similar to FSN. Van der Heide *et al*. [114] also used the interaction between the dye Eosin Y and a POx hydrogel network for staining and as a result make the hydrogel network structures visible under a fluorescence microscope.

In summary, it was observed that the uptake of the more hydrophilic dye depended more on the ability of the hydrogel to swell. In contrast, the uptake of the more hydrophobic dye MB was less dependent on the swelling degree but much more on the hydrophilicity of the network.

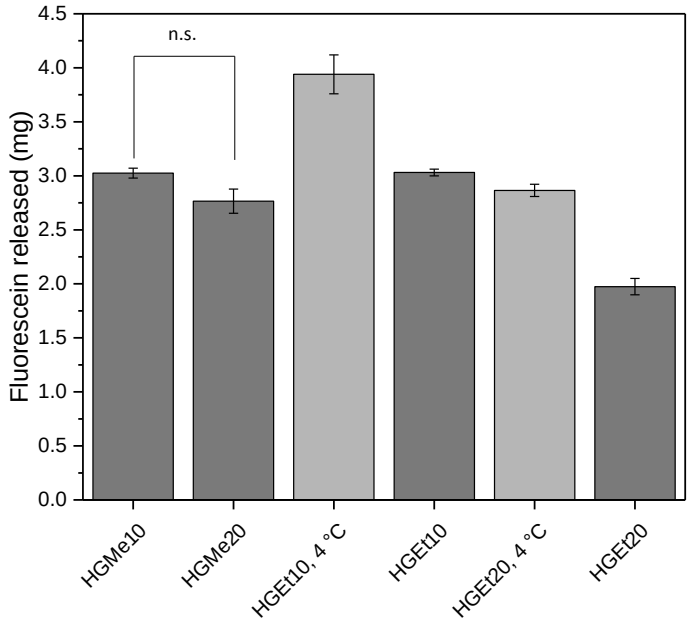

Figure 89: Amount of fluorescein sodium salt after 48 h. Mean and standard deviation shown (n = 3). There is a significant difference between the hydrogel types ($p < 0.05$) unless otherwise stated by n.s. (not significant).

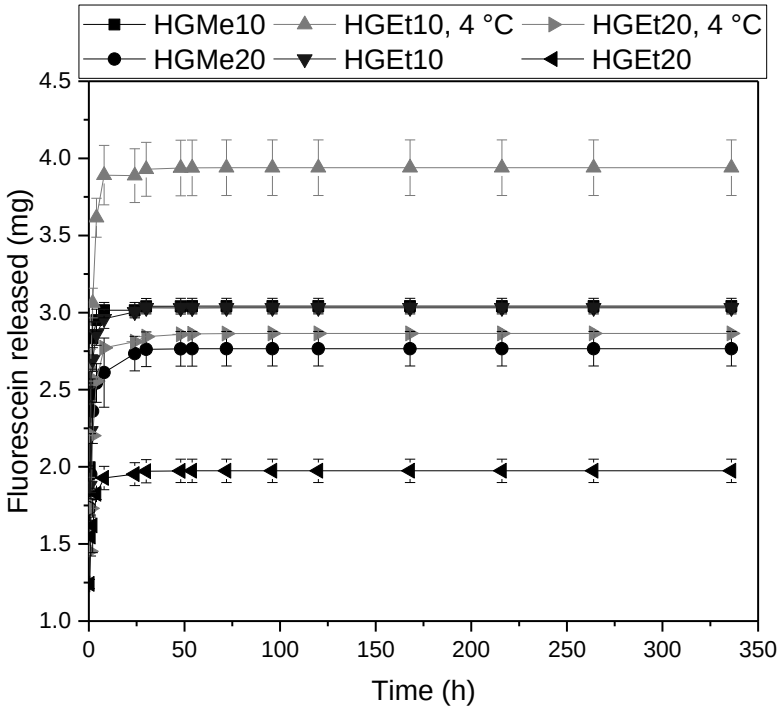

Figure 90: Release profile of fluorescein sodium salt for 14 days. Mean and standard deviation shown (n = 3).

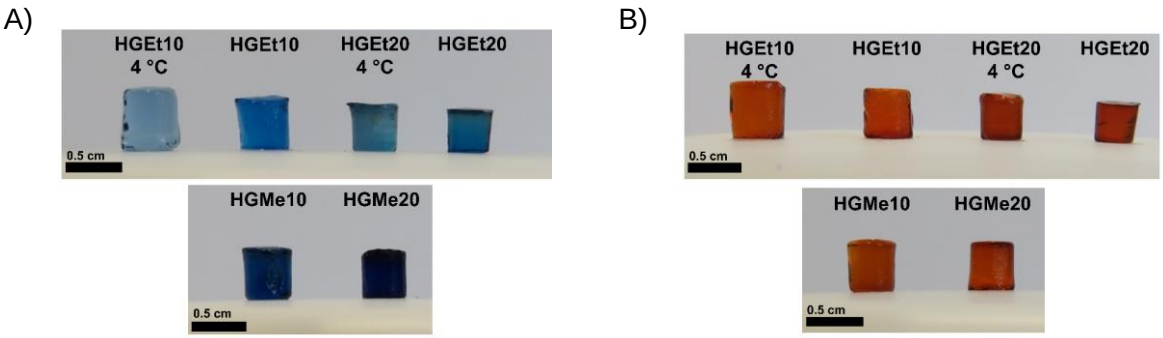

Figure 91: Exemplary photographs of hydrogels incubated in A) methylene blue and B) fluorescein sodium salt after 72 h in PBS.

3.3.2 Catechol Cross-linked Hydrogels

The catechol-functionalized copolymers, described in section 3.2.2, were used to form hydrogels based on the oxidation of a catechol group to a quinone group, which will react with other available quinones to form dicatechols [119]. Through the side chain functionalization, a three-dimensional network can be created (Figure 92, top). In addition, the catechol groups can react with a variety of nucleophiles, even under wet conditions, making it an ideal candidate to react with organic surfaces like tissues, e.g. cartilage.

Berdichevski *et al*. examined the influence of different biological macromolecules in hydrogels and found that PEG-fibrinogen and PEG-albumin hydrogels had only a mild cellular response [168]. For this reason, fibrinogen was added to the functionalized POx copolymers to improve overall cell compatibility and generate cell adhesive hydrogels. Fibrinogen also offers several nucleophiles, for example amine and thiol groups through amino acids like cysteine and lysine. These can react with the quinone group through Michael addition or Schiff base reaction [169] (Figure 92, bottom). Additionally, the protein fibrinogen is organized by a long α-helical coiled coil, which transforms into an extended β-strand conformation when mechanical force is applied [170]. This transformation makes fibrinogen a stretchable and soft fiber and positively influences the mechanical properties of the biohybrid hydrogel.

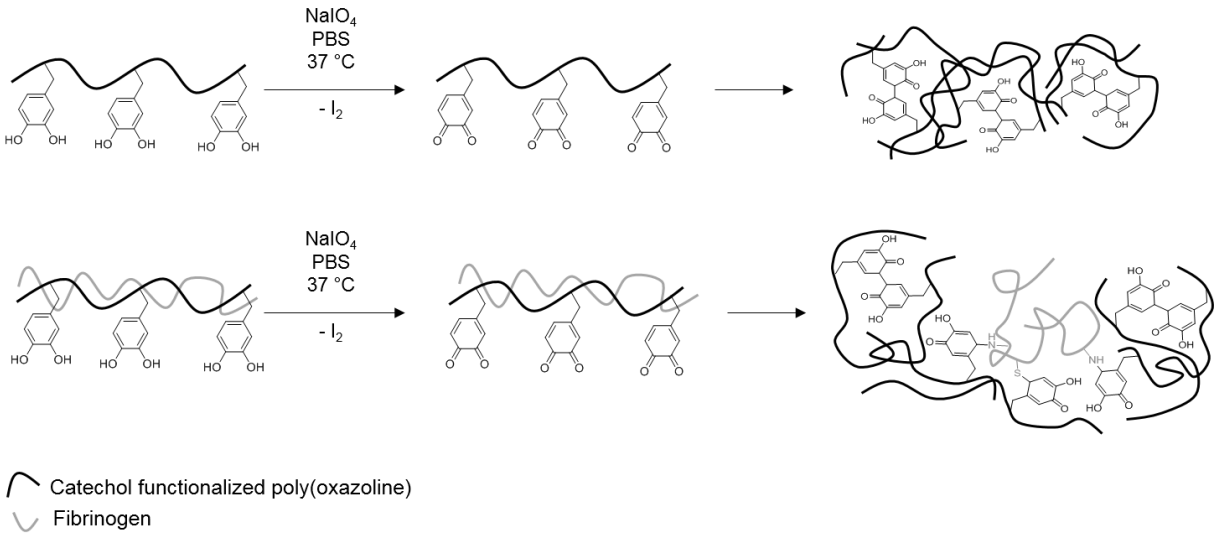

Figure 92: Reaction scheme of the hydrogel formation through oxidation of catechol-functionalized poly(oxazoline) with and without fibrinogen using $NaIO_4$ as oxidizing agent.

3.3.2.1 Hydrogel Preparation

Hydrogels without and with fibrinogen were prepared to analyze the influence of fibrinogen on the hydrogel characteristics.

First, the polymers P(EtOx-*co*-ButOxDOPAm) or P(MeOx-*co*-ButOxDOPAm) for hydrogels without fibrinogen were dissolved in 1xPBS to the desired w/v%. 40 µL of the stock solution was pipetted into the silicon molds with a volume of 50 µL. Then, 10 µL of an aqueous sodium periodate stock solution was pipetted to the hydrogel solution, which became brown colored and solid (Figure 93), when the colorless $NaIO_4$ was reduced to water insoluble iodine (I_2).

For hydrogels containing fibrinogen, a stock solution of the desired w/v% of the polymers P(EtOx-*co*-ButOxDOPAm) or P(MeOx-*co*-ButOxDOPAm) was prepared and always combined with a 12.5 w/v% stock solution of fibrinogen in PBS. Hydrogels were further prepared as described before.

Hydrogels containing only P(EtOx-*co*-ButOxDOPAc) or P(MeOx-*co*-ButOxDOPAc) could not be synthesized as the reaction kinetics were so fast that the pipette tip would clog as soon as the $NaIO_4$ solution came into contact with the hydrogel solution. Therefore, stock solutions where 25 % and 50 % of the total polymer mass contained polymer with hydrolyzable ester bonds were prepared, combined with fibrinogen as described above and cross-linked using $NaIO_4$. All hydrogels were cured under humid conditions at 37 °C before they were removed from the silicon mold and immersed in PBS.

A) B)

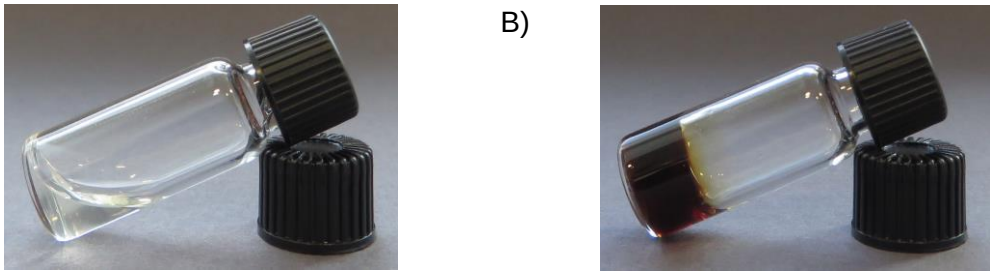

Figure 93: Photographs of A) hydrogel solution before addition of $NaIO_4$ (clear, colorless) and B) after addition of $NaIO_4$ (brown, solid).

3.3.2.2 Hydrogel Characterization

To determine how the different catechol functionalization degrees and the addition of fibrinogen influenced the elastic modulus, hydrogels with 12.5 w/v% polymer content of P(EtOx-*co*-ButOxDOPAm) or P(MeOx-*co*-DOPAm) (5 % vs. 8 % catechol functionality) without fibrinogen were prepared. In addition, hydrogels with 5, 7.5 and 10 w/v% polymer content and a constant 5 w/v% of fibrinogen were prepared to determine the right ratio of polymer to fibrinogen and to evaluate the influence of the protein on the mechanical properties. Figure 94A shows the results of the hydrogels made from P(EtOx-*co*-ButOxDOPAm) and Figure 94B shows the result of the hydrogels made from P(MeOx-*co*-DOPAm) after 24 h incubation at 37 °C in PBS. The Young's modulus of hydrogels, prepared from the polymer with 5 % catechol functionality based on EtOx, is ~10 kPa compared to ~50 kPa for 8 % catechol functionality, which was expected as the cross-linking density increases with increasing side chain functionality leading to denser networks and stronger mechanical properties. Hydrogels made of 5 w/v% P(EtOx-*co*-ButOxDOPAm) and fibrinogen were too soft to be analyzed. Whereas hydrogels made from 5 w/v% P(MeOx-*co*-DOPAm) with fibrinogen had a YM of ~6 kPa. Comparing hydrogels with the same mass content, 12.5 w/v% pure synthetic hydrogel versus 7.5 w/v% polymer plus 5 w/v% fibrinogen, it becomes obvious that the addition of fibrinogen increases the elasticity. Hydrogels based on P(EtOx-*co*-ButOxDOPAm) have a YM of ~7 kPa compared to ~10 kPa without fibrinogen and hydrogels based on P(MeOx-*co*-DOPAm) have a YM of ~15 kPa compared to ~50 kPa without fibrinogen. Only by increasing the polymer content up to 10 w/v%, the values for the YM resemble the one without fibrinogen. The overall trend that hydrogels with a higher degree of catechol functionality are stiffer continues for hydrogels with fibrinogen. Regarding application, a higher degree of functionalization seems to be desirable as it increases mechanical strength and in combination with fibrinogen maintains elasticity. Nevertheless, application wise, it is better to fabricate hydrogels with a low mass content so that cells have more room to penetrate the network.

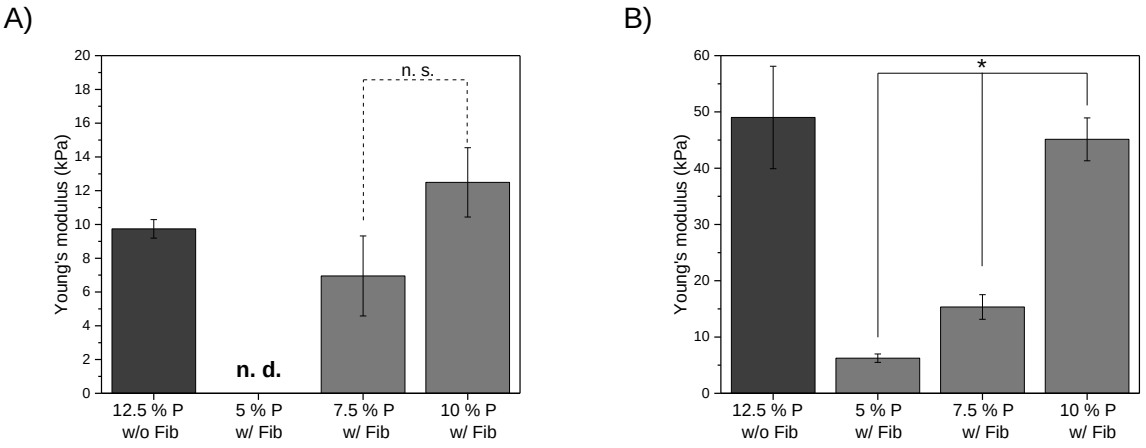

Figure 94: Young's moduli of hydrogels based on A) P(EtOx-*co*-ButOxDOPAm) and B) P(MeOx-*co*-ButOxDOPAm) of different w/v% with (w/) and without (w/o) 5 w/v% fibrinogen after 24 h incubation in PBS at 37 °C. Hydrogels with 5 w/v% P(EtOx-*co*-ButOxDOPAm) were too soft so that the Young's modulus could not be determined (n. d.). Mean and standard deviation shown (n = 3). Statistical significance shown with * ($p < 0.050$). and n.s. (not significant).

Therefore, for the following experiments, a constant polymeric content of 7.5 w/v% with 5 w/v% fibrinogen was used. Additionally, 0 %, 25 % or 50 % of the total polymer mass was replaced by the corresponding polymer with the labile ester bond in the side chain, P(EtOx-*co*-ButOxDOPAc) or P(MeOx-*co*-ButOxDOPAc), to examine the influence on the swelling and mechanical properties during incubation at 37 °C in PBS.

Figure 95A shows the mass change of hydrogels made from P(EtOx-*co*-ButOxDOPAm) with 0 %, 25 % or 50 % of P(EtOx-*co*-ButOxDOPAc). The hydrogels showed a quick mass increase within one day. The general trend that can be observed is that hydrogels with ester bonds showed a stronger swelling with increasing ester content so that hydrogels with 50 % ester increased in mass by ~160 % after 24 h in comparison to only ~130 % for hydrogels without ester. The mass of the latter did not change much over the time course of three weeks. However, hydrogels with ester showed a slight increase in mass over time, which can be related to an increase of hydrolyzed ester bonds resulting in a widened network. After 3 weeks, there is a slight drop in mass, which might be related to the fact that the fibrinogen content is metabolized by bacteria as those samples were not stored under sterile conditions. Nevertheless, no complete degradation of the hydrogel samples could be observed. As described earlier, it was not possible to prepare stable homogeneous hydrogels consisting solely of polymer with ester side chains, which could further be analyzed gravimetrically or mechanically. However, it was

possible to observe hydrogels with 100 % ester content macroscopically, shown in Figure 97. The pictures show, in accordance with the results of the gravimetrical analysis, that the morphology of hydrogels with 0 % to 50 % ester content stay intact over three weeks but with 100 % ester, the hydrogels start to disintegrate after one week. Of course, these conditions only simulate the conditions in the human body to some extent. It can be expected that the degradation *in vivo* or *in vitro* will be more advanced when the material is in contact with living cells.

Figure 94B shows the YM of the hydrogels over the time course of three weeks. One expected that the Young's modulus would change over time due to a progressing degradation. However, the YM did not change significantly over time. The YM decreased with increasing amount of ester starting from approximately 7 kPa for hydrogels without ester and decreasing to ~3 kPa for hydrogels where 50 % of the polymeric phase consisted of P(EtOx-*co*-ButOxDOPAc). There was no significant difference between hydrogels without and with 25 % ester. The YM only changed significantly when 50 % ester had been incorporated. This can be explained by an increased swelling and additional network inhomogeneities. The higher elasticity of these hydrogels might however be favorable for cell invasion.

Hydrogels made from P(MeOx-*co*-ButOxDOPAm) with 0 %, 25 % or 50 % of P(MeOx-*co*-ButOxDOPAc) showed a lesser mass increase compared to hydrogels based on EtOx (Figure 96A). Hydrogels without ester showed a slight initial swelling to ~105 % during the first three days, after that they reached a stable mass with a minimal mass decrease to ~100 %. When 25 % of the polymeric phase was replaced with P(MeOx-*co*-ButOxDOPAc), the mass was initially similar to the specimens without ester but started to increase after 7 days to ~110 %. Replacing the polymeric phase with 50 % ester containing polymer led to a stronger increase in mass of ~120 % after one day which steadily increased to ~130 % after three weeks. These results show that the higher degree of functionality leads to denser networks, which will, as a result, be less able to swell. The denser network also influenced the YM (Figure 96B). The same trend of a decreasing YM with increasing ester content could be observed, however, the hydrogels were about twice to three times as stiff starting at ~24 kPa for hydrogels without ester decreasing to ~7 kPa for hydrogels with 50 % ester. In addition, the YM did not change over time as it had also been the case for EtOx based hydrogels. It could also be noted that 25 % of P(MeOx-*co*-ButOxDOPAc) already influenced the hydrogel stiffness significantly, which was not the case for

EtOx based hydrogels. This can be explained by the fact that P(MeOx-*co*-ButOxDOPAc) had a lower degree of functionalization (6 % compared to 8 % for PMeOx-*co*-DOPAm), which directly influenced the cross-linking extent.

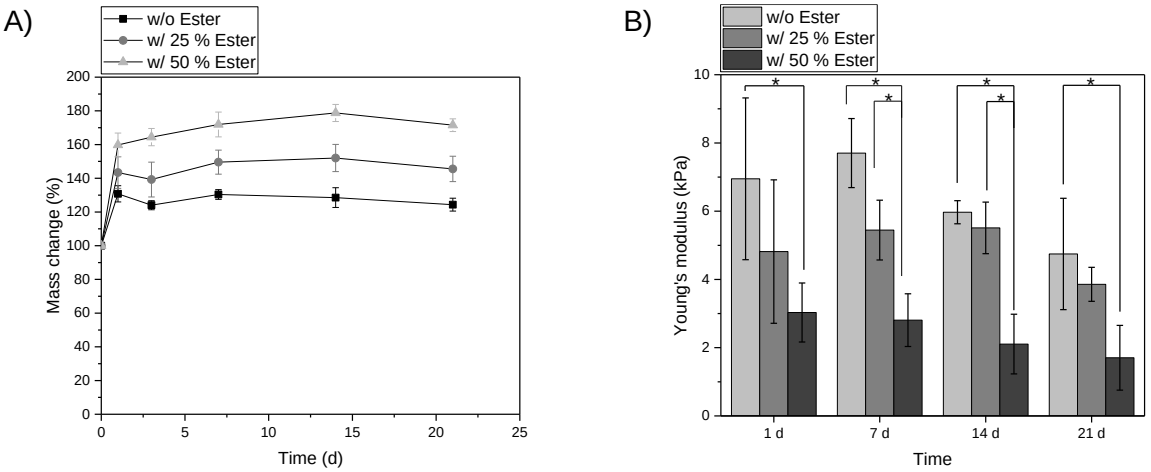

Figure 95: Development of A) mass and B) Young's modulus of hydrogels made from P(EtOx-*co*-ButOxDOPAm) and P(EtOx-*co*-ButOxDOPAc) (7.5 w/v% polymer + 5 w/v% fibrinogen) for three weeks incubation in PBS at 37 °C. Mean and standard deviation shown (n = 3). Statistical significance shown with * ($p < 0.050$).

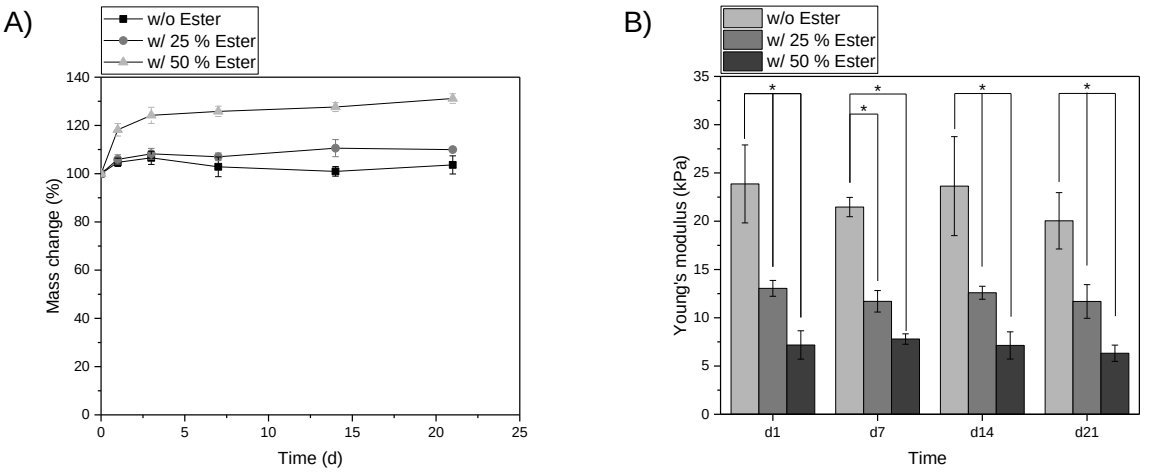

Figure 96: Development of A) mass and B) Young's modulus of hydrogels made from P(MeOx-*co*-ButOxDOPAm) and P(MeOx-*co*-ButOxDOPAc) (7.5 w/v% polymer + 5 w/v% fibrinogen) for three weeks incubation. Mean and standard deviation shown (n = 3). Statistical significance shown with * ($p < 0.050$).

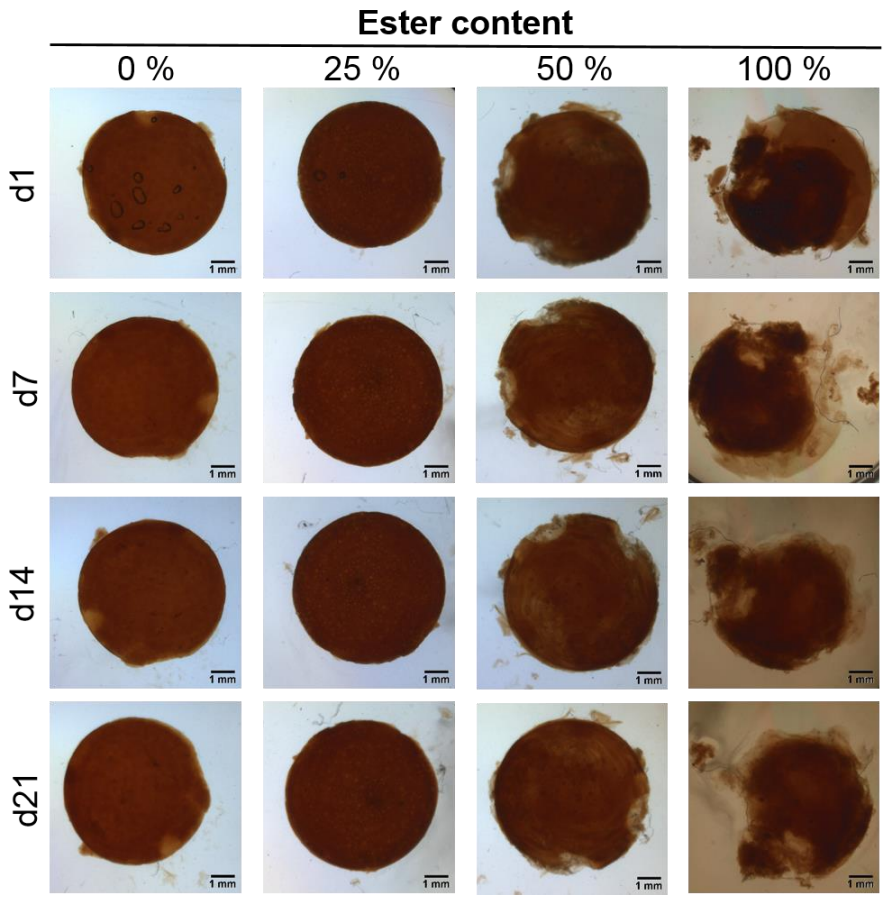

Figure 97: Macroscopic pictures of hydrogels with fibrinogen and varying ester content in the polymeric phase, stored at 37 °C in PBS over the time course of three weeks.

3.3.2.3 Biological Evaluation

The prepared hydrogels without and with ester and fibrinogen were also tested for cytotoxicity *in vitro* by Oliver Berberich in the course of his doctoral thesis. The MTT viability stain and microscopic evaluation showed excellent cell viability when tested on cartilage plugs harvested from pigs aged 2 – 3 months.

The long-term cartilage integration for hydrogels based on P(EtOx-*co*-ButOxDOPAm) and P(EtOx-*co*-ButOxDOPAc) plus fibrinogen showed increased cell invasion for hydrogels with increasing ester content. The microscopic analysis after three weeks and immunofluorescent staining for typical cartilage extracellular matrix components (collagen type II and aggrecan) showed an unsuccessful integration for the hydrogel without ester (Figure 98, left picture). The non-degradable hydrogel network can be seen in green as a barrier for the cells, which could not migrate and bridge the gap. In contrast to this, hydrogels with ester content showed neocartilage formation and

freely migrating chondrocytes across the gap as soon as 25 % of the polymer was replaced by P(EtOx-*co*-ButOxDOPAc), middle and right pictures in Figure 98. Here, the gap is completely of a light red color and cells are visible in pink/violet across the complete defect site.

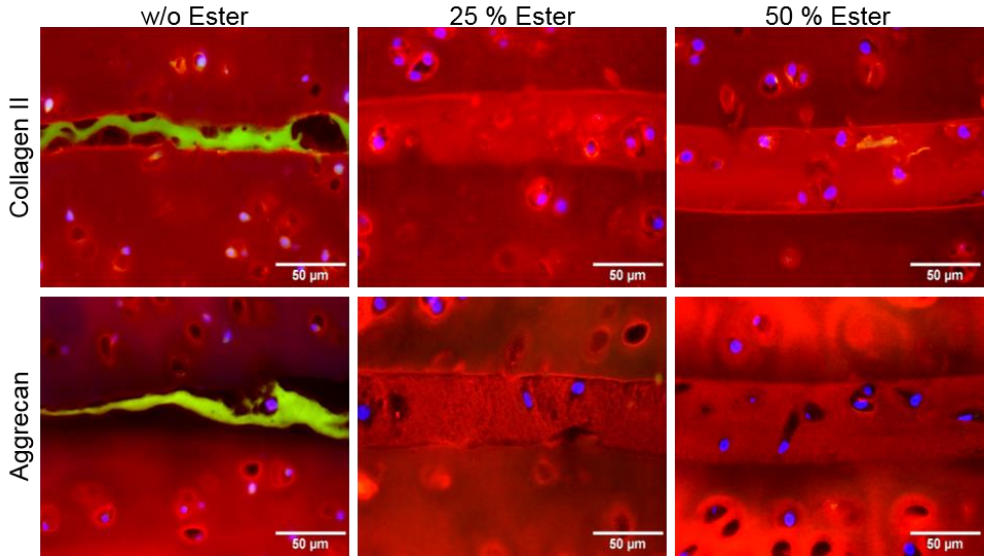

Figure 98: Immunofluorescent staining for cartilage ECM markers collagen type II and aggrecan after 21 days, performed by the collaboration partner Oliver Berberich, workgroup Prof. Dr. T. Blunk, Universitätsklinikum Würzburg.

3.3.3 Peptide Attachment

A model peptide with the amino acid sequence CGGGF with a N-terminal cysteine was attached to the side chain of POx with different side chain functionality. This peptide was chosen as it is soluble in most common solvents and minimal sterical hindrance is expected. Large, sterically demanding peptides can be difficult partners for linking reactions as it has been demonstrated by Schmitz *et al*. [147]. The second peptide used possessed the amino sequence CKFKFQF. This peptide sequence was provided by the workgroup of Prof. Tanja Weil in Ulm, Germany, and was expected to be sterically more demanding than CGGGF and not freely soluble in all solvents.
The easiest way is to use thiol-ene chemistry to bind the thiol of the cysteinyl group of the peptide to the double bond of vinyl functional copolymers. The second option presented is to use a thiolactone side functional copolymer that will react with the cysteine to form an amide bond. Very similar to this, the third option is to use an azlactone side functional copolymer, which will react with amines as well as cysteines forming an amide bond. The advantage of using the two latter approaches is that one or even two thiols, in case of the thiolactone group, are still present at the coupling site after the reaction. Free thiols are rather uncommon in nature, hence it is especially interesting to use these free thiols for further reactions, for example for a thiol-ene reaction.

3.3.3.1 Peptide Attachment via Thiol-ene Chemistry

The copolymer P(EtOx$_{0.91}$-*co*-ButEnOx$_{0.09}$)$_{56}$ (P19) was dissolved in deuterated water or DMSO and degassed with argon. Afterwards, 1 – 3 eq. of the peptide CGGGF (CG3F) or CKFKFQF (CKF) and a photo-initiator were added. The solution was irradiated under UV light using LED cubes or a UV handlamp.
It was expected that the thiol of the cysteine amino acid at the N-terminus of the peptide would react with the vinyl group at the side chain of copolymer (Figure 99). ^{1}H NMR spectroscopy revealed whether there were still double bonds present at their characteristic value of 5.80 ppm (CH_2=C*H*) and 4.97 ppm (C*H*$_2$=CH). When the double bond reacts with a thiol compound, new signals for the CH_2 group adjacent to the thiol at 2.62 ppm and for the other two CH_2 groups not directly neighboring the carbonyl group at 1.59 ppm appear, marked with grey boxes in Figure 100.

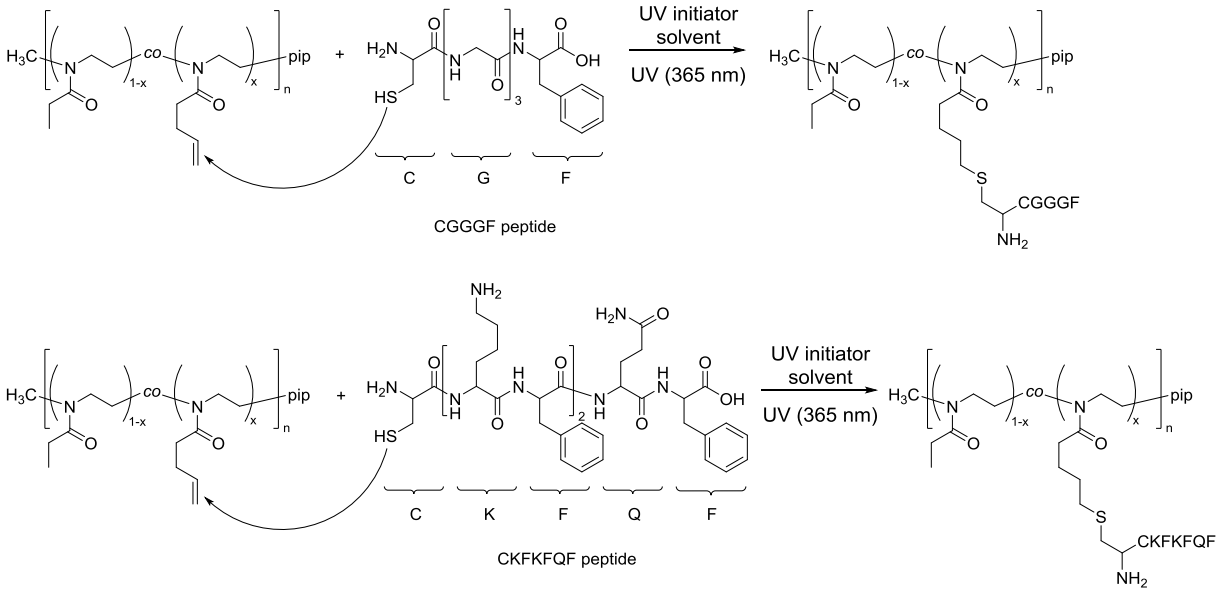

Figure 99: Synthesis scheme of vinyl functional POx reacting with peptide CGGGF or CKFKFQF with N-terminal cysteine.

The thiol-ene reaction between the polymer P19 and the peptide CG3F did not work well in DMSO-d_6 but good results were obtained in D_2O, where only 20 % of unreacted double bonds were left when 1 eq. peptide per vinyl group was used. When the equivalency was raised to 2 eq. or higher, all vinyl groups had reacted (Table 9). The solvent also played an important role when trying to bind the sterically more demanding and rather hydrophobic peptide CKF, from which is known that it will build fibrils in water. This behavior was observed from transmission electron microscopy recordings made in the research group of Prof. Tanja Weil.

No reaction occurred when a mixture of DMSO-d_6 and CD_3CN and 1.5 eq. of CKF were used (Table 9). Increasing the equivalents of the peptide led to better results, but complete conversion was still not achieved. Pure DMSO-d_6 showed similar results with even 3 eq. of peptide. Mixing D_2O with CD_3CN led to 100 % conversion of the double bonds when 3 eq. of the peptide were used, however best results were obtained when mixing D_2O and DMSO-d_6. Here, only 1.5 eq. of the peptide were needed to reach full conversion of the double bonds. These results show that depending on the peptide, one should look for the best solvent combination to reach a high coupling efficiency whilst keeping peptide equivalents as low as possible.

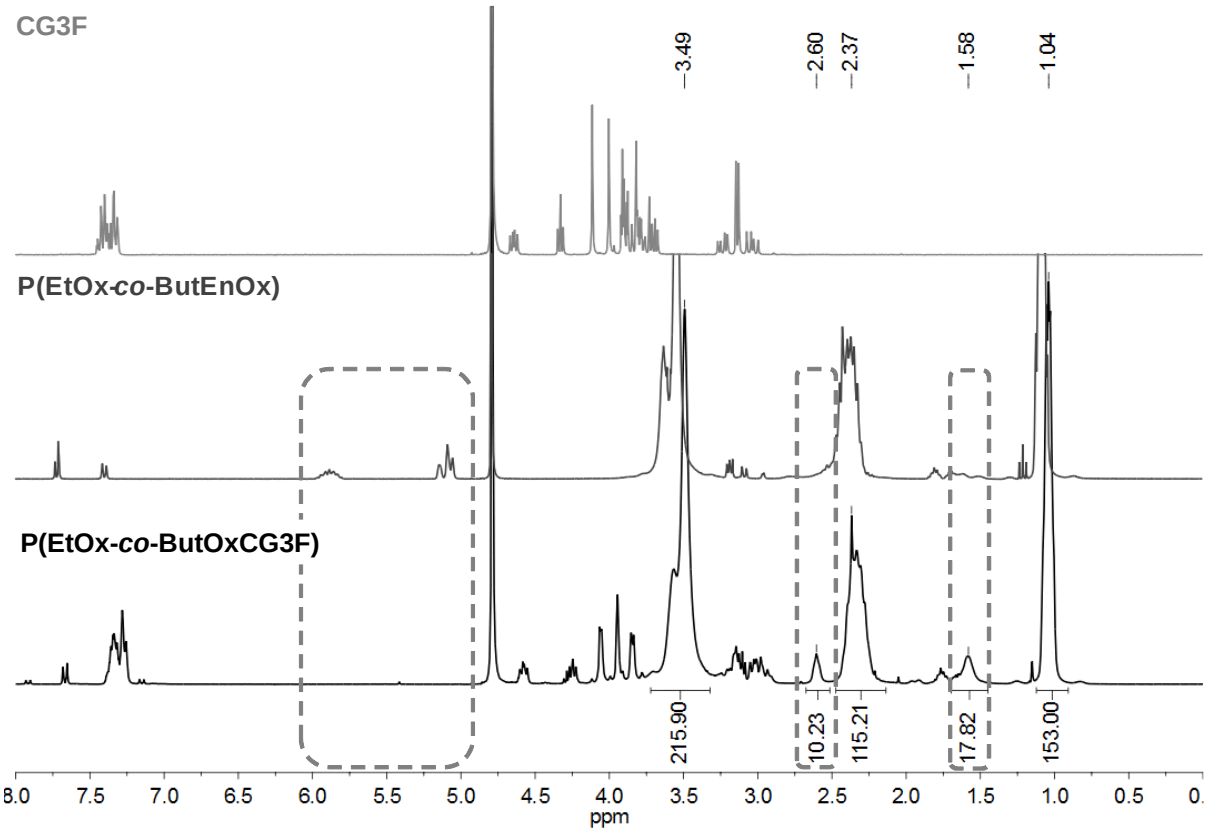

Figure 100: Stacked ^{1}H NMR spectra of peptide (light grey, top), vinyl functional copolymer (grey, middle) and peptide-polymer conjugate after the reaction (black, bottom).

Table 9: Result of thiol-ene reaction between peptide and vinyl side chain POx copolymer.

Sample name	Solvent (v:v)	Eq. CG3F	Eq. CKF	Unreacted vinyl groups (%)*
P19-CG3F-1	DMSO-d_6	3	-	82
P19-CG3F-2	D_2O	1	-	20
P19-CG3F-3	D_2O	2	-	0
P19-CG3F-4	D_2O	3	-	0
P19-CKF-1	DMSO-d_6	-	3	55
P19-CKF-2	D_2O/CD_3CN (1:1)	-	2	23.6
P19-CKF-3	D_2O/CD_3CN (1:1)	-	3	0
P19-CKF-4	CD_3CN/DMSO-d_6 (2:1)	-	1.5	100
P19-CKF-5	CD_3CN/DMSO-d_6 (2:1)	-	2	44
P19-CKF-6	D_2O/DMSO-d_6 (2:1)	-	1.5	0

* Determined by ^{1}H NMR end group analysis

3.3.3.2 Peptide Attachment via Thiolactone Chemistry

The model peptide CG3F with a N-terminal cysteine was conjugated to a thiolactone functionalized copolymer (Figure 101) following the native chemical ligation protocol of Schmitz *et al*. [147]. A buffer containing NaH_2PO_4, TCEP (reducing agent) and 4-mercaptophenylacetic acid (MPAA) as catalyst [171] was used as reaction medium

and 2 eq. of peptide per thiolactone functionality were added. The reaction mixture was stirred over night at pH 7 and room temperature. Purification was carried out by means of dialysis to remove any unbound peptide and any salts. The native chemical ligation mechanism between the thiolactone, which is cyclic thioester, is shown in Figure 102. The additional aryl thiol, MPAA, acts as a catalyst as it creates an intermediate in situ active thioester facilitating the attack of the cysteine functionality [172].

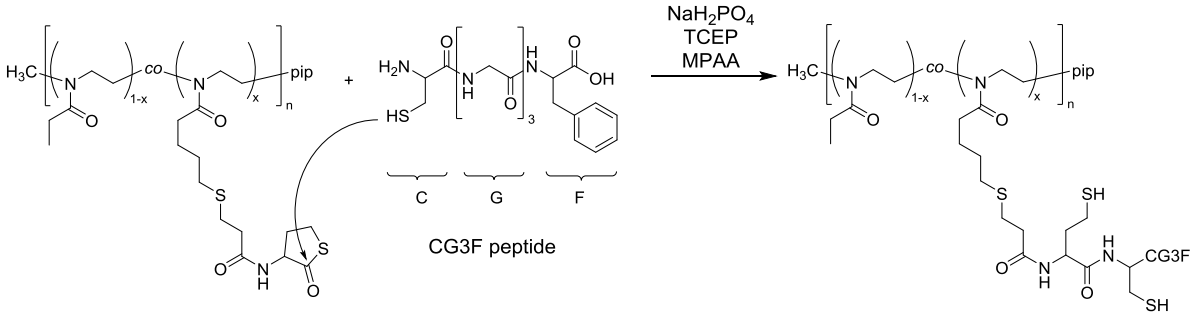

Figure 101: Synthesis scheme of thiolactone functional POx reacting with CG3F peptide.

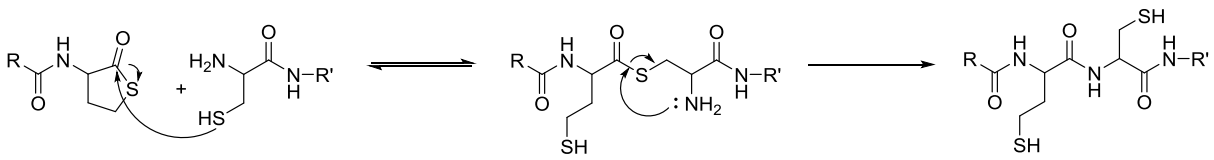

Figure 102: Reaction mechanism of thiolactone with cysteine showing the intramolecular rearrangement by a S,N-acyl shift.

Two copolymers with increasing thiolactone content (10 mol% and 20 mol%) were used. The reaction was more successful for the polymer with the higher thiolactone content with a peptide attachment of ~85 % to the functional groups in contrast to only ~28 %, which was determined by ^{1}H NMR end group analysis by integrating the aromatic signals of the phenyl alanine amino acid of CG3F. However, the residual thiolactone groups might still have reacted with the catalyst MPAA. Nevertheless, the thioester bond between MPAA and the polymer side chain would have been destroyed during dialysis against water. The IR spectrum also showed an increase in intensity of the amino and amide vibration at 3200 cm^{-1} – 3120 cm^{-1} and 1540 cm^{-1} respectively (Figure 103). The successful binding of the peptide to the polymer could also be confirmed by HPLC analysis. The HPLC traces at 210 nm (Figure 104) reveal that no unbound peptide is present in the product of P(EtOx$_{0.89}$-*co*-ButOxLac$_{0.08}$-*co*-ButOxCG3F$_{0.03}$)$_{56}$-pip as there is no signal at 15 min where the pure peptide CG3F

elutes. This means that the aromatic signals, which are visible in the NMR spectrum, can only originate from bound peptides. The trace of the peptide polymer conjugate also shows an increased intensity at 254 nm, where the aromatic ring of the amino acid phenyl alanine absorbs (Figure 105), compared to the thiolactone functionalized polymer confirming the attachment of the peptide to the polymer.

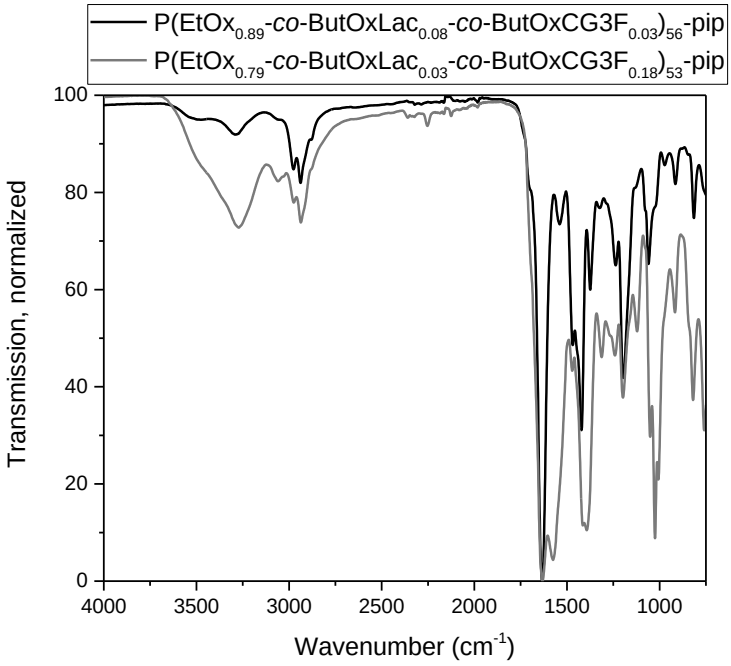

Figure 103: IR spectra of thiolactone functionalized POx copolymers after the reaction with the peptide CG3F.

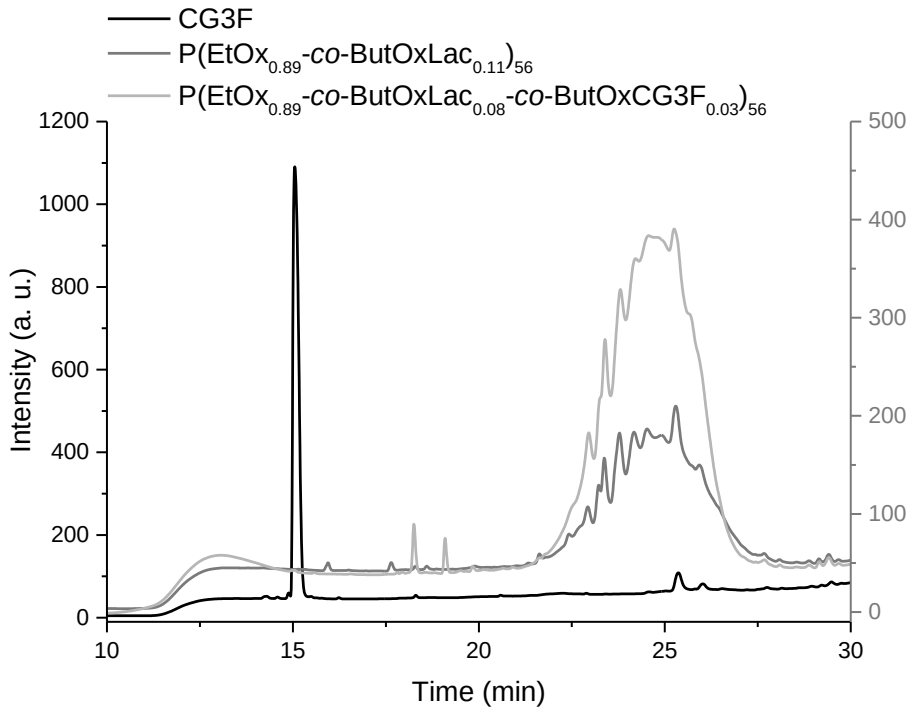

Figure 104: HPLC trace of peptide (black), thiolactone functional copolymer (dark grey) and peptide-polymer conjugate (light grey) at 210 nm. Concentration was 10 mg/mL for each sample.

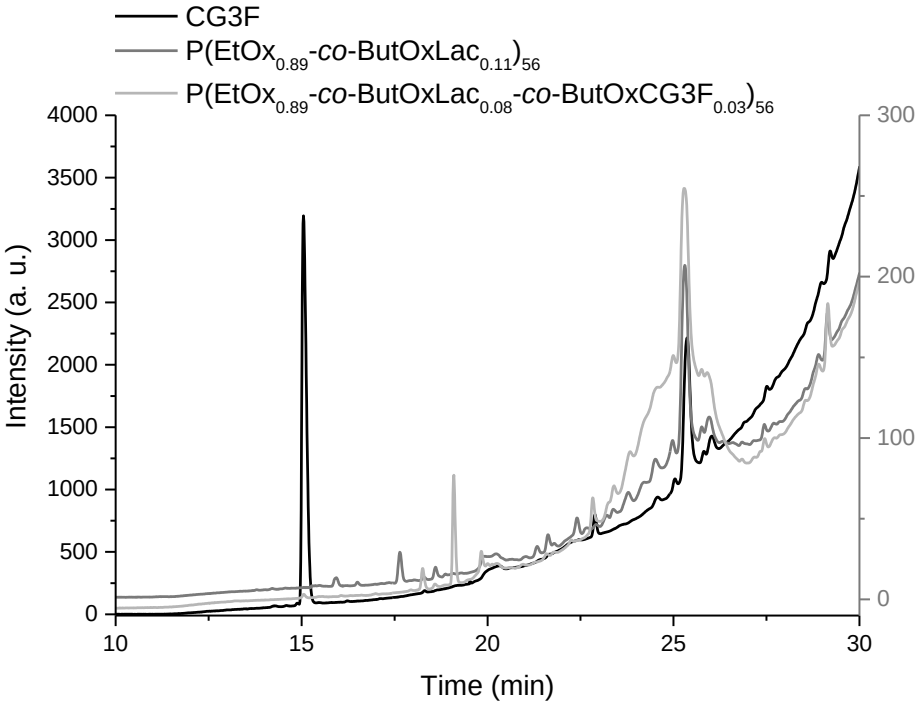

Figure 105: HPLC trace of peptide (black), thiolactone functional copolymer (dark grey) and peptide-polymer conjugate (light grey) at 254 nm. Concentration was 10 mg/mL for each sample. The trace of the copolymer and peptide-polymer conjugate are scaled to the same intensity.

3.3.3.3 Peptide Attachment via Azlactone Chemistry

The conjugation of the peptide CG3F to the azlactone side functional polymer (Figure 106) was performed according to Ho *et al*. [162]. As postulated by Schmitt *et al*. the azlactone group can be attacked by a cysteine, which will undergo a rearrangement similar to the native chemical ligation mechanism [139] (Figure 107). They discussed that is likely that the thiol of the cysteine attacks at the carbonyl carbon of the cyclic ester forming a thioester followed by an intramolecular S→N transfer leading to a stable amide bond [139]. The two methyl groups at the 5 position of the azlactone ring are essential so that an electron pair shift to an enol is impossible and the reactive anhydride structure of the azlactone ring is preserved.

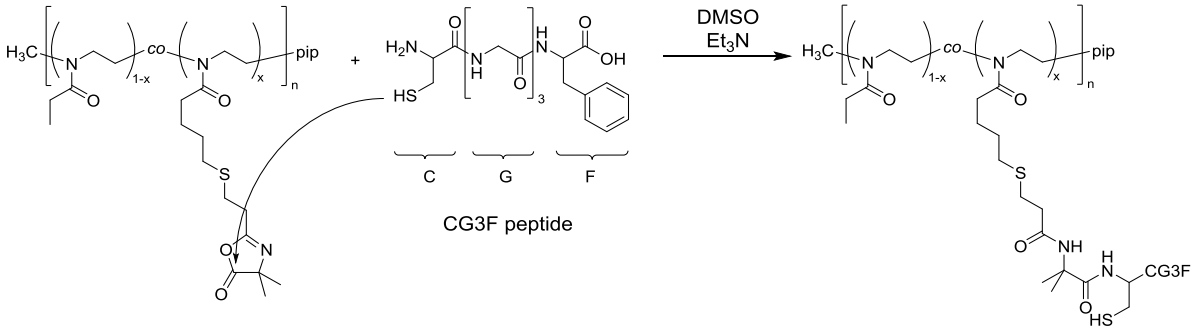

Figure 106: Synthesis scheme of azlactone functional POx reacting with CG3F peptide.

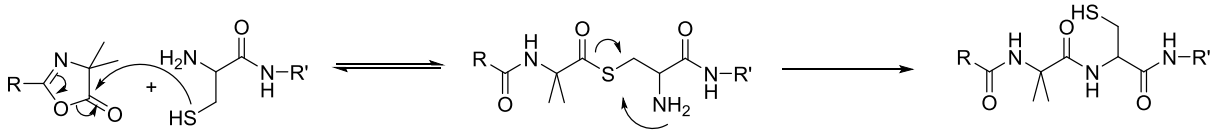

Figure 107: Reaction scheme of azlactone ring with cysteine.

The peptide and the polymer were dissolved in dry DMSO to prevent hydrolysis of the azlactone group. It was shown by Schmitt *et al*. that the azlactone functionality is very susceptible to the reaction with nucleophiles such as -OH, -SH and -NH_2 [173]. In addition, it was shown by Ho *et al*. that azlactone functional copolymers were conjugated to a more complex protein, lysozyme, with higher efficiency in DMSO than in aqueous buffer [138, 174]. Hence, DMSO was chosen as solvent to keep any possible unwanted nucleophile away from the reaction site. As catalyst, triethylamine was added, and the reaction mixture was stirred for 20 h and afterwards purified by dialysis to remove any unbound peptide.

The conjugate was analyzed via ^{1}H NMR end-group analysis to determine how much peptide had been bound to the polymer. It revealed that in case of P(EtOx$_{0.89}$-co-

ButOxAL$_{0.11}$)$_{56}$-pip ~55 % of all azlactone groups had been functionalized with the peptide, which could be determined from the aromatic signals at 7.22 ppm and the amide signals at 8.34 ppm – 7.94 ppm (Figure 108). Further characteristic peptide signals could also be found in the NMR at 4.41 ppm, 3.72 ppm and 2.92 ppm.

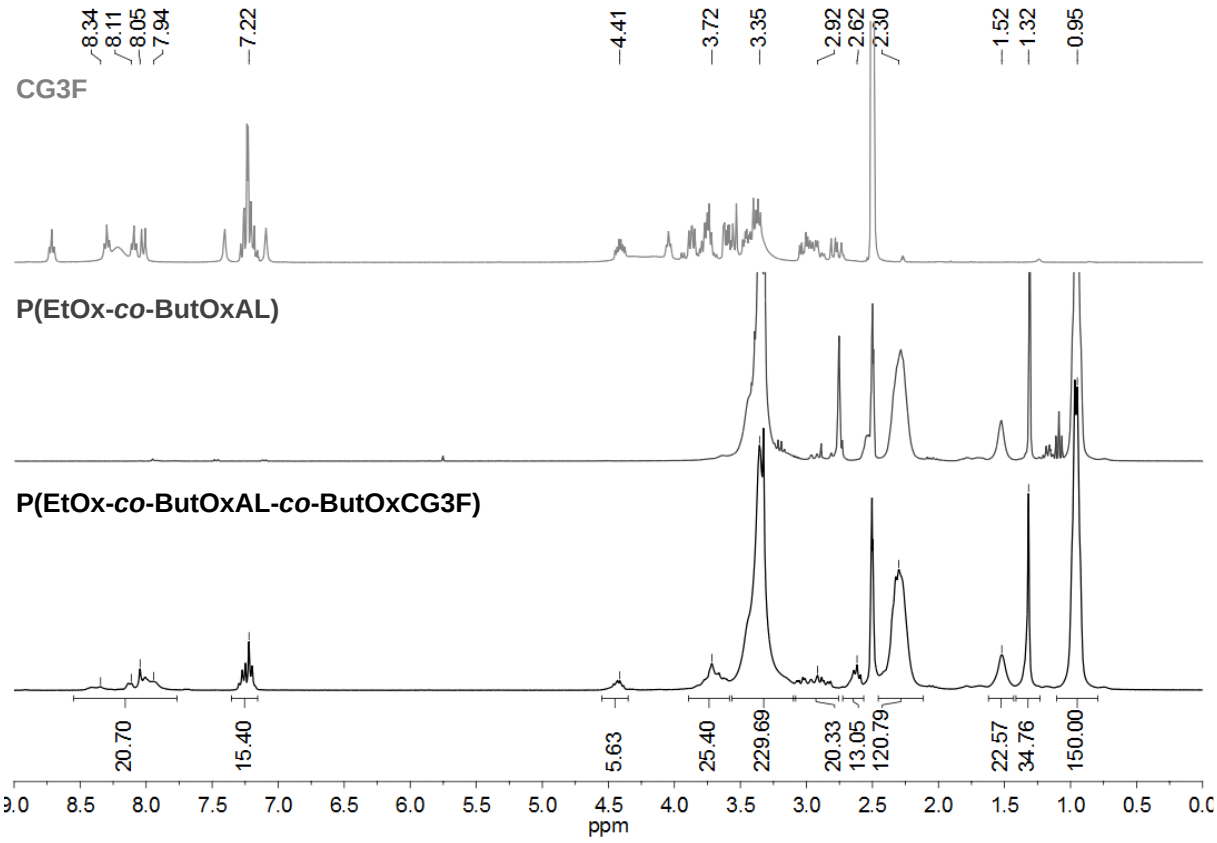

Figure 108: ^{1}H NMR stack of the peptide-polymer conjugate P(EtOx$_{0.89}$-*co*-ButOxAL$_{0.05}$-*co*-ButOxCG3F$_{0.06}$)$_{56}$-pip (black, bottom), the azlactone functionalized polymer P(EtOx$_{0.89}$-*co*-ButOxAL$_{0.11}$)$_{56}$-pip (dark grey, middle) and the peptide CG3F (light grey, top) in DMSO-d$_6$.

In case of P(EtOx$_{0.79}$-*co*-ButOxAL$_{0.21}$)$_{53}$-pip, ^{1}H NMR analysis revealed that only ~35 % of the azlactone groups were functionalized. The lower conversion can be explained by the longer storage time of the polymer, where azlactone groups might have already reacted with air moisture. The polymer with the lower azlactone groups was used for the coupling reaction within two days and had been stored under dry conditions.

The successful coupling was also visible in the IR spectra (Figure 109), where the typical peptide vibrations in the region of 3700 cm^{-1} – 3120 cm^{-1} (OH, NH stretching) and at 1542 cm^{-1} (NH deformation) are visible. The peak of the carbonyl of the azlactone ring at 1815 cm^{-1} has completely disappeared, but as the azlactone groups

that had not reacted with a peptide were converted back into carboxylic acid, there is also a peak at 1730 cm^{-1} visible.

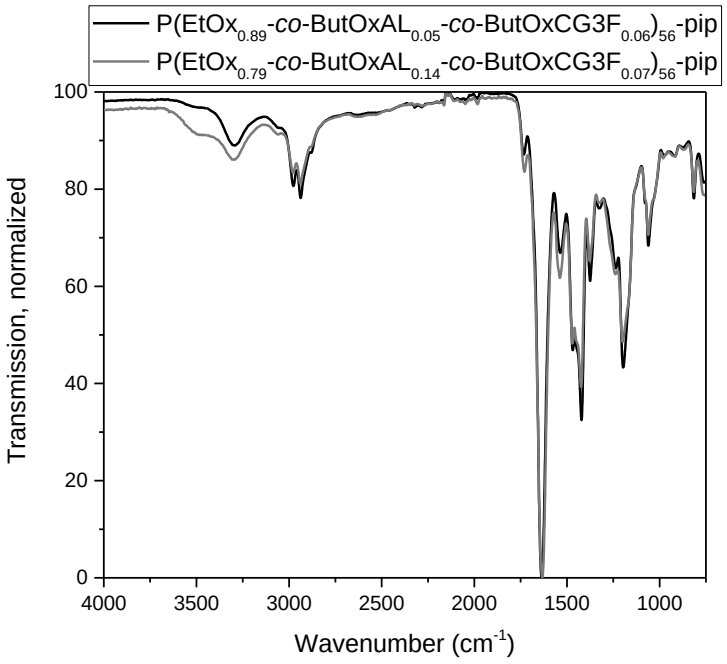

Figure 109: IR spectra of peptide-polymer conjugates based on azlactone coupling.

HPLC measurements also revealed the presence of the peptide. On the one hand, there is not peak visible in the trace of the peptide-polymer conjugate at the elution time where the peptide alone elutes (12.4 min), neither at 210 nm nor at 254 nm (Figure 110 and Figure 111). This means that the aromatic signals in the ^{1}H NMR spectrum do not originate from unbound peptide in the product, but indeed from polymer bound peptide. On the other hand, the peak shape of the peptide functionalized polymer differs to the one of the original parent copolymer (Figure 36), indicating a change in hydrophobicity. The azlactone functionalized polymer is more hydrophilic as the azlactone groups are transformed back into carboxylic acid due to hydrolysis in the eluent (ACN/water) and elute earlier due to weaker interaction with the hydrophobic column material. In addition, the intensity of the peak of the peptide-polymer conjugate at 254 nm, where the aromatic ring of phenyl alanine absorbs, is higher than for the azlactone-functionalized copolymer, which interestingly also shows an increased intensity at 254 nm. As both samples were measured at the same concentration, it can be assumed that the increase in intensity really originates from the additional peptide bound to the copolymer.

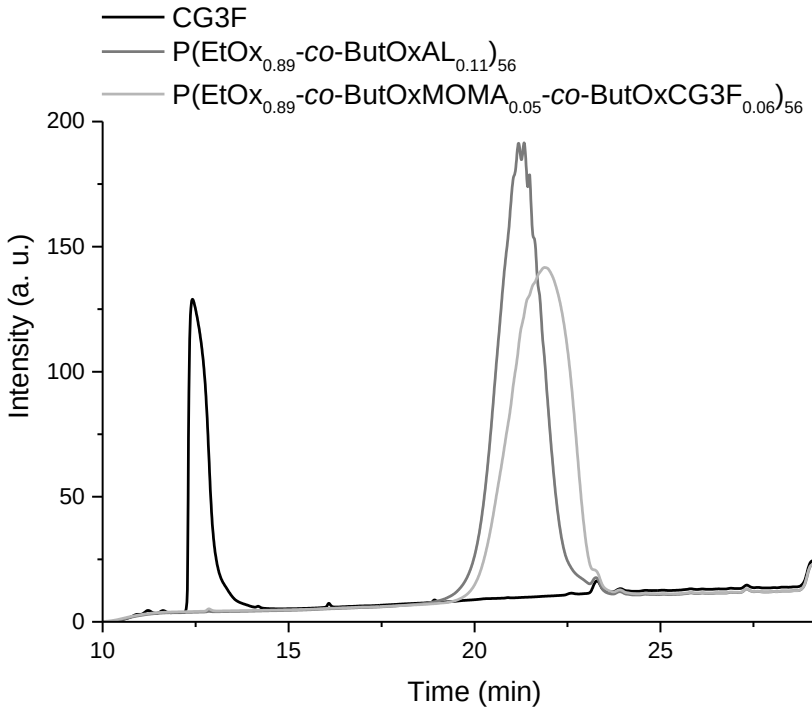

Figure 110: HPLC trace of peptide (black), azlactone functional copolymer (dark grey) and peptide-polymer conjugate (light grey) at 210 nm. Concentration was 10 mg/mL for each sample.

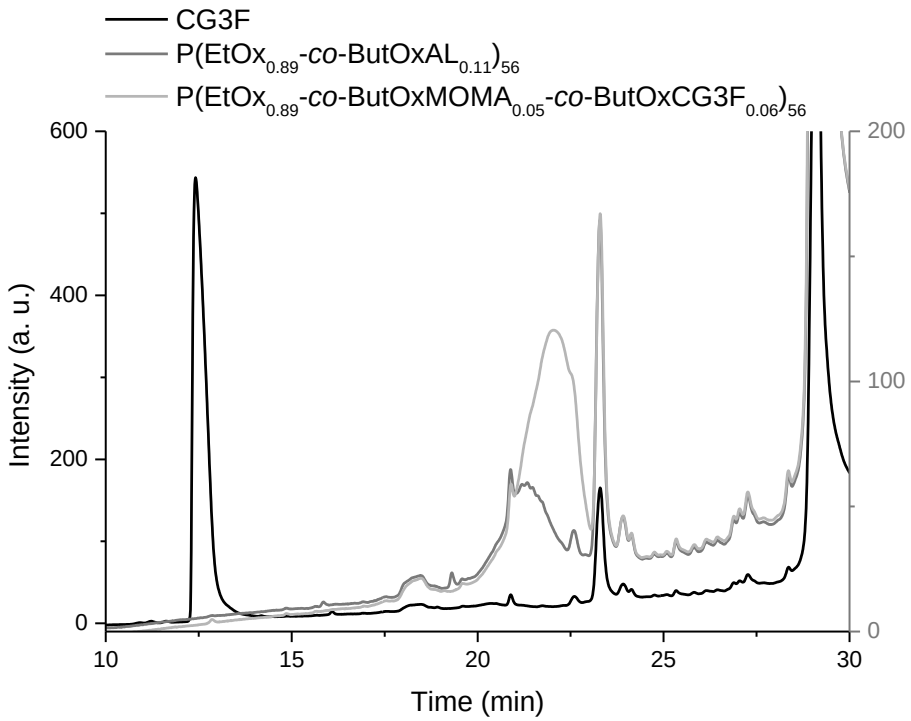

Figure 111: HPLC trace of peptide (black), azlactone functional copolymer (dark grey) and peptide-polymer conjugate (light grey) at 254 nm. Concentration was 10 mg/mL for each sample. The trace of the copolymer and peptide-polymer conjugate are scaled to the same intensity.

4 Summary / Zusammenfassung

The aim of the thesis was to develop water soluble poly(2-oxazoline) copolymers with new side group functionalities, which can be used for the formation of hydrogels in biomedical applications and for the development of peptide-polymer conjugates.

The synthesis of simple homopolymers based on the monomers MeOx, EtOx and *n*PropOx was performed in the flask or in a microwave reactor at 100 °C, 120 °C and 140 °C. The initiator for the CROP was methyl tosylate (MeTos) and piperidine, allylamine and a methanolic potassium hydroxide solution were used as terminating agents. The predetermined degree of polymerization (DP), which was set by the initiator to monomer ratio, was met with a deviation of 5 % – 10 % as determined by ^{1}H NMR end group analysis. The distribution and dispersity were evaluated using size exclusion chromatography (SEC). PEtOx homopolymers were monomodal and exhibited a dispersity below 1.2 when polymerized at 100 °C. Bimodal distributions were often observed for PMeOx terminated with piperidine and for PPrOx with high degrees of polymerization (DP > 100). In the next step, copolymers of the monomer MeOx or EtOx with ButEnOx and EtOx with DecEnOx were synthesized and characterized. The monomers were randomly copolymerized by adding both monomers to the reaction vessel from the start. The vinyl functionality brought into the copolymer by the monomers ButEnOx and DecEnOx would later serve for post-polymerization functionalization. The DP was kept constant at 50 and P(EtOx-*co*-ButEnOx) with 10 mol% to 40 mol% vinyl functionality, P(EtOx-*co*-DecEnOx) with 7 mol%, 11 mol% and 17 mol% vinyl functionality and P(MeOx-*co*-ButEnOx) with 9 mol%, 12 mol% and 20 mol% vinyl functionality were synthesized. Copolymers based on EtOx showed monomodal distributions with low dispersities in contrast to copolymers based on MeOx, where the dispersity was between 1.2 – 1.3. The copolymers showed different thermo-responsive behavior. Whereas P(MeOx-*co*-ButEnOx) was water soluble without restriction, the effect of the longer side chain of ButEnOx already became apparent with 20 mol% functionality, when EtOx was used as the main co-monomer. Here the T_{CP} decreased to 55 °C and decreased even further to 25 °C, when 40 mol% ButEnOx was incorporated. The effect of the co-monomer DecEnOx was even more dramatic with a decrease of the T_{CP} to 25 °C with only 7 mol% DecEnOx. The copolymers with 10 mol% and 20 mol% ButEnOx were also tested for cytocompatibility and showed good results. In direct comparison, copolymers based on MeOx were slightly less cytocompatible than the ones based on EtOx.

The synthesized copolymers were further functionalized with thiols via post-polymerization functionalization using a newly developed synthesis protocol. In the first step, a thioester was attached to the vinyl side chain through radical thiol-ene chemistry and was deprotected in the second step using cysteine under mild reaction conditions. The successful functionalization could be observed by ^{1}H NMR and Raman spectroscopy. The Ellman's assay also confirmed the theoretical mol% of thiols and SEC analysis showed that the reaction conditions had not led to a degradation of the polymer as it had first been observed when using basic conditions and high temperatures to remove the thioester. The thiol functionalized copolymers were less cytocompatible compared to the unfunctionalized parent polymers. At 15 mg/mL – 5 mg/mL, all thiol polymers showed moderate cytotoxicity but not cytotoxicity at 1 mg/mL.

For the formation of peptide-polymer conjugates, a cyclic thioester, namely thiolactone acrylamide and an azlactone precursor, whose synthesis was newly developed, were attached to the side chain of P(EtOx-*co*-ButEnOx) copolymers. The successful functionalization could be confirmed by ^{1}H NMR and IR spectroscopy.

The cooperation project with the workgroup of Prof. Dr. Blunk involved the development of a catechol-based hydrogel system. As the catechol functionality increases the hydrophobicity of the polymer, two copolymers with a higher degree of polymerization (80 – 90) based on EtOx and on MeOx, which would render the system more hydrophilic and allow a higher catechol functionalization, were synthesized. After radical thiol-ene post-polymerization functionalization with cysteamine or 2-mercaptoethanol, the protected catechol molecule was bound to the polymer side chain by amidation/esterification. The presence of the catechol at the side chain was confirmed by ^{1}H NMR and UV/Vis spectroscopy. The functionalization efficiency proved to be not as good compared to thiol-ene chemistry with only 58 % – 83 % of all side chains functionalized.

Chapter 3.3 presents the different applications of the functionalized copolymers starting with hydrogels based on radical thiol-ene chemistry in aqueous solutions using the initiator Irgacure 2959. Copolymers with the same thiol and vinyl content were paired and cross-linked at a concentration of 15 wt% for 15 min under UV irradiation. Their swelling behavior and mechanical properties (Young's modulus) were characterized. The hydrophilicity of the network as well as the cross-linking density strongly influenced the swelling behavior and the mechanical strength of the

hydrogels. Hydrogels based on the more hydrophilic monomer MeOx showed the highest degree of swelling and hydrogels based on the less hydrophilic monomer EtOx showed limited swelling at 37 °C due to their thermo-responsive behavior. The swelling was also influenced by the addition of salts in a way that hydrogels were able to swell 1.5 times more in ultrapure water compared to PBS. The Young's moduli of the hydrogels fabricated were 100 kPa to 380 kPa, depending on the copolymer composition and degree of functionalization. All hydrogels showed good cell viability results.

Hydrogels based on EtOx were also loaded with FITC-labeled dextran of different molecular weight. It could be observed that dextran with 500 kDa was not able to diffuse out of the network, whereas the amount of dextran with 40 kDa released from the network with the lower cross-linking degree was twice as high. The hydrogel networks based on MeOx and EtOx were also loaded with two dyes, fluorescein and methylene blue. It was observed that the uptake of the more hydrophilic dye fluorescein depended more on the ability of the hydrogel to swell. In contrast, the uptake of the more hydrophobic dye methylene blue was less dependent on the swelling degree, but much more on the hydrophilicity of the network.

For the cartilage glue project in cooperation with the workgroup of Prof. Dr. Blunk, (biohybrid) hydrogels were synthesized based on the catechol-functionalized copolymers, with and without additional fibrinogen, using sodium periodate as the oxidizing agent. The system allowed for degradation due to the incorporated ester linkages at the cross-linking points. The swelling behavior as well as the mechanical properties (Young's modulus) were characterized. As expected, hydrogels with higher degrees of cross-linking showed less swelling and higher elastic modulus. The addition of fibrinogen however increased the elasticity of the network, which can be favorable for the intended application as a cartilage glue. Biological evaluation, performed in the lab of Prof. Dr. Blunk, clearly demonstrated the advantage of degradable ester links in the hydrogel network, where chondrocytes were able to bridge the artificial gap in contrast to hydrogels without any ester motifs.

The last section presents different ways to form peptide-polymer conjugates. Peptides were attached with the thiol of the terminal cysteine group to the vinyl side chain of P(EtOx-*co*-ButEnOx) copolymers by radical thiol-ene chemistry. The success of the reaction was determined via ^{1}H NMR analysis. Two peptides, CGGGF and CKFKFQF, the second being more hydrophobic than the first one, were reacted

with the copolymer in different solvents. It could be shown that the success of the reaction was strongly dependent on the solvent (mixtures) chosen and that with the right solvent, peptide equivalents could be reduced to 1.5 eq. for each eq. of vinyl functional group. Another approach was to use a cyclic thioester, thiolactone. It was used to bind the peptide CGGGF to the polymer side chain of P(EtOx-*co*-ButOxLac) via native chemical ligation. ^{1}H NMR end group analysis confirmed the attachment of the peptide to the polymer and HPLC measurements showed an increased intensity at a wavelength of 254 nm, indicating the presence of the aromatic ring of the amino acid phenyl alanine.
Furthermore, azlactone functionalized copolymers were reacted with CGGGF in dry DMSO to prevent any unwanted hydrolysis of the azlactone ring by water molecules. The successful binding could be determined by ^{1}H NMR end group analysis, IR spectroscopy and HPLC measurements. The two latter named strategies to bind peptides to POx side chains are especially interesting as one and in the case of thiolactone two free thiols are still present at the binding site after the reaction, which can, for example, be used for further thiol-ene cross-linking to form POx hydrogels.

In summary, side functional poly(oxazoline) copolymers show great potential for numerous biomedical applications. The various side chain functionalities can be introduced by an appropriate monomer or by post-polymerization functionalization, as demonstrated. By their multi-functionality, hydrogel characteristics, such as cross-linking degree and mechanical strength, can be fine-tuned and adjusted depending on the application in the human body. In addition, the presented chemoselective and orthogonal reaction strategies can be used in the future to synthesize polymer conjugates, which can, for example, be used in drug delivery or in tissue regeneration.

Das Ziel der Arbeit war es, wasserlösliche Poly(2-oxazolin) Copolymere mit neuen Seitenkettenfunktionalitäten zu entwickeln, welche zur Synthese von Hydrogelen für biomedizinische Anwendungen und zur Entwicklung von Peptid-Polymer Konjugaten genutzt werden können.

Zunächst wurde die Synthese von einfachen Homopolymeren basierend auf den Monomeren MeOx, EtOx und *n*PropOx, welche im Kolben oder im Mikrowellenreaktor bei 100 °C, 120 °C and 140 °C durchgeführt wurden, beschrieben. Der Initiator der kationischen Ringöffnungspolymerisation war Methyltosylat (MeTos) und als Terminationsreagenzien wurden Piperidin, Allylamin oder methanolische Kaliumhydroxid Lösung verwendet. Der gewünschte Polymerisationsgrad, welcher durch das Verhältnis von Initiator zu Monomer eingestellt wird, wurde mit einer Abweichung von 5 % – 10% erreicht, welche durch ^{1}H NMR Endgruppen Analyse bestimmt wurde. Die Verteilung und Dispersität wurde über Gelpermeationschromatographie (GPC) ermittelt. PEtOx Homopolymere waren monomodal und wiesen eine Dispersität kleiner 1.2 auf, wenn sie bei 100 °C polymerisiert worden waren. Es wurden jedoch häufig bimodale Verteilungen beobachtet, wenn PMeOx mit Piperidin terminiert wurde oder wenn bei PPrOx versucht wurde, hohe Polymerisationsgrade (größer 100) zu erreichen. Im nächsten Schritt wurden Copolymere aus den Monomeren MeOx oder EtOx mit ButEnOx und EtOx mit DecEnOx synthetisiert und anschließend charakterisiert. Die Monomere wurden statistisch miteinander copolymerisiert, indem sie zusammen zum Start der Reaktion in das Reaktionsgefäß gegeben wurden. Die Vinyl Funktionalität, die durch die Monomere ButEnOx und DecEnOx eingebracht wurde, kann später zur nachträglichen Funktionalisierung am Polymer verwendet werden. Der Polymerisationsgrad wurde konstant bei 50 gehalten und P(EtOx-*co*-ButEnOx) mit 10 mol% bis 40 mol% Vinyl Funktionalität, P(EtOx-*co*-DecEnOx) mit 7 mol%, 11 mol% und 17 mol% Vinyl Funktionalität und P(MeOx-*co*-ButEnOx) mit 9 mol%, 12 mol% und 20 mol% Vinyl Funktionalität wurden synthetisiert. Copolymere basierend auf EtOx zeigten monomodale Verteilungen mit niedrigen Dispersitäten, im Gegensatz zu Copolymeren basierend auf MeOx, wo die Dispersität zwischen 1.2 und 1.3 lag. Die Copolymere wiesen ein unterschiedliches thermoresponsives Verhalten auf. Die P(MeOx-*co*-ButEnOx) Copolymere waren ohne Einschränkung wasserlöslich, wohingegen der Einfluss der längeren Seitenkette von ButEnOx in Kombination mit dem Monomer EtOx schon bei 20 mol% ButEnOx ersichtlich war. In

diesem Fall fiel die Temperatur, bei der der Trübungspunkt erreicht wurde, auf 55 °C und sank noch weiter auf 25 °C, wenn 40 mol% ButEnOx in das Copolymer eingebunden war. Der Effekt des Co-Monomers DecEnOx war noch deutlicher und führte zu einer Erniedrigung des Trübungspunktes auf 25 °C bei einem DecEnOx Anteil von 7 mol%. Die Copolymere mit 10 mol% und 20 mol% ButEnOx wurden ebenfalls auf ihre Zytokompatibilität getestet und zeigten gute Ergebnisse. Im direkten Vergleich waren die Copolymere basierend auf MeOx etwas weniger zellverträglich als die auf EtOx Basierenden. Die synthetisierten Copolymere wurden weiterhin mit Thiolen über ein neues Syntheseprotokoll funktionalisiert. Im ersten Schritt wird ein Thioester an die Vinyl Seitengruppe mit Hilfe von radikalischer Thiol-en Chemie angebracht, welcher im zweiten Schritt mittels Cystein unter milden Bedingungen entschützt wird. Die erfolgreiche Funktionalisierung wurde mittels ^{1}H NMR und Raman Spektroskopie bewiesen. Das Ellman's Assay bestätigte ebenfalls den erwarteten Anteil an Thiolen und die GPC zeigte, dass unter den gegebenen Reaktionsbedingungen keine Degradation, wie erst unter basischen Bedingungen und hohen Temperaturen beobachtet, stattgefunden hatte. Die Thiol-funktionalisierten Copolymere waren etwas weniger zellfreundlich als die Elternpolymere. Bei 15 mg/mL – 5 mg/mL zeigten alle Thiol-haltigen Polymere moderate Zelltoxizität, jedoch keine Zelltoxizität bei 1 mg/mL.

Um Peptid-Polymer Konjugate zu bilden, wurden zyklische Thioester, genauer Thiolacton acrylamid und ein Azlacton Präkursor, dessen Synthese neu entwickelt wurde, an die Seitenkette von P(EtOx-*co*-ButEnOx) Copolymere angebunden. Die erfolgreiche Anbindung konnte mittels ^{1}H NMR und IR Spektroskopie nachgewiesen werden.

Das Kooperationsprojekt mit der Arbeitsgruppe von Prof. Dr. Blunk beinhaltete die Entwicklung eines Catechol-basierenden Hydrogel Systems. Da die Catechol Gruppe die Hydrophobizität des Polymers erhöht, wurden zwei Copolymere mit einem höheren Polymerisationsgrad (80 – 90) basierend auf den Monomeren EtOx und MeOx, welches das Polymer hydrophiler und somit einen höheren Funktionalisierungsgrad erlauben würde, hergestellt. Nach der Funktionalisierung der Seitengruppe mit Cysteamin oder 2-Mercaptoethanol mittels radikalischer Thiol-en Chemie wurde das geschützte Catechol Molekül an die Polymerseitenkette mittels Amidierung/Esterfizierung angebunden. Die erfolgreiche Anbindung wurde mittels ^{1}H NMR und UV/Vis Spektroskopie nachgewiesen. Die Funktionalisierungseffizienz

zeigte sich nicht so erfolgreich wie mittels Thiol-en Chemie und nur 58 % – 83 % der Seitengruppen konnten funktionalisiert werden.

Das dritte Kapitel des Ergebnisteils stellt die verschiedenen Anwendungen der funktionalisierten Copolymere vor. Zunächst werden Hydrogele, welche basierend auf radikalischer Thiol-ene Chemie in wässriger Lösung mit dem Photoinitiator Irgacure 2959 hergestellt wurden, präsentiert. Copolymere mit dem gleichen Thiol- und Vinylanteil wurden miteinander kombiniert und bei einer Polymerkonzentration von 15 wt% für 15 min unter UV-Strahlung vernetzt. Das Quellverhalten und die mechanischen Eigenschaften (Young's Modulus) wurden analysiert. Sowohl die Hydrophilie des Netzwerkes als auch die Vernetzungsdichte beeinflusste das Quellverhalten und die mechanische Festigkeit stark. Hydrogele, welche auf dem hydrophileren Monomer MeOx basierten, zeigten den höchsten Quellungsgrad und Hydrogele, welche auf dem weniger hydrophilen Monomer EtOx basierten, zeigten ein eingeschränktes Quellvermögen bei 37 °C durch ihr thermoresponsives Verhalten. Das Quellverhalten wurde außerdem durch die Zugabe von Salzen beeinflusst, so dass die Gele 1.5-mal stärker in ultrareinem Wasser quellen konnten im Vergleich zu in PBS gelagerten Gelen. Die Young's Moduli lagen zwischen 100 kPa bis 380 kPa, abhängig von der Copolymer Zusammensetzung und dem Funktionalisierungsgrad. Alle Hydrogele zeigten gute Zellverträglichkeit. Zudem wurden Hydrogele basierend auf EtOx auch mit FITC funktionalisierten Dextran unterschiedlichen Molekulargewichts beladen. Es konnte beobachtet werden, dass Dextran mit 500 kDa nicht mehr aus dem Netzwerk herausdiffundieren konnte, wohingegen Dextran mit 40 kDa Molekulargewicht aus dem Netzwerk mit niedriger Vernetzungsdichte in einer zweifach so großen Menge herausdiffundierte wie aus dem stärker vernetzten Hydrogel. Die Hydrogele basierend auf MeOx und EtOx wurden außerdem mit den Farbstoffen Fluorescein und Methylenblau beladen. Es wurde beobachtet, dass von den beiden Farbstoffen die Aufnahme des hydrophileren Farbstoffs Fluorescein stärker vom Quellungsgrad des Hydrogels abhing. Hingegen war die Aufnahme des hydrophoberen Farbstoffs Methylenblau weniger davon abhängig wie sehr das Hydrogel quellen konnte, sondern stärker von der Hydrophilie des Hydrogel-Netzwerkes. Für das Knorpelkleber Projekt mit dem Arbeitskreis von Prof. Dr. Blunk wurden (biohybride) Hydrogele basierend auf Catechol-funktionalisiertem Copolymeren mit und ohne zusätzliches Fibrinogen und dem Oxidationsmittel Natriumperiodat synthetisiert. Das System war durch die

eingebauten Ester Vernetzungspunkte abbaubar. Das Quellverhalten und die mechanischen Eigenschaften (Young's Modulus) wurden charakterisiert. Wie zu erwarten, zeigten Hydrogele mit stärkerer Vernetzung eine geringe Quellung und einen höheren elastischen Modulus. Die Zugabe von Fibrinogen jedoch erhöhte die Elastizität des Netzwerkes, welches förderlich für die avisierte Anwendung als Knorpelkleber sein kann. Die biologische Auswertung, die im Labor von Prof. Dr. Blunk durchgeführt wurde, zeigte, dass die Ester-haltigen, abbaubaren Vernetzungspunkte von großem Vorteil sind. Die Chondrozyten konnten ohne Probleme den Defektspalt überbrücken, was nicht möglich war, sobald keine Ester Funktionalitäten im Hydrogel eingebunden waren.

Im letzten Abschnitt werden verschiedene Möglichkeiten Peptid-Polymer Konjugate zu synthetisieren präsentiert. Zum einen wurden Peptide mit der Thiolgruppe des endständigen Cysteins an die Vinyl Seitenkette der P(EtOx-*co*-ButEnOx) Copolymere mittels radikalischer Thiol-en Chemie angebunden. Die erfolgreiche Umsetzung wurde mittels ^{1}H NMR Spektroskopie untersucht. Die beiden Peptide, CGGGF und CKFKFQF, wobei letzteres das Hydrophobere ist, wurden in verschiedenen Lösungsmitteln angebunden. Es zeigte sich, dass der Erfolg der Reaktion stark von der Wahl des Lösungsmittels abhing und dass die benötigten Äquivalente an Peptid bis auf 1.5 Äquivalente reduziert werden konnten, wenn das richtige Lösungsmittel gewählt wurde. Des Weiteren wurde ein zyklischer Thioester, das Thiolacton, verwendet, um das Peptid CGGGF an die Seitenkette von P(EtOx-*co*-ButOxLac) mittels nativer chemischer Ligation zu binden. Die ^{1}H NMR Spektroskopie bestätigte die Anbindung des Peptids und HPLC Messungen zeigten einen Anstieg der Intensität bei einer Wellenlänge von 254 nm, was auf die Anwesenheit des Aromaten des Phenylalanins hinweist. Im letzten Abschnitt des Kapitels wurde das Peptid CGGGF an Azlacton-funktionalisierte Copolymere in DMSO gebunden, um die frühzeitige Hydrolyse des Azlacton Ringes durch Wassermoleküle zu verhindern. Die erfolgreiche Anbindung konnte über ^{1}H NMR und IR Spektroskopie und über HPLC Messung bestätigt werden. Die zwei zuletzt genannten Strategien, um Peptide an Polymere zu binden, sind besonders interessant, da hier ein beziehungsweise im Fall der Thiolacton Funktionalität zwei freie Thiole an der Bindungsstelle nach der Reaktion entstehen. Diese könnten genutzt werden, um zum Beispiel über Thiol-en Chemie Peptid-haltige Hydrogele herzustellen.

Zusammenfassend zeigen seitenkettenfunktionale Poly(oxazolin) Copolymere ein großes Potenzial für biomedizinische Anwendungen. Die vielen verschiedenen Seitenkettenfunktionalitäten können durch das passende Monomer oder durch Post-Polymerisationsfunktionalisierung eingebracht werden, wie in dieser Arbeit gezeigt. Durch ihre Multifunktionalität können Hydrogel Charakteristika, wie der Vernetzungsgrad und die mechanische Festigkeit, fein eingestellt und angepasst werden, je nach Anwendungsbereich im menschlichen Körper. Die entwickelten chemoselektiven und orthogonalen Reaktionswege können in der Zukunft genutzt werden, um Polymer Konjugate zu synthetisieren, welche zum Beispiel für das Drug Delivery oder im Bereich der Geweberegneration zum Einsatz kommen.

5 Experimental section

Parts of this chapter have already been published in

Julia Blöhbaum, Ilona Paulus, Ann-Christin Pöppler, Jörg Tessmar and Jürgen Groll; Influence of charged groups on the cross-linking efficiency and release of guest molecules from thiol-ene cross-linked poly(2-oxazoline) hydrogels, *Journal of Materials Chemistry B* **2019**, *7*, p. 1782-1794.

Julia Blöhbaum, Oliver Berberich, Stefanie Hölscher-Doht, Rainer Meffert, Jörg Teßmar, Torsten Blunk, Jürgen Groll; Catechol-modified Poly(oxazoline)s with Tunable Degradability Facilitate Cell Invasion and Lateral Cartilage Integration, *Journal of Industrial and Engineering Chemistry* **2019**, *80*, p. 757-769.

Julia Liebscher, Jörg Tessmar, Jürgen Groll; In situ polymer analogue generation of azlactone functions at poly(oxazoline)s for peptide conjugation, *Macromolecular Chemistry and Physics*, November 2019, accepted.

5.1 Materials

All chemicals and solvents used are commercially available and were used as received, unless stated otherwise.

CaH_2 (92 %, abcr GmbH, Karlsruhe, Germany), chloroethylamine HCl (99.8 %, Alfa Aesar, Haverhill, MA, USA), cysteamine*HCl (BioChemica, AppliChem, Darmstadt, Germany), diethyl ether (Staub & Co., Nürnberg, Germany), 1-ethyl-3-(3-dimethylaminopropyl)carbodiimide hydrochloride (CarboSynth, Compton, UK), formic acid (98/100 %, Bernd Kraft, Duisburg, Germany), thiobenzoic acid (94 %, Alfa Aesar, Haverhill, MA, USA), tris(2-carboxyethyl)phosphine hydrochloride (TCEP) (≥ 98 %, Carl Roth GmbH + Co KG, Karlsruhe, Germany).

Acetic acid anhydride (98 %) and dichloromethane (reagent grade) were purchased from VWR (Radnor, PA, USA).

Chloroform (reagent grade), 1,4-dioxane (reagent grade), ethyl acetate (reagent grade), methanol (reagent grade), potassium hydroxide (85 %), sodium borhydride (99 %), sodium hydrogen carbonate (99 %) and sodium dihydrogen phosphate (99 %) were purchased from Fisher Scientific (Hampton, NH, USA).

Acryloyl chloride (stabilized with phenothiazine for synthesis, > 98 %), aqueous ammonia (32 %), hydrochloric acid (32 %), sodium hydroxide (ACS, Reag. Ph Eur), fluorescein sodium salt (extra pure), methylene blue B (for microscopy) and pyridine (> 99 %) were purchased from Merck (Darmstadt, Germany).

Acetone (≥ 99.5 %), acetonitrile (anhydrous, 99.8 %), allylamine (98 %), 1-boc-piperazine (≥ 98.0 %), 2-aminoisobutyric acid (98 %), 3-bromopropionyl chloride (technical grade), butyronitrile (≥ 99.0 %), 1,1′-carbonyldiimidazole (CDI) (reagent grade), 2-chloroethylammonium chloride (99 %), L-cysteine hydrochloride monohydrate (≥ 98 %), FITC-dextran (average molecular weight 4000, 40,000 and 500,000), *N,N*'-dicyclohexylcarbodiimide (99 %), 3,4-dihydroxyphenylacetic acid (DOPAC) (98 %), 4-(dimethylamino)pyridine (≥ 99.0 %), dimethylformamide (99.8 %, anhydrous), 2,2-dimethoxy-2-phenylacetophenone (99 %), dimethylphenylphosphine (99 %), *N,N*'-disuccinimidyl carbonate (≥ 95 %), 5,5'-dithiobis(2-nitrobenzoic acid) (Ellman's reagent) (99 %), dopamine hydrochloride, ethanolamine (≥ 98 %), 2-ethyl-2-oxazoline (≥ 99 %, distilled and dried over CaH_2 prior to use), ethyl chloroformate (97 %), fibrinogen from bovine plasma (Type I-S, 65-85 % protein), D,L-

homocysteine thiolactone hydrochloride (> 99 %), 2-hydroxy-4′-(2-hydroxyethoxy)-2-methylpropiophenone (Irgacure 2959), N-hydroxysuccinimide (98 %), magnesium sulfate (≥ 99.5 %), 2-mercaptoethanol (≥ 99.0 %), 4-mercaptophenylacetic acid (97 %), methanol (99.8 %, anhydrous), 2-methyl-2-oxazoline (≥ 99 %, distilled and dried over CaH_2 prior to use), methyl tosylate (98 %), methyl trifluoromethanesulfonate (≥ 98.0 %), pentenoic acid (≥ 98 %), piperidine (≥ 99.5 %, anhydrous, purified by redistillation), sodium formiate (≥ 99 %), thioacetic acid (96 %), triethylamine (≥ 99 %), thioglycolic acid (98 %), 10-undecenoyl chloride (97 %) and zinc acetate dihydrate (reagent grade) were purchased from Sigma-Aldrich (St. Louis, MO, USA).

The peptides CGGGF (≥ 95 %) and CGRGDS (≥ 95 %) were purchased from GeneCust (Ellange, Luxembourg).

The deuterated solvents deuterium oxide (D_2O), deuterated chloroform ($CDCl_3$), dimethyl sulfoxide-d_6 (DMSO-d_6), acetonitrile-d_3 (CD_3CN) and methanol-d_4 (CD_3OD) were purchased from Deutero GmbH (Kastellaun, Germany).

To prepare 1x phosphate buffered saline (1xPBS), sodium chloride (8.00 g, 136.89 mmol), potassium dihydrogen phosphate (0.2 g, 1.47 mmol, Merck, Darmstadt, Germany), sodium hydrogen phosphate (1.11 g, 7.82 mmol, Merck) and potassium chloride (0.2 g, 2.68 mmol, Merck) were dissolved in 1 L of deionized water. Ultrapure (Milli-Q) water was obtained from an ultrapure water system (arium® pro, Sartorius, Göttingen, Germany).

5.2 Methods

5.2.1 Monomer and Polymer Characterization

5.2.1.1 Dynamic Light Scattering

Diluted aqueous solutions (1 – 10 mg/mL) were measured in plastic or glass cuvettes in a Zetasizer Nano-ZSP from Malvern Panalytical GmbH (Herrenberg, Germany). The instrument is equipped with a 633 nm HeNe Laser and works at measurement angles of 13° and 173°. To determine the cloud point of the aqueous polymer solutions, a temperature program was run in 0.5 °C steps with 3 measurements of 3x10 s at each temperature point.

5.2.1.2 Electron Impact Mass Spectrometry

Electron impact mass spectrometry (EI-MS) was measured on a Finnigan MAT90 from Finnigan MAT, Bremen, Germany.

5.2.1.3 Fluorescence Spectroscopy

The fluorescence intensity of fluorescently-labeled dextran was measured in black flat 96-well plates (Greiner Bio-One GmbH, Kremsmünster, Austria) on a Tecan Spark® 20 M multimode microplate reader (Tecan, Crailsheim, Germany) at an excitation wavelength of 485 nm and an emission wavelength of 535 nm.

5.2.1.4 Fourier Transformed Infrared Spectroscopy

The FT-IR spectroscopy measurements were performed on a Nicolet iS10 with a Smart iTR diamond attenuated total reflectance unit (Waltham, Massachusetts, USA). The beam splitter consists of KBr and the spectral region reaches from 4200 cm^{-1} to 650 cm^{-1}. The instrument is operated with OMNIC. The characteristic vibrations of each functional group were assigned according to [175].

5.2.1.5 High Performance Liquid Chromatography

High Performance Liquid Chromatography (HPLC) is a method to separate molecules based on their affinity to the column material. Depending on the ability of the molecule to adsorb to the solid phase of the column, the sample will elute at a different time point than the other molecules in the sample mixture. The HPLC system that was used consisted of a series-type double plunger (LC-20AT), an autosampler (SIL-20AC), fluorescence detector (RF-20A), a photodiode array detector (SPD-M20A), a column oven (CTO-20AC), a system controller (CBM-20A), a refractive index detector (RID-20A) and a fraction collector (FRC-10A) from Shimadzu (Kyoto, Japan). The columns used were a Luna 5 µm C18(2) 100 Å LC column (150x4.6 mm) from Phenomenex Inc. (Torrance, CA, USA) or a XBridge C18 3.5 µm column (250x4.6 mm) from Waters Corporation (Milford, MA, USA). The measurement was run as a gradient starting with 10 % acetonitrile in water to 90 % acetonitrile. The samples were dissolved in water and filtered through a syringe filter (0.25 µm, nylon) prior to injection.

5.2.1.6 Nuclear Magnetic Resonance

Nuclear magnetic resonance (NMR) spectroscopy was used for structural identification of all low and high molecular weight compounds. All NMR spectra were measured on a Fourier 300 from Bruker (Billerica, MA, USA) operating at 300 MHz. All spectra were referenced to the signal of the non-deuterated solvent. Samples were dissolved and measured in deuterium oxide (D_2O), deuterated chloroform ($CDCl_3$), dimethyl sulfoxide-d_6 (DMSO-d_6), acetonitrile-d_3 (CD_3CN) or methanol-d_4 (CD_3OD).

5.2.1.7 Solid-state Nuclear Magnetic Resonance

Solid-state nuclear magnetic resonance (NMR) was measured of freeze-dried polymers or hydrogels which had been gently ground and filled in a solid-state NMR rotor. A 600 MHz Bruker Avance III spectrometer at 14.1 T and 12.5 kHz MAS using a Bruker 3.2 mm double-resonance probe was used for the experiments. The temperature of the measurement was set to 23.25 °C. The ^1H 90° pulse length was

of 2.5 µs duration. In ^{13}C detection experiments, SPINAL64 heteronuclear decoupling was applied during acquisition. A ramp on the ^{1}H channel was used for the CP contact time in ^{1}H-^{13}C cross polarization experiments. The contact time was 2 ms. ^{13}C NMR spectra were referenced with respect to trimethylsilane (TMS) by using adamantane and assigned with additional information from 2D ^{1}H-^{13}C cross polarization correlations in the solid state and a set of standard 1 and 2D spectra in solution.

5.2.1.8 Raman Spectroscopy

Raman spectroscopy was measured using a DXR Raman microscope from Thermo Fisher Scientific (Waltham, MA, USA) equipped with a 780 nm laser. For the measurement, a 10x objective was used with fluorescence correction of 5th degree polynomial order and a signal to noise ratio of 500 at a laser power of 24 mV. The characteristic Raman bands of each functional group were assigned according to [160].

5.2.1.9 Cryo Scanning Electron Microscopy

Cryo scanning electron microscopy (SEM) was performed on a Crossbeam 340 from Zeiss (Carl Zeiss Jena GmbH, Jena, Germany) equipped with a GEMINI e-beam column (Carl Zeiss Jena GmbH, Jena, Germany). A polymer precursor solution in MilliQ-water with photo-initiator was prepared and 2 – 3 µL were pipetted on an aluminum carrier plate Type B (Ø 3 x 0.5 mm) from Baltic Präparation (Niesgrau, Germany). The polymer solution was cross-linked for 5 min using a UV handlamp. The carrier plate was transferred into a nitrogen slush and immediately frozen. Afterwards, the samples were freeze-etched for 10 min at -85 °C and vapor coated with 4 mm of platinum in a high vacuum coater Leica EM ACE 600 (Emitech, Molfetta, Italy).

5.2.1.10 Size Exclusion Chromatography

Size exclusion chromatography (SEC) is an analytical method to characterize the molecular weight distribution of macromolecules and with the right detectors, even

the degree of branching can be determined. The principle of SEC is that the macromolecules are separated according to their hydrodynamic volume on a gel packed matrix. In contrast to High Performance Liquid Chromatography (HPLC), an interaction with the column material is undesired. SEC can further be used to estimate the molecular weight of polymers by calibrating the instrument with known polymer standards. The results can then be used to generate a calibration curve. When only the refractive detector is used for the evaluate the results, it is called a conventional calibration. When a combination of refractive index detector and viscometer detector is used, a universal calibration can be performed. As the intensity of the scattered light by a molecule is proportional to the molecular weight of the molecule, the molar mass that is calculated, when a light scattering detector is additionally used, is the most exact.

One of the GPC systems used to analyze parent and functionalized POx polymers is an OmniSEC Resolve & Reveal system from Malvern Panalytical GmbH (Herrenberg, Germany) consisting of an autosampler, pump, column oven (45 °C), RI detector (45 °C), viscometer detector (45 °C), right angle light scattering (RALS) detector (45 °C) and low angle light scattering (LALS) detector (45 °C). The columns were a set of a precolumn (Dguard), a D2000 (300x7.8 mm, exclusion limit poly(styrene): 5,000 g/mol, particle size: 6 µm) and a D3000 (300x7.8 mm, exclusion limit poly(styrene): 70,000 g/mol, particle size: 6 µm) from Viscotek (Malvern Panalytical GmbH). The eluent is dimethyl formamide (DMF) with 1 g/L lithium bromide and a monodisperse poly(methyl methacrylate) purchased from Malvern with a molecular weight of 50 kDa was used for the calibration using the RI and viscometer detectors in combination with the light scattering detectors. This calibration method is named triple detection. The SEC elugram displayed show the RI, viscometer and RALS signal only as the LALS signal is usually rather weak for polymers with a molecular weight below 10 kDa.

A few of the earlier synthesized polymers were measured on a SEC system from Polymer Standard Service SECurity (PSS, Mainz, Germany) equipped with an MDS RI detector (Agilent technologies, Santa Clara, USA), a 50 mm GRAM precolumn (pore size 30 Å) and a 300 mm GRAM column (pore size 1000 Å) running on DMF with 1 g/L LiBr. The column oven was set at 40 °C and the flow rate was 1 mL/min. Narrow PEG standards with a molecular weight from 106 Da to 1,015 kDa were used for the conventional calibration of the system.

The polymer samples were dissolved in the eluent to a concentration of 3 – 5 mg/mL. After complete dissolution, the samples were filtered through a PTFE syringe filter with a pore size of 0.25 µm.

5.2.1.11 UV/Vis Spectroscopy

UV/Vis spectroscopy of diluted aqueous solutions were measured at a Genesys 10S Bio spectrophotometer (Thermo Fisher Scientific, Waltham, MA, USA) equipped with a xenon lamp and a wavelength region of 190 nm to 1100 nm.

5.2.1.12 Polymer Purification

Water soluble POx could be purified by means of dialysis. For this method, the polymer was dissolved in an adequate amount of water and placed in cellulose dialysis membranes Spectra/Por® with a molecular weight cut-off of 1 kDa or 3.5 kDa purchased from Carl Roth GmbH + Co KG (Karlsruhe, Germany) in 2 L of Milli-Q water.
Frequent water changes every two hours for several days ensured good results.
Depending on the cloud point of the polymer, the dialysis water was constantly cooled by an ice bath. Thiol functionalized POx was dialyzed in water that had been degassed for at least two hours with argon prior to use.

After dialysis, the aqueous polymer solution was frozen in liquid nitrogen and placed on an Alpha 1-2 LD or an Epsilon 2-4 LSCplus freeze dryer from Martin Christ Gefriertrocknungsanlagen GmbH (Osterode am Harz, Germany).

5.2.1.13 Polymer Synthesis

Polymer synthesis was performed, unless otherwise stated, in microwave synthesizer Discover SP from CEM GmbH (Kamp Lintfort, Germany) using 10 mL or 35 mL vessels with a silicon cap. The microwave irradiation provides for a quick and homogenous heating and the sealed vessels allow working above the boiling point of the solvent and monomers.

5.2.1.14 Glovebox

The purified and dried monomers as well as thiol functionalized POx copolymers which are susceptible to oxidation were stored in a glovebox, model GS046711 (Glovebox Systemtechnik, Malsch, Germany).

5.2.1.15 UV Sources

UV reactions for polymer functionalization were performed using three UV LED cubes (365 nm, 77 mW/cm^2) from Polymerschmiede (Aachen, Germany).
To cross-link hydrogels, a UV handlamp with filter set to 365 nm (1 mW/cm^2) from A. Hartenstein (Würzburg, Germany) was used.

5.2.1.16 Ellman Assay

The Ellman assay was used to quantify the amount of thiol functionality at the polymer by using a dilution series of 2-mercaptoethanol as the reference. A stock solution of 36 µL 2-mercaptoethanol in 49.964 mL water was prepared and 16 different concentrations ranging from 9 µM to 255.73 µM 2-mercaptoethanol were created. A dilution series of the polymer was prepared so that the expected amount of thiol/polymer would be in the range of the molarity of the 2-mercaptoethanol reference. The assay was performed in a 96 well plate (Thermo Scientific, Nunclon Delta Surface). In one well, 10 µL of the polymer sample, standard or in case of the blank pure water was pipetted. 40 µL of a 1 M $NaBH_4$ solution in 0.01 M NaOH was added and the mixture was incubated for 60 min at room temperature. Afterwards, 24 µL of a 1 M HCl was added. After incubation for 30 min, 116 µL of 0.8 M PBS was added, the solution gently mixed with the pipette and measured at 412 nm in a Tecan Spark® 20 M multimode microplate reader (Tecan, Crailsheim, Germany). The values of the 2-mercaptoethanol standard was used to create a linear calibration curve according to which the functionality degree on the polymer chain could be calculated.

5.2.2 Hydrogel Preparation

5.2.2.1 Thiol-ene Cross-linked Hydrogels

Hydrogels were prepared in Milli-Q water or in 1xPBS to the desired wt%. Vinyl and thiol functionalized POx copolymers with the same functionality degree were combined in an equimolar amount (ratio vinyl:thiol was 1:1). First, the vinyl functional polymer was dissolved in the appropriate amount of water or PBS in which the thiol functionalized copolymer was further dissolved. A 2.5 mg/mL stock solution of the photoinitiator Irgacure I2959 was prepared and added to the polymer precursor solution so that overall photoinitiator concentration in the hydrogel solution was 0.05 wt%. The hydrogel solution was pipetted into clear cylindrical silicon molds (Ø = 4 mm and h = 4 mm) and irradiated for 15 min with the UV handlamp.

5.2.2.2 Catechol Cross-linked Hydrogels

Hydrogels without additional fibrinogen were fabricated by preparing stock solutions of catechol-functionalized POx in 1xPBS. The stock solutions were pipetted into cylindrical molds and a 300 mM sodium periodate ($NaIO_4$) stock solution was added to induce cross-linking. The hydrogels were fabricated with either 7.5 w/v% or 12.5 w/v% of the polymer with the $NaIO_4$ concentration always being kept at 60 mM.
Hydrogels with additional fibrinogen were prepared by mixing a stock solution of the catechol-functionalized POx in PBS with a 12.5 % (w/v) solution of fibrinogen in PBS. The well-mixed solution was again pipetted into a silicon mold and a 300 mM stock solution of $NaIO_4$ was added. All hydrogels were made with 5 w/v% fibrinogen but with 5 w/v%, 7.5 w/v% or 10 w/v% of catechol-functionalized POx. In addition, the polymer content was made up of 0 %, 25 % or 50 % (in mass) of POx to which the catechol group had been bound by an ester linkage.
The silicon molds were of 2 mm in height and had a diameter of 6 mm for gravimetrical analysis and of 4 mm in height and had a diameter of 4 mm for mechanical testing.

5.2.3 Hydrogel Characterization

5.2.3.1 Swelling Studies and Gel Fraction

Hydrogels were incubated in Milli-Q water or in 1xPBS at 37 °C and at 4 °C for thermo-responsive hydrogels for up to four weeks to analyze the swelling over time. The hydrogel specimens were weighed directly after preparation (w_0) and at defined time points (w_t). Before weighing, the hydrogel specimens were blotted on tissue paper to remove excess water. The mass change in wt% can be calculated as follows: $\text{Mass change (wt\%)} = \frac{w_t}{w_0} x\ 100.$

To determine the equilibrium swelling degree (SD) the hydrogel specimen was incubated for 1 d incubation in 1xPBS at 37 °C or 4 °C and its weight was measured (w_s). The specimen was further freeze-dried, and the weight was measured again (w_d). The SD can be calculated as follow: $\text{SD} = \frac{w_s - w_d}{w_d}$.

The gel fraction, meaning the amount of polymer that has reacted and was built into the hydrogel network, was determined by fabricating hydrogels in Milli-Q water which were directly freeze-dried and afterwards weighed (w_i). The same hydrogel specimen was further incubated in Milli-Q water for three days at 37 °C with frequent water changes to wash away any non-bound polymer. The hydrogel specimen was freeze-dried again and weighed (w_g). The gel fraction was calculated as follows: $\text{Gel fraction (\%)} = \frac{w_g}{w_i} x\ 100.$

All measurements were done in triplicates.

5.2.3.2 Mechanical Testing

The mechanical testing of the hydrogel specimens was performed on a mechanical test instrument (ElectroForce 5000, TA Instruments, Eden Prairie, MN, USA) equipped with a load cell of 22 N or 250 g depending on the softness of the hydrogel. The hydrogels were prepared as described before in a cylindrical shape with a diameter of 4 mm and a height of 4 mm, but the dimensions were additionally measured with a sliding caliper before each measurement. The specimens were compressed by 1.25 mm in height between two metal cylinders with a speed of 0.0025 mm/s. All measurements were done in triplicates. When the 250 g load cell

was used, the obtained values were multiplied with the gravitational acceleration constant (9.81 m/s^2) to convert the value from Gram into Newton.
The strain was calculated by dividing the displacement, which had been recorded during the measurement, by the original height. The stress was calculated as follows:

$$\text{Stress (MPa)} = load(N)\ x\ \frac{height_{hydrogel}\ (mm) - displacement\ (mm)}{volume_{hydrogel}\ (mm^3)}$$

The stress was plotted versus the strain and a linear fit was applied from 0.1 to 0.2 strain to obtain the Young's modulus, which was the slope of the linear fit.

5.2.4 Loading and Release of Fluorescein Isothiocyanate-Dextran

Thiol-ene cross-linked hydrogels based on copolymers synthesized with EtOx were prepared as described earlier in 1xPBS and fluorescein isothiocyanate-dextran (FITC-dextran) with different molar mass was mixed with the hydrogel precursor solution prior to cross-linking. One hydrogel specimen would contain either 0.008 ng of 4 kDa or 500 kDa dextran or 0.016 ng of 40 kDa. It was chosen to add more 40 kDa dextran to the hydrogel as the degree of substitution was only 0.001 mol – 0.008 mol FITC/mol glucose compared to 0.002 mmol – 0.020 mol FITC/mol glucose for dextran with a molar mass of 4 kDa and 500 kDa. The hydrogels were incubated in 1 mL of PBS at 37 °C and additionally at 4 °C for hydrogels with 20 mol% functionality for 15 d. At each time point, 0.8 mL of buffer were removed and measured by fluorescence spectroscopy (excitation wavelength = 485 nm, emission wavelength = 535 nm) and replaced with 0.8 mL of fresh buffer.

5.2.5 Loading and Release of Small Molecular Weight Substances

Thiol-ene cross-linked hydrogels with 15 wt% polymer were prepared as described earlier in 1xPBS. Directly after fabrication, they were immersed in saturated buffered methylene blue solution (40 g/L) or in buffered fluorescein sodium salt solution (60 g/L) at room temperature or at 4 °C for thermo-responsive hydrogels. It was observed that methylene blue did not dissolve as well at 4 °C and it is anticipated from UV/Vis measurements that the concentration of dissolved methylene blue is only 11.76 g/L at 4 °C. The hydrogels that had been incubated at room temperature overnight were placed at 37 °C for one hour.

All hydrogels were taken out of the dye solution, blotted on tissue paper to remove excess dye solution and placed in clean vials containing 9 mL of fresh tempered (4 or 37 °C) PBS. At timepoints 0.5 h, 1 h, 2 h, 4 h, 8 h and 24 h, 1 mL was removed and replaced with 1 mL of fresh tempered PBS. After one day, the hydrogels were removed and placed in fresh 9 mL of PBS for fluorescein loaded hydrogels and in only 5 mL for methylene blue loaded hydrogels. Samples of 1 mL were taken and replaced with fresh PBS at time points 30 h, 48 h, 54 h, 72 h and 96 h. After 96 h, the hydrogels were removed and placed in Eppendorf tubes with 0.5 mL of PBS. Samples of 0.2 mL were taken and replaced with fresh PBS at time points 5 d, 7 d, 9 d, 11 d and 14 d.

5.2.6 Cell Viability Assays

Mouse fibroblasts (L 929 CC1) were cultured in Dulbecco's Modified Eagle Medium (DMEM, Life Technologies) containing 10 % fetal bovine serum (Sigma-Aldrich) and 1 % penicillin-streptomycin (Thermo Fisher Scientific) in a T75 cell culture bottle (BD Falcon, Bioswisstec AG, Schaffhausen, Switzerland) at 37 °C and 5 % CO_2. The cells were washed two times with 1xPBS and detached with 1 mL of Accutase® solution (Sigma-Aldrich) for five minutes.

5.2.6.1 CellTiter-Glo® Luminescent Assay

The cell toxicity of the functional (vinyl and thiol) POx copolymers was tested with a CellTiter-Glo® Luminescent cell viability assay (Promega Corporation, Madison, WI, USA), as the standard cytotoxicity assays based on tetrazolium salts (MTT or WST) were not applicable for thiol functional copolymers. After determination of the cell number, the concentration was diluted to 50,000 cells/mL. In each well of a 48 well plate, 0.5 mL of the cell suspension were seeded and cultivated for 24 h at 37 °C/5 % CO_2. The vinyl functional polymers P(MeOx$_{0.89}$-*co*-ButEnOx$_{0.11}$)$_{44}$, P(MeOx$_{0.78}$-*co*-ButEnOx$_{0.22}$)$_{53}$, P(EtOx$_{0.91}$-co-ButEnOx$_{0.09}$)$_{60}$ and P(EtOx$_{0.79}$-co-ButEnOx$_{0.21}$)$_{53}$, as well as the thiol functionalized version of these polymers except for P(EtOx$_{0.79}$-co-ButOxSH$_{0.21}$)$_{53}$ due to its low cloud point were tested at concentrations of 15, 5, 1 and 0.1 mg/mL prepared in cell media. The cells were incubated for 48 h at 37 °C/5 % CO_2 with the polymer solutions which were tested in fourfold, as well as the controls.

The negative control was poly(styrene) (Nunc, Thermo Fisher Scientific) and as the positive control, the eluate of 1 mL per 1.25 cm^2 of a Vekoplan KT poly(vinyl chloride) plate (König GmbH, Wendelstein, Germany), incubated for 24 h, was used. The well plates and the assay reagent were tempered at room temperature for 30 min before the assay. The reagent was diluted in a 1:1 ratio with the cell culture media. Before 0.5 mL of the diluted assay reagent was added, the media supernatant was carefully removed. The diluted assay reagent acted as blank. The well plates were mixed on an orbital shaker for two minutes and incubated for 10 min at room temperature to stabilize the luminescence signal. From each well, two times 0.2 mL were pipetted into a white 96 well plate and the luminescence was measured on a Tecan Spark® 20 M multimode microplate reader (Tecan, Crailsheim, Germany).

5.2.6.2 WST-1 Assay

The cell proliferation in direct contact with the hydrogels was tested with a water-soluble tetrazolium (WST-1) assay (WST reagent by Roche purchased from Sigma-Aldrich). The hydrogels were prepared in triplicates as described earlier but under sterile conditions. The hydrogels precursor polymers were P(MeOx$_{0.91}$-*co*-ButEnOx$_{0.09}$)$_{56}$, P(MeOx$_{0.82}$-*co*-ButEnOx$_{0.18}$)$_{49}$, P(EtOx$_{0.91}$-*co*-ButEnOx$_{0.09}$)$_{60}$ and P(EtOx$_{0.79}$-*co*-ButEnOx$_{0.21}$)$_{53}$ always partnered with the thiol functionalized version of the vinyl functional polymer. Silicon molds with a diameter of 6 mm and a height of 1 mm (volume = 30 µL) were used and the hydrogels were only cross-linked for 10 min due to the smaller dimensions of the silicon mold. The cell number for this test was only 40,000 cells/mL as the intended assay time was 7 days. 0.5 mL of the cell suspension was seeded per well in a 48 well plate and cultivated for 24 h. Afterwards, the media supernatant was removed, and the hydrogel specimen were placed on top of the cells in the middle of the well. New media was added to each well and the hydrogels were incubated for 7 days, with cell culture media change after 3 days. As positive control, the eluate of 1 mL per 1.25 cm^2 of a Vekoplan KT poly(vinyl chloride) plate (König GmbH, Wendelstein, Germany) and as negative control, poly(styrene) and 2 wt% agarose hydrogels (Ø = 6 mm, h = 1 mm) were used. The agarose hydrogels were used to exclude any mechanical effect caused by the hydrogel covering the cells.

After 7 days, the cell culture media was removed from each well. The WST reagent was diluted in a ratio of 1:10 with culture media and 0.5 mL of the diluted reagent was added to each well and incubated for 30 min at 37 °C. Duplicates of 0.2 mL of each well were pipetted into a 96 well plate and measured at a wavelength of 450 nm on a Tecan Spark® 20 M multimode microplate reader (Tecan, Crailsheim, Germany). A reference wavelength at 620 nm was subtracted from each measurement.

5.2.7 Statistical Analysis

Statistical analysis was performed with SigmaPlot12.5 (Systat Software, Erkrath, Germany) using a two way analysis of variance (two way ANOVA) for the time dependent swelling behavior. A one way ANOVA was used for the comparison of the Young's modulus, the swelling degree and the release of fluorescein sodium salt and methylene blue. Significant differences were determined using post-hoc Tukey test with a significance level of $p > 0.05$.

5.3 Synthesis

5.3.1 Monomer Synthesis

5.3.1.1 2-(3-Butenyl)-2-oxazoline

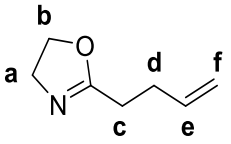

The synthesis of 2-(3-butenyl)-2-oxazoline (ButEnOx) was performed according to Gress *et al*. [21]. The first step involved the activation of the carboxylic acid group of pentenoic acid (14.700 g, 147 mmol, 1 eq.) with N-hydroxysuccinimide (27.037 g, 235 mmol, 1.6 eq.) using 1-(3-dimethylaminopropyl)-3-ethylcarbodiimide Hydrochloride (EDC·HCl, 33.775 g, 176 mmol, 1.2 eq.) in 600 mL of dichloromethane (DCM). After stirring overnight under argon atmosphere, the organic solvent was removed, and the residual product was dissolved in diethyl ether (Et_2O) and washed five times with water. The organic solvent is dried with $MgSO_4$ and removed under reduced pressure to isolate the final product. *N*-succinimidyl-4-pentenate (22.949 g, 114 mmol, 1 eq.) was dissolved in 200 mL of DCM and cooled in an ice bath. Chloroethylamine HCl (26.463 g, 228 mmol, 2 eq.) was dissolved in 100 mL of water, cooled, and sodium hydroxide (9.126 g, 228 mmol, 2 eq.) was added. The aqueous solution was introduced dropwise to the organic phase and left stirring over night at room temperature.

The aqueous phase was removed, and the organic phase was washed five times with water, dried and removed under reduced pressure to receive the final product. *N*-(2-chloroethyl)-4-pentenamide (23.244 g, 144 mmol, 1 eq.) and in a second flask potassium hydroxide (8.069 g, 144 mmol, 1 eq.) was dried under reduced pressure ($1 \cdot 10^{-3}$ mbar) in a flame-dried flask for one hour. To both flasks, 60 mL of dry methanol was added and flushed with argon for 45 min. The potassium hydroxide solution was added dropwise to the pentenamide solution and afterwards stirred for 24 h at 70 °C under inert atmosphere. The precipitated KCl was filtered off and the solvent was removed under reduced pressure. The product, ButEnOx, was dissolved in DCM and washed five times with distilled water. The organic phase was dried over

$MgSO_4$ and evaporated under reduced pressure. The monomer was fractionally distilled over CaH_2 at $1 \cdot 10^{-3}$ mbar at 45 °C and received as a colorless liquid (9.681 g, 77 mmol, 54 % yield).

^{1}H NMR of ButEnOx (300 MHz, $CDCl_3$, ppm): δ = 5.83 (m, 1 H, H-**e**), 5.03 (m, 2 H, H-**f**), 4.24 (t, 2 H, H-**b**), 3.83 (t, 2 H, H-**a**), 2.39 (s, 4 H, H-**c**, **d**).

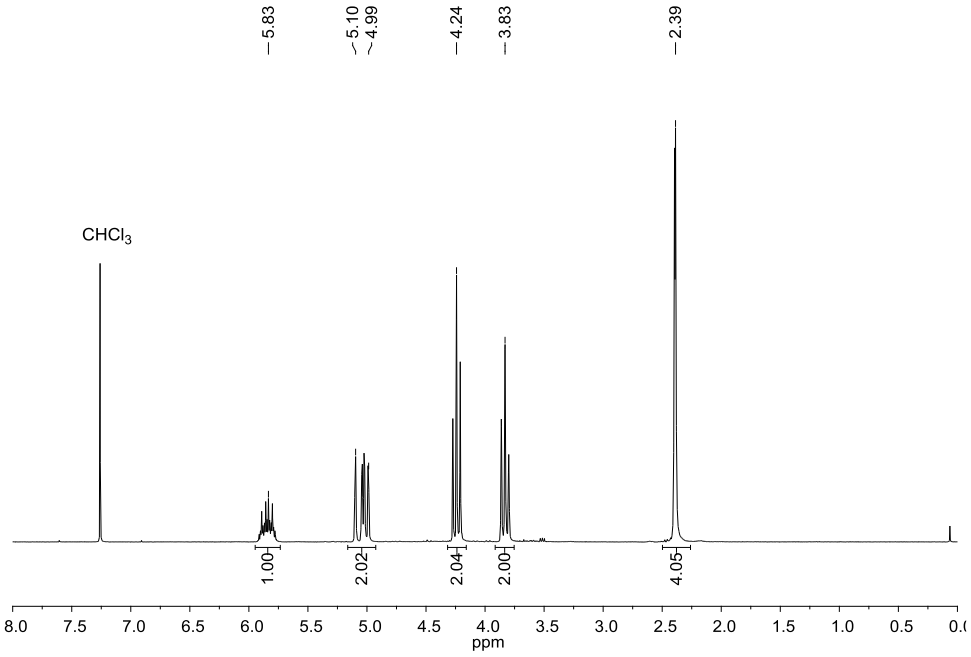

Figure 112: ^{1}H NMR of ButEnOx in $CDCl_3$.

5.3.1.2 2-Decenyl-2-oxazoline

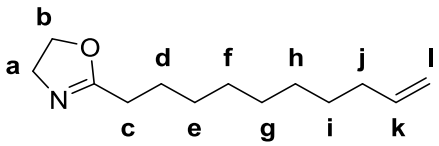

The monomer 2-decenyl-2-oxazoline (DecEnOx) was synthesized following the protocol of Kempe *et al*. [159].

In flame-dried flask, 2-chloroethylammonium chloride (7.497 g, 65 mmol, 1 eq.) was dissolved in 160 mL dry DCM (dried over $CaCl_2$) and 10-undecenoyl chloride (13.216 g, 65 mmol, 1 eq.) was added. After the solution had been stirred under inert atmosphere for 1.5 h, it was cooled down to 0 °C and triethylamine (15.173 g, 150 mmol, 2.3 eq.) was slowly added dropwise. The solution was stirred for 0.5 h

followed by stirring over night at room temperature. 100 mL of DI water were added, and the reaction mixture was extracted three times with 35 mL of DCM. The organic phase was washed three times with water (35 mL), three times with saturated NaCl solution (35 mL) and afterwards dried over $MgSO_4$. DCM was removed under reduced pressure and dried in vacuum ($1 \cdot 10^{-3}$ mbar).

In the second step of the synthesis, the oxazoline ring closure, *N*-(2-chloroethyl)-undec-10-enamide (11.695 g, 48 mmol, 1 eq.) was dissolved in 20 mL of dry methanol (dried over molecular sieve) and in a separate flame-dried flask, ground KOH (2.670 g, 48 mmol, 1 eq.) was dissolved in 10 mL of dry methanol. The methanolic KOH solution was added and the reaction mixture stirred under reflux at 80 °C for 48 h. The KCl, which had developed, was filtered off and 80 mL DI water was added. The product was extracted three times with Et_2O (50 mL) followed by washing of the organic phase with DI water and saturated NaCl solution (brine). The organic phase was then dried with $MgSO_4$ and DCM was removed under reduced pressure. The monomer was fractionally distilled over CaH_2 at 130 °C and $1 \cdot 10^{-3}$ mbar and received as a colorless liquid (6.93 g, 33 mmol, 69 % yield).

^{1}H NMR of DecEnOx (300 MHz, $CDCl_3$, ppm): δ = 5.80 (m, 1 H, H-**k**), 5.02-4.90 (m, 2 H, H-**l**), 4.24 (t, 2 H, H-**b**), 3.83 (t, 2 H, H-**a**), 2.28 (t, 4 H, H-**j**), 2.00 (m, 2H, **d**), 1.63 (m, 2 H, **c**), 1.30 (m, 10 H, **e-i**).

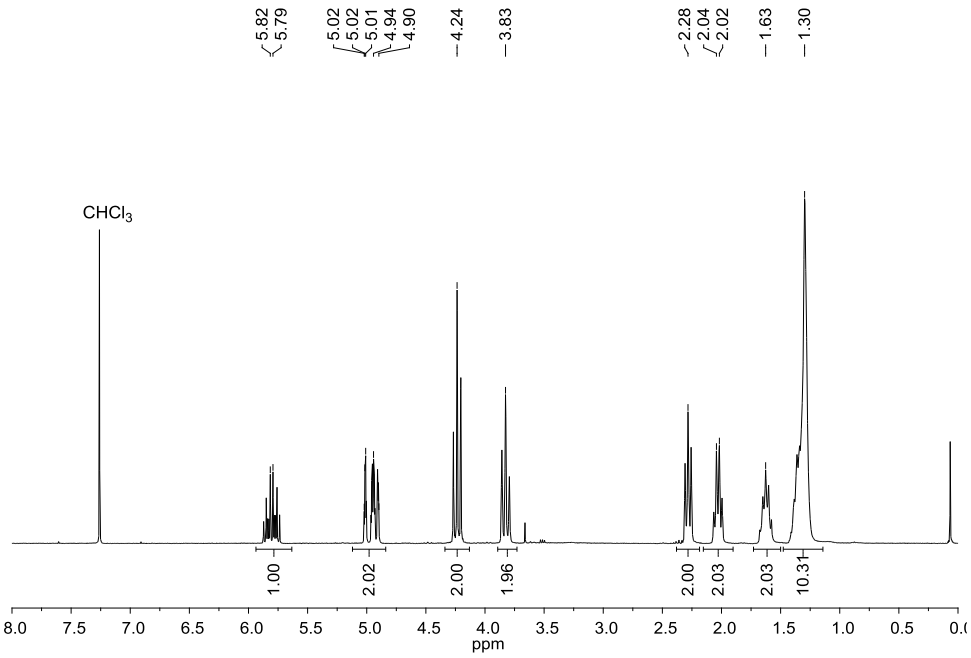

Figure 113: ^{1}H NMR of DecEnOx in $CDCl_3$.

5.3.1.3 2-*n*-Propyl-2-oxazoline

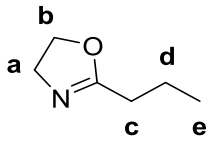

The monomer 2-*n*-propyl-2-oxazoline (*n*PropOx) was synthesized according to Boerman *et al*. [176].

Zinc acetate dihydrate (3.970 g, 18 mmol, 0.025 eq.) was weighed in a three neck round bottom flask and butyronitrile (50.0 g, 724 mmol, 1 eq.) was added. The solution was heated up to 130 °C under reflux and ethanolamine (53.029 g, 868 mmol, 1.2 eq.) was added dropwise. The solution was stirred over night at 130 °C. Afterwards, 50 mL DCM was added, and the organic phase was washed five times with 30 mL DI water and twice with 20 mL of brine. DCM was removed under reduced pressure and the monomer was fractionally distilled over CaH_2 at 65 °C and 1 mbar. The product was received as a colorless liquid.

^{1}H NMR of *n*PropOx (300 MHz, $CDCl_3$, ppm): δ = 4.13 (t, 2 H, H-**b**), 3.73 (t, 2 H, H-**a**), 2.17 (t, 2 H, H-**c**), 1.58 (sx, 2 H, H-**d**), 0.89 (t, 3 H, H-**e**).

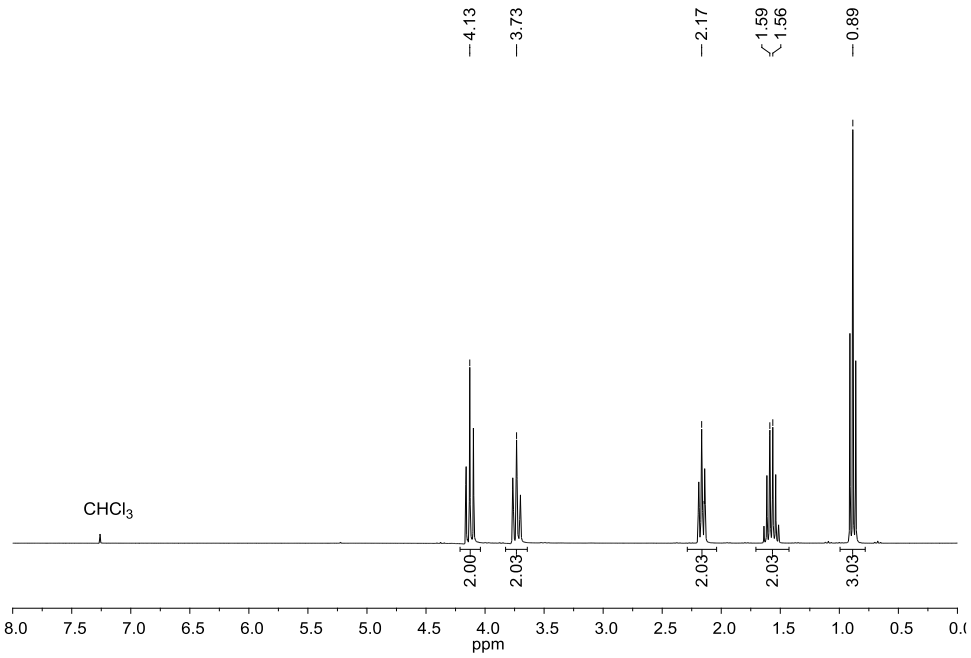

Figure 114: ^{1}H NMR of *n*PropOx in $CDCl_3$.

5.3.2 Polymer Synthesis

5.3.2.1 Poly(2-ethyl-2-oxazoline) (PEtOx)

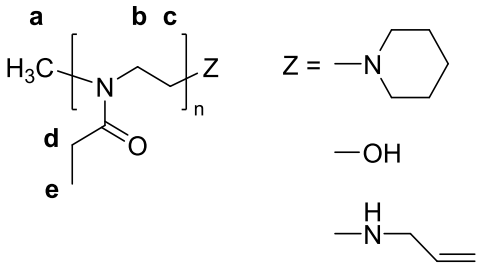

Poly(2-ethyl-2-oxazoline) (PEtOx) was synthesized according to Wiesbrock *et al*. [16]. The initiator methyl tosylate (MeTos) was dried in vacuum before use, when the synthesis was performed in a flask, or distilled to dryness over CaH_2 and stored in the glovebox, when the synthesis was performed in the microwave reactor. For two experiments, an alternative initiator, methyl trifluoromethanesulfonate, was used in the same way. The number of repeating units of the polymer was set by the molar ratio of initiator to monomer. The monomer molarity was set at 2 M for synthesis in a flask in the oil bath at 70 °C or at 4 M for polymerizations carried out in the microwave reactor. A typical synthesis for a polymer with 50 repeating units was

carried out as follows. MeTos (0.205 g, 1.1 mmol, 1 eq.) was weighed in a microwave vial in the glovebox. Acetonitrile (8.5 mL) was added with a syringe and the monomer EtOx (5.456 g, 5.556 mL, 55 mmol, 50 eq.) was added with an Eppendorf pipette. The solution was transferred outside of the glovebox and into the microwave reactor. The reaction was performed at different temperatures for different periods of time to investigate the effect of the temperature on the polymerization. Usually, the polymerization was carried out at 100 °C for 1 h. The polymerization was terminated with piperidine (room temperature, 12 h), methanolic KOH (room temperature, 12 h) or allylamine (45 °C, 48 h).

After the termination, the solvent was evaporated, and the polymer was dissolved in a small amount of chloroform and precipitated in ice cold Et_2O. The precipitate was separated from Et_2O by centrifugation and dissolved again in chloroform. This procedure was repeated at least three times. Afterwards, residual Et_2O was removed under reduced pressure and the polymer was received as a white powder. For further purification, the polymer was dissolved in water, dialyzed against water (MWCO of the dialysis membrane was 1 or 3.5 kDa) and freeze-dried.

^{1}H NMR of PEtOx$_{50}$-pip (300 MHz, CD_3CN, ppm): δ = 7.61 (d, aromat., tosylate anion), 7.17 (d, tosylate anion), 3.41 (m, 184 H, H-**b**, **c**), 2.96 (d, 2 H, H-**a**), 2.86 (s, 1H, H-**a**), 2.33 (m, 99 H, H-**d**), 1.76 – 1.37 (m, 10 H, -N(CH_2)$_5$), 1.02 (m, 139 H, H-**e**).

^{1}H NMR of PEtOx$_{50}$-OH (300 MHz, CD_3CN, ppm): δ = 7.61 (d, aromat., tosylate anion), 7.17 (d, aromat., tosylate anion), 3.60 (m, 3 H, H-**c** adjacent to OH), 3.41 (m, 245 H, H-**b**, **c**), 2.96 (d, 2 H, H-**a**), 2.86 (s, 1H, H-**a**), 2.33 (m, 112 H, H-**d**), 1.02 (m, 175 H, H-**e**).

^{1}H NMR of PEtOx$_{50}$-allyl (300 MHz, CD_3CN, ppm): δ = 7.61 (d, aromat., tosylate anion), 7.17 (d, aromat., tosylate anion), 5.86 (m, 1 H, -CH=CH_2), 5.24 (m, 2 H, -CH=CH_2), 3.95 (dd, 2 H, -CH_2-CH=CH_2) 3.41 (m, 190 H, H-**b**, **c**), 2.96 (d, 2 H, H-**a**), 2.86 (s, 1H, H-**a**), 2.33 (m, 108 H, H-**d**), 1.02 (m, 140 H, H-**e**).

Table 10: Overview of polymerization with EtOx and piperidine as terminating agent.

Sample name	MeTos	EtOx	ACN	Piperidine	Heating	Temp.	Time
$PEtOx_{50}$-pip (**P1**)	0.083 g, 0.447 mmol	2.216 g, 22.35 mmol	2.9 mL	0.114 g, 1.34 mmol	Microwave	140 °C	20 min
$PEtOx_{50}$-pip (**P2**)	0.039 g, 0.209 mmol	1.038 g, 10.5 mmol	1.5 mL	0.053 g, 0.63 mmol	Microwave	100 °C	1 h

Table 11: Overview of polymerization with EtOx and KOH as terminating agent.

Sample name	MeTos	EtOx	ACN	1 M KOH	Heating	Temp.	Time
$PEtOx_{20}$-OH (**P3**)	0.262 g, 1.407 mmol	2.789 g, 28.14 mmol	4.5 mL	2.110 mL, 2.11 mmol	Microwave	100 °C	1 h
$PEtOx_{50}$-OH (**P4**)	0.097 g, 0.521 mmol	2.582 g, 26.04 mmol	4 mL	0.781 mL, 0.78 mmol	Microwave	100 °C	1 h

Table 12: Overview of polymerization with EtOx and allylamine as terminating agent.

Sample name	MeTos	EtOx	ACN	Allylamine	Heating	Temp.	Time
$PEtOx_{20}$-allyl (**P5**)	0.272 g, 1.5 mmol	2.896 g, 29.2 mmol	4.4 mL	0.834 g, 14.6 mmol	Microwave	100 °C	0.5 h
$PEtOx_{25}$-allyl (**P6**)	0.155 g, 0.8 mmol	2.063 g, 20.8 mmol	3.4 mL	0.475 g, 8.3 mmol	Microwave	100 °C	1 h
$PEtOx_{30}$-allyl (**P7**)	0.263 g, 1.4 mmol	4.200 g, 42.4 mmol	7 mL	0.806 g, 14.1 mmol	Microwave	100 °C	1 h
$PEtOx_{50}$-allyl (**P8**)	0.151 g, 0.8 mmol	4.019 g, 40.5 mmol	6 mL	0.463 g, 8.1 mmol	Microwave	100 °C	1 h

Table 13: Reaction overview of the polymerization of EtOx initiated with MeOTf.

Sample name	MeOTf	EtOx	ACN	Piperidine	Heating	Temp.	Time
$PEtOx_{50}$ (**P9**)	16.2 mg, 0.1 mmol	491 mg, 5 mmol	1.9 mL	25 mg, 0.30 mmol	Oilbath	70 °C	48 h
$PEtOx_{60}$ (**P10**)	65 mg, 0.4 mmol	2.356 g, 23.8 mmol	3.1 mL	101 mg, 1.6 mmol	Microwave	140 °C	20 min

Table 14: Molecular weight of synthesized PEtOx determined by ^{1}H NMR and SEC.

Sample name	Rpt. units[$]	M_n (g/mol) [$]	M_n (g/mol)	M_w (g/mol)	Đ
P1[#]	-	-	3617	4790	1.32
P2[#]	55	5445	3765	4069	1.08
P3*	22.5	2262	3088	3296	1.07
P4*	58	5782	6549	7240	1.11
P5*	16	1657	2574	2720	1.06
P6*	20	2054	3124	3441	1.10
P7*	28	2847	4467	4825	1.08
P8*	46.5	4681	5041	5642	1.12
P9[#]	-	-	4065	5459	1.34
P10[#]	-	-	4438	6602	1.49

[$]determined by ^{1}H NMR spectroscopy *measured on Malvern SEC system (triple detection) [#]measured on PSS SEC system (conventional calibration)

A)

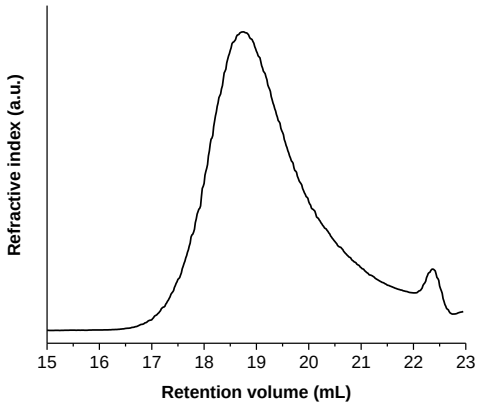
Refractive index (a.u.)
15 16 17 18 19 20 21 22 23
Retention volume (mL)

B)

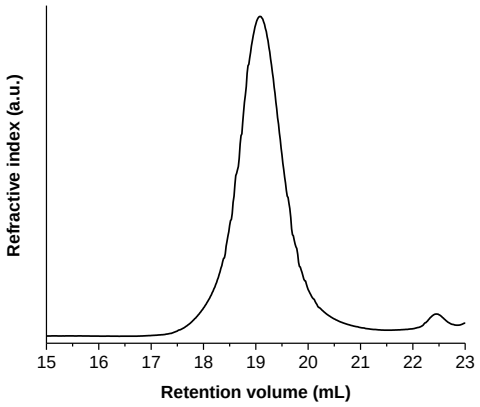
Refractive index (a.u.)
15 16 17 18 19 20 21 22 23
Retention volume (mL)

C)

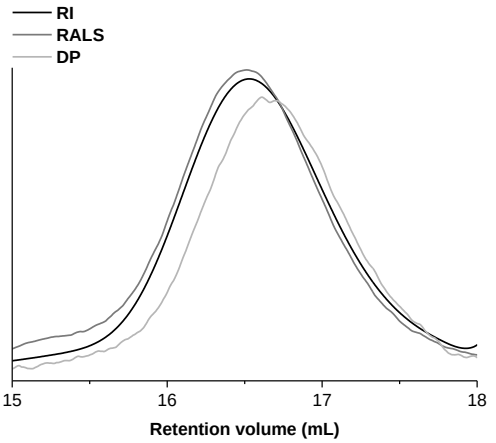
RI
RALS
DP
15 16 17 18
Retention volume (mL)

D)

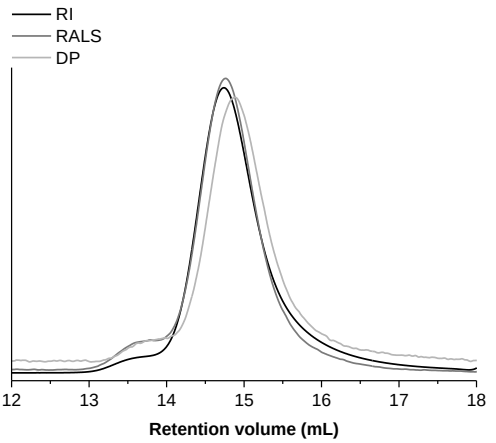
RI
RALS
DP
12 13 14 15 16 17 18
Retention volume (mL)

E)

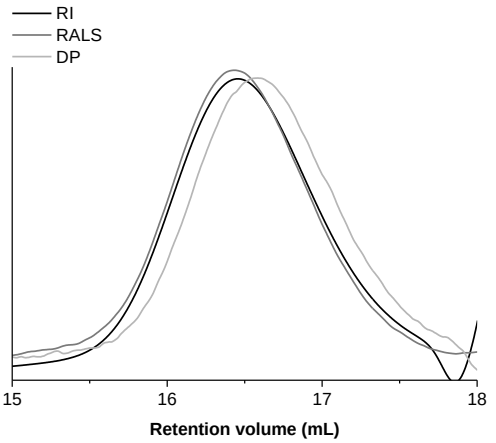
RI
RALS
DP
15 16 17 18
Retention volume (mL)

F)

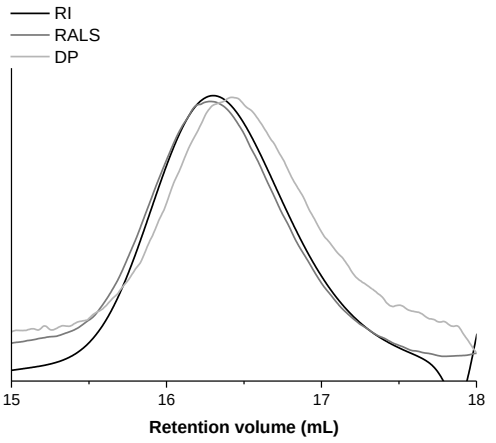
RI
RALS
DP
15 16 17 18
Retention volume (mL)

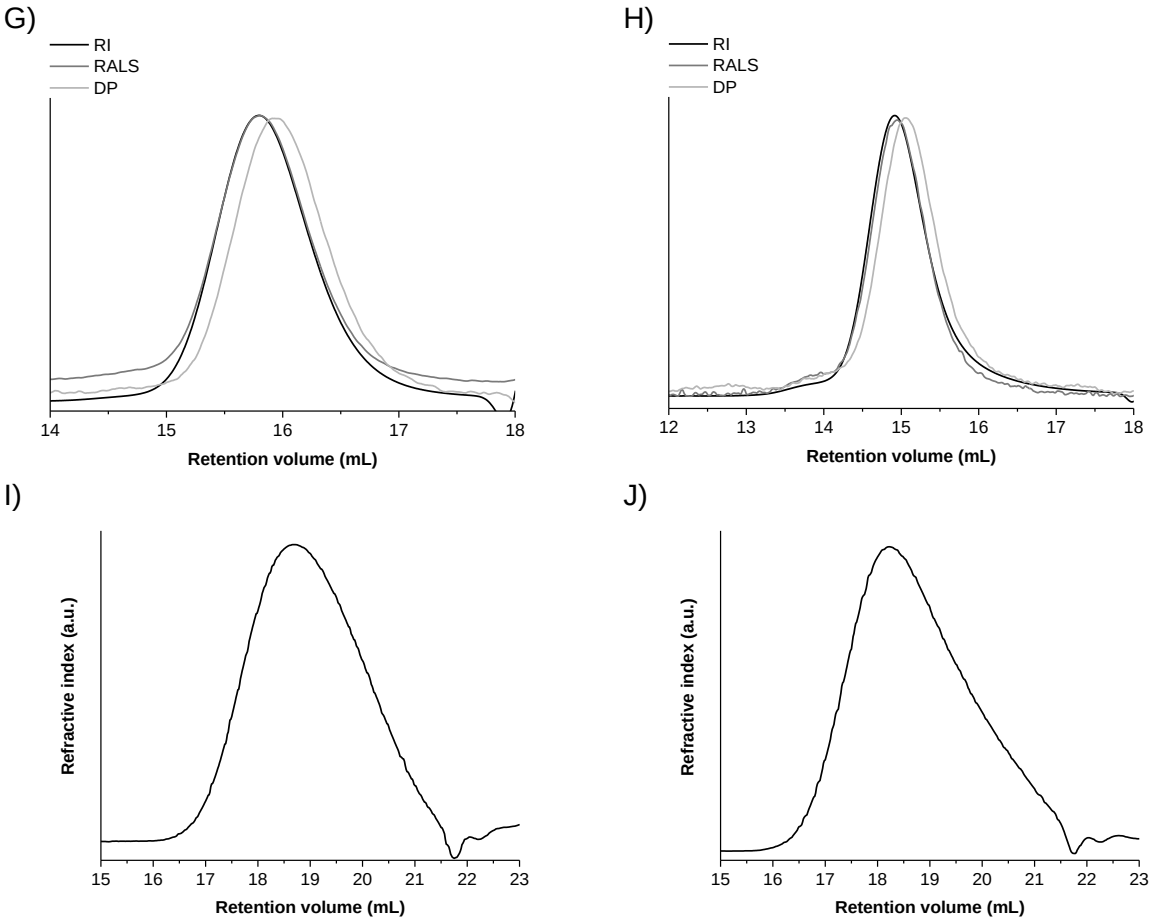

Figure 115: SEC elugrams of A) P1, B) P2, C) P3, D) P4, E) P5, F) P6, G) P7, H) P8, I) P9 and J), P10; (RI = refractive index, RALS = right angle light scattering, DP = differential pressure/viscometer signal in arbitrary units).

5.3.2.2 Poly(2-methyl-2-oxazoline) (PMeOx)

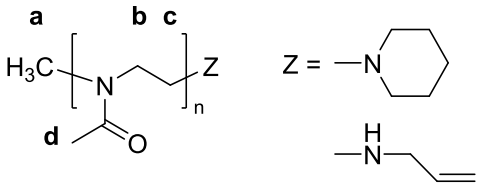

The synthesis of poly(2-methyl-2-oxazoline) (PMeOx) was carried out as described for PEtOx. The initiator was always MeTos and the terminating agents were piperidine, water or allylamine.

^{1}H NMR of PMeOx$_{50}$-pip (300 MHz, CD_3CN, ppm): δ = 7.61 (d, aromat., tosylate anion), 7.17 (d, aromat., tosylate anion), 3.42 (m, 185 H, H-**b**, **c**), 2.99 (d, 2 H, H-**a**), 2.85 (s, 1H, H-**a**), 2.01 (m, H, H-**d**), 1.76 – 1.37 (m, 10 H, -N(C*H*$_2$)$_5$).

^{1}H NMR of PMeOx$_{30}$-allyl (300 MHz, CD_3CN, ppm): δ = 7.61 (d, aromat., tosylate anion), 7.17 (d, aromat., tosylate anion), 5.85 (m, 1 H, -C*H*=CH_2), 5.24 (m, 2 H, -CH=C*H*$_2$), 3.95 (dd, 3 H, -C*H*$_2$-CH=CH_2) 3.39 (m, 105 H, H-**b**, **c**), 2.96 (d, 2 H, H-**a**), 2.86 (s, 1H, H-**a**), 2.01 (m, 77 H, H-**d**).

Table 15: Overview of polymerization with MeOx and piperidine as terminating agent.

Sample name	MeTos	MeOx	ACN	Piperidine	Heating	Temp.	Time
PMeOx$_{50}$-pip (**P11**)	0.035 g, 0.2 mmol	0.800 g, 9.3 mmol	1.6 mL	0.048 g, 0.6 mmol	Microwave	140 °C	20 min
PMeOx$_{50}$-pip (**P12**)	0.035 g, 0.1 mmol	0.795 g, 9.3 mmol	3 mL	0.159 g, 1.9 mmol	Microwave	100 °C	1 h

Table 16: Overview of polymerization with MeOx and allylamine as terminating agent.

Sample name	MeTos	MeOx	ACN	Allylamine	Heating	Temp.	Time
PMeOx$_{30}$-allyl (P13)	0.246 g, 1.3 mmol	3.372 g, 39.6 mmol	7 mL	0.754 g, 13.2 mmol	Microwave	100 °C	1 h

Table 17: Molecular weight of synthesized PMeOx determined by ^{1}H NMR and SEC.

Sample name	Rpt. units[$]	M_n (g/mol) [$]	M_n (g/mol)	M_w (g/mol)	Đ
P11[#]	46	4014	4481	5268	1.18 (bimodal)
P12*	42	3683	7254	8152	1.12 (bimodal)
P13*	26	2282	3904	4304	1.02

[$]determined by ^{1}H NMR spectroscopy *measured on Malvern SEC system (triple detection) [#]measured on PSS SEC system (conventional calibration)

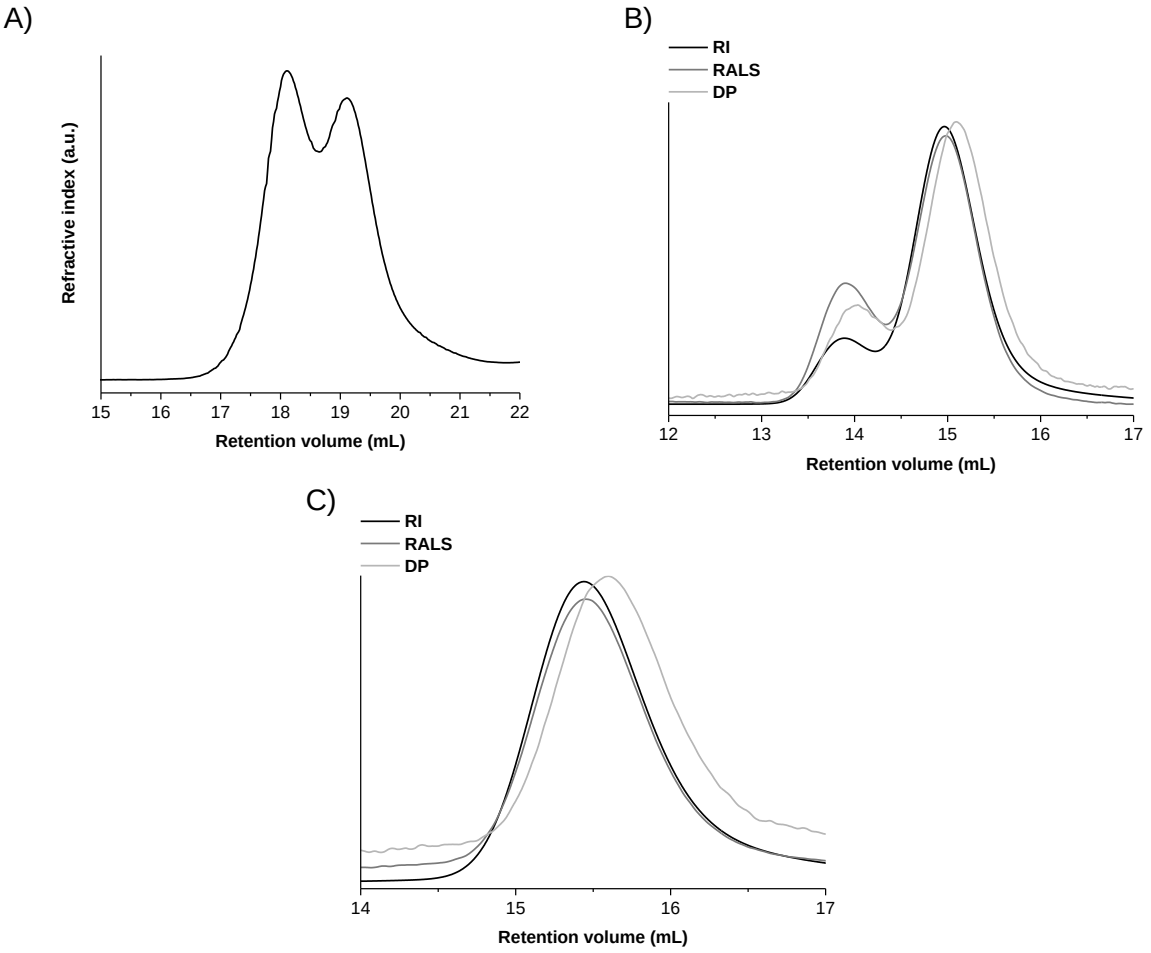

Figure 116: SEC elugrams of A) $PMeOx_{50}$-pip (P11), B) $PMeOx_{50}$-pip (P12) and C) $PMeOx_{30}$-allyl (P13) measured in DMF, with piperidine terminated PMeOx showing a bimodal distribution.

5.3.2.3 Poly(*n*-propyl-2-oxazoline) (P(PrOx))

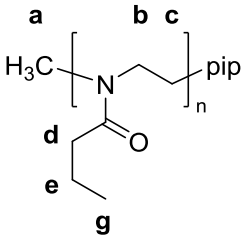

The synthesis of poly(*n*-propyl-2-oxazoline) (PPrOx) was carried out as described for PEtOx and PMeOx with the variation that either benzonitrile was used as a solvent and the synthesis was carried out in a Schlenk flask under inert conditions at 100 °C for 40 h or the microwave reactor was used with the solvent acetonitrile and the reaction was carried out at 120 °C for 5 – 6 h.

To obtain a polymer with 400 repeating units, MeTos (0.220 g, 1.2 mmol, 1 eq.) was weighed in a Schlenk flask and dried under HV ($1 \cdot 10^{-3}$ mbar) for 1 h. The dry

monomer 2-*n*-propyl-2-oxazoline (53.434 g, 472.5 mmol, 400 eq.) and the solvent benzonitrile (BZN) (100 mL) was added. The solution was stirred in an oil bath at 100 °C for 40 h. The polymerization was terminated using piperidine (0.302 g, 0.351 mL, 3.5 mmol, 3 eq.) at room temperature. Afterwards, the polymer was precipitated in cold Et_2O and dialyzed against cold Milli-Q water (MWCO = 3.5 kDa) for 3 d. The product was received as a white powder after freeze-drying.

^{1}H NMR of $PPrOx_{100}$ (300 MHz, CD_3CN, ppm): δ = 3.39 (m, 447 H, H-**b**, **c**), 2.98 (d, 2 H, H-**a**), 2.85 (s, 1H, H-**a**), 2.28 (m, 219 H, H-**d**), 1.55 (m, 227 H, H-**e**), 0.90 (m, 339 H, H-**f**).

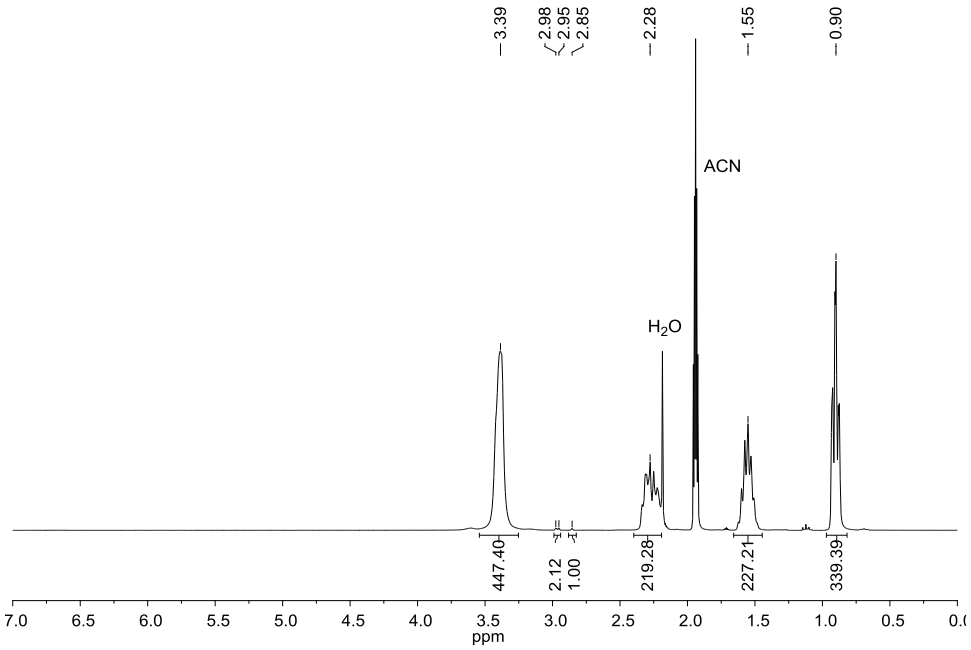

Figure 117: ^{1}H NMR of $PPrOx_{100}$ measured in CD_3CN.

Table 18: Overview of polymerizations of *n*PropOx.

Sample name	MeTos	*n*PropOx	Solvent	Piperidine	Heating	Temp.	Time
P(PrOx)100 (P14)	0.081 g, 0.435 mmol	4.918 g, 43.495 mmol	10 mL ACN	0.111 g, 1.305 mmol	Microwave	140 °C	3 h
P(PrOx)200 (P15)	0.068 g, 0.363 mmol	8.197 g, 72.491 mmol	15 mL ACN	0.093 g, 1.087 mmol	Microwave	120 °C	5 h
P(PrOx)300 (P16)	0.034 g, 0.183 mmol	6.194 g, 54.771 mmol	12 mL ACN	0.047 g, 0.548 mmol	Microwave	120 °C	5 h
P(PrOx)400 (P17)	0.012 g, 0.066 mmol	2.963 g, 26.204 mmol	9 mL ACN	0.017 g, 0.197 mmol	Microwave	120 °C	6 h
P(PrOx)400 (P18)	0.220 g, 1.181 mmol	53.434 g, 472.5 mmol	100 mL BZN	0.302 g, 3.544 mmol	Flask	100 °C	40 h

Table 19: Molecular weight of synthesized PPrOx determined by ^{1}H NMR and SEC.

Sample name	Rpt. units[$]	M_n (g/mol) [$]	M_n (g/mol)*	M_w (g/mol)	Đ
P14	102	11559	13090	14410	1.10 (bimodal)
P15	207	23558	26170	29140	1.11 (bimodal)
P16	343	38886	37710	45020	1.19 (bimodal)
P17	391	44314	41600	52720	1.27
P18	397	44993	41720	54340	1.30

[$]determined by ^{1}H NMR spectroscopy *measured on Malvern SEC system (triple detection)

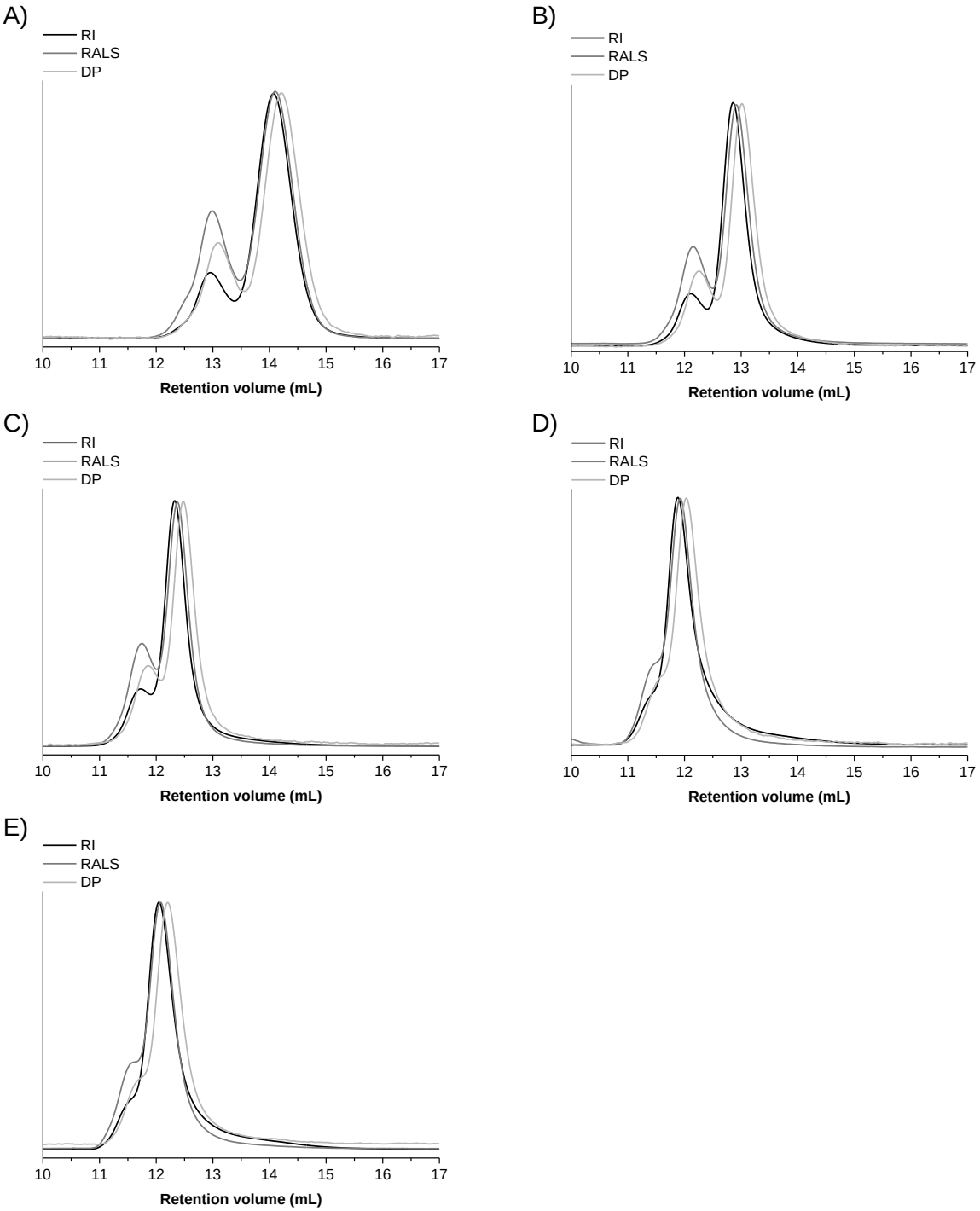

Figure 118: SEC elugrams of A) P14, B) P15, C) P16, D) P17 and E) P18 measured in DMF.

5.3.2.4 Poly(2-ethyl-2-oxazoline-*co*-2-(3-butenyl)-2-oxazoline)

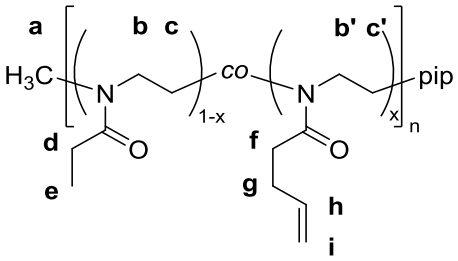

The synthesis of poly(2-ethyl-2-oxazoline-*co*-2-(3-butenyl)-2-oxazoline) (PEtOx-*co*-ButEnOx) was performed according to Gress *et al*. [21] and Hoogenboom *et al*. [177]. The dry initiator MeTos was weighed in a microwave vial inside the glovebox, the monomer ButEnOx was weighed on top and the monomer EtOx was added with an Eppendorf pipette. The solvent acetonitrile was added so that the overall monomer concentration would be 4 M. The solution was heated in a microwave reactor at 100 °C for 2 h. The initiator to monomer ratio determined the number of repeating units per polymer chain. A typical reaction was carried out as follows: The initiator (0.303 g, 1.627 mmol, 1 eq.) was weighed in a microwave vial inside the glovebox. The monomer ButEnOx (1.018 g, 8.135 mmol, 5 eq.) was added and the second monomer EtOx (8.064 g, 8.212 mL, 81.350 mmol, 50 eq.) was added with an Eppendorf pipette. The solvent acetonitrile (13 mL) was added with a syringe. The microwave vial, equipped with a stirring bar, was put in the microwave reactor and the solution was stirred for 2 h at 100 °C. The polymerization was terminated with piperidine (0.416 g, 4.881 mmol, 3 eq.) at room temperature overnight under inert atmosphere. The solvent ACN was removed and the polymer was dissolved in a small volume of chloroform and precipitated three times from chloroform in ice cold diethyl ether. The residual solvent was removed under reduced pressure to receive the polymer as a white powder.

^{1}H NMR of P(EtOx$_{0.91}$-*co*-ButEnOx$_{0.09}$)$_{56}$-pip (300 MHz, CD_3CN, ppm): δ = 7.61 (d, aromat., tosylate anion), 7.17 (d, aromat., tosylate anion), 5.85 (m, 5 H, H-**h**), 4.99 (m, 10 H, H-**i**), 3.42 (m, 225 H, H-**b**, **c**, **b'**, **c'**), 2.96 (d, 2 H, H-**a**), 2.86 (s, 1H, H-**a**), 2.33 (m, 129 H, H-**d, f, g**), 1.76 – 1.37 (m, 10 H, -N(CH_2)$_5$), 1.03 (m, 154 H, H-**e**).

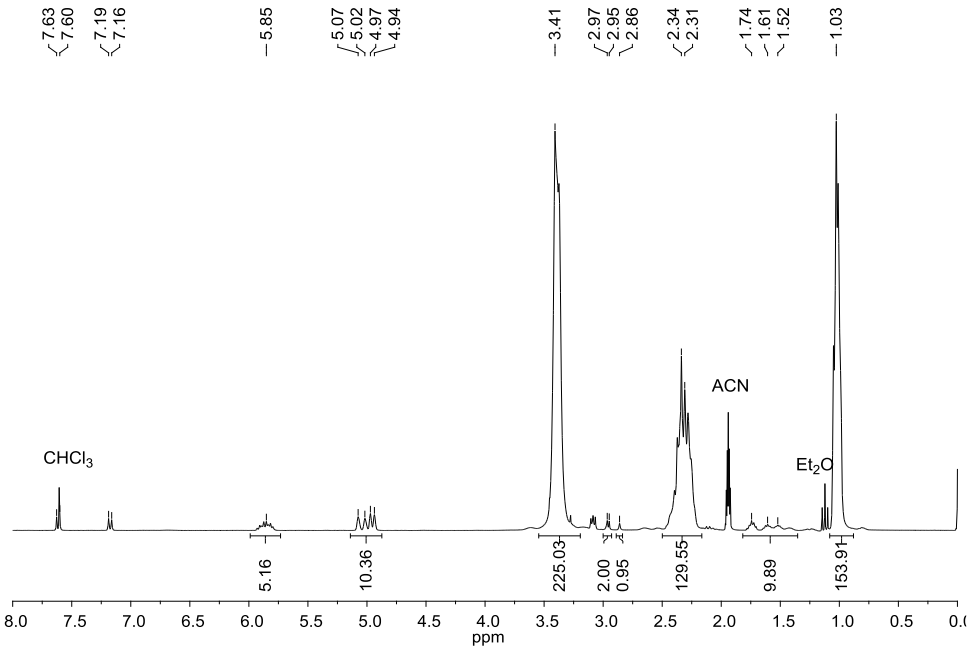

Figure 119: ^{1}H NMR of P(EtOx$_{0.91}$-*co*-ButEnOx$_{0.09}$)$_{56}$ in CD_3CN.

Table 20: Molecular weight of synthesized P(EtOx-*co*-ButEnOx) determined by ^{1}H NMR and SEC.

Sample name	EtOx/ButEnOx theoretical	EtOx/ButEnOx*	M_n* (g/mol)	M_n# (g/mol)	M_w# (g/mol)	Đ
P19	50/5	51/5	5782	6907	7510	1.09
P20	45/5	50/6	5801	6799	7430	1.09
P21	40/10	42/11	5633	7557	8402	1.11
P22	35/15	43/19	6732	6746	7313	1.08
P23	30/20	34/23	6341	7243	7961	1.10
P24	77/5	85/6	9265	11140	12700	1.18

*determined by ^{1}H NMR spectroscopy #measured on Malvern SEC system (triple detection)

Table 21: Cloud point temperature (T_{CP}) of P(EtOx-*co*-ButEnOx) copolymers in Milli-Q water.

Polymer	T_{CP} (°C)
P19	> 85
P20	> 85
P21	55.5
P22	37
P23	25

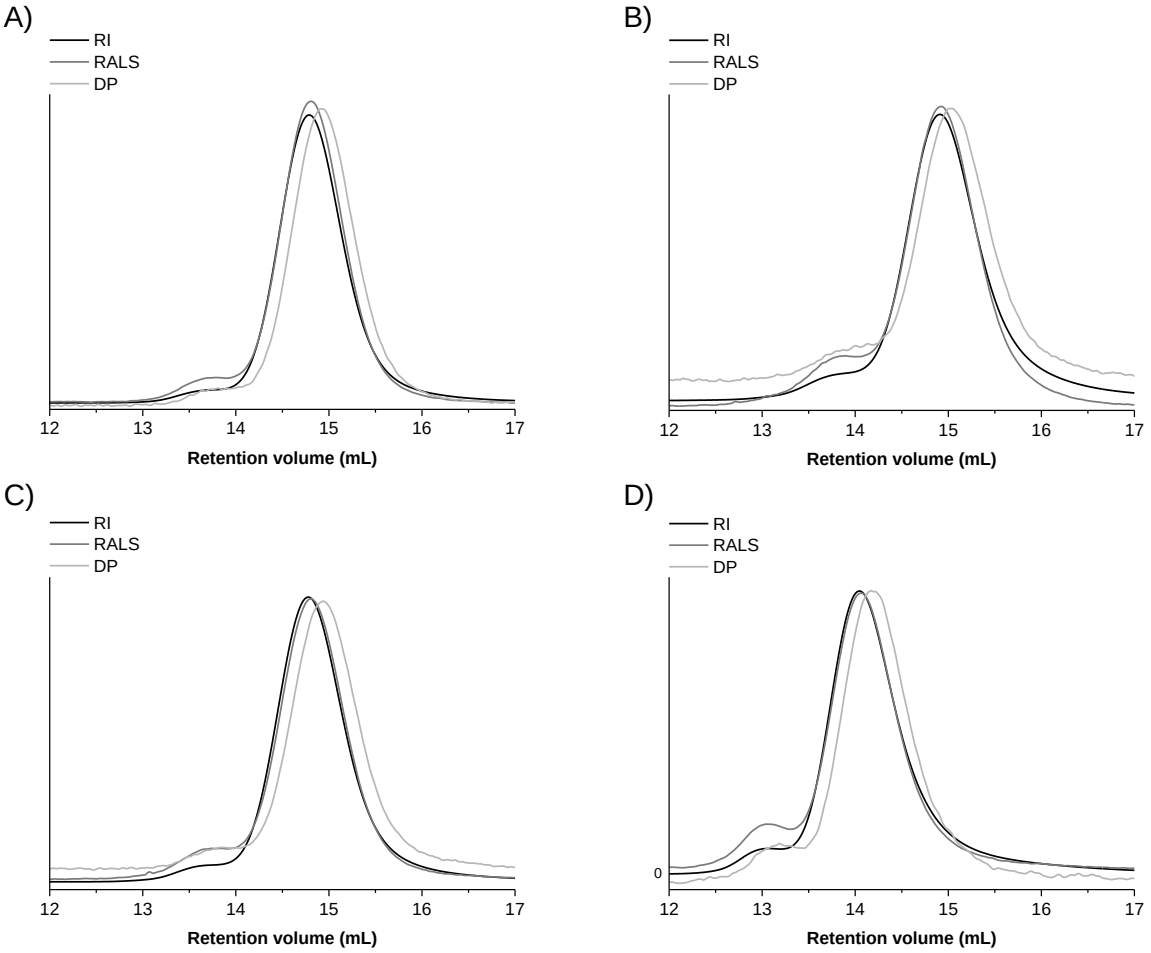

Figure 120: Exemplary SEC elugrams of A) P19, B) P21, C) P23 and D) P24.

5.3.2.5 Poly(2-ethyl-2-oxazoline-*co*-2-decenyl-2-oxazoline)

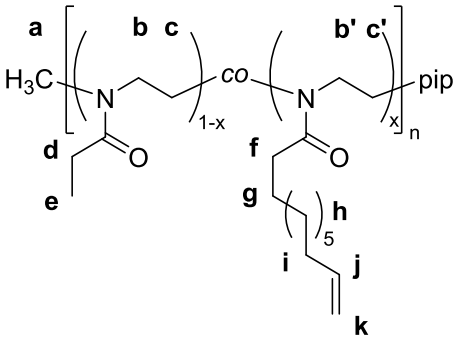

The synthesis of poly(2-ethyl-2-oxazoline-*co*-2-decenyl-2-oxazoline) (PEtOx-*co*-DecEnOx) was performed according to Kempe *et al*. [159] and the synthesis protocol of the synthesis of P(EtOx-*co*-ButEnOx) was followed. For example, MeTos (0.064 g, 0.344 mmol, 1 eq.) was weighed in a microwave vial inside the glovebox. DecEnOx (0.360 g, 1.718 mmol, 5 eq.) was weighed on top and EtOx (1.703 g, 1.735 mL, 17.180 mmol, 50 eq.) was added with an Eppendorf pipette. Acetonitrile (2.6 mL) was added and the polymerization was carried out in a microwave reactor for 5 h at 100 °C. Afterwards, the reaction was terminated with piperidine (0.088 g, 1.031 mmol, 3 eq.) overnight and the polymer was precipitated three times from chloroform in ice cold diethyl ether. Afterwards, residual solvent was removed under reduced pressure.

^{1}H NMR of P(EtOx$_{0.92}$-*co*-DecEnOx$_{0.08}$)$_{55}$-pip (300 MHz, CD_3CN, ppm): δ = 7.61 (d, aromat., tosylate anion), 7.17 (d, aromat., tosylate anion), 5.83 (m, 4.5 H, H-**j**), 4.94 (m, 9 H, H-**k**), 3.41 (m, 223 H, H-**b**, **c**, **b'**, **c'**), 2.96 (d, 2 H, H-**a**), 2.86 (s, 1H, H-**a**), 2.33 (m, 122 H, H-**d, f**), 2.03 (m, 11 H, H-**i**), 1.76 – 1.37 (m, 10 H, -N(CH_2)$_5$), 1.51 (m, 11 H, H-**g**), 1.29 (m, 47 H, H-**h**), 1.03 (m, 154 H, H-**e**).

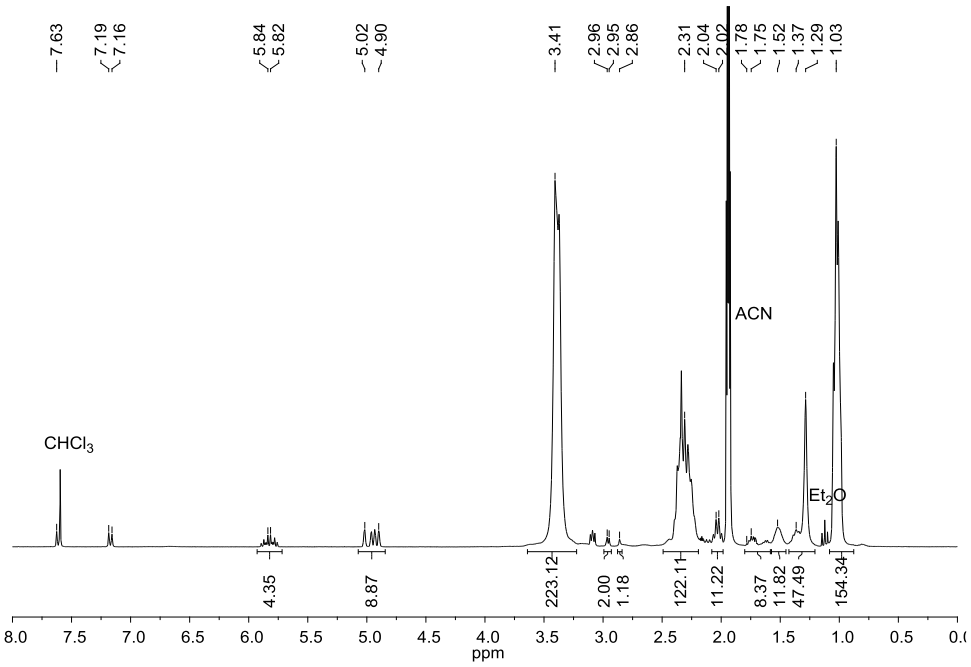

Figure 121: ^{1}H NMR of P(EtOx$_{0.92}$-*co*-DecEnOx$_{0.08}$)$_{55}$ in CD_3CN.

Table 22: Molecular weight of synthesized P(EtOx-*co*-DecEnOx) determined by ^{1}H NMR and SEC.

Sample name	EtOx/DecEnOx theoretical	EtOx/DecEnOx*	M_n* (g/mol)	$M_n^{\#}$ (g/mol)	$M_w^{\#}$ (g/mol)	Đ
P25	50/5	51/4	5986	6974	7895	1.13
P26	50/7.5	63/8	8012	8101	9252	1.14
P27	40/10	48/10	6945	7335	8362	1.14

*determined by ^{1}H NMR spectroscopy $^{\#}$measured on Malvern SEC system (triple detection)

Table 23: Cloud point temperature (T_{CP}) of P(EtOx-*co*-DecEnOx) copolymers in Milli-Q water.

Polymer	T_{CP} (°C)
P25	25
P26	12
P27	not water soluble

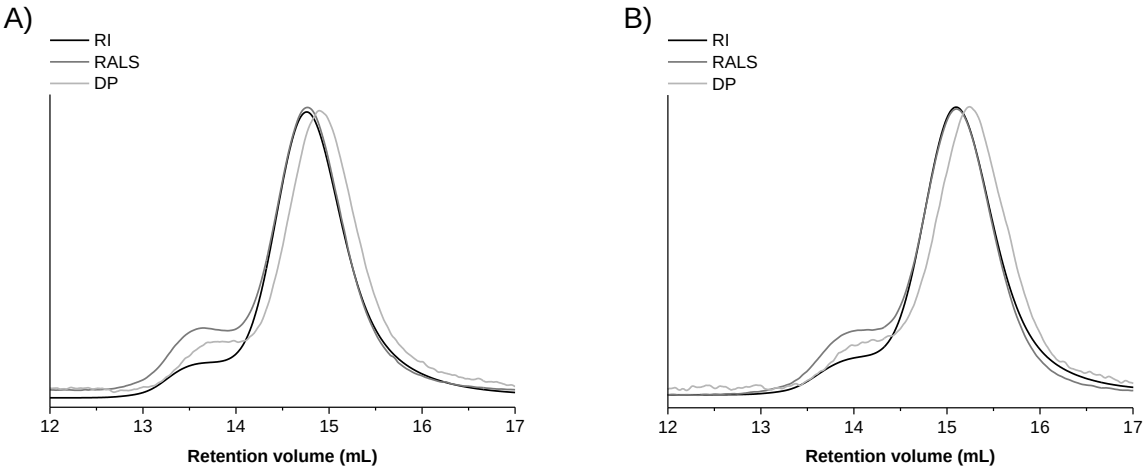

Figure 122: SEC elugrams of A) P25 and B) P27 measured in DMF.

5.3.2.6 Poly(2-methyl-2-oxazoline-*co*-2-(3-butenyl)-2-oxazoline)

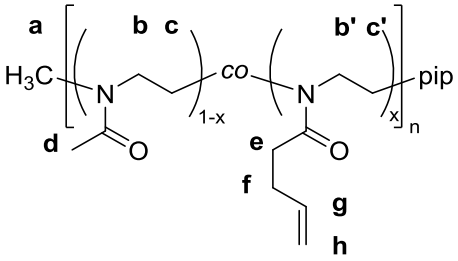

The synthesis of poly(2-methyl-2-oxazoline-*co*-2-(3-butenyl)-2-oxazoline) (PMeOx-*co*-ButEnOx) was performed according to Gress *et al*. [21] and carried out as described in 5.3.2.4. For example, MeTos (0.055 g, 0.295 mmol, 1 eq.) was weighed in a microwave vial inside the glovebox. ButEnOx (0.185 g, 1.477 mmol, 5 eq.) was weighed on top and MeOx (1.257 g, 1.250 mL, 14.767 mmol, 50 eq.) was added with an Eppendorf pipette. Acetonitrile (2.6 mL) was added and the polymerization was carried out in a microwave reactor for 1.5 h at 100 °C. Afterwards, the reaction was terminated with piperidine (0.075 g, 0.886 mmol, 3 eq.) overnight and the polymer was precipitated three times from methanol/chloroform (v/v 1:1) in ice cold diethyl ether.

^{1}H NMR of P(MeOx$_{0.91}$-*co*-ButEnOx$_{0.09}$)$_{56}$-pip (300 MHz, CD_3CN, ppm): δ = 7.61 (d, aromat., tosylate anion), 7.17 (d, aromat., tosylate anion), 5.87 (m, 5 H, H-**g**), 5.00 (m, 10 H, H-**h**), 3.40 (m, 232 H, H-**b**, **c**, **b'**, **c'**), 2.96 (d, 2 H, H-**a**), 2.85 (s, 1H, H-**a**), 2.42 (m, 10 H, H-**f**), 2.31 (m, 10 H, H-**e**), 2.01 (m, 153 H, H-**d**), 1.76 – 1.37 (m, 10 H, -N(CH_2)$_5$).

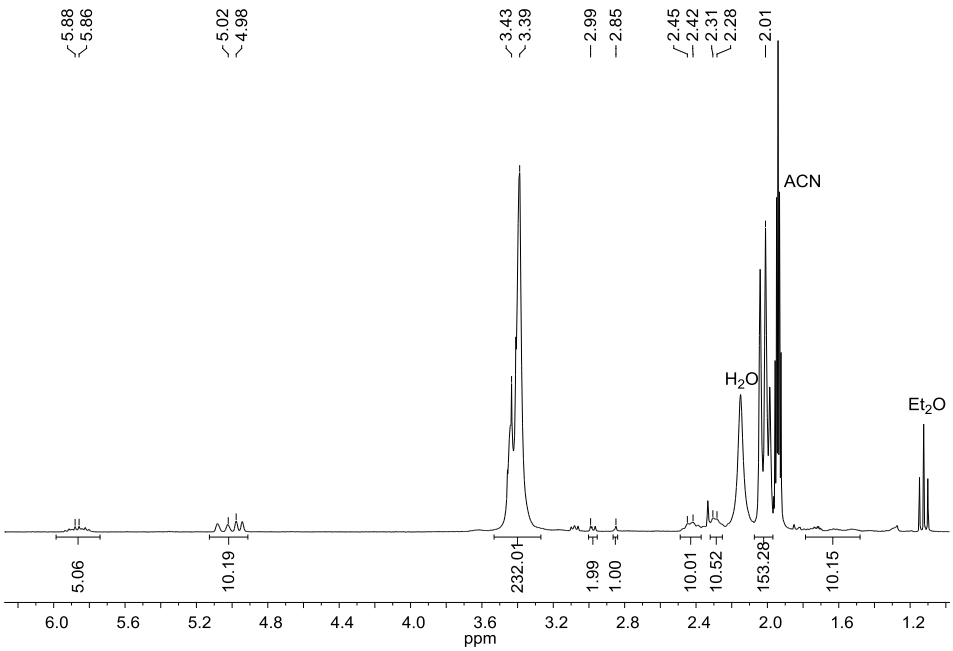

Figure 123: ^{1}H NMR of P(MeOx$_{0.91}$-*co*-ButEnOx$_{0.09}$)$_{56}$-pip in CD_3CN.

Table 24: Molecular weight of synthesized P(MeOx-*co*-ButEnOx) determined by ^{1}H NMR and SEC.

Sample name	MeOx/ButEnOx theoretical	MeOx/ButEnOx*	M_n* (g/mol)	M_n# (g/mol)	M_w# (g/mol)	Đ
P28	50/5	51/5	5986	8264	10160	1.23 (bimodal)
P29	40/10	40/9	4631	6821	8795	1.29 (bimodal)
P30	72/8	71/8	7143	11750	14930	1.27 (bimodal)

*determined by ^{1}H NMR spectroscopy #measured on Malvern SEC system (triple detection)

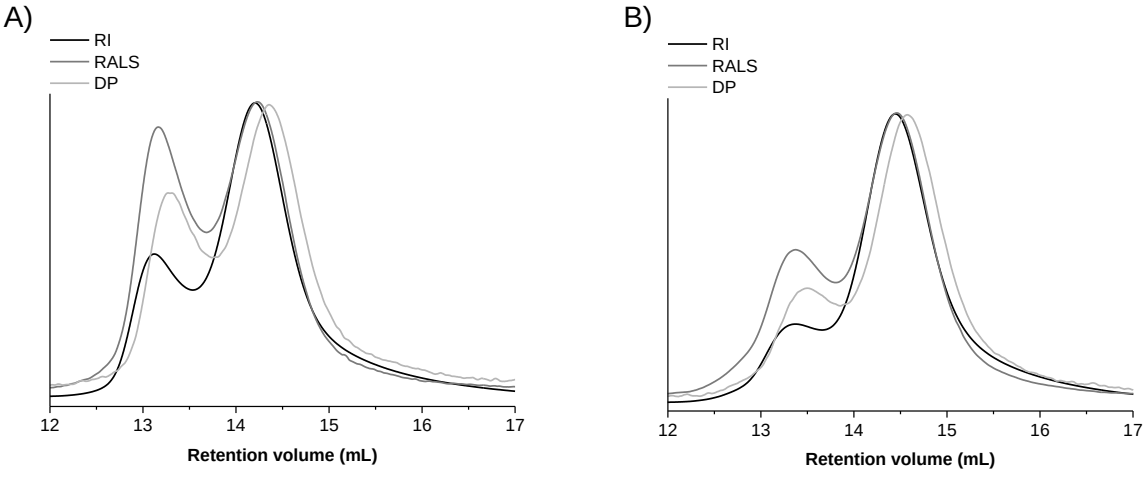

Figure 124: SEC elugrams of A) P28 and B) P29 in DMF.

5.3.3 Polymer Functionalization

5.3.3.1 Thiol Functionalization

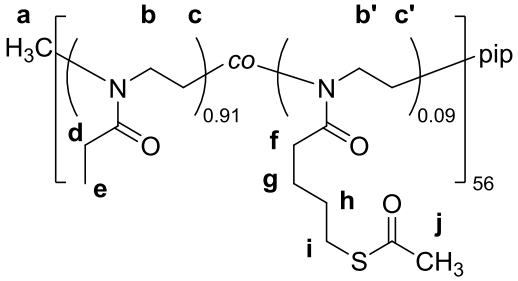

The copolymers P19, P20, P21, P28 and P29 were functionalized with thioacetic acid at the side chain using thiol-ene chemistry. The copolymer was dissolved in methanol and was degassed with argon for 15 min. 3 equivalents of thioacetic acid per double bond available and 0.5 eq. of the photo-initiator 2,2-dimethoxy-2-phenylacetophenone (DMPA) were added. The solution was stirred under UV irradiation (365 nm, UV LED-cubes, Polymerschmiede, Aachen, Germany) for 0.5 h. Afterwards, the solvent was removed under reduced pressure and the polymer was precipitated in cold Et_2O three times from chloroform or chloroform/methanol. The polymer was received as a white powder after removal of residual solvent.

^{1}H NMR of P(EtOx$_{0.91}$-*co*-ButOxTAAc$_{0.09}$)$_{56}$-pip (300 MHz, CD_3CN, ppm): δ = 7.61 (d, aromat., tosylate anion), 7.17 (d, aromat., tosylate anion), 3.42 (m, 238 H, H-**b**, **c**, **b'**, **c'**), 2.96 (d, 2 H, H-**a**), 2.86 (m, 13 H, H-**a**, H-**i**), 2.33 (m, 129 H, H-**d, f**), 1.57 (m, 22 H, H-**g**, **h**), 1.03 (m, 168 H, H-**e**).

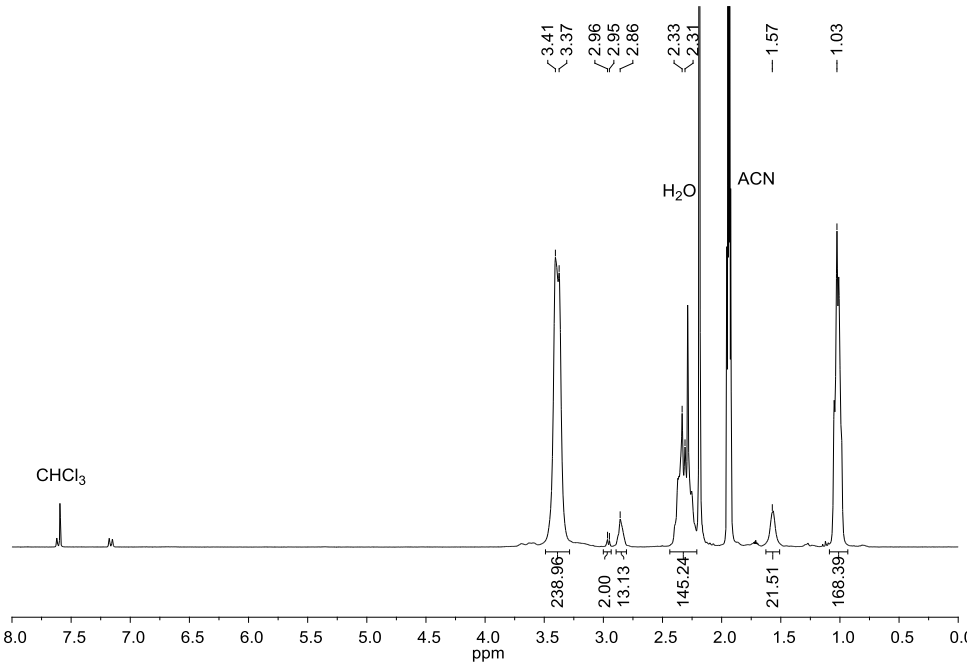

Figure 125: ^{1}H NMR of P19 functionalized with thioacetic acid in CD_3CN.

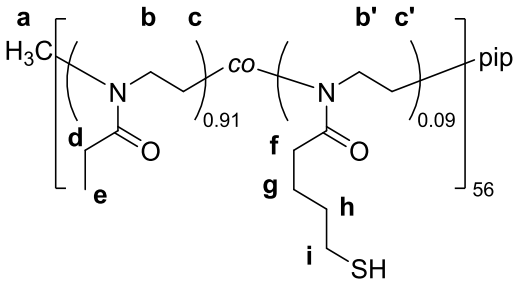

The second step involves the deprotection of the thioester using cysteine. The polymer and 1.5 eq. of cysteine for 1 eq. of thioester were dissolved in methanol in two separate Schlenk flasks and the solutions were degassed for 15 min. Then, 3 eq. of sodium borohydride ($NaBH_4$) for 1 eq. of thioester were added to the cysteine solution. Attention, strong gas formation. The polymer solution was added to the cysteine solution and stirred overnight under inert atmosphere. The solution was filtered to remove the precipitate, excess cysteine, and the solvent was removed under reduced pressure. The polymer was precipitated three times from chloroform/methanol (1:1 v/v) in cold Et_2O. To reduce any disulfides that might have formed during the process, 1 eq. tris(2-carboxyethyl)phosphine hydrochloride (TCEP·HCl) for 1 eq. of thiol was added to an aqueous solution of the polymer and stirred for 2 h at pH 7 before the solution was dialyzed against degassed water

(MWCO = 3.5 kDa) to remove the water soluble side product acetylcysteine. After dialysis against degassed water for 3 days with frequent water changes, the polymer was freeze-dried and received as a white powder.

^{1}H NMR of P(EtOx$_{0.91}$-*co*-ButOxSH$_{0.09}$)$_{56}$-pip (300 MHz, D_2O, ppm): δ = 3.58 (m, 220 H, H-**b**, **c**, **b'**, **c'**), 3.09 (d, 2 H, H-**a**), 2.95 (m, 1 H, H-**a**), 2.58 (m, 10 H, H-**i**) 2.39 (m, 114 H, H-**d, f**), 1.65 (m, 20 H, H-**g**, **h**), 1.08 (m, 152 H, H-**e**).
Raman: υ = 2980 – 2820 (-CH, -CH_2), 2570 (-S-H).

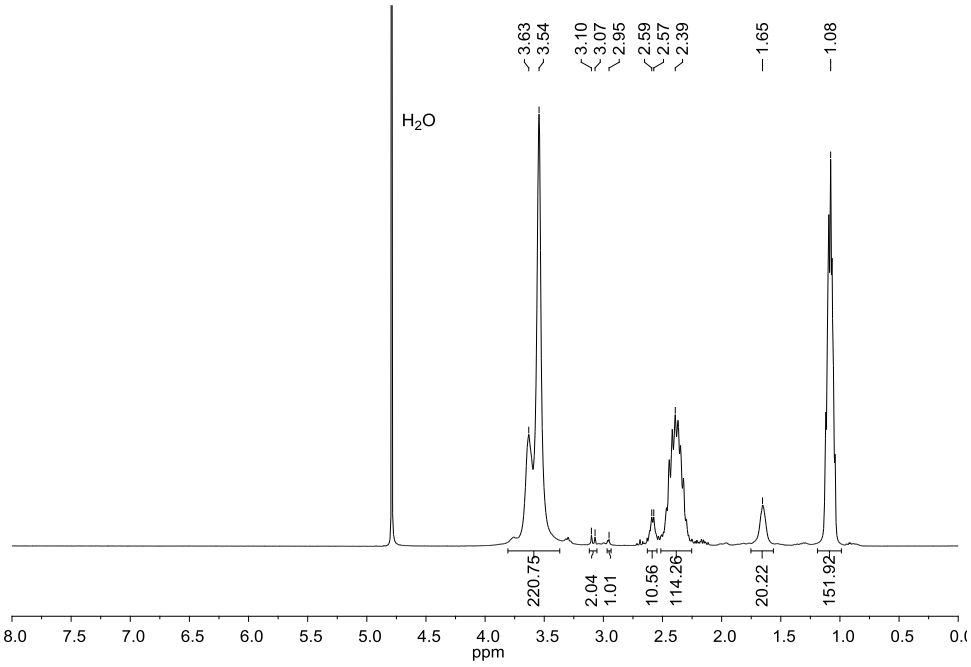

Figure 126: ^{1}H NMR of thiol functionalized P(EtOx$_{0.91}$-*co*-ButOxSH$_{0.09}$)$_{56}$-pip in D_2O.

Table 25: SEC results of thiol functionalized POx copolymers.

Polymer	M_n (g/mol)	M_w (g/mol)	Đ
P(EtOx$_{0.91}$-*co*-ButOxSH$_{0.09}$)$_{56}$-pip (P19-thiol)	11880	13350	1.12 (shoulder at high MW)
P(EtOx$_{0.89}$-*co*-ButOxSH$_{0.11}$)$_{56}$-pip (P20-thiol)	9484	10940	1.15 (shoulder at high MW)
P(EtOx$_{0.79}$-*co*-ButOxSH$_{0.21}$)$_{53}$-pip (P21-thiol)	12990	15430	1.19 (shoulder at high MW)
P(MeOx$_{0.91}$-*co*-ButOxSH$_{0.09}$)$_{56}$-pip (P28-thiol)	7729	9212	1.19 (shoulder at high MW)
P(MeOx$_{0.81}$-*co*-ButOxSH$_{0.19}$)$_{49}$-pip (P29-thiol)	8258	9783	1.18 (shoulder at high MW)

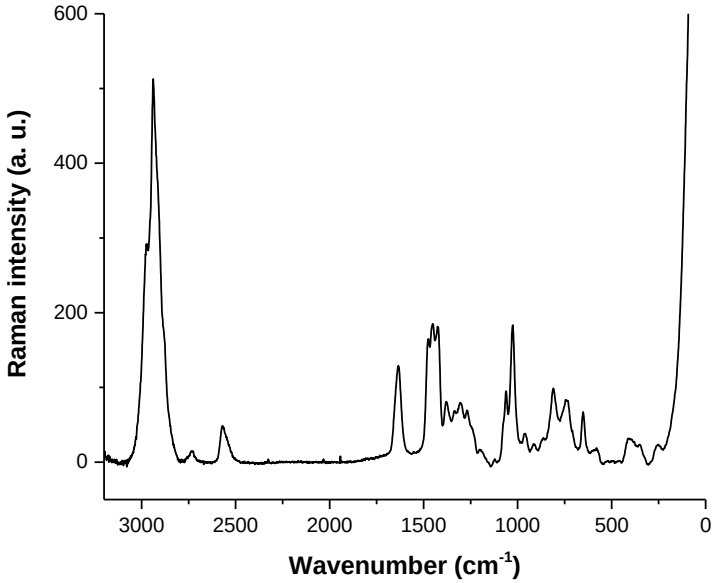

Figure 127: Raman spectrum of P(EtOx$_{0.79}$-*co*-ButOxSH$_{0.21}$)$_{53}$.

Table 26: Thiol content determined by Ellman's assay of thiol functionalized P(EtOx-*co*-ButOxSH) and P(MeOx-*co*-ButOxSH) copolymers and their T_{CP} in 1xPBS measured with the zetasizer.

Polymer	Theoretical thiol content (mol%)	Thiol content determined by Ellman's assay (mol%)	T_{CP} (°C)
P(EtOx$_{0.91}$-*co*-ButOxSH$_{0.09}$)$_{56}$-pip (P19-thiol)	8.93	9.70	53
P(EtOx$_{0.89}$-*co*-ButOxSH$_{0.11}$)$_{56}$-pip (P20-thiol)	10.71	9.17	53.5
P(EtOx$_{0.79}$-*co*-ButOxSH$_{0.21}$)$_{53}$-pip (P21-thiol)	20.75	16.99	23.5
P(MeOx$_{0.91}$-*co*-ButOxSH$_{0.09}$)$_{56}$-pip (P28-thiol)	9.09	6.54	> 85
P(MeOx$_{0.81}$-*co*-ButOxSH$_{0.19}$)$_{49}$-pip (P29-thiol)	18.37	18.42	> 85

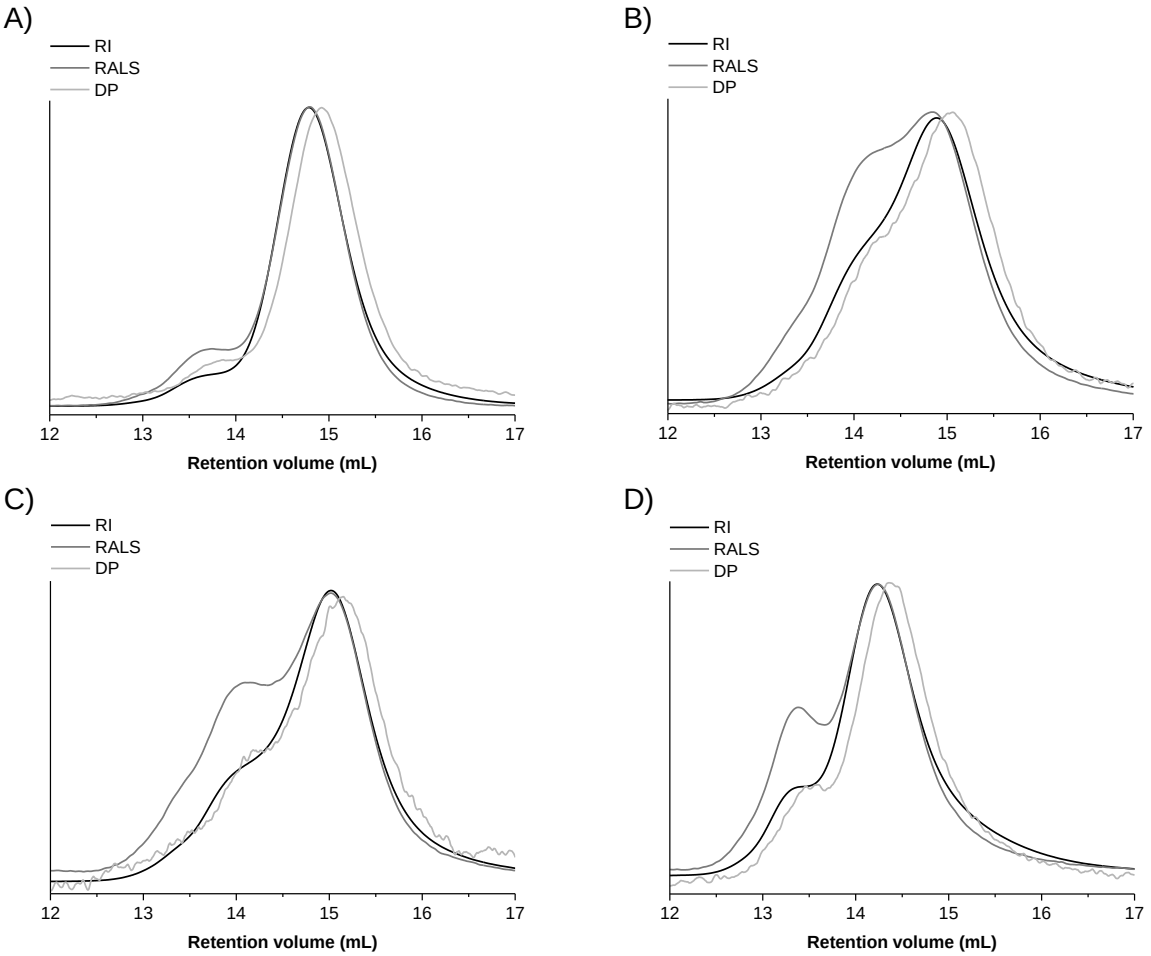

Figure 128: Exemplary SEC elugram of A) P(EtOx$_{0.89}$-*co*-ButOxTAAc$_{0.11}$)$_{56}$-pip, B) P(EtOx$_{0.89}$-*co*-ButOxSH$_{0.11}$)$_{56}$-pip, C) P(EtOx$_{0.79}$-*co*-ButOxSH$_{0.21}$)$_{53}$-pip and D) P(MeOx$_{0.91}$-*co*-ButOxSH$_{0.09}$)$_{56}$-pip.

5.3.3.2 Thiolactone Functionalization

Synthesis of thiolactone acrylamide

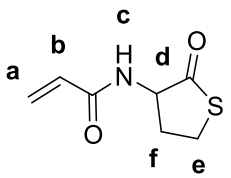

The synthesis of thiolactone acrylamide was performed according to Reinicke *et al*. [161]. Homocysteine thiolactone hydrochloride (5.591 g, 36.39 mmol, 1 eq.) was dissolved in a solution of water/1,4-dioxane (1:1 v/v) cooled at 0 °C with an ice bath. $NaHCO_3$ (15.287 g, 181.96 mmol, 5 eq.) was added and the solution was stirred for

0.5 h at 0 °C. Acryloyl chloride (6.588 g, 72.79 mmol, 2 eq.) was added dropwise and the reaction mixture was left stirring at room temperature for 12 h. Brine (20 mL) was added and the product was extracted three times with ethyl acetate (30 mL). The organic phases were combined and dried over $NaSO_4$. The solvent was removed under reduced pressure and colorless to slightly yellowish viscous oil was obtained. The crude product was directly recrystallized under reflux at 50 °C in DCM and white crystals were received.

^{1}H NMR of thiolactone acrylamide (300 MHz, DMSO-d_6, ppm): δ = 8.46-8.43 (d, 1 H, H-**c**), 6.19 (m, 2 H, H-**a**, **b**), 5.65 (m, 1H, **a**), 4.69 (m, 1 H, H-**d**), 3.47 – 3.27 (m, 2 H, H-**e**), 2.48 – 2.03 (m, 2 H, H-**f**).
IR spectrum (cm^{-1}): 3268 (amide, NH valency), 1693 (-C=O valency, amide band I), 1656 (-C=C valency), 1621 (NH deformation), 1536 (NH deformation), 1406 – 696 (CH_2 deformation).

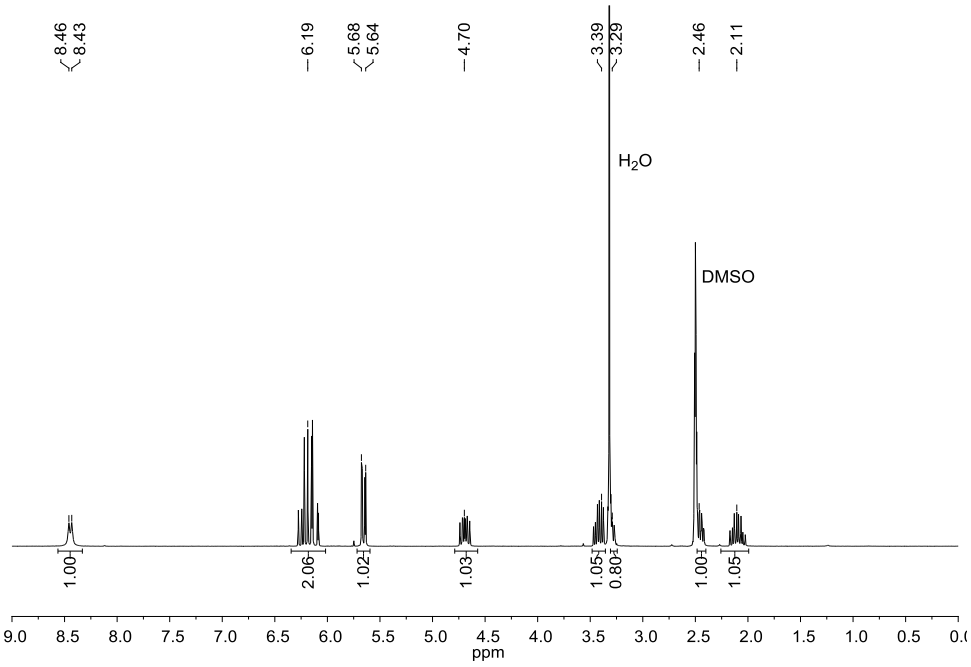

Figure 129: ^{1}H NMR of thiolactone acrylamide.

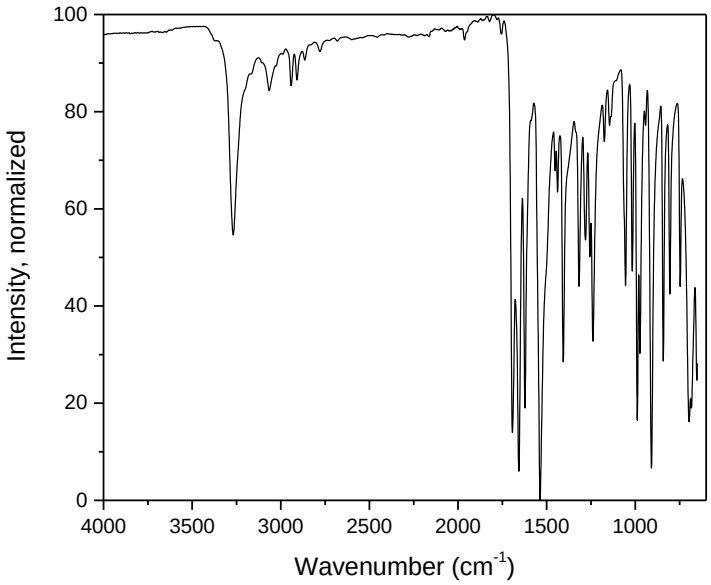

Figure 130: IR spectrum of thiolactone acrylamide.

Thiolactone functionalization of P(EtOx-co-ButOxSH)

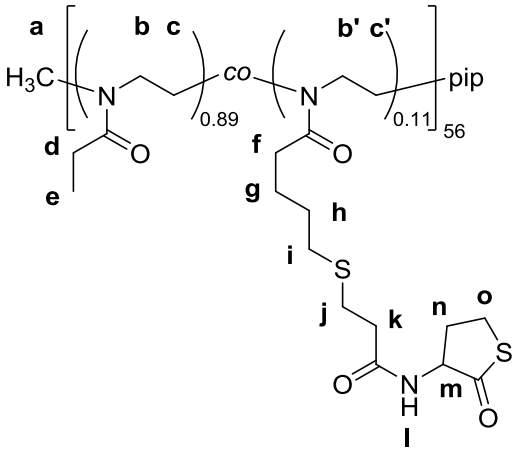

Thiolactone acrylamide (0.058 g, 0.400 mmol, 2 eq. in respect to thiol groups) was dissolved in DMSO (1 mL) and degassed with argon. DMPP (0.023 g, 0.024 mL, 0.034 mmol, 1 eq. in respect to thiol groups) was added to the solution. The polymer P(EtOx$_{0.89}$-*co*-ButOxSH$_{0.11}$)$_{56}$-pip was dissolved in DMSO (1 mL) and added to the thiolactone acrylamide solution and the reaction was stirred for 2 h. Chloroform (4 mL) was added and the polymer was precipitated in cold Et$_2$O. The polymer was

dissolved in methanol/DCM (1:1 v/v) and precipitated in cold Et_2O three times. Residual solvent was removed under reduced pressure.

^{1}H NMR of P(EtOx$_{0.89}$-*co*-ButOxLac$_{0.11}$)$_{56}$-pip (300 MHz, DMSO-d$_6$, ppm): δ = 4.57 (m, 6 H, H-**m**), 3.35 (m, 282 H, H-**b**, **c**, **b'**, **c'**), 2.94 (d, 2 H, H-**a**), 2.77 (m, 8 H, H-**a**, **o**), 2.65 (m, 10 H, H-**j**) 2.29 (m, 149 H, H-**d**, **f**, **k**, **n**), 2.05 (m, 11 H, H-**i**), 1.52 (m, 22 H, H-**g**, **h**), 0.95 (m, 153 H, H-**e**).

SEC (DMF): M_n = 9970 g/mol, M_w = 12150 g/mol, Đ = 1.22.

IR spectrum (cm^{-1}): 3274 (amide, NH valency), 1702 (-C=O valency, amide band I), 1628 (-C=O valency, carbonyl backbone), 1540 (NH deformation), 1469 – 658 (CH_2, CH_3 deformation).

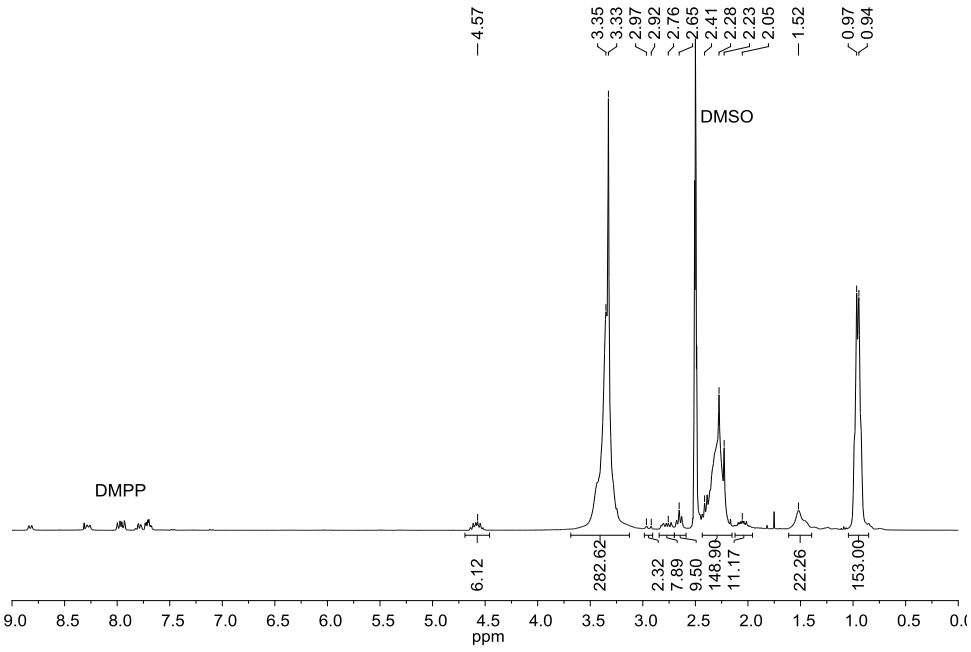

Figure 131: ^{1}H NMR of P(EtOx$_{0.89}$-*co*-ButOxLac$_{0.11}$)$_{56}$-pip in DMSO-d$_6$.

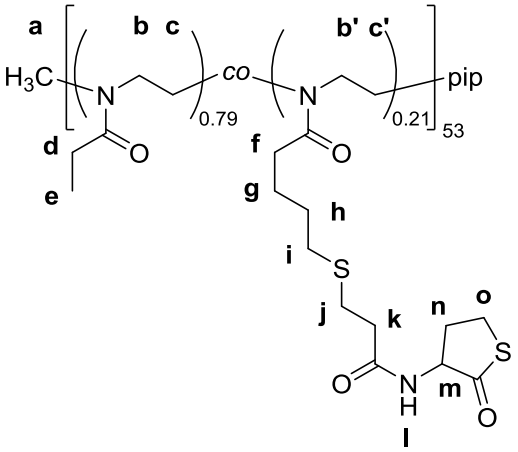

Thiolactone acrylamide (0.287 g, 1.680 mmol, 2 eq. in respect to thiol groups) was dissolved in DMSO (2 mL) and degassed with argon. DMPP (0.077 g, 0.080 mL, 0.051 mmol, 1 eq. in respect to thiol groups) was added to the solution. The polymer P(EtOx$_{0.79}$-*co*-ButOxSH$_{0.21}$)$_{53}$-pip was dissolved in DMSO (4 mL) and added to the thiolactone acrylamide solution and the reaction was stirred for 2 h. Methanol (10 mL) was added and the polymer was precipitated in cold Et_2O. The polymer was dissolved in methanol/chloroform (1:1 v/v) and precipitated in cold Et_2O three times. Residual solvent was removed under reduced pressure.

^{1}H NMR of P(EtOx$_{0.79}$-*co*-ButOxLac$_{0.21}$)$_{53}$-pip (300 MHz, DMSO-d$_6$, ppm): δ = 4.59 (m, 11 H, H-**m**), 3.35 (m, 335 H, H-**b**, **c**, **b'**, **c'**), 2.96 (d, 2 H, H-**a**), 2.77 (m, 18 H, H-**a**, **o**), 2.65 (m, 21 H, H-**j**) 2.29 (m, 206 H, H-**d**, **f**, **k**, **n**), 2.05 (m, 30 H, H-**i**), 1.52 (m, 54 H, H-**g**, **h**), 0.97 (m, 153 H, H-**e**).
SEC (DMF): M_n = 12740 g/mol, M_w = 15740 g/mol, Đ = 1.24.

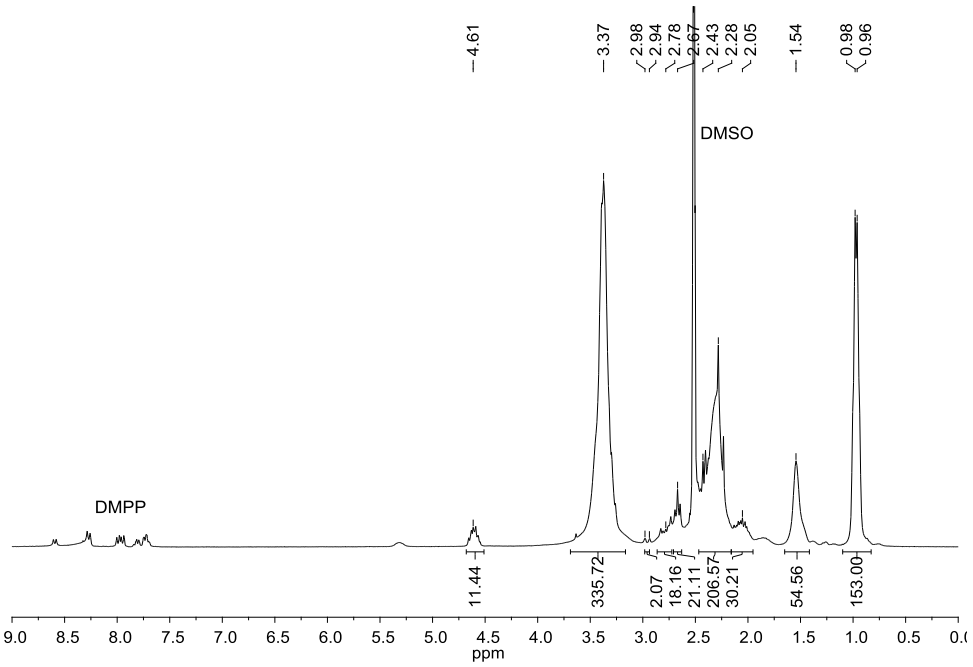

Figure 132: ^{1}H NMR of P(EtOx$_{0.79}$-*co*-ButOxLac$_{0.21}$)$_{53}$-pip in DMSO-d$_6$.

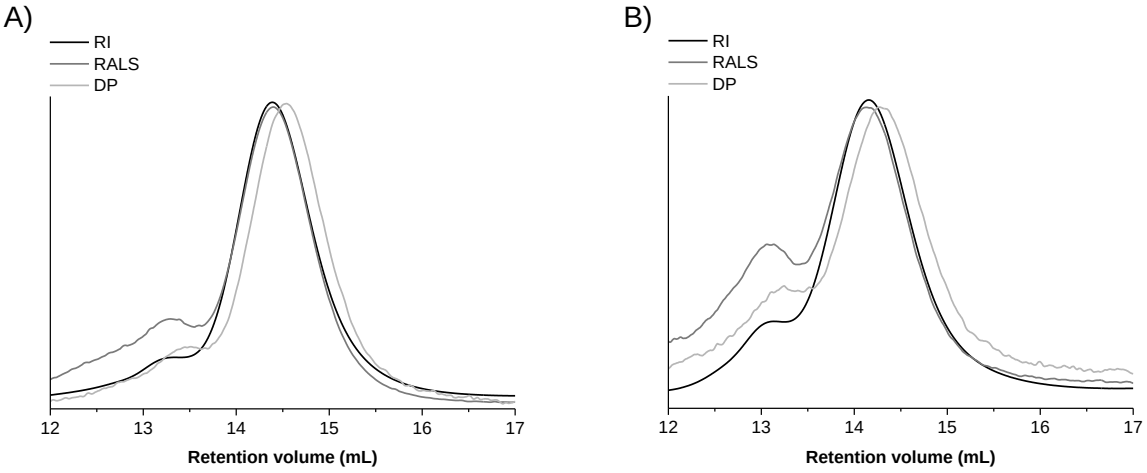

Figure 133: SEC elugram of A) P(EtOx$_{0.89}$-*co*-ButOxLac$_{0.11}$)$_{56}$-pip and B) P(EtOx$_{0.79}$-*co*-ButOxLac$_{0.21}$)$_{53}$-pip.

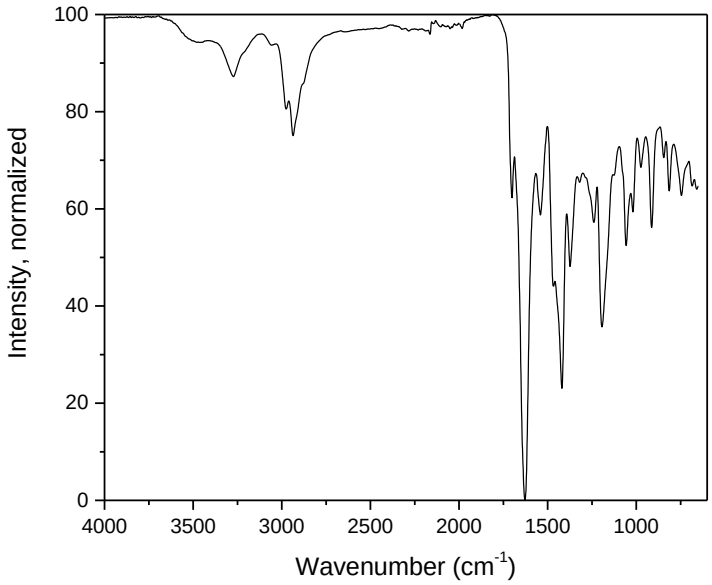

Figure 134: IR spectrum of P(EtOx$_{0.79}$-*co*-ButOxLac$_{0.21}$)$_{53}$-pip.

5.3.3.3 Azlactone Functionalization

Synthesis of N-(3-mercapto-1-oxopropyl)-2-methyl-alanine

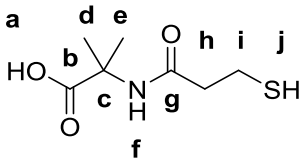

The synthesis of *N*-(3-mercapto-1-oxopropyl)-2-methyl-alanine (MOMA) was performed based on the synthesis of mercaptoacyl amino acids by Condon *et al*. [163].

At first, *N*-[3-(benzoylthio)-1-oxopropyl]-2-methylalanine was synthesized. 2-Aminoisobutyric acid (6.0 g, 58 mmol, 1 eq.) was dissolved in 1.5 M NaOH (90 mL) and cooled to 0 °C with an ice bath. 3-Bromopropionyl chloride (9.966 g, 58 mmol, 1 eq.) was added and the solution was stirred for 0.5 h at room temperature. The pH was set to 7 and the solution was stirred for another 3 h. Thiobenzoic acid (8.837 g, 64 mmol, 1.1 eq.) was dissolved in a 0.7 M aqueous solution of potassium carbonate solution (90 mL) which was added to the reaction mixture and stirred overnight.

Concentrated hydrochloric acid (HCl) was added until the pH was acidic, and a white precipitate formed. Ethyl acetate (100 mL) was used to extract the precipitate. The organic phase was reduced, and the product was received from crystallization in cold Et_2O.

Yield: 4.109 g, 13.912 mmol, 23.91 %.

^{1}H NMR of *N*-[3-(benzoylthio)-1-oxopropyl]-2-methylalanine (300 MHz, DMSO-d_6, ppm): δ = 12.13 (s, 1 H, COO*H*), 8.11 (s, 1 H, N*H*), 8.11 (d, 2 H, aromatic ring), 7.69 (m, 1 H, aromatic ring), 7.56 (t, 2 H, aromatic ring), 3.19 (t, 2 H, CH_2SCO), 2.45 (t, 2 H, NHCOCH_2), 1.33 (s, 6 H, 2xCH_3).

^{13}C NMR of *N*-[3-(benzoylthio)-1-oxopropyl]-2-methylalanine (300 MHz, DMSO-d_6, ppm): δ = 191.21 (thioester C=O), 175.41 (carboxylic acid C=O), 169.41 (amide C=O), 136.42 (aromatic C), 133.86 (aromatic CH), 129.09 (aromatic CH), 126.72 (aromatic CH), 54.78 (CO-*C*(CH_3)$_2$-NH), 34.62 (CO-CH_2-*C*H_2-S), 24.92 (C(*C*H_3)$_2$), 24.33 (CO-*C*H_2-CH_2-S).

N-[3-(benzoylthio)-1-oxopropyl]-2-methylalanine (3.0 g, 10.157 mmol, 1 eq.) was dissolved in water (11 mL) and concentrated ammonia (7.5 mL) was added. A white precipitate formed after a few minutes from the clear solution and the suspension was stirred for 2 h. Water (10 mL) was added and the precipitate was filtered out. The aqueous solution was washed three times with ethyl acetate (15 mL). The pH of the aqueous solution was lowered using concentrated HCl and the product precipitated as a white solid, which was filtered and freeze-dried to dryness.

Yield: 0.858 g, 4.486 mmol, 44.17 %.

^{1}H NMR of MOMA (300 MHz, DMSO-d_6, ppm): δ = 12.12 (s, 1 H, H-**a**), 8.09 (s, 1 H, H-**f**), 2.62 (t, 2 H, H-**i**), 2.37 (q, 2 H, H-**h**), 2.22 (s, 1 H, H-**j**), 1.33 (s, 6 H, H-**d**, **e**).

^{13}C NMR of MOMA (300 MHz, DMSO-d_6, ppm): δ = 174.37 (carboxylic acid C=O, C^b), 168.57 (amide C=O, C^g), 53.61 (CO-*C*(CH_3)$_2$-NH, C^c), 38.66 (CO-CH_2-*C*H_2-S,C^h, hidden by solvent peak), 23.82 (C(*C*H_3)$_2$, $C^{d, e}$), 18.86 (CO-*C*H_2-CH_2-S, C^i).

EI-MS: Calculated $[M+H]^+$: 191.6, found 191.0.

IR spectrum (cm^{-1}): 3308 (amide, NH valency), 3247-2688 (CH_2, CH_3 valency), 1720 (C=O valency), 1612 (NH deformation), 1545 (NH deformation), 1465 – 672 (CH_2, CH_3 deformation).

Raman spectrum (cm^{-1}): 2984 – 2870 (ν(C-H)), 2572 (ν(S-H)), 773 (ν(C-S)).

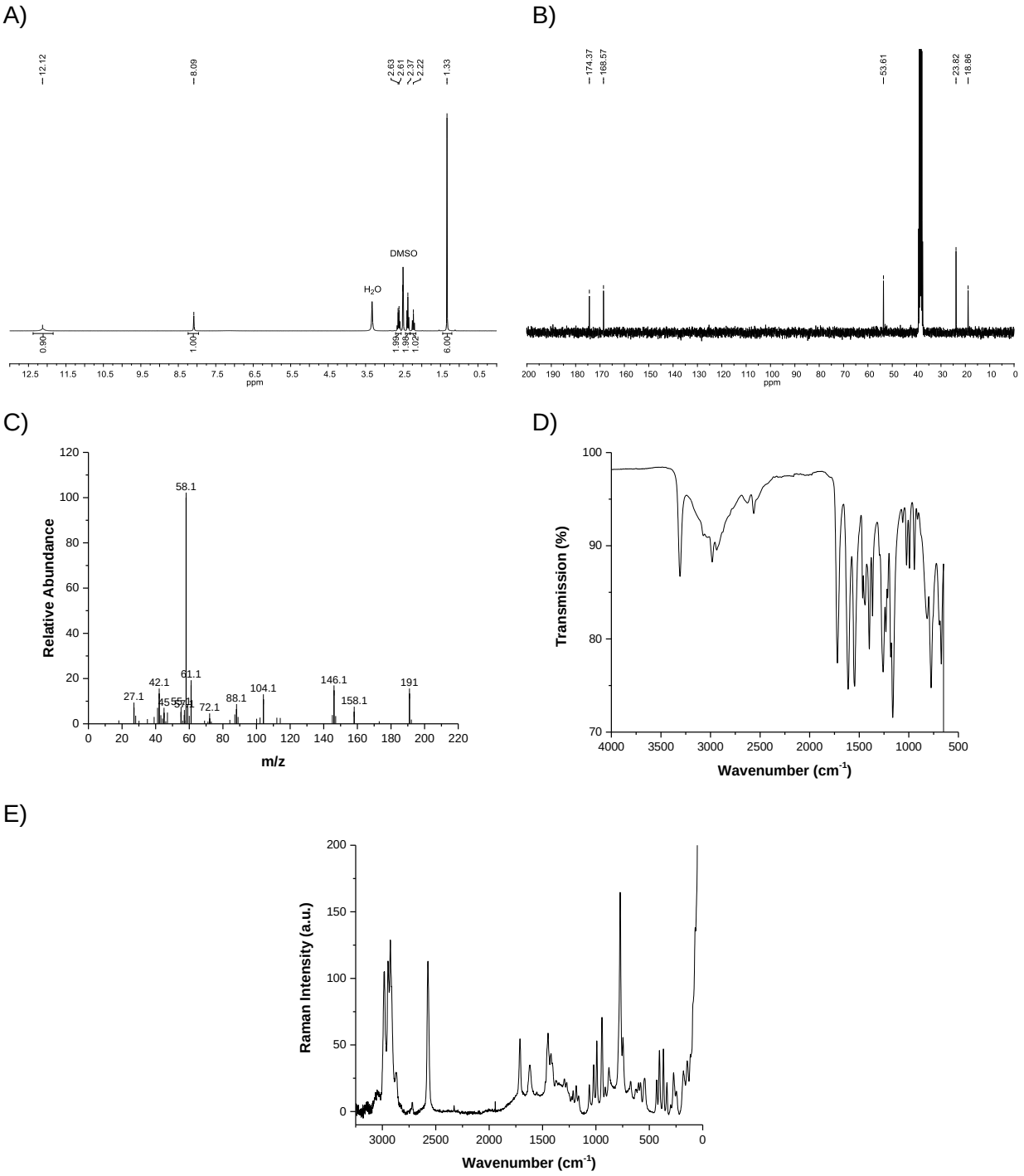

Figure 135: A) ^{1}H NMR, B) ^{13}C NMR, C) EI-MS spectrum, D) IR spectrum and E) Raman spectrum of MOMA.

Functionalization of P(EtOx-co-ButEnOx) with MOMA

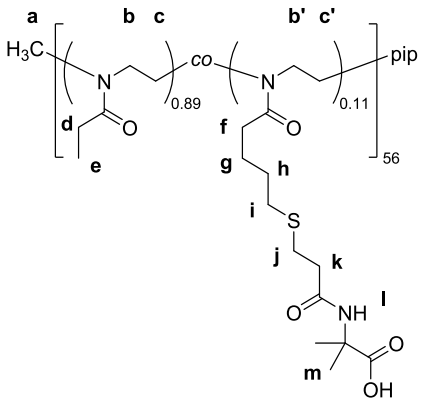

The copolymer P($EtOx_{0.89}$-*co*-$ButEnOx_{0.11}$)$_{56}$-pip (P20) was dissolved in methanol and the solution was degassed for 15 min. MOMA (1.5 eq. per double bond functionality) and 0.5 eq. of the photo-initiator DMPA were added. The solution was stirred under UV light for 0.5 eq. and the solvent was removed under reduced pressure.

The polymer was dissolved in water and dialyzed against Milli-Q water for 1 d to remove unbound MOMA. The polymer was received as a white powder after freeze-drying.

^{1}H NMR of P($EtOx_{0.89}$-*co*-$ButOxMOMA_{0.11}$)$_{56}$-pip (300 MHz, DMSO-d_6, ppm): 8.03 (s, 5.6 H, H-**l**), 3.35 (m, 245 H, H-**b**, **c**, **b'**, **c'**), 2.97 – 2.92 (d, 2 H, H-**a**), 2.81 (s, 1 H, H-**a**), 2.61 (m, 14 H, H-**j**), 2.30 (m, 124 H, H-**d, f, i**, **k**), 1.52 (m, 27 H-**g**, **h**), 1.32 (s, 36 H, H-**m**), 1.03 (m, 153 H, H-**e**).

IR spectrum (cm^{-1}): ν = 3040 – 2755 (CH_2, CH_3 valency), 1730 (C=O valency, carboxylic acid), 1633 (C=O valency, amide), 1542 (NH deformation), 1507 – 990 (CH_2, CH_3 deformation).

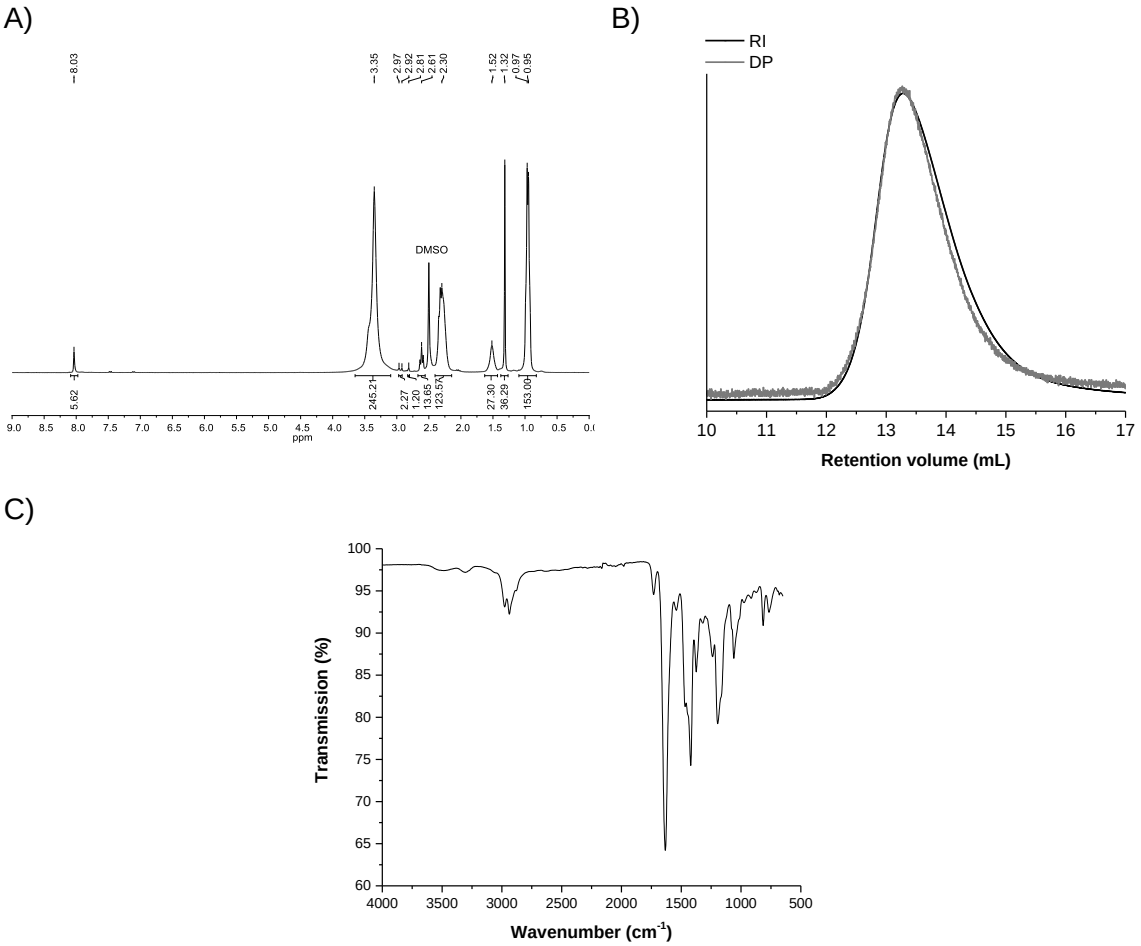

Figure 136: A) ^{1}H NMR and B) SEC elugram measured in water and C) IR spectrum of P(EtOx$_{0.89}$-*co*-ButOxMOMA$_{0.11}$)$_{56}$-pip.

In situ ring closure of azlactone ring at P(EtOx-co-MOMA)

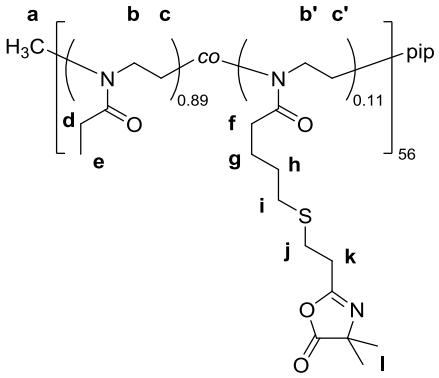

P(EtOx$_{0.89}$-*co*-ButOxMOMA$_{0.11}$)$_{56}$-pip dried under vacuum (1·10^{-3} mbar) for several hours in a flame-dried flask before it was dissolved in dry DMF. Triethylamine (3 eq. per MOMA functionality) was added and the solution was cooled to 0 °C. Ethyl

chloroformate (2 eq. per MOMA functionality) was added and the reaction mixture was stirred for 3 h at 0 °C. The precipitate was filtered, and the organic solvent was removed under reduced pressure. The polymer was precipitated three times from dry DCM in cold Et_2O. The residual solvent was removed under reduced pressure.

^{1}H NMR of P(EtOx$_{0.89}$-*co*-ButOxAL$_{0.11}$)$_{56}$-pip (300 MHz, DMSO-d$_6$, ppm): 3.35 (m, 251 H, H-**b**, **c**, **b'**, **c'**), 2.97 – 2.92 (d, 2 H, H-**a**), 2.81 (s, 1 H, H-**a**), 2.75 (m, 23 H, H-**j**, **k**), 2.55 (m, 11 H, H-**i**), 2.29 (m, 112 H, H-**d**, **f**), 1.52 (m, 23 H-**g**, **h**), 1.31 (s, 35 H, H-**l**), 1.03 (m, 153 H, H-**e**).

SEC (DMF): M_n = 6987 g·mol^{-1}, M_w = 7776 g·mol^{-1}, Đ = 1.11.

IR spectrum (cm^{-1}): *v* = 3040 – 2755 (CH_2, CH_3 valency), 1815 (C=O valency, azlactone carbonyl), 1633 (C=O valency, amide), 1507 – 990 (CH_2, CH_3 deformation).

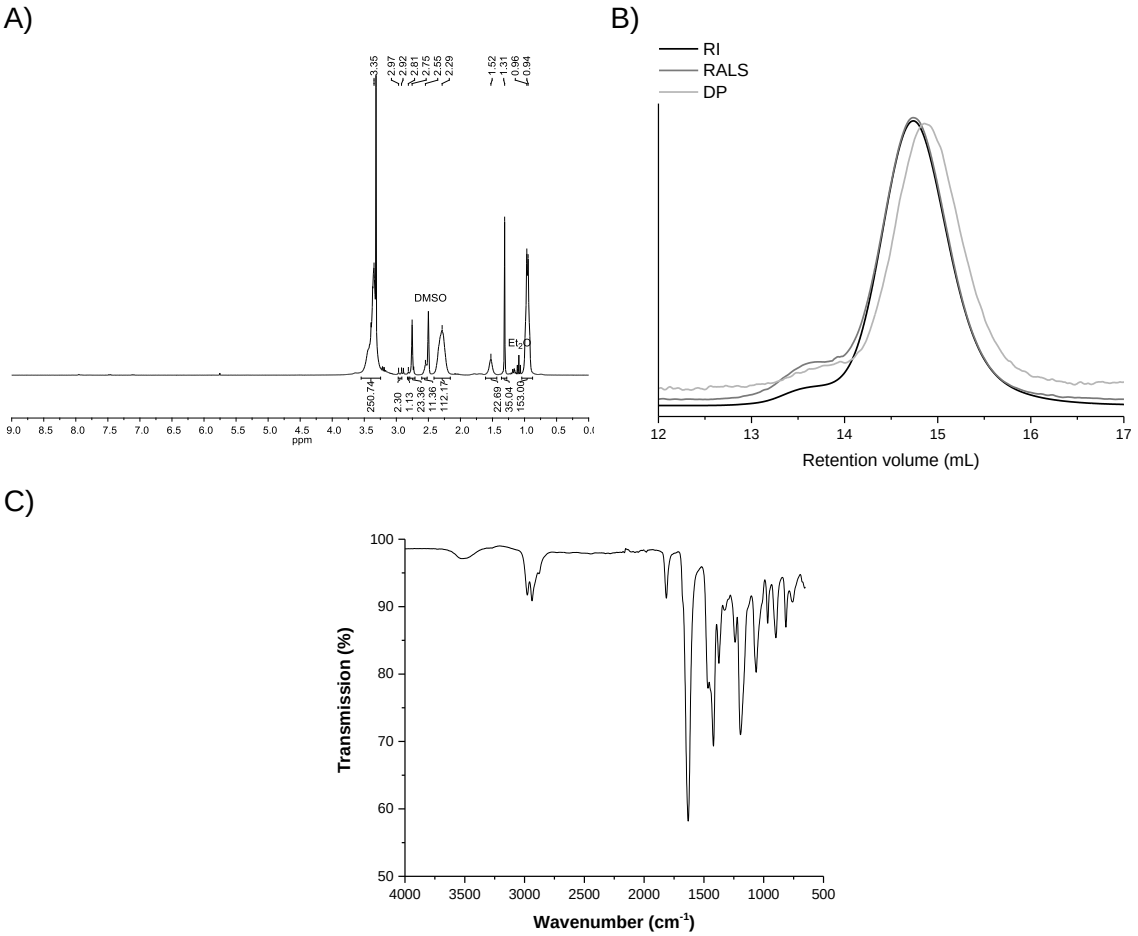

Figure 137: A) ^{1}H NMR and B) SEC elugram measured in DMF and C) IR spectrum of P(EtOx$_{0.89}$-*co*-ButOxAL$_{0.11}$)$_{56}$-pip.

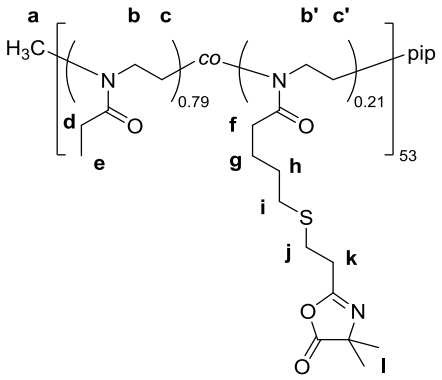

The synthesis of P(EtOx$_{0.79}$-*co*-ButOxAL$_{0.21}$)$_{53}$-pip starting from P(EtOx$_{0.79}$-*co*-ButEnOx$_{0.21}$)$_{53}$-pip (P16) was performed as described for P(EtOx$_{0.89}$-*co*-ButOxAL$_{0.11}$)$_{56}$-pip.

^{1}H NMR of P[(EtOx)$_{0.79}$-*co*-(ButOxAL)$_{0.21}$]$_{53}$-pip (300 MHz, DMSO-d$_6$, ppm): 3.35 (m, 232 H, H-**b**, **c**, **b'**, **c'**), 2.97 (d, 2 H, H-**a**), 2.92 (s, 1H, H-**a**), 2.75 (m, 42 H, H-**j**, **k**), 2.55 (m, 17 H, H-**i**), 2.29 (m, 105 H, H-**d**), 1.52 (m, 44 H-**g**, **h**), 1.31 (s, 66 H, H-**l**), 1.03 (m, 123 H, H-**e**).

IR spectrum (cm^{-1}): *v* = 3040 – 2755 (CH_2, CH_3 valency), 1815 (C=O valency, azlactone carbonyl), 1633 (C=O valency, amide), 1507 – 990 (CH_2, CH_3 deformation).

A)

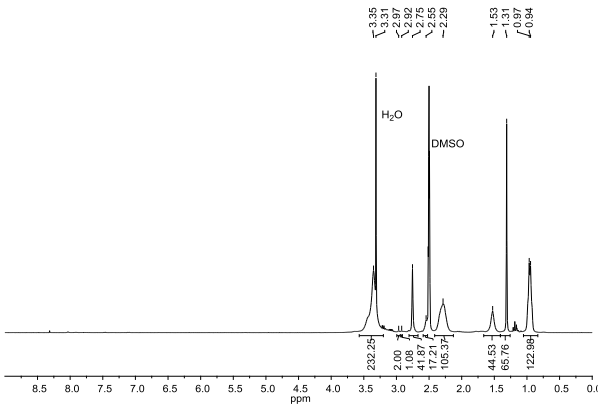

B)

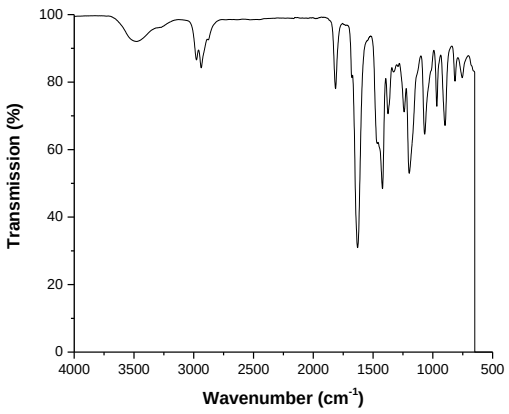

Figure 138: A) ^{1}H NMR (residues of ethyl chloroformate visible at 1.19 ppm) and B) IR spectrum of P(EtOx$_{0.79}$-*co*-ButOxAL$_{0.21}$)$_{53}$-pip.

5.3.3.4 Catechol Functionalization

Protected catechol building block

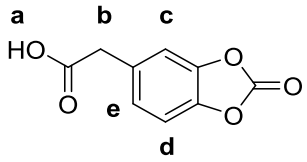

The protected catechol building block 2-oxo-1,3-benzodioxole-5-acetic acid (BDAA) was synthesized according to Li Shao and Xiaohu Zhang [129]. 3,4-dihydroxyphenylacetic acid (4.0 g, 23.788 mmol, 1 eq.) was stirred in 100 mL of dry DCM and *N,N*'-disuccinimidyl carbonate (6.703 g, 26.167 mmol, 1.1 eq.) was added. The solution was degassed with argon for 15 min. Triethylamine (2.888 g. 28.546 mmol, 1.2 eq.) was added to the reaction mixture. After stirring for 12 h, the organic phase was extracted twice with 1 M HCl and once with brine followed by drying over $MgSO_4$. The solvent was narrowed down under reduced pressure and the product was precipitated in cold cyclohexane as a white powder.

Yield: 2.771 g (58.7 %).

^{1}H NMR of BDAA (300 MHz, DMSO-d_6, ppm): δ = 12.41 (br-s, 1 H, H-**a**), 7.42 (s, 1 H, H-**c**), 7.39 (d, 1 H, H-**d**), 7.18-7.15 (dd, 1 H, H-**e**), 3.65 (s, 2 H, H-**b**).

^{13}C NMR of BDAA (300 MHz, DMSO-d_6, ppm): δ = 172.34 (carboxylic acid C=O), 151.11 (carbonate C=O), 142.84 (aromatic C), 141.75 (aromatic CH), 132.15 (aromatic CH), 125.72 (aromatic CH), 111.44 (aromatic CH), 109.89 (aromatic CH), 39.80 (hidden by solvent peaks, CO-CH_2-CH).

EI-MS: Calculated $[M+H]^+$: 194.02 ; found: 194.

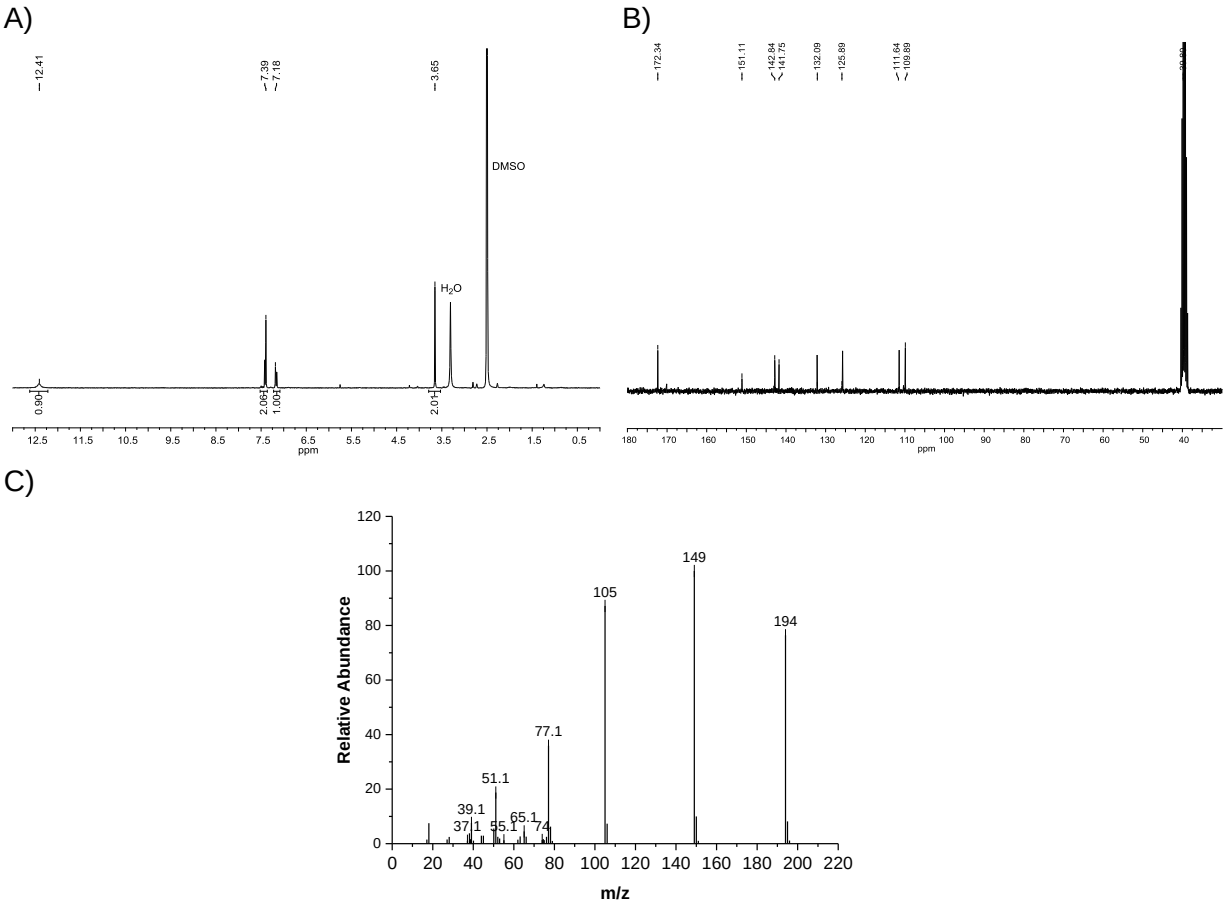

Figure 139: A) ^{1}H NMR, B) ^{13}C NMR and C) EI-MS of BDAA.

Catechol-functionalized P(EtOx-co-ButEnOx) with amide linkage

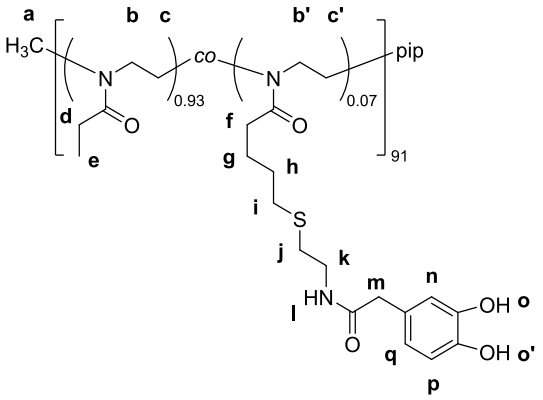

The copolymer P($EtOx_{0.93}$-*co*-$ButEnOx_{0.07}$)$_{91}$-pip (P24) was dissolved in methanol and 3 eq. of cysteamine·HCl per double bond. The solution was degassed for 15 min with argon and 0.5 eq. of the photo-initiator DMPA was added. The reaction was stirred

under UV light for 30 min. Afterwards, the polymer was precipitated in cold Et_2O and dialyzed against Milli-Q water for 3 d to remove any excess cysteamine.
After lyophilization, P[$(EtOx)_{0.93}$-*co*-$(ButOxNH_2)_{0.07}$]$_{91}$-pip was dissolved in dry DMF in a flame-dried flask. 3 eq. of the protected catechol building block BDAA per amine functionality and 3 eq. of *N,N*'-dicyclohexylcarbodiimide (DCC) per amine functionality were added and the solution was stirred for 12 h at room temperature. The solvent was removed under reduced pressure and the functionalized polymer was dialyzed against slightly acidic water (pH 4) for 2 d. The polymer was received as a white powder after lyophilization.

^{1}H NMR of P[$(EtOx)_{0.93}$-*co*-$(ButOxNH_2)_{0.02}$-*co*-$(ButOxDOPAm)_{0.05}$]$_{91}$-pip (300 MHz, DMSO-d_6, ppm): δ = 8.76-8.66 (s, 8 H, H-**o, o'**), 7.99 (m, 4 H, H-**l**), 7.49 (d, aromat., tosylate anion), 7.12 (d, aromat., tosylate anion), 6.66 – 6.62 (m, 9 H, H-**n**, **p**), 6.49 (m, 4 H, H-**q**), 3.37 (m, 474 H, H-**b**, **c**, **b'**, **c'**, **m**), 3.21 (m, 27 H, H-**i**, **j**, **k**), 2.96 (d, 2 H, H-**a**), 2.83 (m, 1 H, H-**a**), 2.30 (m, 179 H, H-**d, f**), 1.53 (m, 20 H, H-**g**, **h**), 0.97 (m, 256 H, H-**e**).

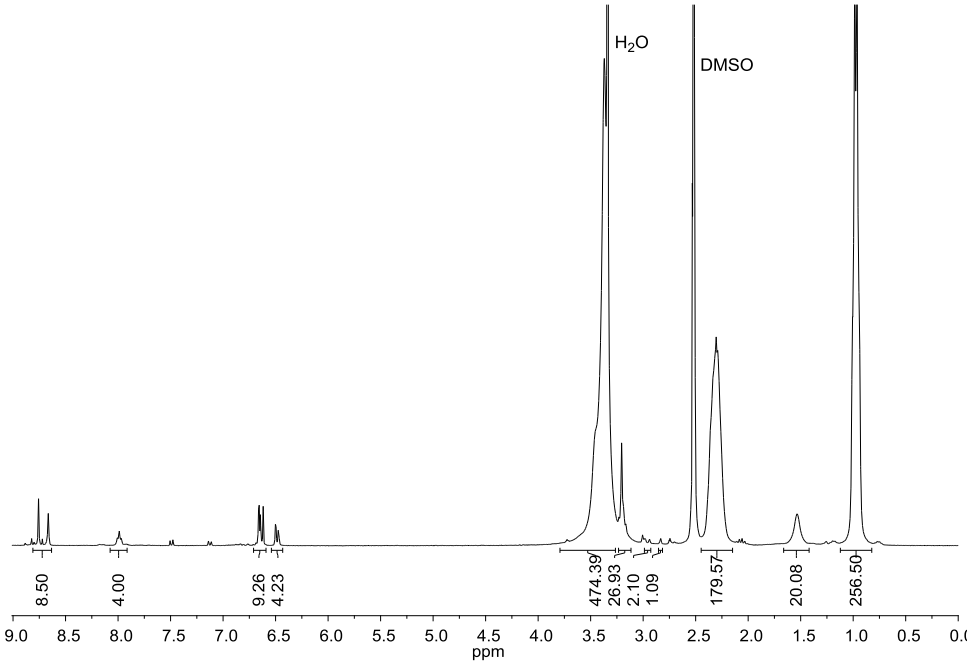

Figure 140: ^{1}H NMR of catechol-functionalized POx.

Catechol-functionalized P(EtOx-co-ButEnOx) with ester linkage

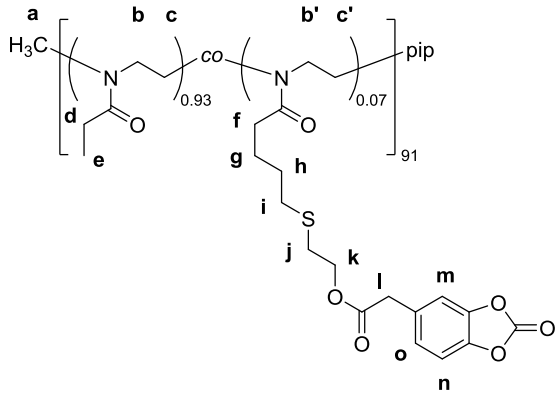

The copolymer P($EtOx_{0.93}$-*co*-$ButEnOx_{0.07}$)$_{91}$-pip (P24) was dissolved in methanol degassed for 15 min. 3 eq. of 2-mercaptoethanol per double bond and 0.5 eq. of the photo-initiator DMPA were added. The solution was irradiated under UV light for 30 min. The polymer was precipitated three times from chloroform in ice-cold Et_2O and residual solvent was removed. Afterwards, the polymer P($EtOx_{0.93}$-*co*-$ButOxOH_{0.07}$)$_{91}$-pip was transferred into a flame-dried flask and dry DMF was added. 3 eq. of the protected catechol BDAA per hydroxyl functionality and 10 mol% of DMAP were added. The reaction mixture was cooled down to 0 °C using an ice bath and 3 eq. of DCC per hydroxyl functionality were added. The solution was stirred for another 15 min at 0 °C and then left stirring overnight at room temperature. The polymer was purified by dialysis against DMF (MWCO = 3.5 kDa) for several days, followed by removal of DMF and precipitation from chloroform in Et_2O.

^{1}H-NMR of P($EtOx_{0.93}$-*co*-$ButOxOH_{0.02}$-*co*-$ButOxDOPAc_{0.05}$)$_{91}$-pip (300 MHz, DMSO-d_6, ppm): δ = 7.40 (m, 8 H, H-**m**, **n**), 7.20 (m, 4 H, H-**o**), 4.17 (t, 8 H, H-**k**), 3.76 (s, 7 H, H-**l**), 3.35 (m, 511 H, H-**b**, **c**, **b'**, **c'**, residual water in deuterated solvent), 2.94 (d, 2 H, H-**a**), 2.81 (m, 1 H, H-**a**), 2.71 (t, 11 H, H-**j**), 2.28 (m, 184 H, H-**d, f**), 1.52 (m, 28 H, H-**g**, **h**, **i**), 0.95 (m, 256 H, H-**e**).

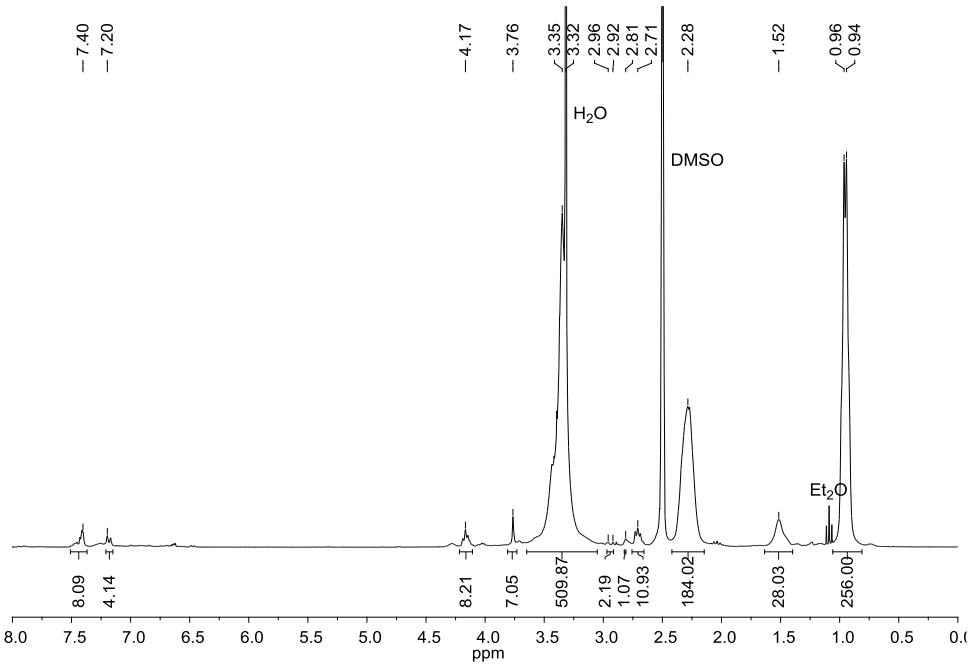

Figure 141: ^{1}H NMR of P(EtOx$_{0.93}$-*co*-ButOxOH$_{0.02}$-*co*-ButOxDOPAc$_{0.05}$)$_{91}$-pip.

Catechol-functionalized P(MeOx-co-ButEnOx) with amide linkage

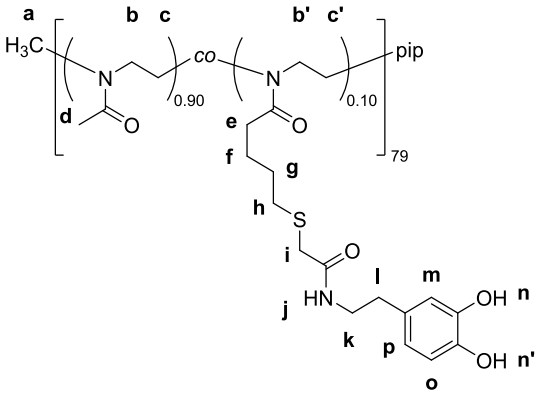

The copolymer P(MeOx$_{0.90}$-*co*-ButEnOx$_{0.10}$)$_{79}$-pip (P30) was dissolved in methanol and degassed for 15 min with argon. 3 eq. of thioglycolic acid per double bond functionality and 0.5 eq. DMPA were added. The reaction mixture was irradiated for 30 min under UV light and afterwards precipitated four times from chloroform/methanol (v/v 1:1) in cold Et$_2$O. Residual solvent was removed under reduced pressure. The polymer P(MeOx$_{0.90}$-*co*-ButOxCOOH$_{0.10}$)$_{79}$-pip was transferred into a flame-dried flask and was dissolved in dry DMF. 3.5 eq. of NHS, 3.5 eq. of EDC and 3.5 eq. of dopamine hydrochloride per carboxyl functionality were

added and the reaction mixture was stirred overnight at room temperature. The organic solvent was removed, and the polymer was purified by dialysis for 3 days against acidic Milli-Q water (pH 3).

^{1}H NMR of P(MeOx$_{0.90}$-*co*-ButOxCOOH$_{0.02}$-*co*-ButOxDOPAm$_{0.08}$)$_{79}$-pip (300 MHz, DMSO-d$_6$, ppm): δ = 8.74-8.65 (s, 13.3 H, H-**n, n'**), 7.98 (m, 6.7 H, H-**j**), 6.66 – 6.62 (m, 14.8 H, H-**m**, **o**), 6.49 (m, 6.7 H, H-**p**), 3.34 (m, 389 H, H-**b**, **c**, **b'**, **c'**, **h**), 3.07 (m, 15 H, H-**i**), 3.19 (m, 22 H, H-**k**), 2.97 (d, 2 H, H-**a**), 2.81 (m, 1 H, H-**a**), 2.55 (m, 16 H, H-**l**), 2.30 (m, 17 H, H-**e**), 2.00 (m, 213 H, H-**d**), 1.54 (m, 35 H, H-**f**, **g**).

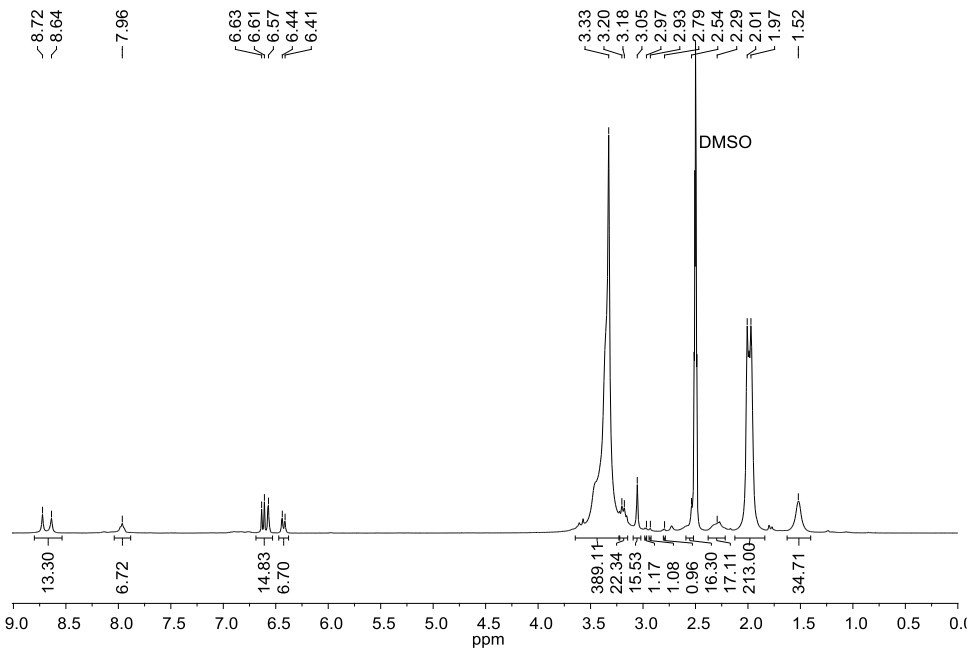

Figure 142: ^{1}H NMR of P(MeOx$_{0.90}$-*co*-ButOxCOOH$_{0.02}$-*co*-ButOxDOPAm$_{0.08}$)$_{79}$-pip.

Catechol-functionalized P(MeOx-co-ButEnOx) with ester linkage

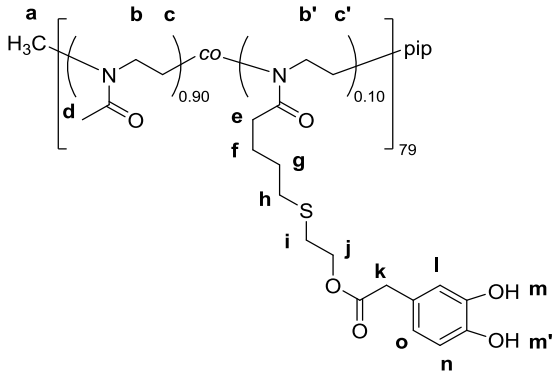

The copolymer P(MeOx$_{0.90}$-*co*-ButEnOx$_{0.10}$)$_{79}$-pip (P30) was dissolved in methanol and degassed for 15 min with argon. 3 eq. of 2-mercaptoethanol per double bond functionality and 0.5 eq. DMPA were added. The reaction mixture was irradiated for 30 min under UV light and afterwards precipitated four times from chloroform/methanol (v/v 1:1) in cold Et_2O. Residual solvent was removed under reduced pressure. The polymer P(MeOx$_{0.90}$-*co*-ButOxOH$_{0.10}$)$_{79}$-pip was transferred into a flame-dried flask and was dissolved in dry DMF. 3 eq. of BDAA per hydroxyl functionality and 10 mol% of DMAP were added under inert atmosphere. The solution was cooled to 0 °C and 3 eq. of DCC per hydroxyl functionality were added. The solution was stirred for 15 min at 0 °C and 12 h at room temperature. The precipitated salt was removed with a PTFE syringe filter and the solvent was removed under reduced pressure. The polymer was precipitated from chloroform/methanol in cold Et_2O and dialyzed against DMF (MWCO = 1 kDa) for 3 days. DMF was removed under reduced pressure and the polymer was precipitated twice from chloroform/methanol in cold Et_2O. The residual solvent was removed under reduced pressure.

^{1}H NMR of P(MeOx$_{0.90}$-*co*-ButOxOH$_{0.04}$-*co*-ButOxDOPAc$_{0.06}$)$_{79}$-pip (300 MHz, DMSO-d_6, ppm): δ = 8.81 (br s, 8.8 H, H-**m**, **m'**), 6.64 (m, 9.8 H, H-**l**, **n**), 6.50 (m, 4.65 H, H-**o**), 4.13 (t, 15 H, H-**j**), 3.69 (s, 8 H, H-**k**), 3.35 (m, 450 H, H-**b**, **c**, **b'**, **c'**, residual water in deuterated solvent), 2.95 (d, 2 H, H-**a**), 2.80 (m, 1 H, H-**a**), 2.71 (t, 18 H, H-**i**), 2.32 (m, 23 H, H-**e**), 1.99 (m, 213 H, H-**d**), 1.52 (m, 28 H, H-**f**, **g**).

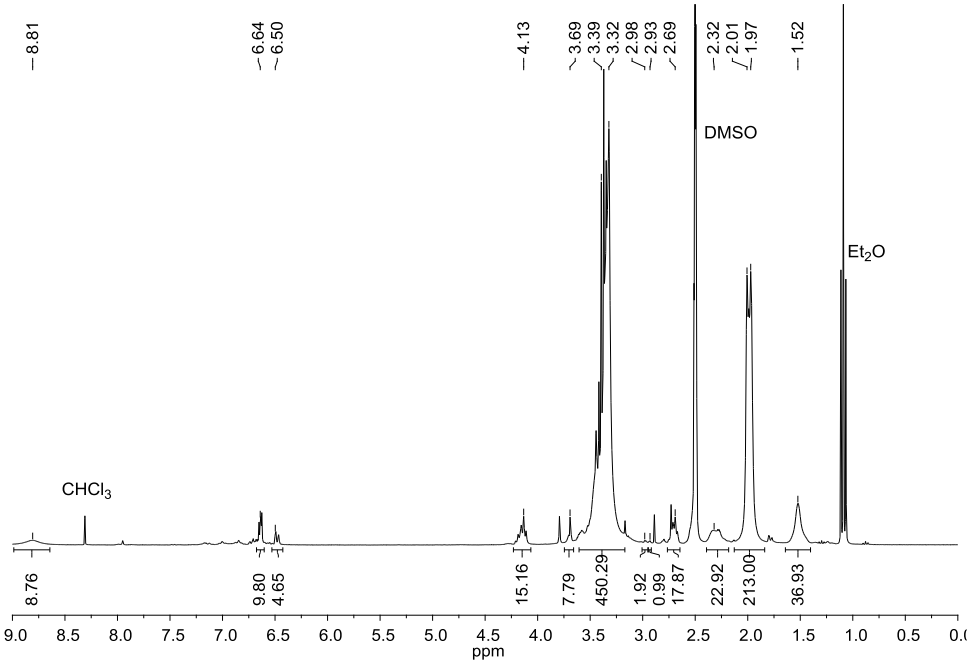

Figure 143: ^{1}H NMR of P(MeOx$_{0.90}$-*co*-ButOxOH$_{0.04}$-*co*-ButOxDOPAc$_{0.06}$)$_{79}$-pip.

5.3.4 Functionalization of POx with Peptide

5.3.4.1 Thiol-ene Chemistry with POx

Polymer peptide conjugate between P(EtOx-co-ButEnOx) and peptide CGGGF

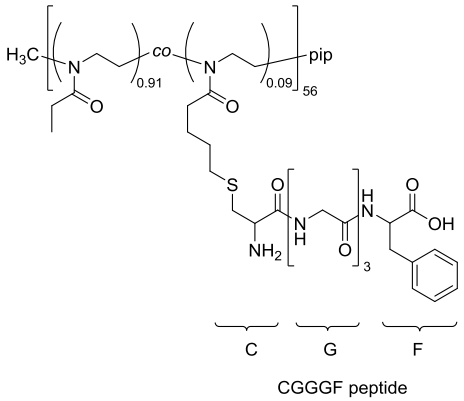

The copolymer P19 and the peptide CGGGF (CG3F) (1 – 3 eq. per double bond available) were dissolved in the deuterated solvent (specified in Table 27) and the solution was degassed with argon for 15 min. Afterwards, the photo-initiator DMPA or Irgacure 2959 (0.5 eq.) was added and the solution was irradiated under UV light for 30 min using the LED cubes (for DMPA) or for 100 min using the UV handlamp (for Irgacure 2959).

The success of the reaction was characterized by means of NMR spectroscopy analyzing the amount of the residual signals belonging to the double bond of the side chain.

Table 27: Reaction of polymer P14 with peptide CGGGF.

Sample name	Solvent	Initiator	Eq. CG3F	Unreacted double bonds (%)
P19-CG3F-1	DMSO-d_6	DMPA	3	82
P19-CG3F-2	D_2O	Irgacure	1	20
P19-CG3F-3	D_2O	Irgacure	2	0
P19-CG3F-4	D_2O	Irgacure	3	0

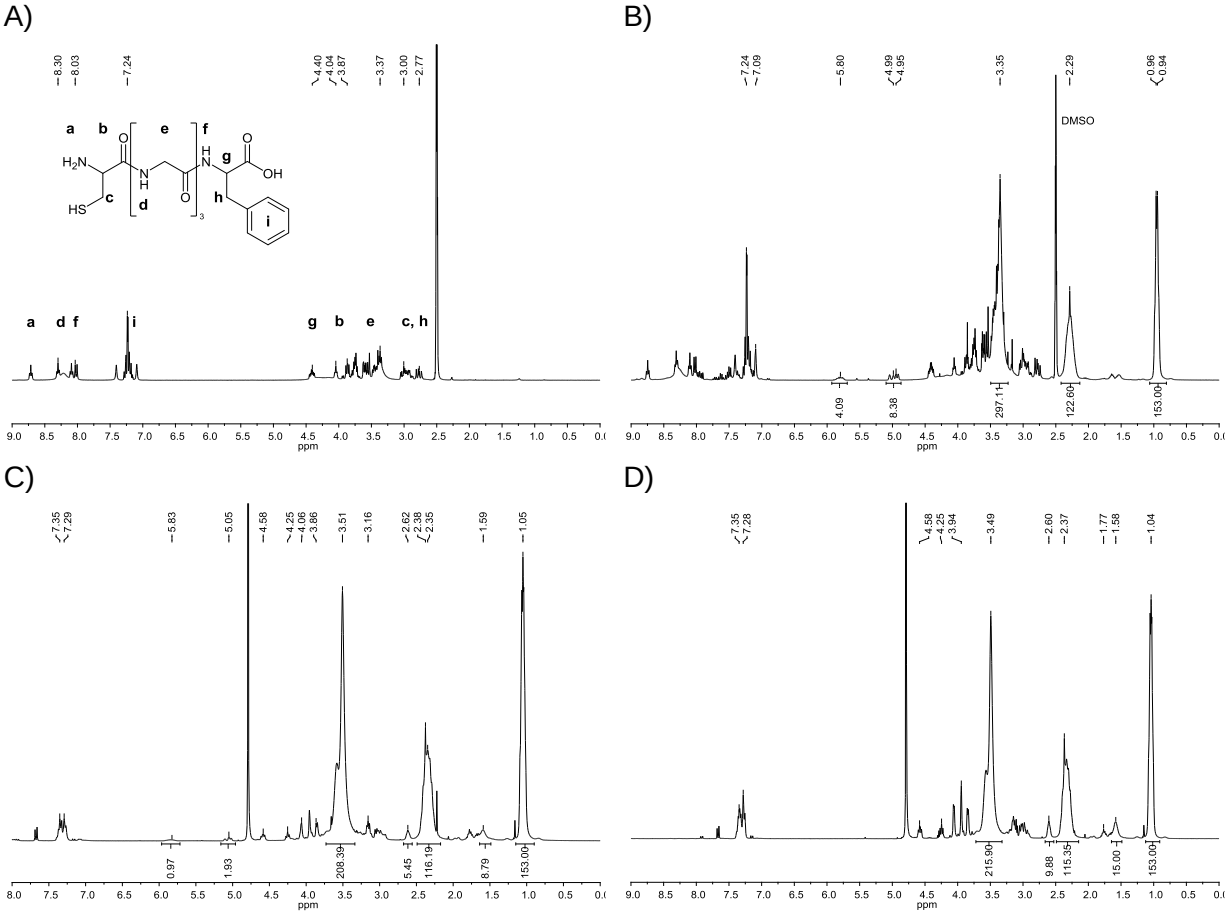

Figure 144: ^{1}H NMR of A) peptide CGGGF, B) P19-CG3F-1 still showing signals of the vinyl double bond, C) P19-CG3F-2 also showing signals of the vinyl double bond and D) P19-CG3F-3, where all double bond signals have vanished.

Polymer peptide conjugate between P(EtOx-co-ButEnOx) and peptide CKFKFQF

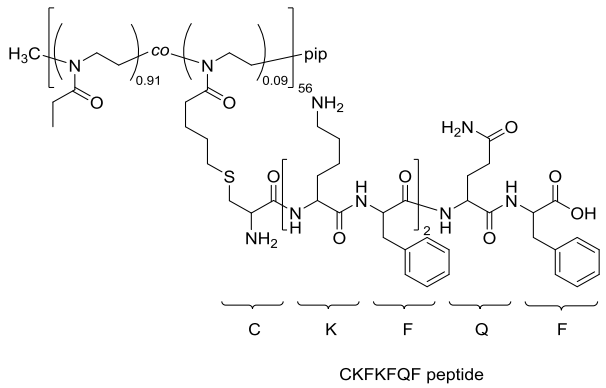

The copolymer P19 and the peptide CKFKFQF (CKF) (1.5 – 3 eq. per double bond available) were dissolved in the deuterated solvent (specified in Table 28) and the solution was degassed with argon for 15 min. Afterwards, the photo-initiator DMPA or

Irgacure 2959 (0.5 eq.) was added and the solution was irradiated under UV light for 30 min using the LED cubes (for DMPA) or for 2 h using the UV handlamp (for Irgacure 2959).

The success of the reaction was characterized by means of NMR spectroscopy analyzing the amount of the residual signals belonging to the double bond of the side chain.

Table 28: Reactions of P14 with peptide CKF.

Sample name	Solvent	Initiator	Eq. CKF	Unreacted double bonds (%)
P19-CKF-1	DMSO-d_6	DMPA	3	55
P19-CKF-2	D_2O/CD_3CN (1:1)	Irgacure	2	23.6
P19-CKF-3	D_2O/CD_3CN (1:1)	Irgacure	3	0
P19-CKF-4	CD_3CN/DMSO-d_6 (2:1)	Irgacure	1.5	100
P19-CKF-5	CD_3CN/DMSO-d_6 (2:1)	Irgacure	2	44
P19-CKF-6	D_2O /DMSO-d_6 (2:1)	Irgacure	1.5	0

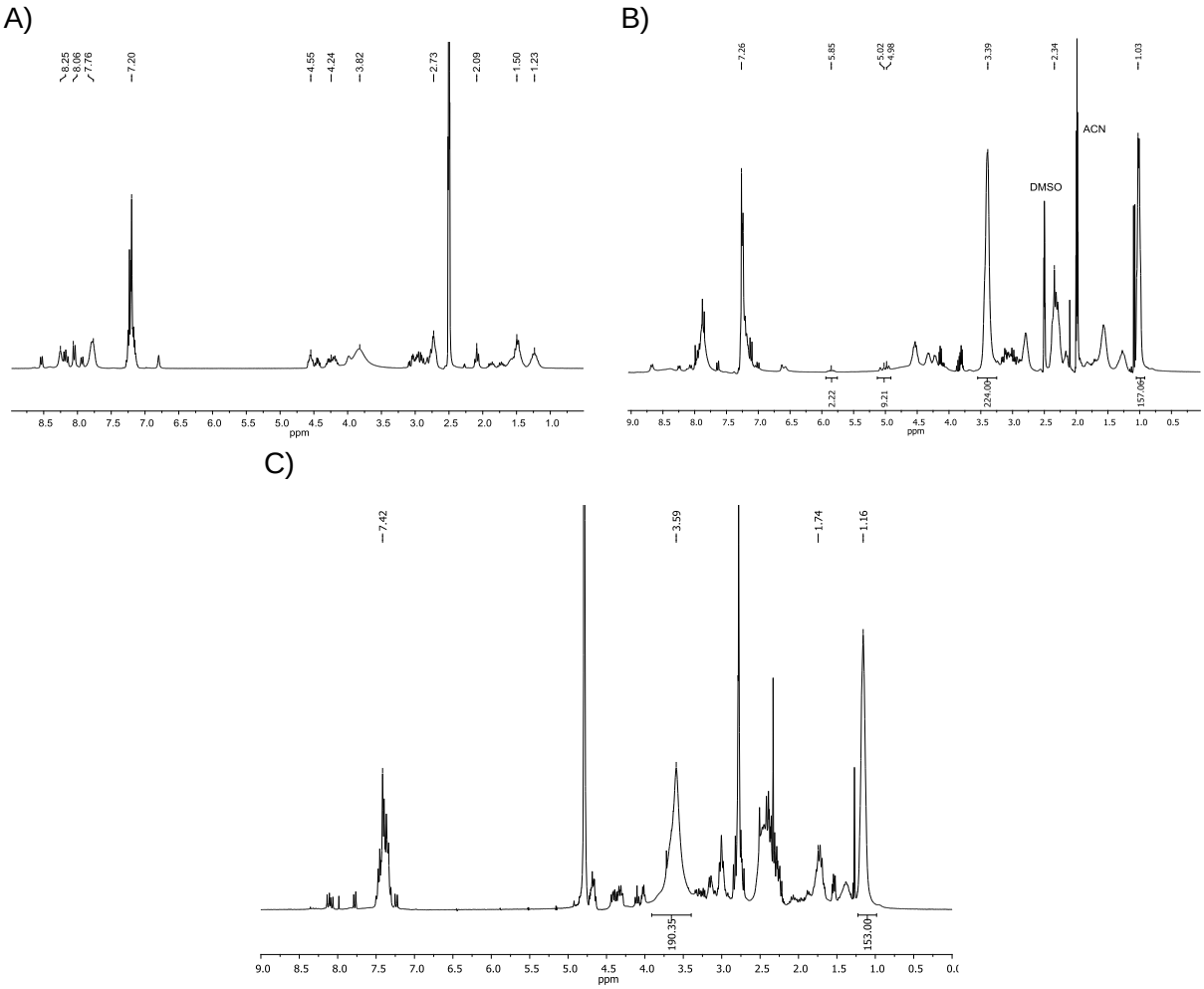

Figure 145: ^{1}H NMR of A) peptide CKFKFQF in DMSO-d_6, B) P19-CKF-5 still showing the signals for the vinyl functionality at 5.85 ppm and 5.00 ppm and C) P19-CKF-6 showing signals in the area of the vinyl functionality.

5.3.4.2 Thiolactone Chemistry with POx

Polymer peptide conjugate between P(EtOx$_{0.89}$-co-ButOxLac$_{0.11}$)$_{56}$-pip and CGGGF

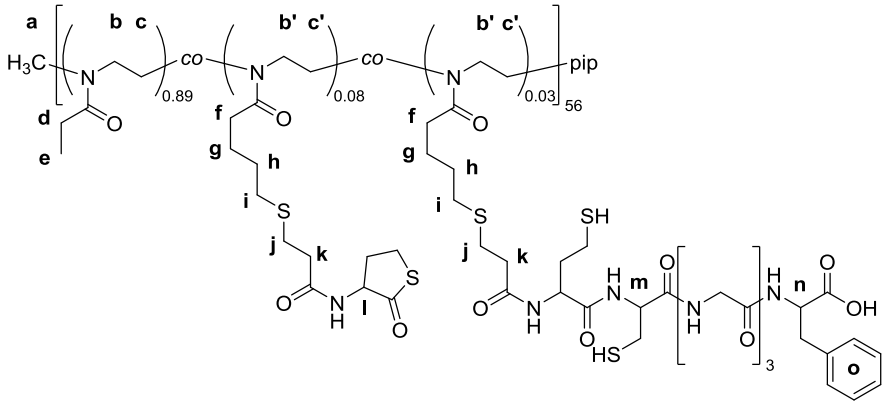

The peptide conjugation was carried out according to Schmitz *et al*. without the addition of guanidinium chloride [147].

A buffer of 100 mM NaH_2PO_4, 50 mM TCEP and 200 mM 4-mercaptophenylacetic acid was prepared and adjusted to pH 7 using NaOH. The buffer was degassed with argon for 15 min. 35 mg (2 eq. per thiolactone side chain) of CGGGF (CG3F) were dissolved in 2 mL of buffer and added to 50 mg of P(EtOx$_{0.89}$-*co*-ButOxLac$_{0.11}$)$_{56}$-pip. The pH was checked and adjusted to pH 7. The reaction solution was agitated for 20 h and afterwards dialyzed against water (MWCO = 3.5 kDa) for two days and freeze-dried. The yield was 27 mg.

^{1}H-NMR of P(EtOx$_{0.89}$-*co*-ButOxLac$_{0.08}$-*co*-ButOxCG3F$_{0.03}$)$_{56}$-pip (300 MHz, D_2O, ppm): δ = 7.36 – 7.28 (m, 8.6 H, H-**o**), 4.71 (m, 6 H, H-**m**, **n**), 4.52 (m, 3 H, H-**l**), 3.54 (m, 213 H, H- **b**, **c**, **b'**, **c'**), 3.10 (d, 2 H, H-**a**), 2.95 (s, 1 H, H-**a**), 2.82 (m, 15 H-**j**), 2.62 (m, 30 H, H-**k**, **n**), 2.39 (m, 107 H, H-**d**, **f**), 2.21 (m, 15 H, H-**i**), 1.65 (m, 23 H, H-**g**, **h**), 1.08 (m, 150 H, H-**e**).

IR spectrum (cm^{-1}): *v* = 3700 – 3120 (OH, NH stretching), 3040 – 2755 (CH_2, CH_3 valency), 1633 (C=O valency, amide), 1540 (NH deformation), 1507 – 990 (CH_2, CH_3 deformation).

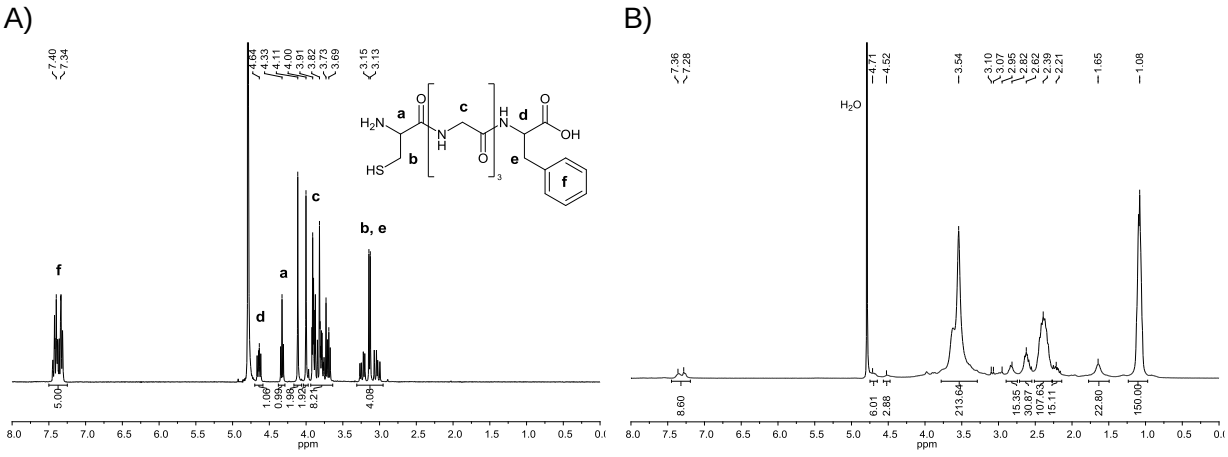

Figure 146: ^{1}H NMR of A) peptide CGF3 in D_2O and B) polymer peptide conjugate P(EtOx$_{0.89}$-*co*-ButOxLac$_{0.08}$-*co*-ButOxCG3F$_{0.03}$)$_{56}$-pip in D_2O.

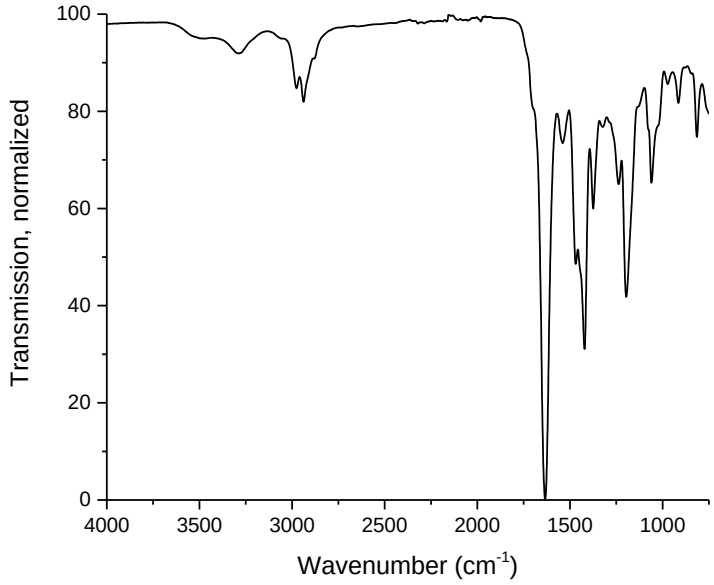

Figure 147: IR spectrum of P(EtOx$_{0.89}$-*co*-ButOxLac$_{0.08}$-*co*-ButOxCG3F$_{0.03}$)$_{56}$-pip.

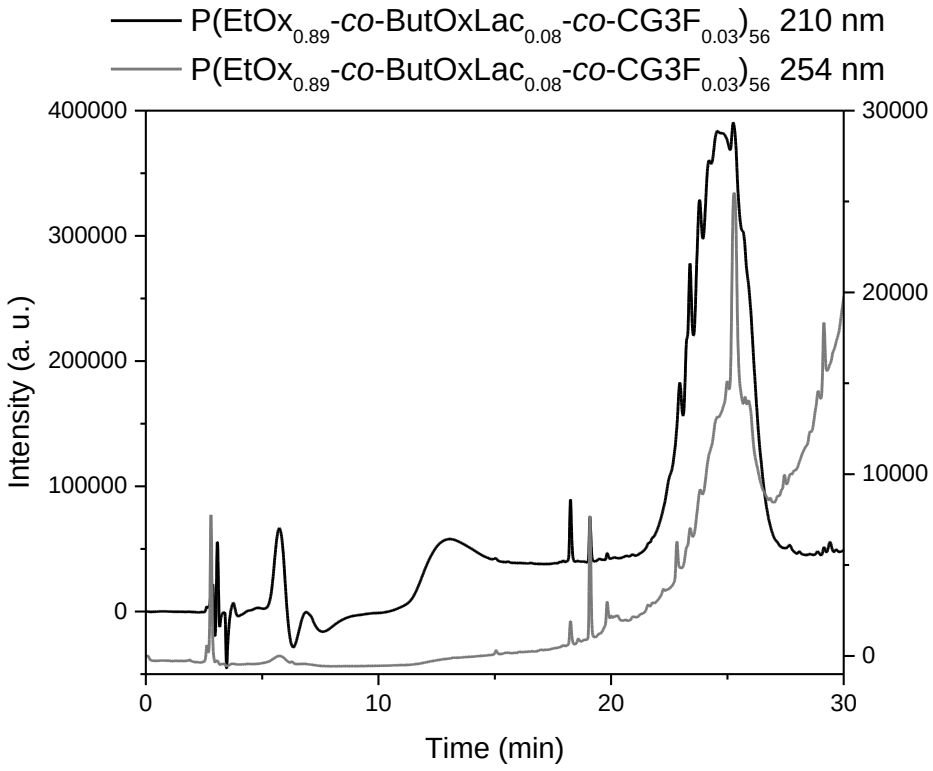

Figure 148: HPLC elugram of P(EtOx$_{0.89}$-*co*-ButOxLac$_{0.08}$-*co*-ButOxCG3F$_{0.03}$)$_{56}$-pip.

Polymer peptide conjugate between P(EtOx$_{0.79}$-co-ButOxLac$_{0.21}$)$_{53}$-pip and CGGGF

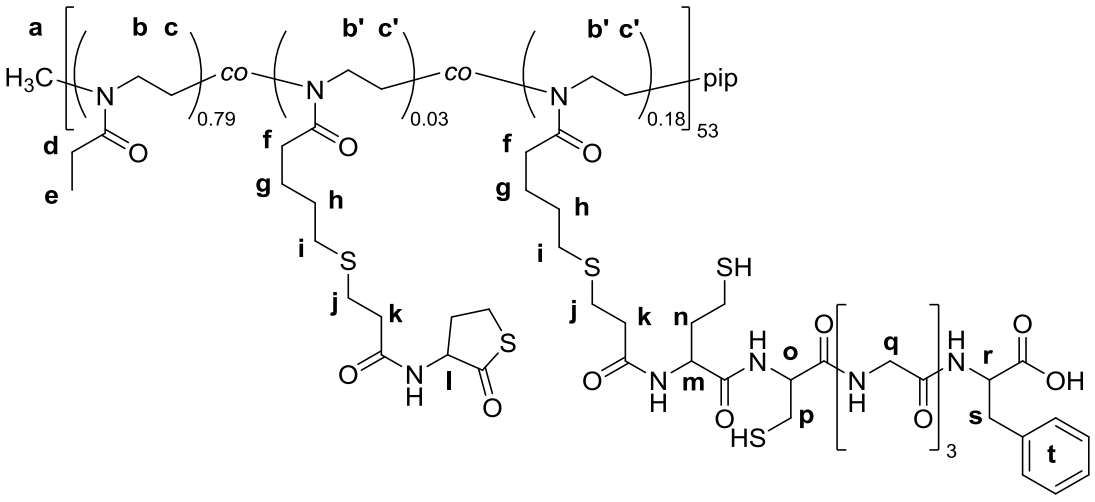

A buffer of 100 mM NaH_2PO_4, 50 mM TCEP and 200 mM 4-mercaptophenylacetic acid (MPAA) was prepared and adjusted to pH 7 using NaOH. The buffer was degassed with argon for 15 min. 49 mg (2 eq. per thiolactone side chain) of CGGGF

were dissolved in 2 mL of buffer and added to 40 mg of P(EtOx$_{0.79}$-*co*-ButOxLac$_{0.21}$)$_{53}$-pip. The pH was checked and adjusted to pH 7. The reaction solution was agitated for 20 h and afterwards dialyzed against water (MWCO = 3.5 kDa) for two days and freeze-dried. The yield was 14 mg.

^{1}H NMR of P(EtOx$_{0.79}$-*co*-ButOxLac$_{0.03}$-*co*-ButOxCG3F$_{0.18}$)$_{53}$-pip (300 MHz, D_2O, ppm): δ = 7.60 (residual MPAA), 7.37 – 7.29 (m, 48 H, H-**t**), 4.69 (m, 7 H, H-**o**, **r**), 4.47 (m, 9 H, H-**m**), 4.06 – 3.86 (m, 64 H, H-**q**) 3.54 (m, 200 H, H- **b**, **c**, **b'**, **c'**), 3.10 (d, 2 H, H-**a**), 2.95 (s, 1 H, H-**a**), 2.83 (m, 22 H-**j**), 2.62 (m, 39 H, H-**k**, **n**), 2.39 (m, 170 H, H-**d**, **f**, residual TCEP), 2.14 (residual TCEP), 1.65 (m, 30 H, H-**g**, **h**), 1.09 (m, 126 H, H-**e**).

IR spectrum (cm^{-1}): *v* = 3700 – 3120 (OH, NH stretching), 3040 – 2755 (CH_2, CH_3 valency), 1633 (C=O valency, amide), 1575 (NH deformation), 1507 – 990 (CH_2, CH_3 deformation).

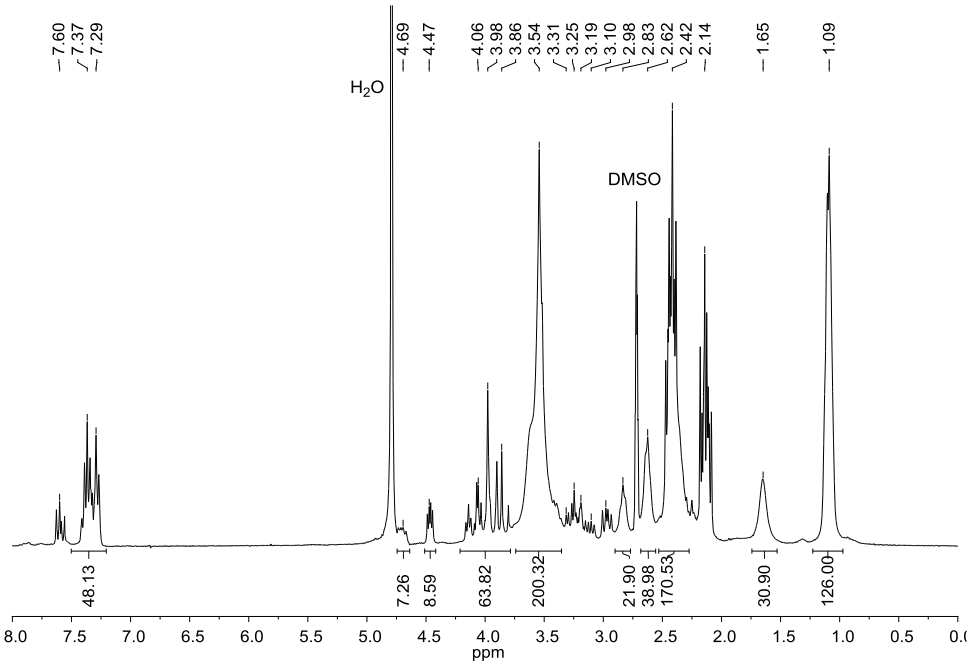

Figure 149: ^{1}H NMR of P(EtOx$_{0.79}$-*co*-ButOxLac$_{0.03}$-*co*-ButOxCG3F$_{0.18}$)$_{53}$-pip in D_2O.

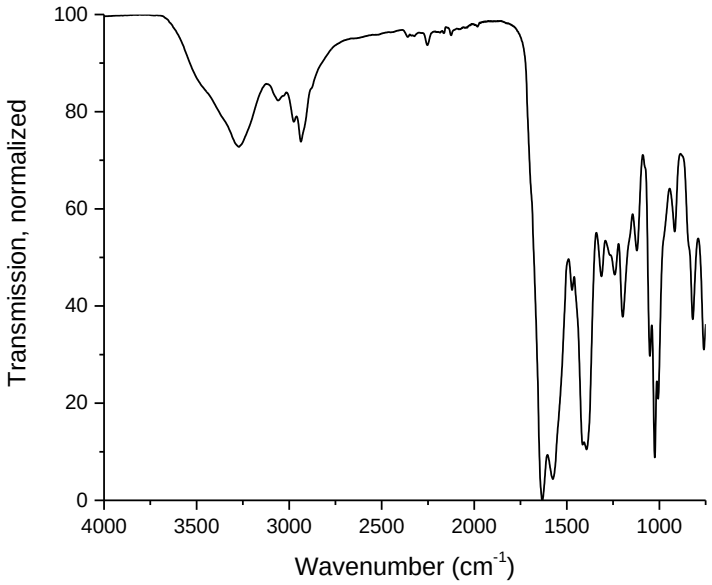

Figure 150: IR spectrum of P(EtOx$_{0.79}$-*co*-ButOxLac$_{0.03}$-*co*-ButOxCG3F$_{0.18}$)$_{53}$-pip.

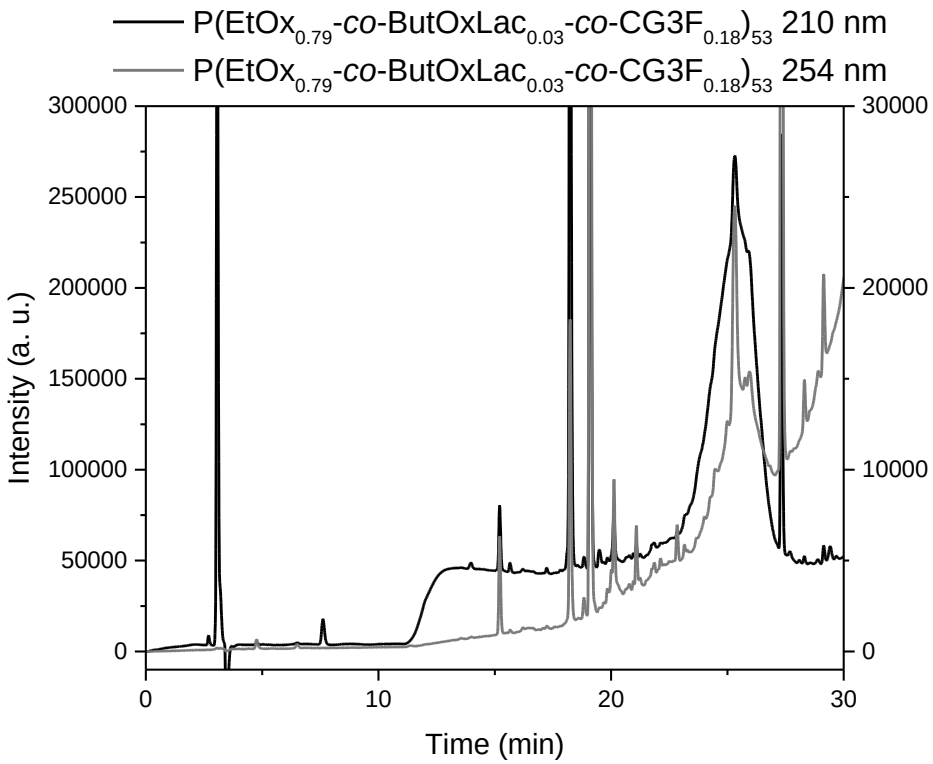

Figure 151: HPLC elugram of P(EtOx$_{0.79}$-*co*-ButOxLac$_{0.03}$-*co*-ButOxCG3F$_{0.18}$)$_{53}$-pip.

5.3.4.3 Azlactone Chemistry with POx

Polymer peptide conjugate between P(EtOx$_{0.89}$-co-ButOxAL$_{0.11}$)$_{56}$-pip and CGGGF

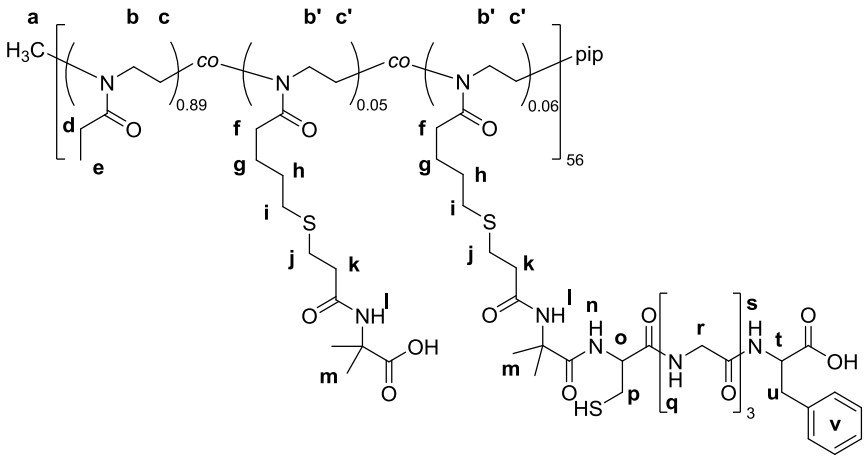

The reaction was carried out following the protocol of Ho *et al*. [162].
110 mg of the peptide CGGGF (CG3F) (3 eq. per azlactone functionality) and 100 mg of P(EtOx$_{0.89}$-*co*-ButOxAL$_{0.11}$)$_{56}$-pip were dissolved separately in 2 mL of dry DMSO and degassed with argon for 10 min. The polymer solution was added to the peptide solution and 0.084 g (10 eq.) of triethylamine were added. The reaction mixture was stirred for 20 h and afterwards purified by dialysis (MWCO = 1 kDa) against acidified water (pH 3). After lyophilization, a white powder was received. The yield was 90 mg.

^{1}H NMR of P(EtOx$_{0.89}$-*co*-ButOxAL$_{0.05}$-*co*-ButOxCG3F$_{0.06}$)$_{56}$-pip (300 MHz, DMSO-d$_6$, ppm): 8.40 – 7.96 (N*H*, 21 H, H-**l**, **n**, **q**, **s**), 7.22 (m, 15 H, H-**v**), 4.43 (m, 5.6 H, H-**t**), 3.71 (m, 24 H, H-**o**, **r**), 3.35 (m, 228 H, H-**b**, **c**, **b'**, **c'**), 3.07 – 2.81 (m, 19 H, H-**a**, **p**, **u**), 2.61 (t, 12 H, H-**j**), 2.30 (m, 120 H, H-**d**, **f**), 1.52 (m, 23 H-**g**, **h**), 1.31 (s, 34 H, H-**m**), 1.03 (m, 150 H, H-**e**).
IR spectrum (cm^{-1}): *v* = 3700 – 3120 (OH, NH stretching), 3040 – 2755 (CH_2, CH_3 valency), 1730 (C=O valency, carboxylic acid), 1633 (C=O valency, amide), 1542 (NH deformation), 1507 – 990 (CH_2, CH_3 deformation).

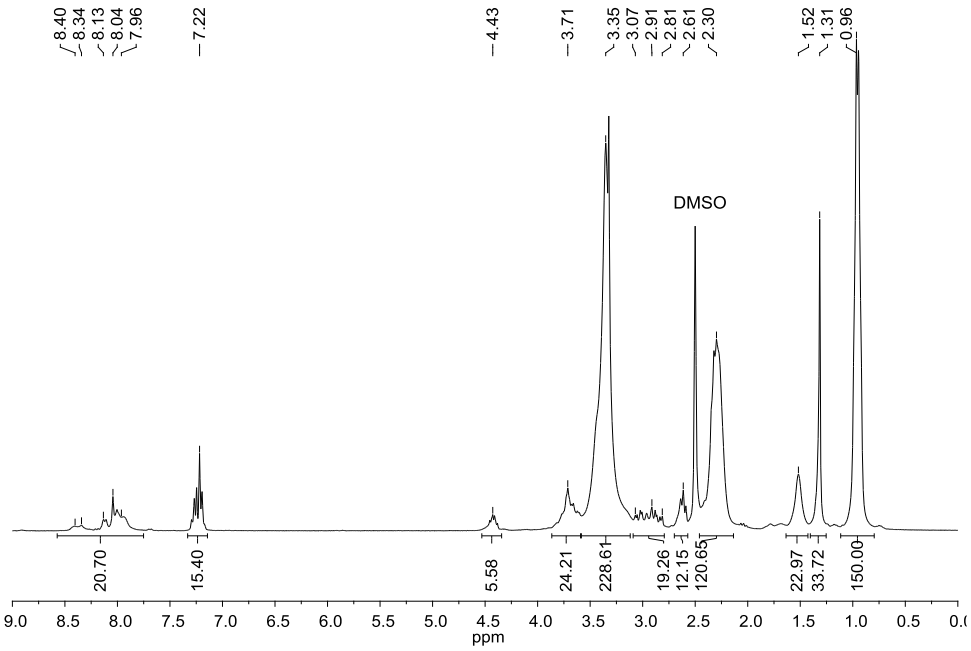

Figure 152: ^{1}H NMR of P(EtOx$_{0.89}$-*co*-ButOxAL$_{0.05}$-*co*-ButOxCG3F$_{0.06}$)$_{56}$-pip measured in DMSO-d$_6$.

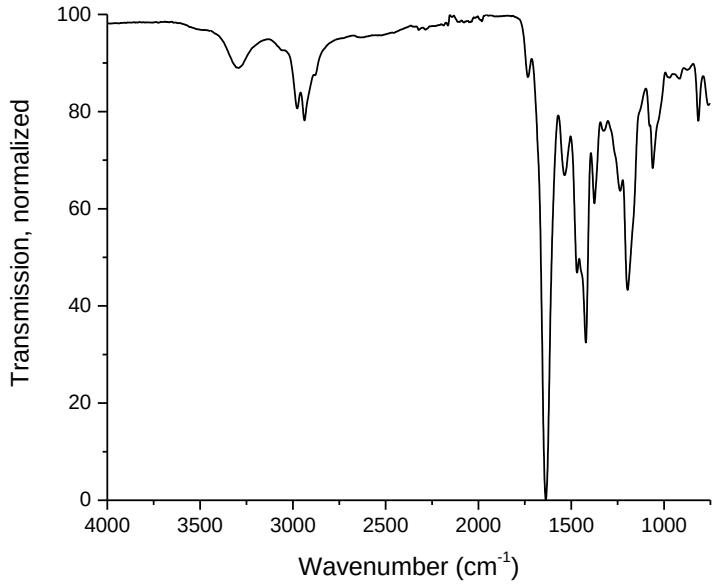

Figure 153: IR spectrum of P(EtOx$_{0.89}$-*co*-ButOxAL-*co*-ButOxCG3F$_{0.11}$)$_{56}$-pip.

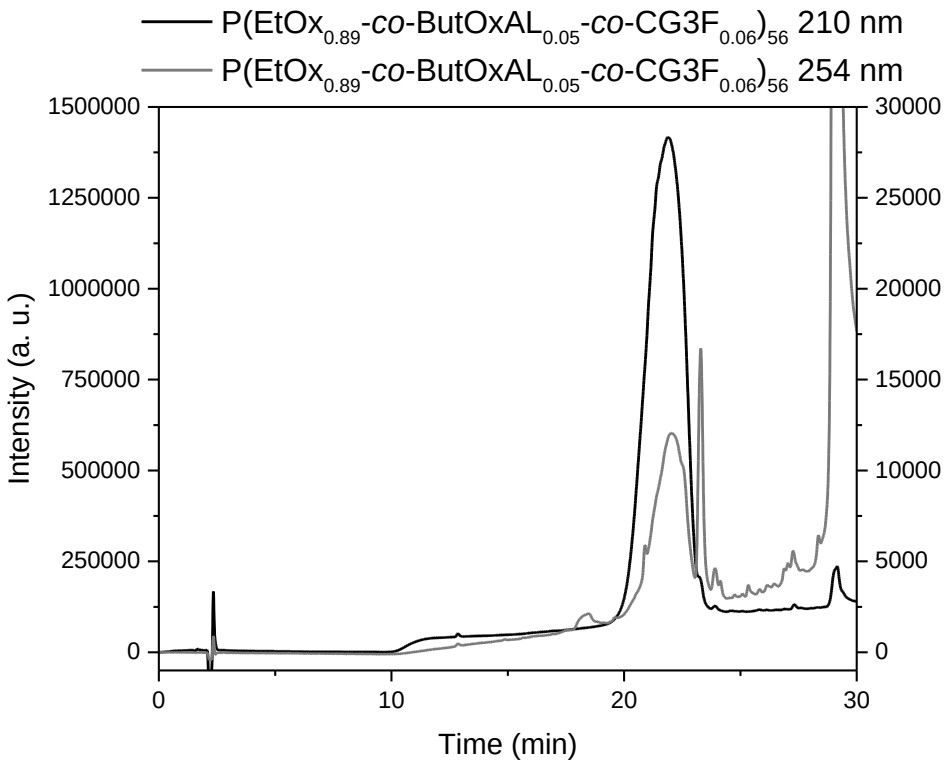

Figure 154: HPLC elugram of P(EtOx$_{0.89}$-*co*-ButOxAL-*co*-ButOxCG3F$_{0.11}$)$_{56}$-pip.

Polymer peptide conjugate between P(EtOx$_{0.79}$-co-ButOxAL$_{0.21}$)$_{53}$-pip and CGGGF

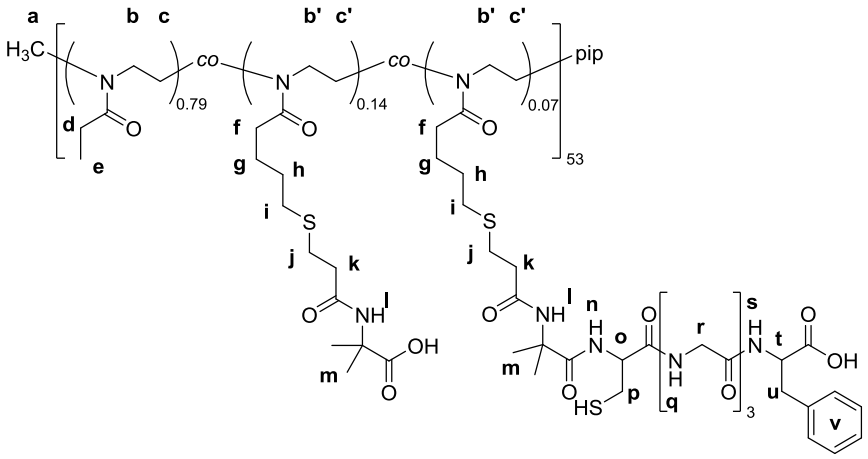

64 mg of the peptide CGGGF (CG3F) (2.5 eq. per azlactone functionality) and 40 mg of P(EtOx$_{0.79}$-*co*-ButOxAL$_{0.21}$)$_{53}$-pip were dissolved separately in 2 mL of dry DMSO and degassed with argon for 10 min. The polymer solution was added to the peptide solution and 0.071 g (12 eq.) of triethylamine were added. The reaction mixture was stirred for 20 h and afterwards purified by dialysis (MWCO = 3.5 kDa) against acidified water (pH 3). After lyophilization, a white powder was received. The yield was 34 mg.

^{1}H NMR of P(EtOx$_{0.79}$-*co*-ButOxAL$_{0.14}$-*co*-ButOxCG3F$_{0.07}$)$_{53}$-pip (300 MHz, DMSO-d$_6$, ppm): 8.40 – 7.96 (N*H*, 27 H, H-**l**, **n**, **q**, **s**), 7.22 (m, 19 H, H-**v**), 4.43 (m, 7 H, H-**t**), 3.71 (m, 35 H, H-**o**, **r**), 3.35 (m, 263 H, H-**b**, **c**, **b'**, **c'**), 3.07 – 2.81 (m, 27 H, H-**a**, **p**, **u**), 2.61 (t, 23 H, H-**j**), 2.30 (m, 119 H, H-**d**, **f**), 1.52 (m, 42 H-**g**, **h**), 1.31 (s, 56 H, H-**l**), 1.03 (m, 126 H, H-**e**).

IR spectrum (cm^{-1}): *v* = 3700 – 3120 (OH, NH stretching), 3040 – 2755 (CH_2, CH_3 valency), 1730 (C=O valency, carboxylic acid), 1633 (C=O valency, amide), 1542 (NH deformation), 1507 – 990 (CH_2, CH_3 deformation).

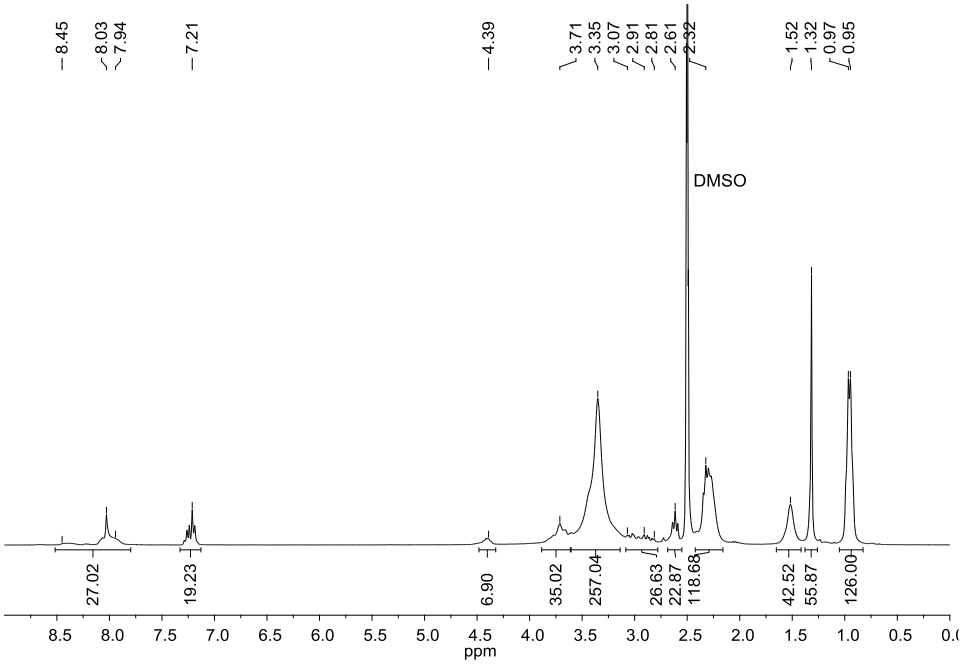

Figure 155: ^{1}H NMR of P(EtOx$_{0.79}$-*co*-ButOxAL$_{0.14}$-*co*-ButOxCG3F$_{0.07}$)$_{53}$-pip measured in DMSO-d$_6$.

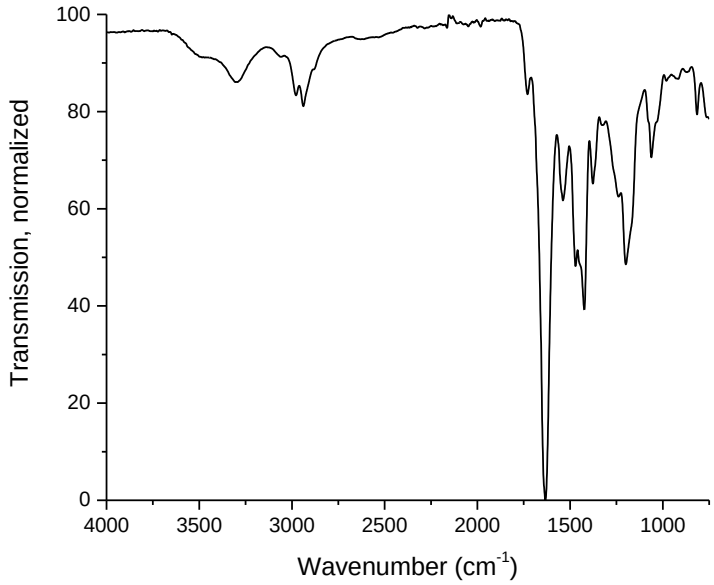

Figure 156: IR spectrum of P(EtOx$_{0.79}$-*co*-ButOxAL-*co*-ButOxCG3F$_{0.21}$)$_{53}$-pip.

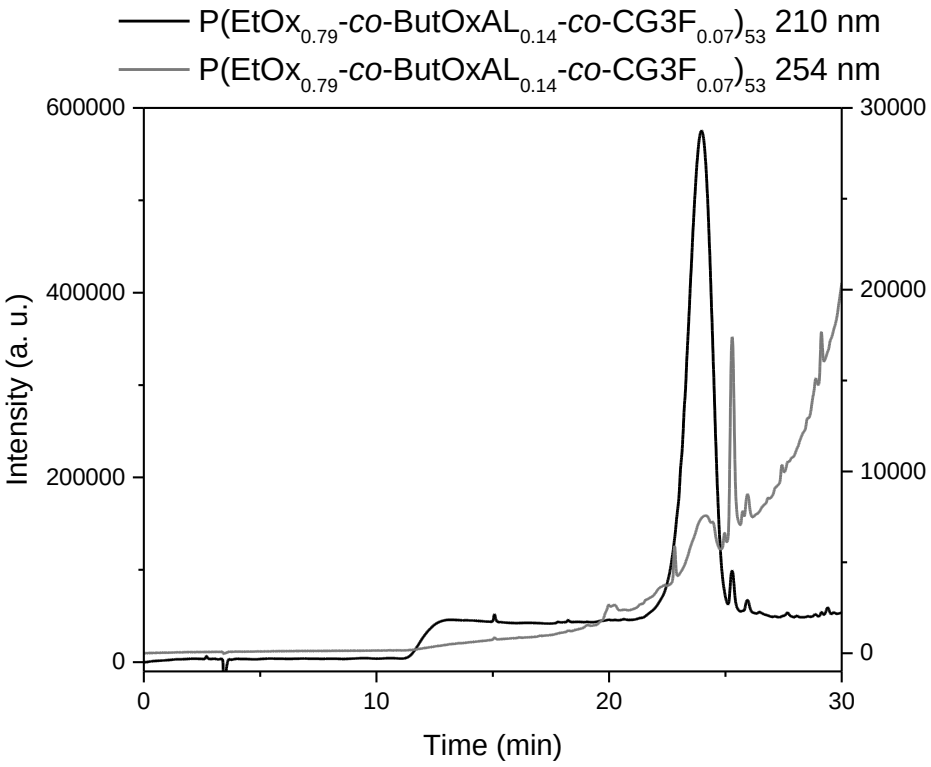

Figure 157: HPLC elugram of P(EtOx$_{0.79}$-*co*-ButOxAL-*co*-ButOxCG3F$_{0.21}$)$_{53}$-pip.

6 References

1. Reis, R.L., Neves, N.M., Mano, J.F., Gomes, M.E., Marques, A.P., Azevedo, H.S., *Natural-based polymers for biomedical applications*. 2008: Woodhead Publishing Limited and CRC Press LLC, ISBN 978-1-84569-264-3.
2. Lee, K.Y., Mooney, D.J., *Alginate: properties and biomedical applications.* Progress in Polymer Science **2012**, *37*, 106-126.
3. Kogan, G., Šoltés, L., Stern, R., Gemeiner, P., *Hyaluronic acid: a natural biopolymer with a broad range of biomedical and industrial applications.* Biotechnology Letters **2007**, *29*, 17-25.
4. Maitz, M.F., *Applications of synthetic polymers in clinical medicine.* Biosurface and Biotribology **2015**, *1*, 161-176.
5. Hoffman, A.S., *Hydrogels for biomedical applications.* Advanced Drug Delivery Reviews **2012**, *64*, 18-23.
6. Kharkar, P.M., Rehmann, M.S., Skeens, K.M., Maverakis, E., Kloxin, A.M., *Thiol–ene Click Hydrogels for Therapeutic Delivery.* ACS Biomaterials Science & Engineering **2016**, *2*, 165-179.
7. Peppas, N.A., *Hydrogels and drug delivery.* Current Opinion in Colloid and Interface Science **1997**, *2*, 531-537.
8. Schöttler, S., Landfester, K., Mailänder, V., *Protein adsorption is required for stealth effect of poly(ethylene glycol)- and poly(phosphoester)-coated nanocarriers.* Nature nanotechnology **2016**, *11*, 372.
9. Bauer, M., Lautenschlaeger, C., Kempe, K., Tauhardt, L., Schubert, U.S., Fischer, D., *Poly(2-ethyl-2-oxazoline) as alternative for the stealth polymer poly(ethylene glycol): comparison of in vitro cytotoxicity and hemocompatibility.* Macromolecular Bioscience **2012**, *12*, 986-98.
10. Shah, S., Prematta, T., Adkinson, N.F., Ishmael, F.T., *Hypersensitivity to polyethylene glycols.* The Journal of Clinical Pharmacology **2013**, *53*, 352-355.
11. Schlaad, H., Diehl, C., Gress, A., Meyer, M., Demirel, A.L., Nur, Y., Bertin, A., *Poly(2-oxazoline)s as smart bioinspired polymers.* Macromolecular Rapid Communications **2010**, *31*, 511-525.
12. Seeliger, W., Aufderhaar, E., Diepers, W., Feinauer, R., Nehring, R., Thier, W., Hellmann, H., *Recent syntheses and reactions of cyclic imidic esters.* Angewandte Chemie International Edition in English **1966**, *5*, 875-888.
13. Kagiya, T., Narisawa, S., Maeda, T., Fukui, K., *Ring-opening polymerization of 2-substituted 2-oxazolines.* Journal of Polymer Science Part B: Polymer Letters **1966**, *4*, 441-445.
14. Tomalia, D., Sheetz, D., *Homopolymerization of 2-alkyl- and 2-aryl-2-oxazolines.* Journal of Polymer Science Part A-1: Polymer Chemistry **1966**, *4*, 2253-2265.
15. Bassiri, T., Levy, A., Litt, M., *Polymerization of cyclic imino ethers. I. Oxazolines.* Journal of Polymer Science Part B: Polymer Letters **1967**, *5*, 871-879.
16. Wiesbrock, F., Hoogenboom, R., Abeln, C.H., Schubert, U.S., *Single-Mode Microwave Ovens as New Reaction Devices: Accelerating the Living Polymerization of 2-Ethyl-2-Oxazoline.* Macromolecular Rapid Communications **2004**, *25*, 1895-1899.
17. Wiesbrock, F., Hoogenboom, R., Leenen, M.A., Meier, M.A., Schubert, U.S., *Investigation of the living cationic ring-opening polymerization of 2-methyl-, 2-ethyl-, 2-nonyl-, and 2-phenyl-2-oxazoline in a single-mode microwave reactor.* Macromolecules **2005**, *38*, 5025-5034.

18. Wiesbrock, F., Hoogenboom, R., Leenen, M., van Nispen, S.F., van der Loop, M., Abeln, C.H., van den Berg, A.M., Schubert, U.S., *Microwave-assisted synthesis of a 4^2-membered library of diblock copoly(2-oxazoline)s and chain-extended homo poly(2-oxazoline)s and their thermal characterization.* Macromolecules **2005**, *38*, 7957-7966.
19. Cesana, S., Auernheimer, J., Jordan, R., Kessler, H., Nuyken, O., *First poly(2-oxazoline)s with pendant amino groups.* Macromolecular Chemistry and Physics **2006**, *207*, 183-192.
20. Cesana, S., Kurek, A., Baur, M.A., Auernheimer, J., Nuyken, O., *Polymer-Bound Thiol Groups on Poly(2-oxazoline)s.* Macromolecular Rapid Communications **2007**, *28*, 608-615.
21. Gress, A., Völkel, A., Schlaad, H., *Thio-Click Modification of Poly[2-(3-butenyl)-2-oxazoline].* Macromolecules **2007**, *40*, 7928-7933.
22. Dargaville, T.R., Forster, R., Farrugia, B.L., Kempe, K., Voorhaar, L., Schubert, U.S., Hoogenboom, R., *Poly (2-oxazoline) hydrogel monoliths via thiol-ene coupling.* Macromolecular Rapid Communications **2012**, *33*, 1695-1700.
23. Guillerm, B., Monge, S., Lapinte, V., Robin, J.J., *How to modulate the chemical structure of polyoxazolines by appropriate functionalization.* Macromolecular Rapid Communications **2012**, *33*, 1600-1612.
24. Rossegger, E., Schenk, V., Wiesbrock, F., *Design strategies for functionalized poly(2-oxazoline)s and derived materials.* Polymers **2013**, *5*, 956-1011.
25. Bludau, H., Czapar, A.E., Pitek, A.S., Shukla, S., Jordan, R., Steinmetz, N.F., *POxylation as an alternative stealth coating for biomedical applications.* European Polymer Journal **2017**, *88*, 679-688.
26. Hoogenboom, R., *Poly(2-oxazoline)s: a polymer class with numerous potential applications.* Angewandte Chemie International Edition **2009**, *48*, 7978-7994.
27. Hoogenboom, R., Schlaad, H., *Bioinspired Poly(2-oxazoline)s.* Polymers **2011**, *3*, 467-488.
28. Luxenhofer, R., Han, Y., Schulz, A., Tong, J., He, Z., Kabanov, A.V., Jordan, R., *Poly(2-oxazoline)s as Polymer Therapeutics.* Macromolecular Rapid Communications **2012**, *33*, 1613-1631.
29. Lorson, T., Lubtow, M.M., Wegener, E., Haider, M.S., Borova, S., Nahm, D., Jordan, R., Sokolski-Papkov, M., Kabanov, A.V., Luxenhofer, R., *Poly(2-oxazoline)s based biomaterials: A comprehensive and critical update.* Biomaterials **2018**, *178*, 204-280.
30. Dargaville, T.R., Park, J.R., Hoogenboom, R., *Poly(2-oxazoline) Hydrogels: State-of-the-Art and Emerging Applications.* Macromolecular Bioscience **2018**, *18*, 1800070.
31. El-Hag Ali, A., AlArifi, A., *Swelling and drug release profile of poly(2-ethyl-2-oxazoline)-based hydrogels prepared by gamma radiation-induced copolymerization.* Journal of Applied Polymer Science **2011**, *120*, 3071-3077.
32. Zahoranová, A., Kronek, J., *Hydrogels Based on Poly(2-oxazoline)s for Pharmaceutical Applications.* Handbook of Polymers for Pharmaceutical Technologies **2015**, 4, 231-258.
33. Hartlieb, M., Schubert, S., Kempe, K., Windhab, N., Schubert, U.S., *Stabilization of factor VIII by poly(2-oxazoline) hydrogels.* Journal of Polymer Science Part A: Polymer Chemistry **2015**, *53*, 10-14.

34. Farrugia, B.L., Kempe, K., Schubert, U.S., Hoogenboom, R., Dargaville, T.R., *Poly(2-oxazoline) hydrogels for controlled fibroblast attachment.* Biomacromolecules **2013**, *14*, 2724-32.
35. Lorson, T., Jaksch, S., Lübtow, M.M., Jüngst, T., Groll, J., Lühmann, T., Luxenhofer, R., *A thermogelling supramolecular hydrogel with sponge-like morphology as a cytocompatible bioink.* Biomacromolecules **2017**, *18*, 2161-2171.
36. Luxenhofer, R., Schulz, A., Roques, C., Li, S., Bronich, T.K., Batrakova, E.V., Jordan, R., Kabanov, A.V., *Doubly amphiphilic poly(2-oxazoline)s as high-capacity delivery systems for hydrophobic drugs.* Biomaterials **2010**, *31*, 4972-4979.
37. He, Z., Wan, X., Schulz, A., Bludau, H., Dobrovolskaia, M.A., Stern, S.T., Montgomery, S.A., Yuan, H., Li, Z., Alakhova, D., *A high capacity polymeric micelle of paclitaxel: Implication of high dose drug therapy to safety and in vivo anti-cancer activity.* Biomaterials **2016**, *101*, 296-309.
38. Eskow Jaunarajs, K.L., Standaert, D.G., Viegas, T.X., Bentley, M.D., Fang, Z., Dizman, B., Yoon, K., Weimer, R., Ravenscroft, P., Johnston, T.H., *Rotigotine polyoxazoline conjugate SER-214 provides robust and sustained antiparkinsonian benefit.* Movement Disorders **2013**, *28*, 1675-1682.
39. Deutsches Kunststoffmuseum. (accessed 03.04.2019); Available from: www.deutsches-kunststoff-museum.de.
40. Grumezescu, V., Mihai Grumezescu, A., *Materials for biomedical engineering: Thermoset and Thermoplastic polymers*. 2019: Elsevier, ISBN 978-0-12-816874-5.
41. Ulery, B.D., Nair, L.S., Laurencin, C.T., *Biomedical applications of biodegradable polymers.* Journal of Polymer Science Part B: Polymer Physics **2011**, *49*, 832-864.
42. Gomes, M.E., Holtorf, H.L., Reis, R.L., Mikos, A.G., *Influence of the porosity of starch-based fiber mesh scaffolds on the proliferation and osteogenic differentiation of bone marrow stromal cells cultured in a flow perfusion bioreactor.* Tissue Engineering **2006**, *12*, 801-809.
43. Entcheva, E., Bien, H., Yin, L., Chung, C.-Y., Farrell, M., Kostov, Y., *Functional cardiac cell constructs on cellulose-based scaffolding.* Biomaterials **2004**, *25*, 5753-5762.
44. Eiselt, P., Lee, K.Y., Mooney, D.J., *Rigidity of two-component hydrogels prepared from alginate and poly(ethylene glycol)−Diamines.* Macromolecules **1999**, *32*, 5561-5566.
45. Janmey, P.A., Winer, J.P., Weisel, J.W., *Fibrin gels and their clinical and bioengineering applications.* Journal of the Royal Society Interface **2008**, *6*, 1-10.
46. Kumbar, S., Laurencin, C., Deng, M., *Natural and synthetic biomedical polymers*. 2014: Elsevier, ISBN 978-0-12-396983-5.
47. Parenteau-Bareil, R., Gauvin, R., Berthod, F., *Collagen-based biomaterials for tissue engineering applications.* Materials **2010**, *3*, 1863-1887.
48. Miranda-Nieves, D., Chaikof, E.L., *Collagen and elastin biomaterials for the fabrication of engineered living tissues.* ACS Biomater Sci Eng **2016**, *3*, 694-711.
49. Kearns, V., MacIntosh, A., Crawford, A., Hatton, P., *Silk-based biomaterials for tissue engineering.* Topics in tissue engineering **2008**, *4*, 1-19.
50. Kundu, S., *Silk biomaterials for tissue engineering and regenerative medicine*. 2014: Elsevier, ISBN 978-0-85709-699-9.

51. Dhandayuthapani, B., Sakthi kumar, D., *Biomaterials for Biomedical Applications*, in *Biomedical Applications of Polymeric Materials and Composites*. 2016, Wiley-VCH Verlag GmbH & Co. KGaA.
52. Knop, K., Hoogenboom, R., Fischer, D., Schubert, U.S., *Poly(ethylene glycol) in drug delivery: pros and cons as well as potential alternatives.* Angewandte Chemie International Edition **2010**, *49*, 6288-6308.
53. Batrakova, E.V., Kabanov, A.V., *Pluronic block copolymers: evolution of drug delivery concept from inert nanocarriers to biological response modifiers.* Journal of Controlled Release **2008**, *130*, 98-106.
54. Jeong, B., Kim, S.W., Bae, Y.H., *Thermosensitive sol–gel reversible hydrogels.* Advanced Drug Delivery Reviews **2012**, *64*, 154-162.
55. Hatefi, A., Amsden, B., *Biodegradable injectable in situ forming drug delivery systems.* Journal of Controlled Release **2002**, *80*, 9-28.
56. Akash, M.S.H., Rehman, K., *Recent progress in biomedical applications of Pluronic (PF127): pharmaceutical perspectives.* Journal of Controlled Release **2015**, *209*, 120-138.
57. Ye, L., Letchford, K., Heller, M., Liggins, R., Guan, D., Kizhakkedathu, J.N., Brooks, D.E., Jackson, J.K., Burt, H.M., *Synthesis and characterization of carboxylic acid conjugated, hydrophobically derivatized, hyperbranched polyglycerols as nanoparticulate drug carriers for cisplatin.* Biomacromolecules **2010**, *12*, 145-155.
58. Saatchi, K., Soema, P., Gelder, N., Misri, R., McPhee, K., Baker, J.H., Reinsberg, S.A., Brooks, D.E., Häfeli, U.O., *Hyperbranched polyglycerols as trimodal imaging agents: design, biocompatibility, and tumor uptake.* Bioconjugate Chemistry **2012**, *23*, 372-381.
59. Feineis, S., Lutz, J., Heffele, L., Endl, E., Albrecht, K., Groll, J., *Thioether–Polyglycidol as Multivalent and Multifunctional Coating System for Gold Nanoparticles.* Advanced Materials **2018**, *30*, 1704972.
60. Stichler, S., Jungst, T., Schamel, M., Zilkowski, I., Kuhlmann, M., Bock, T., Blunk, T., Tessmar, J., Groll, J., *Thiol-ene Clickable Poly(glycidol) Hydrogels for Biofabrication.* Annals of Biomedical Engineering **2016**, *45*, 273-285.
61. Gosecki, M., Gadzinowski, M., Gosecka, M., Basinska, T., Slomkowski, S., *Polyglycidol, its derivatives, and polyglycidol-containing copolymers – Synthesis and medical applications.* Polymers **2016**, *8*, 227.
62. Kainthan, R.K., Janzen, J., Levin, E., Devine, D.V., Brooks, D.E., *Biocompatibility testing of branched and linear polyglycidol.* Biomacromolecules **2006**, *7*, 703-709.
63. Szwarc, M., *'Living'polymers.* Nature **1956**, *178*, 1168.
64. Verbraeken, B., Monnery, B.D., Lava, K., Hoogenboom, R., *The chemistry of poly(2-oxazoline)s.* European Polymer Journal **2017**, *88*, 451-469.
65. Dworak, A., *The role of cationic and covalent active centers in the polymerization of 2-methyl-2-oxazoline initiated with benzyl bromide.* Macromolecular Chemistry and Physics **1998**, *199*, 1843-1849.
66. Monnery, B.D., Jerca, V.V., Sedlacek, O., Verbraeken, B., Cavill, R., Hoogenboom, R., *Defined High Molar Mass Poly(2-Oxazoline)s.* Angewandte Chemie International Edition **2018**, *57*, 15400-15404.
67. Litt, M., Levy, A., Herz, J., *Polymerization of cyclic imino ethers. X. Kinetics, chain transfer, and repolymerization.* Journal of Macromolecular Science: Part A-Chemistry **1975**, *9*, 703-727.

68. Sedláček, O., Monnery, B.D., Hoogenboom, R., *Synthesis of defined high molar mass poly(2-methyl-2-oxazoline).* Polymer Chemistry **2019**, *10*, 825-828.
69. Nuyken, O., Maier, G., Groß, A., Fischer, H., *Systematic investigations on the reactivity of oxazolinium salts.* Macromolecular Chemistry and Physics **1996**, *197*, 83-95.
70. Giardi, C., Lapinte, V., Nielloud, F., Devoisselle, J.M., Robin, J.J., *Synthesis of polyoxazolines using glycerol carbonate derivative and end chains functionalization via carbonate and isocyanate routes.* Journal of Polymer Science Part A: Polymer Chemistry **2010**, *48*, 4027-4035.
71. Kempe, K., *Chain and Step Growth Polymerizations of Cyclic Imino Ethers: From Poly(2-oxazoline)s to Poly(ester amide)s.* Macromolecular Chemistry and Physics **2017**, *218*, 1700021.
72. Witte, H., Seeliger, W., *Simple Synthesis of 2-Substituted 2-Oxazolines and 5,6-Dihydro-4H-1,3-oxazines.* Angewandte Chemie International Edition **1972**, *11*, 287-288.
73. Wenker, H., *The preparation of ethylene imine from monoethanolamine.* Journal of the American Chemical Society **1935**, *57*, 2328-2328.
74. Binder, W.H., Gruber, H., *Block copolymers derived from photoreactive 2-oxazolines, 1. Synthesis and micellization behavior.* Macromolecular Chemistry and Physics **2000**, *201*, 949-957.
75. Luxenhofer, R., Jordan, R., *Click chemistry with poly(2-oxazoline)s.* Macromolecules **2006**, *39*, 3509-3516.
76. Persigehl, P., Jordan, R., Nuyken, O., *Functionalization of amphiphilic poly(2-oxazoline) block copolymers: A novel class of macroligands for micellar catalysis.* Macromolecules **2000**, *33*, 6977-6981.
77. Dargaville, T.R., Lava, K., Verbraeken, B., Hoogenboom, R., *Unexpected Switching of the Photogelation Chemistry When Cross-Linking Poly(2-oxazoline) Copolymers.* Macromolecules **2016**, *49*, 4774-4783.
78. Schmaljohann, D., *Thermo-and pH-responsive polymers in drug delivery.* Advanced Drug Delivery Reviews **2006**, *58*, 1655-1670.
79. Christova, D., Velichkova, R., Loos, W., Goethals, E.J., Prez, F.D., *New thermo-responsive polymer materials based on poly(2-ethyl-2-oxazoline) segments.* Polymer **2003**, *44*, 2255-2261.
80. Hoogenboom, R., Thijs, H.M., Jochems, M.J., van Lankvelt, B.M., Fijten, M.W., Schubert, U.S., *Tuning the LCST of poly(2-oxazoline)s by varying composition and molecular weight: alternatives to poly(N-isopropylacrylamide)?* Chemical Communications **2008**, 5758-5760.
81. Lin, P., Clash, C., Pearce, E.M., Kwei, T., Aponte, M., *Solubility and miscibility of poly(ethyl oxazoline).* Journal of Polymer Science Part B: Polymer Physics **1988**, *26*, 603-619.
82. Tatar Güner, P., Demirel, A.L., *Effect of anions on the cloud point temperature of aqueous poly(2-ethyl-2-oxazoline) solutions.* The Journal of Physical Chemistry B **2012**, *116*, 14510-14514.
83. Kowalczuk, A., Kronek, J., Bosowska, K., Trzebicka, B., Dworak, A., *Star poly(2-ethyl-2-oxazoline)s – synthesis and thermosensitivity.* Polymer International **2011**, *60*, 1001-1009.
84. Bloksma, M.M., Weber, C., Perevyazko, I.Y., Kuse, A., Baumgärtel, A., Vollrath, A., Hoogenboom, R., Schubert, U.S., *Poly(2-cyclopropyl-2-*

oxazoline): from rate acceleration by cyclopropyl to thermoresponsive properties. Macromolecules **2011**, *44*, 4057-4064.
85. Obeid, R., Tanaka, F., Winnik, F.M., *Heat-induced phase transition and crystallization of hydrophobically end-capped poly(2-isopropyl-2-oxazoline)s in water.* Macromolecules **2009**, *42*, 5818-5828.
86. Hoogenboom, R., Schlaad, H., *Thermoresponsive poly(2-oxazoline)s, polypeptoids, and polypeptides.* Polymer Chemistry **2017**, *8*, 24-40.
87. Diehl, C., Schlaad, H., *Thermo-responsive polyoxazolines with widely tuneable LCST.* Macromolecular Bioscience **2009**, *9*, 157-61.
88. Malik, M.I., Pasch, H., *Novel developments in the multidimensional characterization of segmented copolymers.* Progress in Polymer Science **2014**, *39*, 87-123.
89. Naka, K., Nakamura, T., Ohki, A., Maeda, S., *Aggregation behavior and interaction with human serum albumin of 2-oxazoline block copolymers in aqueous solutions.* Macromolecular Chemistry and Physics **1997**, *198*, 101-116.
90. Lambermont-Thijs, H.M., Heuts, J.P., Hoeppener, S., Hoogenboom, R., Schubert, U.S., *Selective partial hydrolysis of amphiphilic copoly(2-oxazoline)s as basis for temperature and pH responsive micelles.* Polymer Chemistry **2011**, *2*, 313-322.
91. Weber, C., Wagner, M., Baykal, D., Hoeppener, S., Paulus, R.M., Festag, G., Altuntas, E., Schacher, F.H., Schubert, U.S., *Easy access to amphiphilic heterografted poly(2-oxazoline) comb copolymers.* Macromolecules **2013**, *46*, 5107-5116.
92. Weber, C., Rogers, S., Vollrath, A., Hoeppener, S., Rudolph, T., Fritz, N., Hoogenboom, R., Schubert, U.S., *Aqueous solution behavior of comb-shaped poly(2-ethyl-2-oxazoline).* Journal of Polymer Science Part A: Polymer Chemistry **2013**, *51*, 139-148.
93. Cook, A.B., Peltier, R., Zhang, J., Gurnani, P., Tanaka, J., Burns, J.A., Dallmann, R., Hartlieb, M., Perrier, S., *Hyperbranched poly (ethylenimine-co-oxazoline) by thiol–yne chemistry for non-viral gene delivery: investigating the role of polymer architecture.* Polymer Chemistry **2019**, *10*, 1202-1212.
94. Hartlieb, M., Kempe, K., Schubert, U.S., *Covalently cross-linked poly(2-oxazoline) materials for biomedical applications – from hydrogels to self-assembled and templated structures.* Journal of Materials Chemistry B **2015**, *3*, 526-538.
95. Kolb, H.C., Finn, M., Sharpless, K.B., *Click chemistry: diverse chemical function from a few good reactions.* Angewandte Chemie International Edition **2001**, *40*, 2004-2021.
96. Barner-Kowollik, C., Du Prez, F.E., Espeel, P., Hawker, C.J., Junkers, T., Schlaad, H., Van Camp, W., *"Clicking" polymers or just efficient linking: what is the difference?* Angewandte Chemie International Edition **2011**, *50*, 60-62.
97. Posner, T., *Beiträge zur Kenntniss der ungesaettigten Verbindungen. II. Ueber die Addition von Mercaptanen an ungesaettigte Kohlenwasserstoffe.* Berichte der Deutschen Chemischen Gesellschaft **1905**, *38*, 28.
98. Lowe, A.B., *Thiol-ene "click" reactions and recent applications in polymer and materials synthesis.* Polymer Chemistry **2010**, *1*, 17-36.
99. Bryant, S.J., Nuttelman, C.R., Anseth, K.S., *Cytocompatibility of UV and visible light photoinitiating systems on cultured NIH/3T3 fibroblasts in vitro.* Journal of Biomaterials Science, Polymer Edition **2000**, *11*, 439-457.

100. Wichterle, O., Lim, D., *Hydrophilic gels for biological use.* Nature **1960**, *185*, 117.
101. Bhattarai, N., Gunn, J., Zhang, M., *Chitosan-based hydrogels for controlled, localized drug delivery.* Advanced Drug Delivery Reviews **2010**, *62*, 83-99.
102. Canal, T., Peppas, N.A., *Correlation between mesh size and equilibrium degree of swelling of polymeric networks.* Journal of Biomedical Materials Research **1989**, *23*, 1183-1193.
103. Munch, J., Candau, S., Herz, J., Hild, G., *Inelastic light scattering by gel modes in semi-dilute polymer solutions and permanent networks at equilibrium swollen state.* Journal de Physique **1977**, *38*, 971-976.
104. Tanaka, T., Hocker, L.O., Benedek, G.B., *Spectrum of light scattered from a viscoelastic gel.* Journal of Chemical Physics **1973**, *59*, 5151.
105. Peppas, N., Huang, Y., Torres-Lugo, M., Ward, J., Zhang, J., *Physicochemical foundations and structural design of hydrogels in medicine and biology.* Annual Review of Biomedical Engineering **2000**, *2*, 9-29.
106. Flory, P.J., Rehner Jr., J., *Statistical mechanics of cross-linked polymer networks I. Rubberlike elasticity.* The journal of chemical physics **1943**, *11*, 512-520.
107. Lin, C.-C., Metters, A.T., *Hydrogels in controlled release formulations: network design and mathematical modeling.* Advanced Drug Delivery Reviews **2006**, *58*, 1379-1408.
108. Cabral, J., Moratti, S.C., *Hydrogels for biomedical applications.* Future Medicinal Chemistry **2011**, *3*, 1877-1888.
109. Zhu, Z., Li, X., *Silicone hydrogels based on a novel amphiphilic poly(2-methyl-2-oxazoline)-b-poly(dimethyl siloxane) copolymer.* Journal of Applied Polymer Science **2014**, *131*, 39867.
110. Hoyle, C.E., Bowman, C.N., *Thiol-ene click chemistry.* Angewandte Chemie International Edition **2010**, *49*, 1540-73.
111. Nguyen, K.T., West, J.L., *Photopolymerizable hydrogels for tissue engineering applications.* Biomaterials **2002**, *23*, 4307-4314.
112. Luef, K.P., Petit, C., Ottersböck, B., Oreski, G., Ehrenfeld, F., Grassl, B., Reynaud, S., Wiesbrock, F., *UV-mediated thiol-ene click reactions for the synthesis of drug-loadable and degradable gels based on copoly(2-oxazoline)s.* European Polymer Journal **2017**, *88*, 701-712.
113. Šrámková, P., Zahoranová, A., Kroneková, Z., Šišková, A., Kronek, J., *Poly(2-oxazoline) hydrogels by photoinduced thiol-ene "click" reaction using different dithiol crosslinkers.* Journal of Polymer Research **2017**, *24*, 1-13.
114. Van der Heide, D.J., Verbraeken, B., Hoogenboom, R., Dargaville, T.R., Hickey, D.K., *Porous poly(2-oxazoline) scaffolds for developing 3D primary human tissue culture.* Biomaterials and Tissue Technology **2017**, *1*, 1-5.
115. Li, L., Smitthipong, W., Zeng, H., *Mussel-inspired hydrogels for biomedical and environmental applications.* Polymer Chemistry **2015**, *6*, 353-358.
116. Li, Y., Meng, H., Liu, Y., Narkar, A., Lee, B.P., *Gelatin microgel incorporated poly(ethylene glycol)-based bioadhesive with enhanced adhesive property and bioactivity.* ACS applied materials & interfaces **2016**, *8*, 11980-11989.
117. Mehdizadeh, M., Weng, H., Gyawali, D., Tang, L., Yang, J., *Injectable citrate-based mussel-inspired tissue bioadhesives with high wet strength for sutureless wound closure.* Biomaterials **2012**, *33*, 7972-7983.
118. Brubaker, C.E., Messersmith, P.B., *Enzymatically degradable mussel-inspired adhesive hydrogel.* Biomacromolecules **2011**, *12*, 4326-4334.

119. Cencer, M., Liu, Y., Winter, A., Murley, M., Meng, H., Lee, B.P., *Effect of pH on the rate of curing and bioadhesive properties of dopamine functionalized poly(ethylene glycol) hydrogels.* Biomacromolecules **2014**, *15*, 2861-2869.
120. Burke, K.A., Roberts, D.C., Kaplan, D.L., *Silk fibroin aqueous-based adhesives inspired by mussel adhesive proteins.* Biomacromolecules **2015**, *17*, 237-245.
121. Fan, C., Fu, J., Zhu, W., Wang, D.-A., *A mussel-inspired double-crosslinked tissue adhesive intended for internal medical use.* Acta Biomaterialia **2016**, *33*, 51-63.
122. Sparks, B.J., Hoff, E.F., Hayes, L.P., Patton, D.L., *Mussel-inspired thiol–ene polymer networks: Influencing network properties and adhesion with catechol functionality.* Chemistry of Materials **2012**, *24*, 3633-3642.
123. Han, L., Wang, M., Li, P., Gan, D., Yan, L., Xu, J., Wang, K., Fang, L., Chan, C.W., Zhang, H., Yuan, H., Lu, X., *Mussel-Inspired Tissue-Adhesive Hydrogel Based on the Polydopamine – Chondroitin Sulfate Complex for Growth-Factor-Free Cartilage Regeneration.* ACS applied materials & interfaces **2018**, *10*, 28015-28026.
124. Kord Forooshani, P., Lee, B.P., *Recent approaches in designing bioadhesive materials inspired by mussel adhesive protein.* Journal of Polymer Science Part A: Polymer Chemistry **2017**, *55*, 9-33.
125. Hu, B.-H., Messersmith, P.B., *Protection of 3, 4-dihydroxyphenylalanine (DOPA) for Fmoc solid-phase peptide synthesis.* Tetrahedron Letters **2000**, *41*, 5795-5798.
126. Liu, Z., Hu, B.-H., Messersmith, P.B., *Convenient synthesis of acetonide-protected 3, 4-dihydroxyphenylalanine (DOPA) for Fmoc solid-phase peptide synthesis.* Tetrahedron Letters **2008**, *49*, 5519-5521.
127. Lee, B.P., Huang, K., Nunalee, F.N., Shull, K.R., Messersmith, P.B., *Synthesis of 3, 4-dihydroxyphenylalanine (DOPA) containing monomers and their co-polymerization with PEG-diacrylate to form hydrogels.* Journal of Biomaterials Science, Polymer Edition **2004**, *15*, 449-464.
128. Van Dyck, S., Lemière, G., Jonckers, T., Dommisse, R., *Synthesis of 4-O-methylcedrusin. Selective protection of catechols with diphenyl carbonate.* Molecules **2000**, *5*, 153-161.
129. Shao, L., Zhang, X., *Preparation of phenylacetic acid derivatives as antitumor agents.* WO 2015018182 **2015**.
130. Dawson, P.E., Muir, T.W., Clark-Lewis, I., Kent, S., *Synthesis of proteins by native chemical ligation.* Science **1994**, *266*, 776-779.
131. Hackenberger, C.P., Schwarzer, D., *Chemoselective Ligation and Modification Strategies for Peptides and Proteins.* Angewandte Chemie **2008**, *120*, 10182-10228.
132. Chen, H., Xiao, Y., Yuan, N., Weng, J., Gao, P., Breindel, L., Shekhtman, A., Zhang, Q., *Coupling of sterically demanding peptides by β-thiolactone-mediated native chemical ligation.* Chemical Science **2018**, *9*, 1982-1988.
133. Fan, Z., Zhang, Y., Ji, J., Li, X., *Hybrid polypeptide hydrogels produced via native chemical ligation.* RSC Advances **2015**, *5*, 16740-16747.
134. de Castro, P.P., Carpanez, A.G., Amarante, G.W., *Azlactone reaction developments.* Chemistry – A European Journal **2016**, *22*, 10294-10318.
135. Coleman, P.L., Walker, M.M., Milbrath, D.S., Stauffer, D.M., *Immobilization of Protein A at high density on azlactone-functional polymeric beads and their use in affinity chromatography.* Journal of Chromatography A **1990**, *512*, 345-363.

136. Levere, M.E., Ho, H.T., Pascual, S., Fontaine, L., *Stable azlactone-functionalized nanoparticles prepared from thermoresponsive copolymers synthesized by RAFT polymerization.* Polymer Chemistry **2011**, *2*, 2878–2887.
137. Gardner, C.M., Brown, C.E., Stöver, H.D., *Synthesis and properties of water-soluble azlactone copolymers.* Journal of Polymer Science Part A: Polymer Chemistry **2012**, *50*, 4674-4685.
138. Ho, H.T., Bénard, A., Forcher, G., Le Bohec, M., Montembault, V., Pascual, S., Fontaine, L., *Azlactone-based heterobifunctional linkers with orthogonal clickable groups: efficient tools for bioconjugation with complete atom economy.* Organic biomolecular chemistry **2018**, *16*, 7124-7128.
139. Schmitt, S.K., Trebatoski, D.J., Krutty, J.D., Xie, A.W., Rollins, B., Murphy, W.L., Gopalan, P., *Peptide Conjugation to a Polymer Coating via Native Chemical Ligation of Azlactones for Cell Culture.* Biomacromolecules **2016**, *17*, 1040-1047.
140. Geng, Y., Discher, D.E., Justynska, J., Schlaad, H., *Grafting Short Peptides onto Polybutadiene-block-poly(ethylene oxide): A Platform for Self-Assembling Hybrid Amphiphiles.* Angewandte Chemie International Edition **2006**, *45*, 7578-7581.
141. Habraken, G.J., Koning, C.E., Heuts, J.P., Heise, A., *Thiol chemistry on well-defined synthetic polypeptides.* Chemical Communications **2009**, 3612-3614.
142. DeForest, C.A., Polizzotti, B.D., Anseth, K.S., *Sequential click reactions for synthesizing and patterning three-dimensional cell microenvironments.* Nature materials **2009**, *8*, 659.
143. Colak, B., Da Silva, J.C., Soares, T.A., Gautrot, J.E., *Impact of the Molecular Environment on Thiol-Ene Coupling For Biofunctionalization and Conjugation.* Bioconjugate Chemistry **2016**, *27*, 2111-23.
144. Jung, B., Theato, P., *Chemical strategies for the synthesis of protein–polymer conjugates.* Advances in Polymer Science **2013**, *253*, 37-70.
145. Luxenhofer, R., López-García, M., Frank, A., Kessler, H., Jordan, R., *First poly(2-oxazoline)-peptide conjugate for targeted radionuclide cancer therapy.* PMSE Preprints **2006**, *95*, 283-284.
146. Luxenhofer, R., Doctoral Thesis, Technical University Munich, Garching, Germany, 2007.
147. Schmitz, M., Kuhlmann, M., Reimann, O., Hackenberger, C.P., Groll, J., *Side-chain cysteine-functionalized poly(2-oxazoline)s for multiple peptide conjugation by native chemical ligation.* Biomacromolecules **2015**, *16*, 1088-94.
148. Nawroth, J.F., McDaniel, J.R., Chilkoti, A., Jordan, R., Luxenhofer, R., *Maleimide-Functionalized Poly(2-Oxazoline)s and Their Conjugation to Elastin-Like Polypeptides.* Macromolecular Bioscience **2016**, *16*, 322-333.
149. Shu, J.Y., Panganiban, B., Xu, T., *Peptide-polymer conjugates: from fundamental science to application.* Annual Review of Physical Chemistry **2013**, *64*, 631-657.
150. Duncan, R., Vicent, M., *Polymer therapeutics-prospects for 21st century: the end of the beginning.* Advanced Drug Delivery Reviews **2013**, *65*, 60-70.
151. Ekladious, I., Colson, Y.L., Grinstaff, M.W., *Polymer–drug conjugate therapeutics: advances, insights and prospects.* Nature Reviews Drug Discovery **2019**, *18*, 273-294.
152. Hu, Y., Hou, Y., Wang, H., Lu, H., *Polysarcosine as an alternative to PEG for therapeutic protein conjugation.* Bioconjugate Chemistry **2018**, *29*, 2232-2238.

153. He, Z., Schulz, A., Wan, X., Seitz, J., Bludau, H., Alakhova, D.Y., Darr, D.B., Perou, C.M., Jordan, R., Ojima, I., *Poly(2-oxazoline) based micelles with high capacity for 3rd generation taxoids: preparation, in vitro and in vivo evaluation.* Journal of Controlled Release **2015**, *208*, 67-75.
154. Pierschbacher, M.D., Ruoslahti, E., *Cell attachment activity of fibronectin can be duplicated by small synthetic fragments of the molecule.* Nature **1984**, *309*, 30.
155. Hersel, U., Dahmen, C., Kessler, H., *RGD modified polymers: biomaterials for stimulated cell adhesion and beyond.* Biomaterials **2003**, *24*, 4385-4415.
156. Hammer, N., Brandl, F.P., Kirchhof, S., Goepferich, A.M., *Cleavable carbamate linkers for controlled protein delivery from hydrogels.* Journal of Controlled Release **2014**, *183*, 67-76.
157. Ramkumar, R., Chandrasekaran, S., *Efficient Catalyst-Free Trans Sulfonamidation/Sulfonamide Metathesis under Mild Conditions.* ChemistrySelect **2018**, *1*, 1-4.
158. Paulus, I., Master thesis, Julius-Maximilians-Universität, Würzburg, Germany, 2017.
159. Kempe, K., Vollrath, A., Schaefer, H.W., Poehlmann, T.G., Biskup, C., Hoogenboom, R., Hornig, S., Schubert, U.S., *Multifunctional poly (2-oxazoline) nanoparticles for biological applications.* Macromolecular Rapid Communications **2010**, *31*, 1869-1873.
160. HORIBA. Raman Data and Analysis. Application Note (accessed 05.02.); Available from: http://www.horiba.com/fileadmin/uploads/Scientific/Documents/Raman/bands.pdf.
161. Reinicke, S., Espeel, P., Stamenović, M.M., Du Prez, F.E., *One-pot double modification of p (NIPAAm): a tool for designing tailor-made multiresponsive polymers.* ACS Macro Letters **2013**, *2*, 539-543.
162. Ho, H.T., Levere, M.E., Pascual, S., Montembault, V., Casse, N., Caruso, A., Fontaine, L., *Thermoresponsive block copolymers containing reactive azlactone groups and their bioconjugation with lysozyme.* Polymer Chemistry **2013**, *4*, 675-685.
163. Condon, M.E., Petrillo Jr, E.W., Ryono, D.E., Reid, J.A., Neubeck, R., Puar, M., Heikes, J.E., Sabo, E.F., Losee, K.A., *Angiotensin-converting enzyme inhibitors: importance of the amide carbonyl of mercaptoacyl amino acids for hydrogen bonding to the enzyme.* Journal of Medicinal Chemistry **1982**, *25*, 250-258.
164. Baker, J.W., Ingold, C.K., *The formation and stability of spiro-compounds.* Journal of the CHemical Society, Transactions **1923**, *123*, 122-133.
165. Williams, C.G., Malik, A.N., Kim, T.K., Manson, P.N., Elisseeff, J.H., *Variable cytocompatibility of six cell lines with photoinitiators used for polymerizing hydrogels and cell encapsulation.* Biomaterials **2005**, *26*, 1211-1218.
166. Blöhbaum, J., Paulus, I., Pöppler, A.-C., Tessmar, J., Groll, J., *Influence of charged groups on the cross-linkingefficiency and release of guest molecules from thiol–ene cross-linked poly(2-oxazoline)hydrogels.* Journal of Materials Chemistry B **2019**, *7*, 1782-1794.
167. Bloksma, M.M., Bakker, D.J., Weber, C., Hoogenboom, R., Schubert, U.S., *The Effect of Hofmeister Salts on the LCST Transition of Poly(2-oxazoline)s with Varying Hydrophilicity.* Macromolecular Rapid Communications **2010**, *31*, 724-728.

168. Berdichevski, A., Shachaf, Y., Wechsler, R., Seliktar, D., *Protein composition alters in vivo resorption of PEG-based hydrogels as monitored by contrast-enhanced MRI.* Biomaterials **2015**, *42*, 1-10.
169. Lee, B.P., Messersmith, P.B., Israelachvili, J.N., Waite, J.H., *Mussel-inspired adhesives and coatings.* Annual review of materials research **2011**, *41*, 99-132.
170. Guthold, M., Liu, W., Sparks, E., Jawerth, L., Peng, L., Falvo, M., Superfine, R., Hantgan, R.R., Lord, S.T., *A comparison of the mechanical and structural properties of fibrin fibers with other protein fibers.* Cell Biochemistry and Biophysics **2007**, *49*, 165-181.
171. Malins, L.R., Payne, R., *Recent extensions to native chemical ligation for the chemical synthesis of peptides and proteins.* Current Opinion in Chemical Biology **2014**, *22*, 70-78.
172. Johnson, E.C., Kent, S.B., *Insights into the mechanism and catalysis of the native chemical ligation reaction.* Journal of the American Chemical Society **2006**, *128*, 6640-6646.
173. Schmitt, S.K., Xie, A.W., Ghassemi, R.M., Trebatoski, D.J., Murphy, W.L., Gopalan, P., *Polyethylene Glycol Coatings on Plastic Substrates for Chemically Defined Stem Cell Culture.* Advanced Healthcare Materials **2015**, *4*, 1555-64.
174. Ho, H.T., Levere, M.E., Fournier, D., Montembault, V., Pascual, S., Fontaine, L., *Introducing the Azlactone Functionality into Polymers through Controlled Radical Polymerization: Strategies and Recent Developments.* Australian Journal of Chemistry **2012**, *65*, 970-977.
175. Becker, H.G.O., Berger, W., Domschke, G., *Organikum*. 2001: WILEY-VCH, ISBN 3-527-29985-8.
176. Boerman, M.A., Van der Laan, H.L., Bender, J.C., Hoogenboom, R., Jansen, J.A., Leeuwenburgh, S.C., Van Hest, J.C., *Synthesis of pH- and thermoresponsive poly(2-n-propyl-2-oxazoline) based copolymers.* Journal of Polymer Science Part A: Polymer Chemistry **2016**, *54*, 1573-1582.
177. Hoogenboom, R., Fijten, M.W.M., Thijs, H.M.L., van Lankvelt, B.M., Schubert, U.S., *Microwave-assisted synthesis and properties of a series of poly(2-alkyl-2-oxazoline)s.* Designed Monomers and Polymers **2012**, *8*, 659-671.